

**Oxazoline and Imidazoline Complexes:
Synthesis, Reactivity and
Asymmetric Catalysis.**

**Thesis Submitted for the Degree of
Doctor of Philosophy**

By

Adam James Davenport

**in the Department of Chemistry
at the
University of Leicester**

October 2000

UMI Number: U141451

All rights reserved

INFORMATION TO ALL USERS

The quality of this reproduction is dependent upon the quality of the copy submitted.

In the unlikely event that the author did not send a complete manuscript and there are missing pages, these will be noted. Also, if material had to be removed, a note will indicate the deletion.



UMI U141451

Published by ProQuest LLC 2013. Copyright in the Dissertation held by the Author.
Microform Edition © ProQuest LLC.

All rights reserved. This work is protected against
unauthorized copying under Title 17, United States Code.



ProQuest LLC
789 East Eisenhower Parkway
P.O. Box 1346
Ann Arbor, MI 48106-1346

Title: Oxazoline and Imidazoline Complexes:

Synthesis, Reactivity and Asymmetric Catalysis.

Author: Adam James Davenport

ABSTRACT

This thesis describes the synthesis and chemistry of “(arene)Ru” and “Cp*Rh” complexes of chiral oxazoline, imidazoline and Schiff-base-containing ligands and their use as asymmetric Lewis-acid catalysts.

Chapter One introduces chiral half-sandwich complexes, with emphasis on the stability of the configuration at the metal, the stereochemistry of substitution reactions at the metal and methods for studying these. This is followed by an overview of the chemistry of arene-ruthenium and Cp*-rhodium complexes in particular their complexes with chiral bidentate ligands.

Chapter Two describes the synthesis and characterisation of chiral-at-metal complexes $[MCl(R\text{-phenmox})(\text{ring})]$ ($M = \text{Rh}$, ring = Cp*; $M = \text{Ru}$, ring = arene) and various derivatives $[\text{RuL}(R\text{-phenmox})(\text{arene})]^{n+}$ ($L = \text{py}$, 2-Me-py, 4-Me-py, PPh₃, $n = 1$; $L = \text{Br}$, I, $n = 0$). The stereochemistry of substitution reactions of $[\text{Ru}(\text{OH}_2)(^i\text{Pr-pymox})(\text{mes})](\text{SbF}_6)_2$, with X⁻ and the kinetics of epimerisation of the products are reported. In the latter part of the chapter, the syntheses of new chiral imidazoline ligands, and half-sandwich complexes of these and of some Schiff-base ligands are described. Throughout the chapter X-ray diffraction (14 structures), variable temperature and 2-D NMR experiments have been used to examine the factors affecting the diastereoselectivity and epimerisation of the complexes.

Chapter Three describes attempts to make cyclometallated *C*, *N*-bonded phenyl-oxazoline half-sandwich complexes. Two cyclometallated tin complexes and a number of palladium derivatives are reported. Finally, the synthesis and X-ray structure of the first example of an arene ruthenium phenyl-oxazoline complex is described.

Chapter Four provides a brief introduction to asymmetric catalysis particularly using half-sandwich complexes as Lewis acid catalysts. The complexes $[\text{Ru}(\text{OH}_2)(L)(\text{arene})](\text{SbF}_6)_n$ ($L = \text{phenmox}$, pymim, ketimine) were found to be moderately efficient and enantioselective catalysts for the Diels-Alder reaction of acrylic dienophiles with simple dienes. Preliminary investigations of other Lewis-acid catalysed reactions including Hetero-Diels Alder, Mukaiyama Aldol and inverse electron-demand Hetero Diels-Alder are reported.

Statement

This thesis is based on work conducted by the author, in the Department of Chemistry of the University of Leicester, during the period between October 1997 and September 2000.

All the work described in the thesis is original unless otherwise stated in the text or in the references. This work is not being presented for any other degree.

Signed: Adam Davenport

Date: 18/03/2001

Adam James Davenport

ACKNOWLEDGEMENTS

I would like to thank my supervisor, Dr D.L. Davies for all the help and guidance throughout the last three years, and also Dr D.R. Russell and especially Dr J. Fawcett for the X-ray structure determinations. Thanks are also due to Dr G.A. Griffith for variable temperature and 2D NMR spectra and to Dr G.A. Eaton for the mass spectra. Thanks also to K. Singh for the synthesis of various starting materials and for helpful discussion in the use of laboratory equipment. Some preliminary observations of the synthesis of $[\text{RuX}(\text{}^i\text{Pr-pymox})(\text{mes})]\text{SbF}_6$ (X = Br, I) was carried out by S. A. Garratt (see Chapter Two).

My thanks are also extended to all the people who have helped enormously in the practical work over the three years, and to everyone working in the organometallic laboratory for numerous helpful discussions.

Acknowledgement is made to the EPSRC for funding this research. Thanks to my family and friends for all their support and encouragement.

Abbreviations and Symbols

General and Physical

br s	=	broad singlet
COSY	=	correlated spectroscopy
d	=	doublet
dd	=	doublet of doublets
dt	=	doublet of triplets
δ	=	chemical shift
°	=	degrees
ES-MS	=	electrospray mass spectrometry
FAB-MS	=	fast atom bombardment mass spectrometry
HOMO	=	highest occupied molecular orbital
h	=	hour
LUMO	=	lowest occupied molecular orbital
m	=	multiplet
min	=	minute
nOe	=	nuclear Overhauser enhancement
NOESY	=	nuclear Overhauser enhancement spectroscopy
NMR	=	nuclear magnetic resonance
ppm	=	parts per million
RT	=	room temperature
s	=	singlet
t	=	triplet
TLC	=	thin layer chromatography

Chemical

aa	=	anion of amino acid
acac	=	anion of pentane-2,4-dione
alaH	=	(L)-alanine
Bn	=	benzyl
Bn-phenmox	=	(4 <i>S</i>)-2-(2-Hydroxyphenyl)-4-benzyl-2-oxazoline
BINAP	=	2,2'-Bis(diphenylphosphino)-1,1'-binaphthyl

bipy	=	2,2'-bipyridine
bom	=	bis-oxazolinyl methane
bop	=	bis-oxazolinyl propane
ⁿ Bu	=	n-Butyl
^t Bu	=	t-Butyl
Chiraphos	=	(2 <i>S</i> ,3 <i>S</i>)-Bis-(diphenylphosphino)-butane
COD	=	cyclooctadiene
Cp	=	cyclopentadienyl anion
CpH	=	cyclopentadiene
Cp*	=	pentamethyl-cyclopentadienyl anion
DCC	=	1,3-dicyclohexylcarbodiimide
DCU	=	1,3-dicyclohexylcarboureia
DMAP	=	<i>N</i> -dimethyl-4-amino-pyridine
DMBD	=	2,3-dimethyl-1,3-butadiene
dopa	=	3,4-dihydroxy-phenylalaninato
DPEN	=	1,2-diphenylethylenediamine
dppe	=	1,2-bis(diphenylphosphino)ethane
dppp	=	1,2-bis(diphenylphosphino)propane
<i>d.e.</i>	=	diastereomeric excess
<i>e.e.</i>	=	enantiomeric excess
HOBt	=	1-hydroxybenzotriazole
LDA	=	lithium diisopropylamide
Me	=	methyl
MeCN	=	acetonitrile
MeOH	=	methanol
2-Me-py	=	2-methyl-pyridine
4-Me-py	=	4-methyl-pyridine
mes	=	1,3,5-trimethylbenzene (mesitylene)
Ms	=	methanesulphonyl
Ns	=	2-nitrobenzenesulphenyl
NOBA	=	3-nitrobenzyl alcohol (matrix)
OAc	=	acetate
OTf	=	triflate
oxaz	=	oxazoline

ⁱ Pr	=	isopropyl
ⁱ Pr-bop	=	2,2'-bis-[(4 <i>S</i>)-isopropyl-oxazolinyl]-propane
ⁱ Pr-phenmox	=	(4 <i>S</i>)-2-(2-hydroxyphenyl)-4-isopropyl-2-oxazoline
R-phenmox	=	(4 <i>S</i>)-2-(2-hydroxyphenyl)-4-R-2-oxazoline
ⁱ Pr-pymox	=	(4 <i>S</i>)-4-isopropyl-2-(2-pyridinyl)-2-oxazoline
(<i>R</i>)-Prophos	=	(<i>R</i>)-(+)-1,2-bis(diphenylphosphino)propane
py	=	pyridine
R,R'-pymimR''	=	(2-pyridinyl)-2-imidazoline (for substituent positions see Figure 2.1)
pymox	=	2-oxazolinyl-pyridine
salald-H	=	(<i>S</i>)- <i>N</i> -(1-phenylethyl)-salicylaldimine
pyrald-H	=	(<i>S</i>)- <i>N</i> -(1-phenylethyl)-pyrrolecarbaldimine
pyald-H	=	(<i>S</i>)- <i>N</i> -(1-phenylethyl)-pyridinecarbaldimine
pyket	=	(<i>S</i>)- <i>N</i> -(1-phenylethyl)-ketimine
proH	=	(<i>L</i>)-proline.
valH	=	(<i>L</i>)-valine
<i>p</i> -cy	=	4-isopropyl-toluene
Ph-phenmox	=	(4 <i>S</i>)-2-(2-hydroxyphenyl)-4-phenyl-2-oxazoline
Ph-pymox	=	(4 <i>S</i>)-4-phenyl-2-(2-pyridinyl)-2-oxazoline
NaOMe	=	sodium methoxide
^t Bu-phenmox	=	(4 <i>S</i>)-2-(2-hydroxyphenyl)-4- <i>tert</i> -butyl-2-oxazoline
THF	=	tetrahydrofuran
Ts	=	toluenesulphonyl
TsDPEN	=	(1 <i>R</i> ,2 <i>R</i>)- <i>N</i> -(<i>p</i> -tolylsulphonyl)-1,2-diphenylethylenediamine

List of Contents

Chapter One – Half-Sandwich Complexes, Synthesis & Chirality	1
(1.1) – Half-Sandwich Chemistry	1
(1.2) – Chirality.....	2
(1.2.1) – Enantiomeric Complexes	2
(1.2.2) – Diastereomeric Complexes	6
(1.3) – Fluxionality, Epimerisation and Mechanism of Substitution.....	7
(1.3.1) – Methods for Studying Epimerisation of Half-sandwich Complexes and Assigning Absolute Stereochemistry.....	7
(1.3.2) – Mechanism of Substitution / Fluxionality.....	9
(1.4) – Arene-Ru (II) and Cp*-Rh (III) half-sandwich chemistry	14
(1.4.1) – Syntheses of Half-sandwich Complexes.....	14
(1.4.2) – Reactions of [RuCl ₂ (arene)] ₂ and [RhCl ₂ (Cp*)] ₂ with Achiral Ligands..	15
(1.4.3) – Reactions with Chiral Ligands.....	18
Chapter Two : Chiral (Arene)Ru & (Cp*)Rh Complexes with Nitrogen-Donor Ligands	38
(2.1) – Introduction.....	38
(2.2) – Results And Discussion	44
(2.2.1) – Half-Sandwich Complexes of Unsymmetrical Oxazoline Ligands	44
(2.2.2) – Mechanism of Substitution	79
(2.2.3) – Half-Sandwich Complexes of Chiral Imidazoline Ligands	89
(2.2.4) - Half-Sandwich Complexes of Chiral Schiff-base Ligands.....	103
(2.3) - Experimental.....	113
Preparation of chiral ligands and precursors.....	113
Preparation of half-sandwich complexes.....	120
Chapter Three – Attempts to Make C-Bonded Phenyl-Oxazolines.....	148
(3.1) – Introduction.....	148
(3.2) – Results and Discussion.....	152
(3.2.1) – Attempted Syntheses of Cyclometallated Phenyloxazoline Half-Sandwich Complexes	152
(3.3) - Experimental.....	169
Chapter Four – Chiral Half-Sandwich Complexes as Asymmetric Catalysts	178

(4.1) – Introduction	178
(4.2) – Results and Discussion.....	186
(4.2.1) – Phenmox Catalysts	187
(4.2.2) – <i>N,N</i> -Donor Catalysts	199
(4.2.3) – Additional Reactions.....	205
(4.3) – Experimental	210
APPENDIX.....	214
BIBLIOGRAPHY.....	229

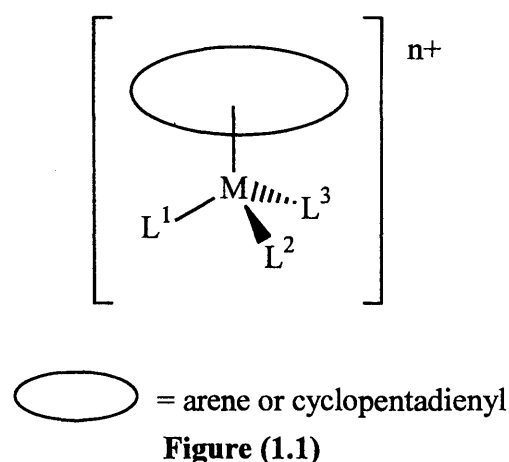
Chapter One:

Half-Sandwich Complexes, Synthesis & Chirality

Chapter One – Half-Sandwich Complexes, Synthesis & Chirality

(1.1) – Half-Sandwich Chemistry

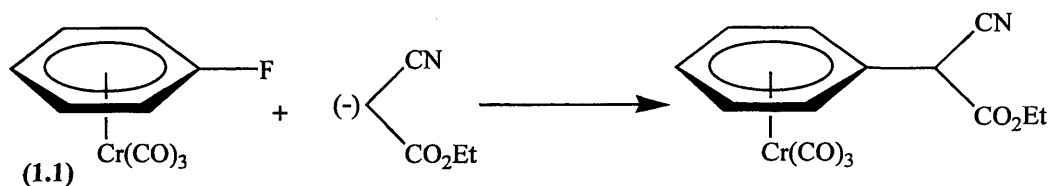
The defining characteristic of a half-sandwich compound is the presence of a π -bound ligand, usually an arene or a cyclopentadienyl ring, occupying three facial coordination sites of the metal centre. The metal may coordinate one to four other ligands, leading to a vast number of half-sandwich complexes that are potentially useful synthetic templates.¹ The focus of this report will be on pseudo-octahedral complexes with three additional donor ligands L^1 - L^3 (**Figure 1.1**).



Half-sandwich complexes are highly versatile tools for both the organometallic and organic chemist. They have been used to investigate the mechanism and stereochemistry of substitution reactions (discussed in Section 1.3.1). In addition, they have found numerous applications in organic synthesis² (resulting from the reactivity of the π -ligand and reactivity at other sites) and more recently, academic and commercial interest has been attracted due to their potential use in asymmetric catalysis,³ (discussed in detail in Chapter Four). The remainder of this chapter will focus on the synthesis, reactivity and chemistry of half-sandwich compounds.

One of the earliest examples of an arene half-sandwich complex was $[\text{Cr}(\text{CO})_3(\text{C}_6\text{H}_6)]$.⁴ X-ray diffraction studies in 1965 showed that the symmetry of the π -bound benzene was not distorted from that of free benzene, this is indicative of a fully delocalised benzene-chromium interaction.⁵ This complex and its derivatives are of synthetic utility since coordination of the arene has a profound effect upon its reaction chemistry.² The arene ring becomes activated towards nucleophilic attack, rather than

the normal electrophilic attack, due to substantial σ -donation of electrons from the arene to chromium. This facilitates previously unfeasible reactions; for example, the fluorine of (1.1) is highly reactive towards substitution by a range of nucleophiles (Scheme 1.1).⁶ This chemistry has been exploited in the synthesis of α -methyl phenyl glycine.⁷



Scheme (1.1)

The majority of research on arene half-sandwich complexes has involved chromium, aside from those, the complexes of ruthenium have attracted a lot of attention, particularly in recent years. The first example of an arene ruthenium half-sandwich complex was $[\text{RuCl}_2(\text{PBU}_3)(\text{C}_6\text{H}_6)]$ reported by Winkaus and Singer in 1967.⁸ The complex was formed by the reaction of PBU_3 with a species of empirical formula $[\text{RuCl}_2(\text{C}_6\text{H}_6)]_n$. One of the first examples of a Cp-ruthenium complex was $[\text{Ru}(\text{CO})_2\text{Cp}]$,⁹ synthesised in 1963 by McCleverty and Wilkinson. The simplest example of a Cp-rhodium complex is $[\text{Rh}(\text{CO})_2\text{Cp}]$,¹⁰ reported by Fischer and Bittler in 1961; these were the first of many related half-sandwich complexes.

The half-sandwich complexes discussed in this report have three donor ligands coordinated to the “(ring)M” fragment, lending the metal a four-coordinate pseudo-tetrahedral geometry. This gives rise to the possibility of generating chiral metal centres based on the half-sandwich structure, see below.

(1.2) – Chirality

This section will look at two classes of half-sandwich complexes; those that are enantiomeric and those that are diastereomeric.

(1.2.1) – Enantiomeric Complexes

Enantiomeric half-sandwich complexes can be categorised into three types:

1. only a chiral metal centre,
2. chiral centre(s) on one of the ligands
3. coordination of a prochiral ligand such as a disubstituted arene or unsymmetrical alkene giving rise to planar chirality.

A general example of a (**type 1**) chiral-at-metal complex is shown in **Figure (1.2)**.

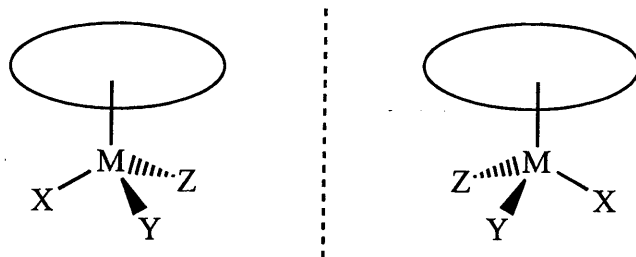


Figure (1.2)

The pseudo-tetrahedral geometry shown in **Figure (1.2)**, is analogous to four-coordinate carbon compounds such that if the three ligands X, Y and Z are all different then the metal is chiral and the complex will usually be formed as a racemate. Similarly, if Y and Z are an unsymmetrical chelate then the metal will be a stereogenic centre and two enantiomers are possible. In 1971 the first examples of chiral ruthenium complexes were synthesised from such a chelate and were indeed formed as racemates, which were not resolved **Figure (1.3)**.¹¹

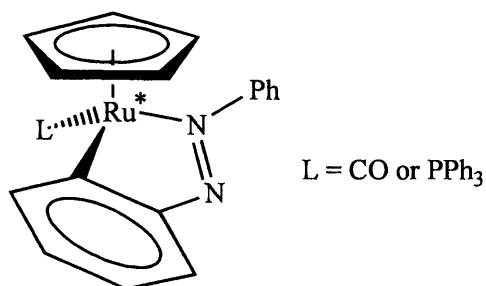
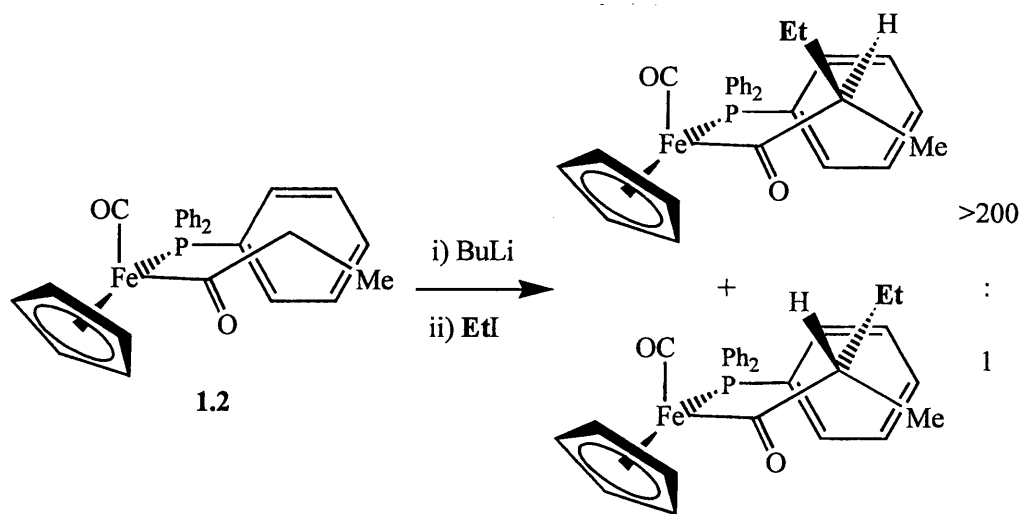


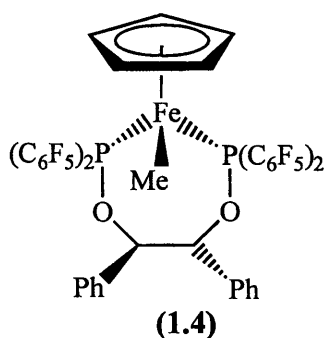
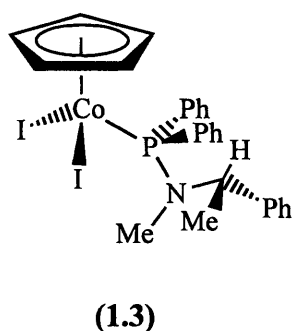
Figure (1.3)

In order to utilise purely chiral-at-metal complexes for asymmetric synthesis a single enantiomer is required; this is often achieved via enantioselective chromatography or crystallisation of their diastereomeric salts. This was first achieved over thirty years ago by Brunner with the manganese complex $[\text{Mn}(\text{CO})(\text{NO})(\text{PPh}_3)\text{Cp}]\text{PF}_6$.¹² The enantiomers were converted to diastereomers by reaction of the carbonyl group with enantiopure menthol, and then separated by selective crystallisation. Acid catalysed hydrolysis of the diastereomerically pure ester yielded the optically pure enantiomer. Particularly impressive examples of stoichiometric asymmetric transformations using CpFe half-sandwich complexes have been achieved by Davies *et al.*¹³ The authors showed that addition of ethyl iodide to the enantiopure lithium enolate of $[\text{Fe}(\text{COEt})(\text{CO})(\text{PPh}_3)\text{Cp}]$ (**1.2**) occurs predominantly from the face opposite to the sterically bulky PPh_3 ligand, resulting in diastereomeric products in a ratio of greater

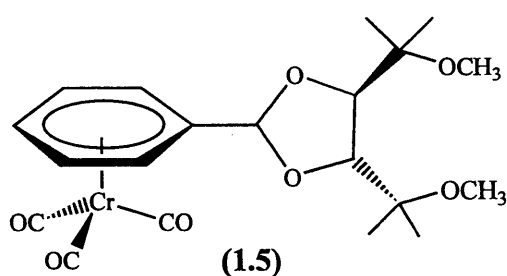
than 200:1 **Scheme (1.2)**¹⁴ This methodology was then utilised in the synthesis of the anti-hypertensive drug (-)-captopril.¹⁵



The second type of optically active half-sandwich complex (**type 2**) has chirality only on a ligand, not at the metal centre. For example, coordination of a chiral monodentate ligand or a C_2 -symmetric bidentate ligand as in **1.3** or **1.4**, respectively. If enantiomerically pure ligands are used enantiomerically pure complexes are formed.



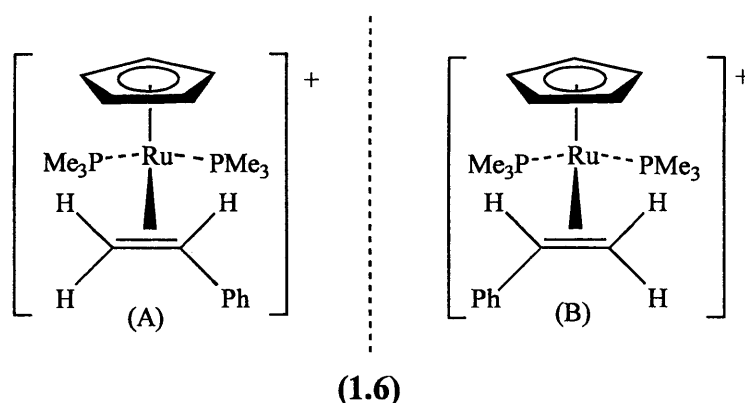
Additionally, this type of chiral complex is formed when the polyhapto ring itself has a chiral auxiliary attached, as in the tartrate derived acetal in **(1.5)**.¹⁶ This arene chromium tricarbonyl complex undergoes *ortho*-functionalisation with high



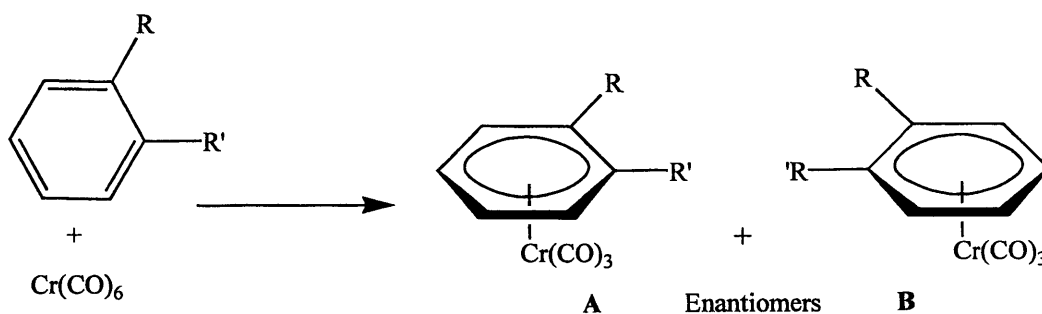
stereocontrol, up to 94% *d.e.* being achieved.

Type 2 chiral half-sandwich complexes have been used in numerous mechanistic studies (these will be discussed in more detail in section 1.3.2).

The third type of enantiomeric half-sandwich complex is that formed by the coordination of a prochiral ligand, such as an unsymmetrical alkene shown in cations (1.6)¹⁷ or an unsymmetrical 1,2- or 1,3-disubstituted polyhapto ring (see **Scheme 1.4**), to an achiral metal centre.



Treatment of $\text{Cr}(\text{CO})_6$ with an unsymmetrical 1,2-disubstituted benzene gives chiral $\text{Cr}(\text{CO})_3(\text{arene})$ complexes, with the enantiomers **A** and **B** corresponding to coordination of the chromium tricarbonyl fragment to either face of the arene (**Scheme 1.3**).¹⁸ The racemates can, in some cases, be resolved by crystallisation of diastereomeric derivatives^{19, 20} and/or be separated by chiral HPLC (these procedures can be problematic on an industrial scale).²¹ Once resolved, highly enantioselective transformations can be achieved since the reactions generally occur from the face opposite the chromium.⁶



Scheme (1.3)

(1.2.2) – Diastereomeric Complexes

The half-sandwich complexes discussed so far have only contained one element of chirality and so are formed as enantiomers (usually as racemates). If there are two or more elements of chirality in the complex then there is the potential to form diastereomers. There are two main types of diastereomeric complexes:

1. chiral metal centre and chiral ligand
2. a chiral ligand and chirality arising from coordination of a prochiral ligand (these will not be discussed further).

The main focus in this section will be on complexes with chirality at both the metal centre and the ligand (**Figure 1.4**), an area of great significance to the study of metal-mediated asymmetric synthesis (see Chapter Four for a detailed discussion). The relationship between A and B (of **Figure 1.4**) is diastereomeric due to the different configuration at the metal centre and identical configuration on the optically pure ligand.

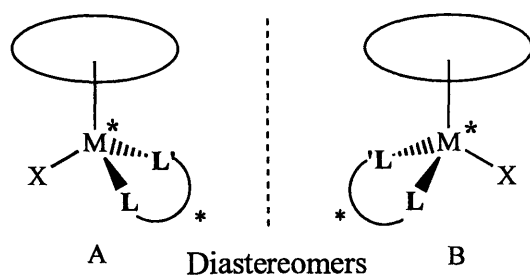
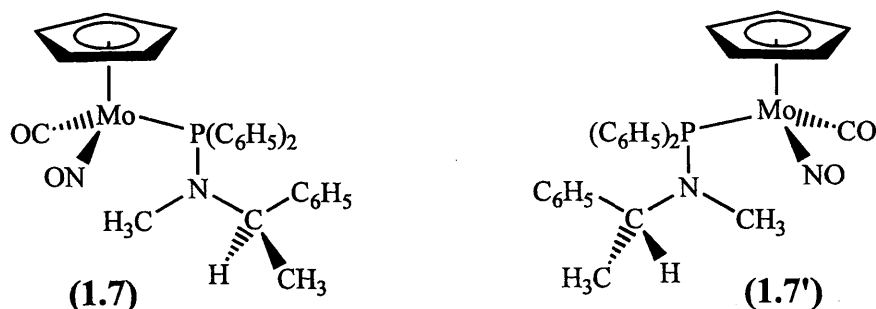


Figure (1.4)

The diastereomeric molybdenum half-sandwich complexes (**1.7/1.7'**) formed from the reaction of (*R*)-Ph₂P-NH(CHMePh) and prochiral [Mo(CO)₂(NO)Cp] are examples of **type 1** diastereomers. They possess opposite configuration at the stereogenic molybdenum with identical configuration, (*R*), on the ligand.²² The two diastereomers (**1.7**) and (**1.7'**), which can be separated by either chromatography or fractional crystallisation, show distinctly different ¹H NMR spectra allowing diastereomer ratios to be measured.



Diastereomers can be formed in different ratios depending upon their stability and the ratio in solution may be different to that in the solid state. So far, the discussion of the types of enantiomeric and diastereomeric complexes has avoided the issue of stability of the configuration of the chiral centres, in particular at the metal, as the configuration at carbon is assumed to be stable. In the following section, the stability of configuration at the metal of half-sandwich complexes, and the methods for studying epimerisation and the mechanism of substitution will be described. These aspects relating to “(arene)Ru” and “Cp*Rh” **type 1** diastereomers will be discussed in more detail and relevance in Section (1.4.3).

(1.3) – Fluxionality, Epimerisation and Mechanism of Substitution

For applications in asymmetric catalysis it is important that the chiral element controlling enantioselectivity is stable under the reaction conditions *i.e.* racemisation should not occur. Clearly therefore, understanding the ease of epimerisation of the relevant chiral elements is important. This section will first look at the methods of observing changing configuration at the metal for both racemates and diastereomers. The mechanism and stereochemistry of substitution at the metal will then be discussed for chiral-at-metal half-sandwich complexes.

Initial work on optically active tetrahedrally coordinated transition metal compounds, such as $[\text{NiFClBrI}]^{2-}$,²³ did not involve attempts to resolve the racemates. Rapid ligand exchange processes would not only quickly interconvert the enantiomers but also result in disproportionation reactions, forming all possible mixed and tetrahalo complexes. In contrast, in general; organometallic compounds are kinetically inert due to the combination of σ -donor and π -acceptor bonds;²³ in principle enabling the syntheses and ligand exchange reactions of these complexes to be controlled and planned. For these reasons half-sandwich complexes are excellent for studying both the fluxionality and the stereochemistry of substitution reactions at the metal.

(1.3.1) – Methods for Studying Epimerisation of Half-sandwich Complexes and Assigning Absolute Stereochemistry

There are several methods of studying the epimerisation within chiral compounds, especially for diastereomers. However, the only methods available for measuring an enantiomer converting into a racemate are polarimetry (optical rotation)

or circular dichroism. Enantiomers usually display an optical rotation ($\alpha_D = \pm x$), whereas, the net optical rotation for a racemate is zero ($\alpha_D = 0$). These methods can also be used to follow diastereomer interconversion ($A \rightarrow B$). The CD spectra for most diastereomeric organometallic complexes which differ only in the configuration at the metal, exhibit curves that are almost mirror images, at least in the visible region.²⁴ NMR spectroscopy cannot usually be used to measure enantiomer interconversion since enantiomers are magnetically equivalent. However, if a molecule possesses prochiral groups on a ligand, epimerisation at the metal may result in them becoming equivalent. If this occurs at a rate comparable to the NMR timescale variable temperature NMR may be used to provide information on the rate and activation energy of the process (see H_A and H_B of **Scheme 1.6**, p11). In contrast, diastereomers are inherently magnetically inequivalent, thus their interconversion can be followed by NMR. The choice of NMR experiment and/or conditions used being dependent on the rate of epimerisation. The timescale over which epimerisation can take place ranges from a number of days at elevated temperature to much faster than the NMR timescale ($k > 10^{-1} \text{ s}^{-1}$). For example, consider a hypothetical sample of two diastereomers, A and B. If epimerisation of A and B is fast on the NMR timescale, time-averaged signals will be observed in the spectrum such that conclusions regarding the number of diastereomers and potential epimerisation cannot be substantiated. Recording the NMR spectrum of this sample at low temperature may slow epimerisation sufficiently to resolve the signals for A and B, thus confirming that A and B were interconverting and enabling the diastereomer ratio to be measured. When following the epimerisation by NMR, if the rate is slow ($\tau_{1/2} \approx 30 \text{ min.}$, $k \approx 10^{-4} \text{ s}^{-1}$), the appearance/disappearance of a species can be followed with time. The reactions can be run over a temperature range of $-80 \text{ }^\circ\text{C}$ to $+80 \text{ }^\circ\text{C}$ to allow adjustment over the total experiment time. When the rate of epimerisation is relatively fast on the chemical timescale ($k > 10^{-3} \text{ s}^{-1}$) but slow on the NMR timescale ($k < 10^{-1} \text{ s}^{-1}$) there is a gap in available NMR experiments to follow the process. This has resulted in the incorrect reporting on the stability of the metal configuration in some arene ruthenium complexes (discussed in more detail in Section 1.4.3). If the rate is just slower than the NMR timescale $k \approx 10^{-1} \text{ s}^{-1}$ magnetisation transfer NMR techniques (1-D or 2-D NOESY) can be used because the diastereomers are interconverting on the same timescale as these NMR experiments. In these, a proton from one isomer is converted into the equivalent proton in the opposite isomer before complete relaxation

T_1 has occurred, resulting in a chemical exchange cross-peak between the two signals in the NOESY spectrum. When the rate of epimerisation increases further, line broadening through to coalescence and then onto averaging of the signals is observed in the 1-D NMR spectrum.

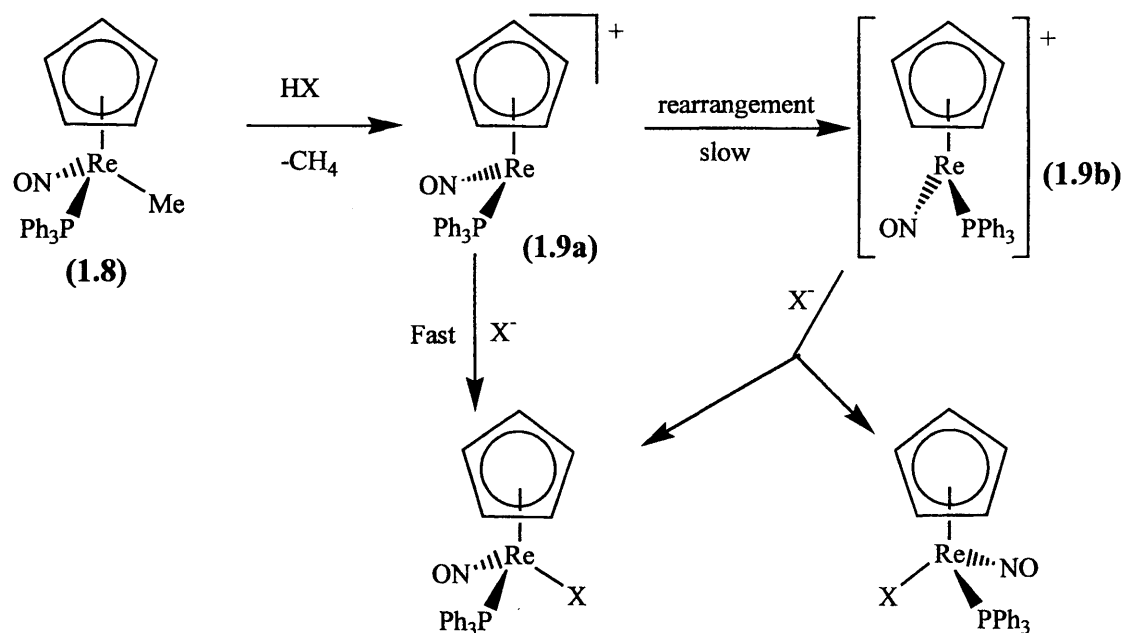
(1.3.2) – Mechanism of Substitution / Fluxionality

In order to determine the stereochemical course of reactions involving substitution at the metal it is necessary to be able to unambiguously assign the absolute stereochemistry at the metal. This can be done by X-ray diffraction, though care needs to be taken to ensure that the isolated crystal is representative of the bulk sample; confirmation that the solid-state structure is retained in solution can often be obtained through nOe experiments. Clearly X-ray diffraction cannot be used “to follow” the epimerisation process, instead circular dichroism can be used to monitor the process. However, problems have arisen when correlations were made between chiroptical properties and the configurations at the metal after one or more ligands had been changed *i.e.* following ligand substitution.²⁵ For example, assignment of absolute configuration at the metal by comparing CD spectra of related ruthenium complexes $[\text{RuCl}(\text{Me})(\text{PPh}_2\text{NHCH}\{\text{Ph}\}\text{Me})(\text{C}_6\text{H}_6)]$ proved impossible.^{26, 27} Note, with diastereomeric complexes it might be possible to assign the configuration at the metal by reference to a known centre on the ligand using nOe experiments.

With enantiomeric complexes that are chiral-at-metal (**type 1**), if substitution at the metal occurs then racemisation may occur depending on the mechanism. The mechanism of substitution of d^6 half-sandwich complexes is believed to be dissociative in nature. Loss of one ligand initially generates a 16-electron pyramidal species. If reaction of the pyramidal species is fast compared with rearrangement to the planar species, then the chirality is retained. If the planar species is formed faster than ligand addition, a racemate is formed (see **Scheme 1.4**).

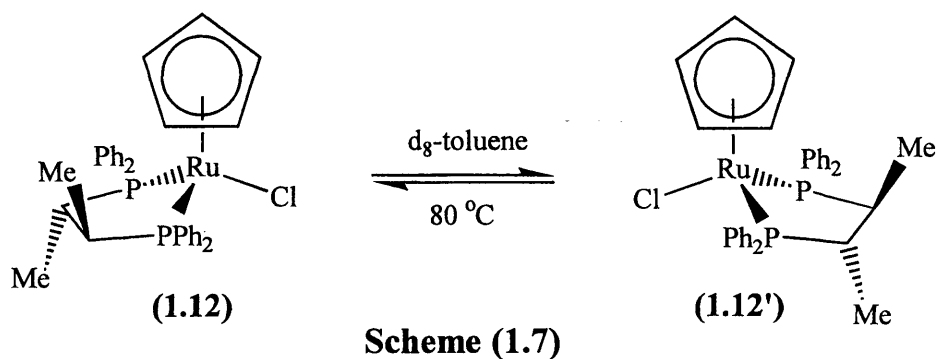
Gładysz *et al.* have extensively studied the half-sandwich rhenium compounds $[\text{Re}(\text{NO})(\text{PPh}_3)\text{LCp}]^{n+}$ ($n = 0,1$), containing a chiral metal centre.²⁸ The complexes are often easily resolved via formation and then separation of their diastereomeric salts, followed by conversion back to the separate enantiomers.²⁹ The enantiopure complexes have been used for numerous reactions and often exhibit excellent stereocontrol. For example, the reaction of $[\text{Re}(\text{CH}_3)(\text{NO})(\text{PPh}_3)\text{Cp}]$ (**1.8**) with electrophiles HX ($X = \text{Cl}$,

Br, I, OTs, OTf), forms complexes $[\text{ReX}(\text{NO})(\text{PPh}_3)\text{Cp}]$ with greater than 99% retention of configuration at Re being observed in most cases.³⁰ These reactions were thought to proceed via the 16-electron chiral pyramidal intermediate (**1.9a**), after elimination of CH_4 from **1.8** (Scheme 1.4).³¹ The high degree of stereoselectivity was attributed to the inversion barrier to the conversion of **1.9a** to the planar species **1.9b** being sufficiently high that the rate of addition of X^- to **1.9a** is much faster than that of rearrangement. Thus, reaction via **1.9b**, which would indisputably result in racemic products, doesn't occur.

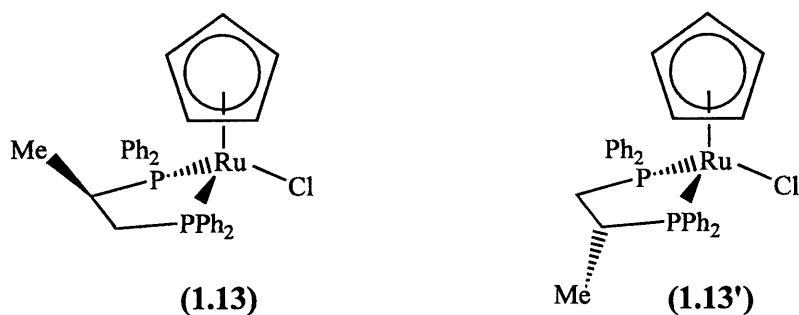


Scheme (1.4)

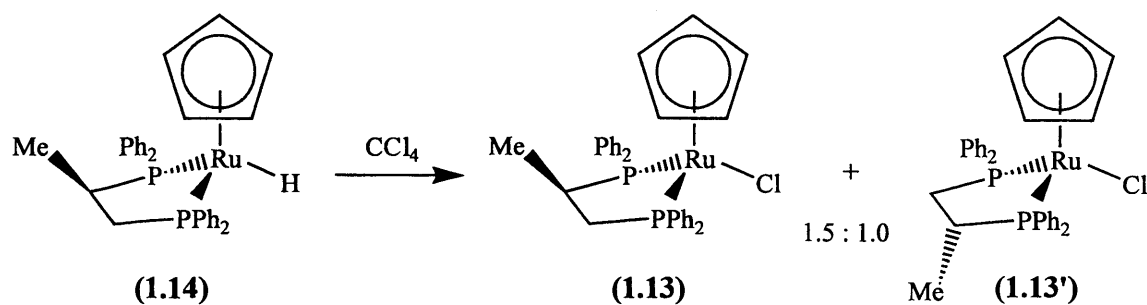
The inversion barriers for interconversion of pyramidal and planar 16-electron half-sandwich intermediates (such as **1.9a/1.9b**) have been calculated by Hoffman *et al.*, who found them to be reasonably low in most cases.³² Pyramidal geometries were found to be especially preferred for systems containing ligands that combined strong π -acceptor and σ -donor properties (such as CS). For these species inversion barriers of 10-15 kcal mol^{-1} were calculated. In contrast, for the rhenium system (**1.9a/1.9b**) the barrier was calculated to be only 0.7 kcal mol^{-1} ; consequently the high stereoselectivity is astonishing. Gladysz has subsequently suggested an associative mechanism (Scheme 1.5) to account for the retention of configuration upon substitution reactions with $[\text{ReL}(\text{NO})(\text{PPh}_3)\text{Cp}]$, in which a 20-electron intermediate (**1.10**) is stabilised by bending



The epimerisation of diastereomeric 18-electron half-sandwich complexes often occurs via a dissociative unimolecular mechanism²⁵ similar to that discussed previously for enantiomeric complexes. However, in contrast to enantiomeric complexes, even if the five-coordinate 16-electron intermediate is pseudo-planar attack by a halide anion from either face is inequivalent, leading to opposite diastereomers. If the rate of epimerisation (between diastereomers) is slow on the chemical timescale then the chiral-at-metal half-sandwich complexes (diastereomeric **type 1**) are ideal substrates for studying the mechanism and stereochemistry of ligand exchange. In fact, the mechanism of substitution, associative or dissociative, and the stereochemical changes at the metal of many cyclopentadienyl and arene ruthenium complexes has been well-studied and the topic has been reviewed.²⁵ The ligand substitution reactions of $[\text{RuCl}\{(R)\text{-Prophos}\}\text{Cp}]$ (**1.13/1.13'**) usually proceed with retention of configuration at ruthenium. For example, treatment of (**1.13**) or (**1.13'**) with the Grignard reagent MeMgBr leads to the corresponding diastereomers of $[\text{RuMe}\{(R)\text{-Prophos}\}\text{Cp}]$ with complete retention of configuration at the metal.³⁶



In contrast, the reaction of either diastereomer of the hydrido complex $[\text{RuH}\{(R)\text{-Prophos}\}\text{Cp}]$ (**1.14/1.14'**) with CCl_4 , which yields the corresponding chloro complex (**1.13/1.13'**) (Scheme 1.8 for conversion of **1.14** into **1.13** and **1.13'**),³⁷ is not stereospecific, diastereomers (**1.13**) and (**1.13'**) form in a molar ratio of 1.5:1.0 independent of which hydride diastereomer is used.



Scheme (1.8)

The configuration at the metal centre in (**1.13/1.13'**) is stable in hydrocarbon solvents. However, in more polar solvents such as chlorobenzene the diastereomers were shown to epimerise.³⁸ Synthesis of (**1.13/1.13'**) from $[\text{RuCl}(\text{PPh}_3)_2\text{Cp}]$ and (*R*)-Prophos in toluene at 80°C resulted in equimolar products.³⁸ However, when the synthesis was carried out at 20°C , rather than at 80°C , the complexes were formed in a diastereomer ratio of 80:20. Heating this sample at 80°C for two hours resulted in an equilibrium ratio of nearly 50:50.³⁵ These findings demonstrate that the configurational stability at the metal for (**1.13/1.13'**) is dependent on both temperature and the choice of solvent. The stereochemical outcome of these substitution reactions depends upon whether the reactions are under kinetic or thermodynamic control and, as such, care needs to be exercised in making conclusions regarding the mechanism of substitution at ruthenium.

As mentioned previously for applications in asymmetric catalysis the chiral element controlling selectivity should be stable under the reaction conditions. Thus, even if a single diastereomer were used as a catalyst, fast epimerisation would mean that both diastereomers would be present in the equilibrium ratio, with one diastereomer selectively favouring one product, whilst the other diastereomer may favour the enantiomeric product thereby reducing the enantiomeric excess of the product. Similarly, if the configuration at the metal is not stable under the reaction conditions, then no conclusions about the stereochemistry of substitution reactions can be gained by mechanistic studies. Thus, the factors affecting the rate and mechanism(s) of

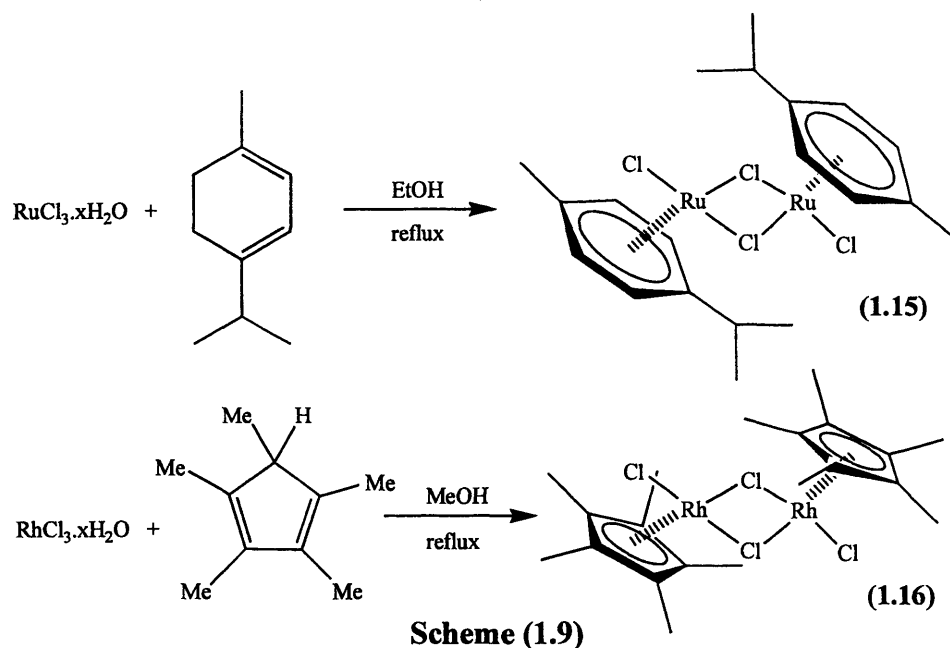
epimerisation are important and will be discussed with relevance to “(arene)Ru” and “(Cp*)Rh” complexes in Section (1.4.3).

(1.4) – Arene-Ru (II) and Cp*-Rh (III) half-sandwich chemistry

This section will discuss the synthesis of arene-Ru (II) and Cp*-Rh (III) half-sandwich complexes, the preparation, and then finally the reactions of, such half-sandwich complexes formed from achiral and chiral ligands. M(ring) will refer to Cp*-Rh or arene-Ru throughout this section.

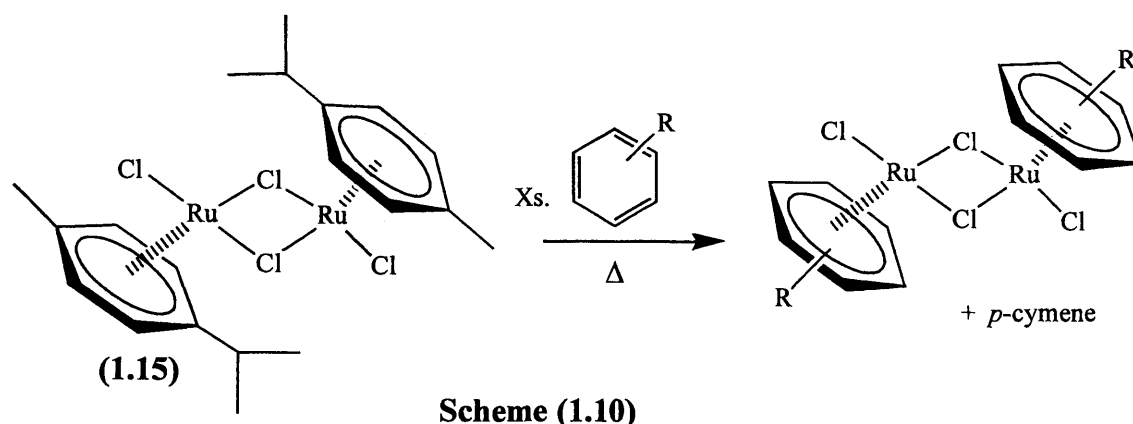
(1.4.1) – Syntheses of Half-sandwich Complexes

The precursors for most arene ruthenium and Cp* rhodium half-sandwich complexes are the chloro-bridged dimers $[\text{RuCl}_2(\text{arene})]_2$ (arene = *p*-cy **1.15**)³⁹ and $[\text{RhCl}_2(\text{Cp}^*)]_2$ (**1.16**),⁴⁰ which are readily synthesised from commercially available $\text{RuCl}_3 \cdot x\text{H}_2\text{O}$ and $\text{RhCl}_3 \cdot x\text{H}_2\text{O}$, respectively (**Scheme 1.9**). In the formation of (**1.15**) the ruthenium is reduced from Ru(III) to Ru(II), which is accompanied by an oxidation of the α -phellandrene mixture to give the arene *p*-cy. In contrast, the rhodium of (**1.16**) remains in the +3 oxidation state. The metal atoms in both these complexes have stable 18-electron configurations and two bridging chloride ligands, X-ray diffraction has shown that the four-membered centre $[\text{M}-\text{Cl}]_2$ has a two-fold axis of symmetry.⁴¹



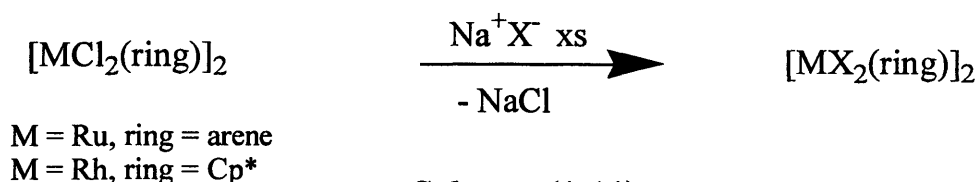
The C_6H_6 derivative of the *p*-cy dimer is synthesised analogously to (**1.15**) by reaction of $\text{RuCl}_3 \cdot x\text{H}_2\text{O}$ with cyclohexadiene. The series of $[\text{RuCl}_2(\text{arene})]_2$ dimers can

be extended by arene exchange reactions of (1.15).⁴² Thus, $[\text{RuCl}_2(\text{C}_6\text{Me}_6)]_2$ can be formed by heating $[\text{RuCl}_2(p\text{-cy})]_2$ in molten hexamethylbenzene,³⁹ whilst other dimers, such as $[\text{RuCl}_2(1,4\text{-Me}_2\text{C}_6\text{H}_4)]_2$, $[\text{RuCl}_2(1,2,3,4\text{-Me}_4\text{C}_6\text{H}_2)]_2$ and $[\text{RuCl}_2(1,2,4,5\text{-Me}_4\text{C}_6\text{H}_2)]_2$, are obtained by heating (1.15) to reflux in neat arene (Scheme 1.10). These arene exchange reactions work best with solid or high-boiling arenes, since high temperatures are required to displace the *p*-cy ligand.⁴² There are no reports of exchange of the Cp* ligand in the rhodium half-sandwich complex (1.16).



(1.4.2) – Reactions of $[\text{RuCl}_2(\text{arene})]_2$ and $[\text{RhCl}_2(\text{Cp}^*)]_2$ with Achiral Ligands

The dimers $[\text{RuCl}_2(p\text{-cy})]_2$ (1.15) and $[\text{RhCl}_2(\text{Cp}^*)]_2$ (1.16) are isoelectronic and undergo many analogous reactions. They both undergo halide exchange reactions with $\text{X} = \text{Br}^-$, I^- and with pseudo halides N_3^- , SCN^- and NCO^- (Scheme 1.11).⁴³⁻⁴⁵



The dimers $[\text{RuCl}_2(\text{arene})]_2$ and $[\text{RhCl}_2(\text{Cp}^*)]_2$ are easily cleaved and undergo a number of similar reactions. Thus, treatment with monodentate ligands L (L = py, PPh₃, DMSO, amines, CO, MeCN) results in half-sandwich complexes $[\text{MCl}_2(\text{L})(\text{ring})]$ (Figure 1.5),⁴⁶⁻⁴⁸ which adopt the well-known ‘piano-stool’ structure. In polar solvents it is possible to add two basic monodentate ligands L to give cations $[\text{MCl}(\text{L})_2(\text{ring})]^+$, or to add ligands L^x and L^y in a step-wise manner to form cations of type $[\text{MCl}(\text{L}^x)(\text{L}^y)(\text{ring})]^+$ (Scheme 1.12).

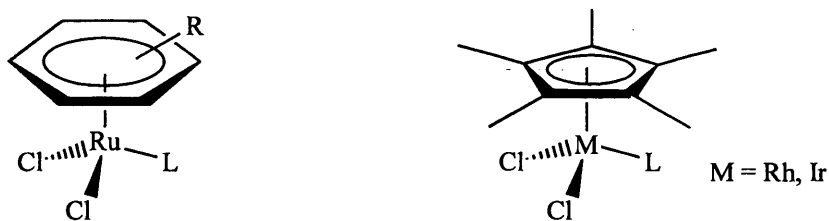
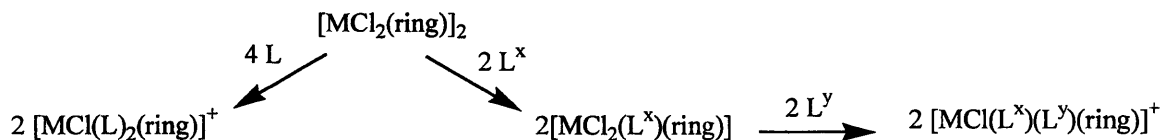
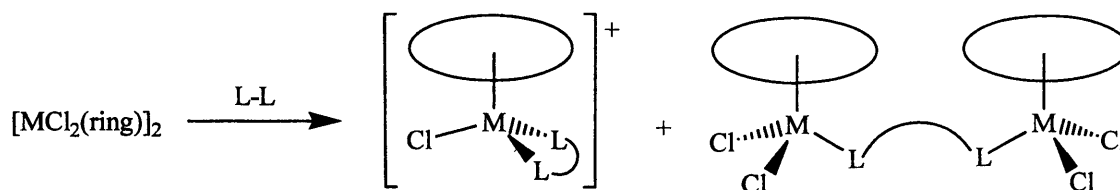


Figure (1.5)



Scheme (1.12)

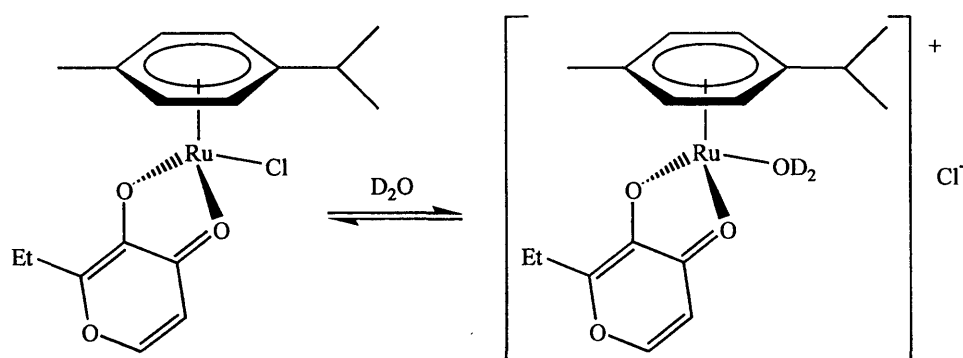
The dimers can also react with bidentate ligands L-L (L-L = bipyridyls, diamines, diphosphines), cleaving the chloride bridges to form two possible types of complex. Usually the ligand will act as a chelate, forming complexes $[\text{MCl}(\text{L-L})(\text{ring})]^+$, but complexes of the type $[\text{M}_2\text{Cl}_4(\mu\text{-L-L})(\text{ring})_2]$ (L-L = diamines, diphosphines) (Scheme 1.13) are also possible.^{39, 49}



Scheme (1.13)

The dimers $[\text{RuCl}_2(\text{arene})]_2$ and $[\text{RhCl}_2(\text{Cp}^*)]_2$ react with acetone or acetonitrile in the presence of a chloride scavenger to form dicationic complexes, $[\text{Ru}(\text{L})_3(\text{arene})]^{2+}$ (L = Me_2CO , arene = C_6Me_6 , mes; L = MeCN, arene = *p*-cy, C_6H_6) and $[\text{Rh}(\text{Me}_2\text{CO})_3(\text{Cp}^*)]^{2+}$.⁵⁰ The weakly coordinated solvent molecules are readily displaced by stronger donor ligands (such as py, DMSO or $\text{P}(\text{OMe})_3$), giving a convenient route to other dicationic complexes.⁵⁰ McCormick *et al.* have extended this synthetic methodology to form monocationic salts $[\text{RuCl}(\text{NCCH}_3)_2(\text{C}_6\text{H}_6)]^+$.⁵¹ These synthetically versatile intermediates will undergo substitution reactions with neutral bidentate ligands, such as 2,2'-bipyridine, to form monocationic complexes of the type $[\text{RuCl}(\text{L-L})(\text{C}_6\text{H}_6)]^+$.⁵¹

With anionic bidentate ligands (*e.g.* the anions of pyranones, pyridinones and 2,4-pentane-dione) neutral complexes $[MCl(L-L)(ring)]$ are formed on reaction with the dimers $[MCl_2(ring)]_2$.^{35, 45, 52} The unsymmetrical pyranone and pyridinone ligands form chiral-at-metal enantiomeric complexes (see Section 1.2.1). Aqueous conductivity and NMR studies with complexes of this type showed that equilibria exist between chloride and water coordinated species (**Scheme 1.14**). The observation of only one set of signals in the NMR spectra recorded in D_2O implies the equilibrium must be rapid on the NMR time-scale. In addition, in d_4 -MeOH the prochiral CH_2 protons (of the Et) are equivalent due to rapid epimerisation at the metal centre.³⁴ This process was only slowed to beneath the NMR time-scale below $-20^\circ C$ for ruthenium complexes, whereas with rhodium only one set of signals was observed, even at $-60^\circ C$. The lability at the metal was attributed to the strong electron donating nature of the pyridinone ligands (O-O).⁵³



Scheme (1.14)

The dimers $[RuCl_2(arene)]_2$ and $[RhCl_2(Cp^*)]_2$ are useful precursors for access to reactive hydrido,⁵⁴ alkyl,⁵⁵ acetylide⁵⁶ and vinylidene⁵⁷ organometallic complexes. The hydrido complexes are key compounds for the formation of intermediates capable of C-H bond activation resulting in new hydrido and cyclometallated arene-ruthenium or Cp^* -rhodium derivatives. The preparation of ruthenium alkyl complexes $[RuX(Y)(L)(arene)]$ ($X = Cl$, $Y = Me$; $X = Y = Me$; $L = PR_3$; arene = C_6H_6 , *p*-cy), albeit in low yields, has been reported.⁵⁸ More recently, Werner *et al.* have shown that the C_6Me_6 analogues are formed in higher yields and the cationic monomethyl complex $[RuMe(PPh_3)_2(C_6Me_6)]PF_6$ can be prepared by treatment of $[RuCl(PPh_3)_2(C_6Me_6)]PF_6$ with methyllithium.^{59, 60} Vinylidene complex $[Ru(=C=CHMe)\{Ph_2PC(Me)-CHPh_2\}(mes)]PF_6$ can be readily accessed via reaction of $[RuCl\{Ph_2PC(Me)-CPh_2\}(mes)]PF_6$ with methylethyne ($MeC\equiv CH$) and NH_4PF_6 .⁶⁰ Whereas, the alkyne

complexes $[\text{Ru}(\text{C}\equiv\text{CR})(\text{alanine})(p\text{-cy})]/[\text{Rh}(\text{C}\equiv\text{CR})(\text{alanine})\text{Cp}^*]$ ($\text{R} = \text{Ph}, \text{CMe}_3, \text{CO}_2\text{Me}$) were prepared by reacting the relevant chloride precursor with the required terminal alkyne in basic (KOH or NEt_3) solution.⁵⁶

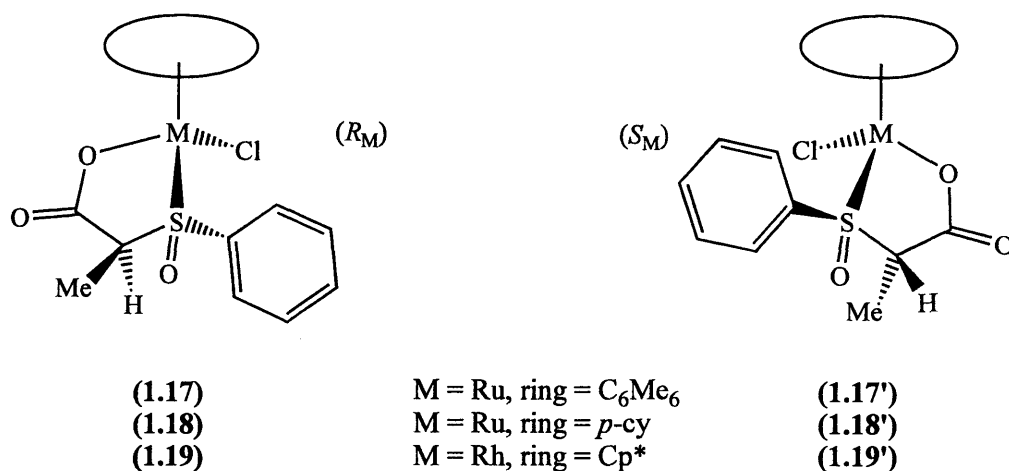
(1.4.3) – Reactions with Chiral Ligands

In the previous section, the synthesis of “(arene)Ru(II)” and “(Cp*)Rh(III)” complexes with achiral ligands was discussed. The chemistry of such complexes with chiral bidentate ligands is summarised below. The complexes will be discussed according to ligand classification (related donor atoms) in three major groups; oxygen-containing, phosphorus-containing and finally nitrogen-containing. The main focus will be to highlight the factors that control the diastereoselectivity of complex formation, the configurational stability at the metal centre and the stereochemistry of substitution reactions for the various diastereomeric half-sandwich complexes. Such information is vital to an understanding of the enantioselectivity of half-sandwich catalysts.

O-Containing Ligands

The first category encompasses *O-O* and *S-O* donor ligands, *N-O* and *P-O* donors will be dealt with in the *P-* and *N-*containing ligand sections, respectively. To our knowledge no arene ruthenium or Cp* rhodium complexes with chiral bidentate *O-O* donor ligands have been reported. As mentioned previously (Section 1.4.2), the reactions of $[\text{RuCl}_2(\text{arene})]_2$ and $[\text{RhCl}_2(\text{Cp}^*)]_2$ with achiral pyranones and pyridinones, in the presence of base, generate chiral-at-metal enantiomeric complexes. Epimerisation was shown to be fast on the NMR time-scale, even at low temperatures.^{45, 52, 53} Arene Ru and Cp*Rh complexes of sulfoxide-carboxylate (*S-O*⁻) ligands were examined by Parr *et al.* for use as asymmetric hetero Diels-Alder catalysts.⁶¹ They reasoned that the combination of a soft S(IV) donor with the hard carboxylate oxygen might show interesting reactivity. The complexes $[\text{MCl}(\text{S-O}^{\ominus})(\text{ring})]$ { $\text{M} = \text{Ru}$, ring = C_6Me_6 (**1.17**), *p-cy* (**1.18**); $\text{M} = \text{Rh}$, ring = Cp* (**1.19**)} are diastereomeric; the ligand has two chiral centres and a third is generated at the metal on complexation. Complexes **1.17–1.19** with fixed (*S_S*) configuration were formed with high diastereoselectivity (at least 90% *d.e.*) and crystallised as single diastereomers with configuration (*R_M*), as shown by X-ray diffraction studies. The principle steric effect that is believed to result in preferential

formation of the (R_M) isomer is that the phenyl substituent on sulphur is orientated away from the polyhapto ring, thus minimising unfavourable steric interactions (see 1.17-1.19), whereas in the (S_M) isomer the phenyl would reside in close proximity to the ring, which would be sterically disfavoured. The carbon configuration is epimerised during complexation, however the stereoselectivity of reprotonation at C(2) is believed to be directed by the metal, to give the (S_C) isomer.



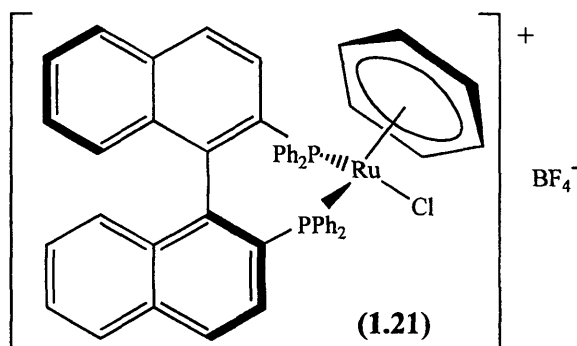
In summary, there are very few complexes of type $[MCl(L-O)(ring)]$ (L-O = bis-oxygen or sulphur-oxygen donor ligands), particularly with chiral ligands. The sulfoxide-carboxylate (S-O) ligands form diastereomeric complexes with excellent stereoselectivity, but to date, the configurational stability and stereochemistry of substitution at the metal for these complexes has not been reported.

P-Containing Ligands

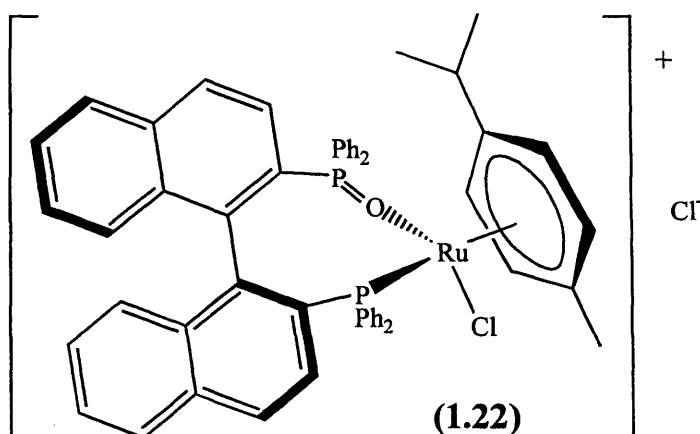
In addition to the mechanistic studies carried out by Consiglio and Morandini with $[RuCl\{(R)\text{-Prophos}\}Cp]$ (1.13/1.13') (see Section 1.3.2),^{25, 37} Carmona *et al.* have studied the analogous complex $[RhCl\{(R)\text{-Prophos}\}Cp^*]PF_6$ (1.20/1.20') which formed with a diastereomer ratio of 77:23 from the reaction of $[RhCl_2Cp^*]_2$ with (*R*)-Prophos.⁶² The configuration at rhodium was found to be stable at room temperature regardless of solvent polarity; epimerisation was not observed in chloroform or d_4 -MeOH, even after 30 days. However, epimerisation did occur in refluxing d_4 -MeOH, after 7 days a 96:4 ratio of diastereomers was obtained; whilst, heating to reflux in chloroform did not result in loss of configurational stability. Addition of excess chloride ions accelerated the rate of epimerisation, which lead the authors to conclude that an associative mechanism was involved.⁶² Although, studies by the research groups of Merbach,^{63, 64}

Consiglio²⁵ and Kurosawa²⁴ have all shown that substitution at the metal, for related half-sandwich complexes, is a dissociative process.

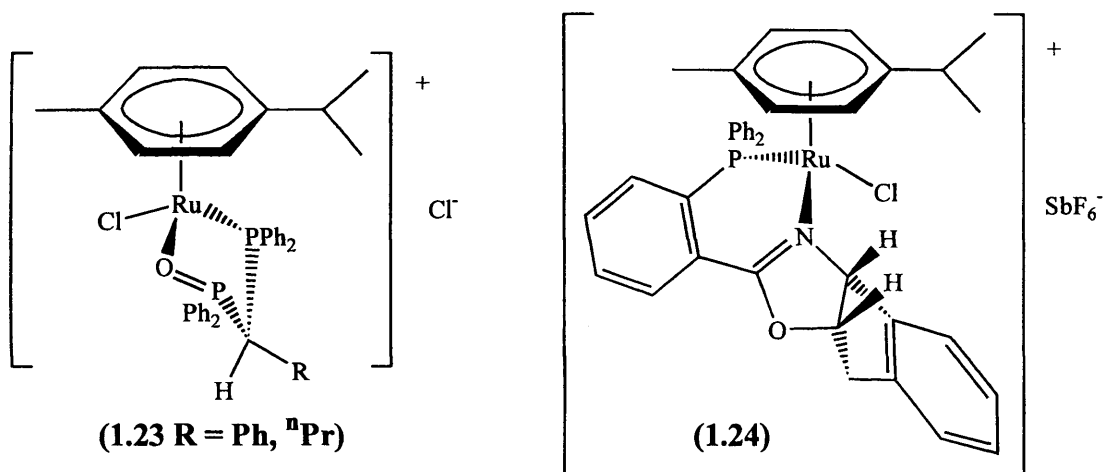
The bis-phosphine complex $[\text{RuCl}(\text{BINAP})(p\text{-cy})]\text{BF}_4$ (**1.21**), which has been used as a precatalyst for asymmetric hydrogenation reactions of substituted alkenes and ketones,⁶⁵ does not undergo pseudoepimerisation in CDCl_3 , as shown by two signals in the ^{31}P NMR spectrum. However, it should be noted that under the catalytic conditions (30-40°C) the arene ring is likely to dissociate from the complex such that the catalytically active species no longer has a half-sandwich structure.



Chelating bisphosphine monoxide (BPMP) ligands that contain (P-O) mixed donor atoms have been used by Bader *et al.*⁶⁶ BPMP ligands have the potential to be “hemilabile” as well as generating electronic asymmetry at the metal, similar to that with sulfoxide-carboxylate (S-O⁻) ligands. (*S*)-BINAP monoxide {(*S*)-BINPO}, prepared by highly selective palladium catalysed monooxidation of (*S*)-BINAP,⁶⁷ was treated with $[\text{RuCl}_2(p\text{-cy})]_2$ forming a single diastereomer product (**1.22**), shown by X-ray diffraction studies to have an (R_{Ru}) configuration.⁶⁸ The high diastereoselectivity was attributed to the large dihedral angle (83.6°) between the naphthyl groups forcing the PPh_2 fragment to adopt a configuration which sterically controls the preference for direction of chelation.⁶⁸



In contrast, reactions of the structurally related ligands $\text{Ph}_2\text{PCH(R)P(O)Ph}_2$ ($\text{R} = \text{Me}, \text{Ph}$ or ^nPr) with $[\text{RuCl}_2(p\text{-cy})]_2$ resulted in either η^1 -, ($\text{R} = \text{Me}$) or η^2 -, ($\text{R} = \text{Ph}, ^n\text{Pr}$) complexes (**1.23**), as observed by ^{31}P NMR spectroscopy.⁶⁹ Thus, increased steric bulk on the ligand backbone ($\text{R} = \text{Ph}$ and ^nPr) results in the formation of solely η^2 -complexes, in an approximate analogy with the Thorpe-Ingold effect.^{70, 71} Furthermore high diastereoselectivity is also achieved (**1.23**, $\text{R} = \text{Ph}, ^n\text{Pr}$). X-ray diffraction studies showed that the R substituent is orientated away from the chloride in each case, presumably to reduce unfavourable steric interactions. Once formed, (**1.23**, $\text{R} = \text{Ph}$ and ^nPr) were found to be configurationally stable at the metal, which is consistent with the related BINAP- (**1.21**) and BINPO-containing complexes (**1.22**).



Carmona *et al.* reported the preparation of $[\text{RuCl}(\text{P-N})(p\text{-cy})]\text{SbF}_6$ (**1.24/1.24'**) { $\text{P-N} = (1S, 2R)$ -phosphinoxazoline}, as a 70:30 mixture of diastereomers from the reaction of $[\text{RuCl}_2(p\text{-cy})]_2$ with the P-N mixed donor ligand.⁷² The two diastereomers were separated by crystallisation and the configuration of the major isomer (**1.24**) determined as (*S*) at ruthenium by both X-ray diffraction studies and solution nOe difference experiments.

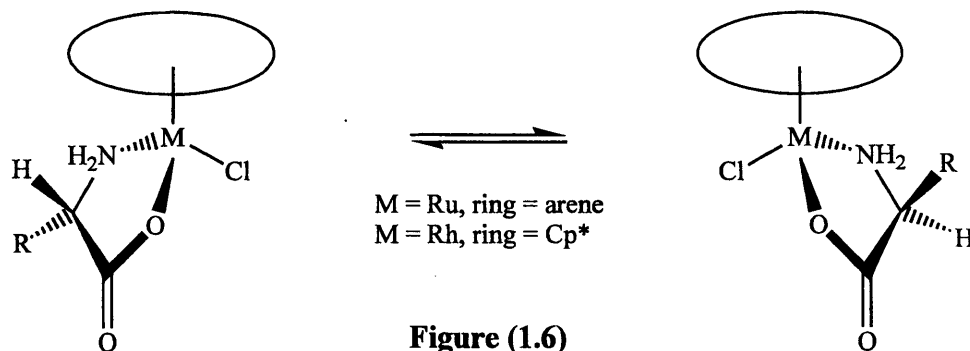
In summary, for complexes of type $[\text{MCl}(\text{P-L})(\text{ring})]^{n+}$ ($\text{P-L} =$ unsymmetrical chiral phosphorus-containing ligand) there is a large variation in diastereoselectivity, although once formed the metal configuration is reasonably stable. However, no studies on the effect of changing the arene have been reported and in some cases it is not easy to vary substituents on the ligands for a systematic study. In many cases, substitution of chloride has been shown to occur with stereospecific retention of configuration at the metal.^{25, 37}

N-Containing Ligands

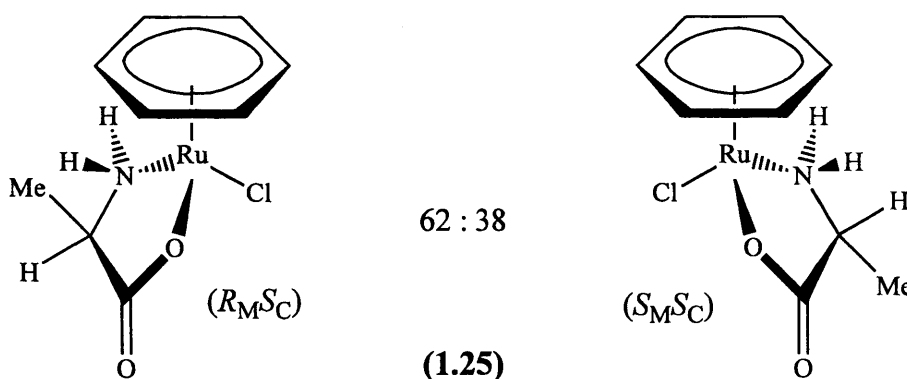
As described above, many detailed mechanistic studies on the reactions of diastereomeric half-sandwich complexes have employed chiral phosphine ligands. There has recently been substantial interest in half-sandwich complexes that incorporate N-containing chiral ligands,⁷³⁻⁷⁵ and these will be discussed in this section. Furthermore, such ligands are often more readily available and/or synthesised than many phosphine ligands, making their complexes potentially very useful in asymmetric synthesis (see Chapter Four).

One of the most widely available and inexpensive sources of chiral ligands is from amino acids ($\text{H}_2\text{NCH(R)CO}_2\text{H}$). These species can bind through both the amine and carboxylate group, depending on pH, to a wide variety of metals. With the exception of achiral glycine ($\text{R} = \text{H}$) all 20 naturally-occurring amino acids have (*S*)-configuration, presenting the potential for many enantiopure complexes with a wide variety of side-chains R.

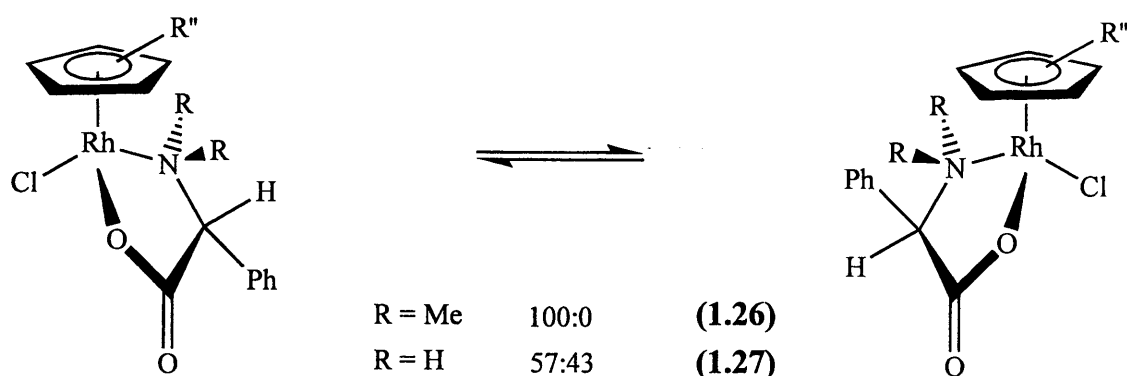
Research on (arene)Ru amino acidate complexes was initially carried out by Dersnah and Baird.⁷³ Subsequently, Beck⁷⁶ and Sheldrick⁷⁷ extended this work to Cp^*Rh . Complexes $[\text{MCl}(\text{aa})(\text{ring})]$ (aa = amino-acidate) (**Figure 1.6**) were synthesised by treatment of the relevant dimer $[\text{MCl}_2(\text{ring})]$ with two equivalents of amino acid in the presence of NaOMe as base.⁷⁶ In general, amino acidate complexes are formed with low diastereoselectivity, typically as 50:50 mixtures (with the exception of aa = proline).⁷⁶ The most likely reason for the low diastereoselectivity, inferred from X-ray crystal structures, is that neither orientation of the R group is particularly sterically hindered, so there is little steric or energetic difference between the two diastereomers (see **Figure 1.6**). This hypothesis is supported by pairs of diastereomers co-crystallising, typically as 50:50 mixtures, as evidenced by X-ray structure determinations.^{78, 79}



The X-ray crystal structure of amino-acidate complex **(1.25)**⁷⁷ contained two diastereomers, and one diastereomer showed the presence of intramolecular H-bonding (N-H \cdots Cl), which was proposed to stabilise this isomer resulting in a diastereomer ratio of 62:38. However, Davies *et al.*⁷⁸ found that similar selectivity was obtained for the related complex (arene = mesitylene) and no intramolecular H-bonding interactions were found in the solid-state molecular structure. Thus, H-bonding interactions are probably not responsible for the diastereoselectivity in the amino acidate complexes. However, the transfer hydrogenation catalyst [RuCl(*p*-TsDPEN)(*p*-cy)], reported by Noyori *et al.*,⁸⁰ was formed completely diastereoselectively and X-ray analysis of this single isomer⁸¹ showed the presence of a short Cl \cdots HN distance of 2.57 Å (expected Van der Waals separation, 3.0 Å). It was surmised that this hydrogen bond was important to the observed selectivity.



The presence of a tertiary nitrogen (-NMe₂) in amino-acidate complexes has been shown to result in very high diastereoselectivity regardless of the metal / R-substituent combination.⁸² This is due to the additional steric bulk at the metal centre when the NMe₂ fragment is present compared to NH₂. With the primary amine terminus it is possible for the puckered chelate ring to adopt two limiting conformations and to flux between the two ring conformations. However, in the case of the tertiary amine terminus, only one ring conformation is observed in which both N-Me bonds are gauche with respect to M-ring and M-Cl bonds.⁸² Conversion to the other conformer does not occur since this would require a pseudo equatorial methyl to pass through an eclipsed conformation with the M-ring bond, which is energetically unfavourable. This conformational selectivity leads to high diastereoselectivity as demonstrated by the ratios for the dimethyl substituted complex [RhCl(NMe₂-aa)(Cp*)] **(1.26)**, 100:0,⁸² compared to unsubstituted [RhCl(aa)(Cp*)] **(1.27)**, 57:43.⁷⁶



Diastereoselectivity is also high in proline complexes, formed in the ratio 95:5 for $[\text{RhCl}(\text{pro})(\text{Cp}^*)]$ (1.28/1.28') and 90:10 for $[\text{RuCl}(\text{pro})(p\text{-cy})]$ (1.29/1.29'), as a result of the secondary nitrogen atom, which becomes an additional chiral centre on coordination (Figure 1.7).⁷⁶ The proline ring is tethered, which helps to fix the position of the ring in space so it cannot orientate (away from bulky groups) into a conformation with lower energy. This has the effect of increasing the relative thermodynamic stability of the isomer with the proline pointing away from the polyhaptic ring, such that it is formed in preference to the other diastereomer.

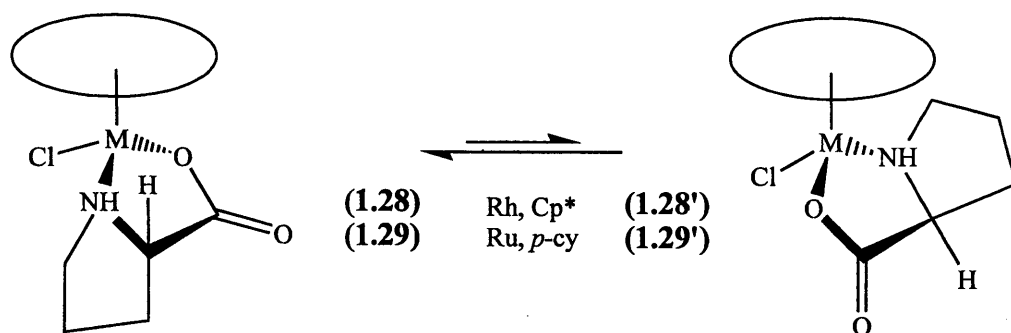


Figure (1.7)

The diastereomer ratios of crystallised amino-acidate complexes can be confirmed by the use of ^1H NMR spectroscopy; the ratios are frequently different in solution and the solid-state. Epimerisation in solution is slow, at least on the NMR time-scale, for complexes $[\text{MCl}(\text{aa})(\text{ring})]$, especially in non-polar solvents such as CDCl_3 .⁷⁴⁷⁸ Diastereomer mixtures do not change their composition after several days in solution, indicating that either the equilibrium is established quickly or the configuration at the metal centre is stable. In D_2O , partial substitution of D_2O for Cl^- occurs in complexes of type $[\text{RuCl}(\text{L}^1)(\text{arene})]$, resulting in equilibria (as shown in Figure 1.8) between two diastereomers with chloride bound and two with D_2O , as observed by ^1H NMR.^{73, 76} At

room temperature the four sets of signals are sharp, indicating slow epimerisation on the NMR timescale. At higher temperatures (50°C), broadening of the resonances attributed to the aqua complex was observed, thus the rate of epimerisation of the D₂O coordinated isomers is comparable with the NMR timescale at 50°C.

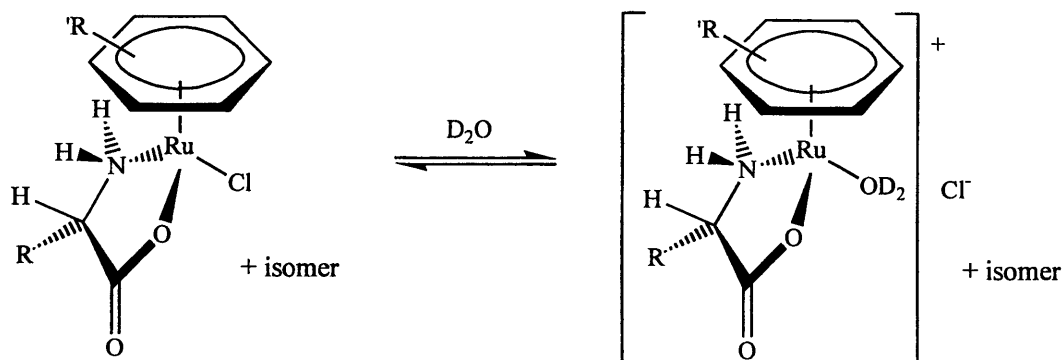


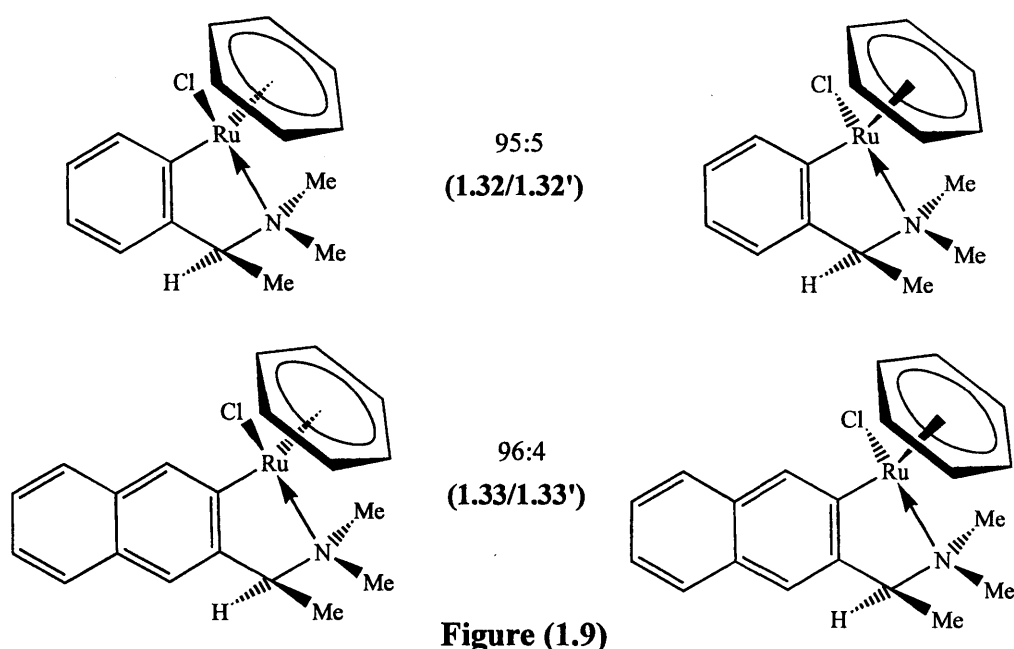
Figure (1.8)

Rapid epimerisation was also found for the solvent-complexes formed after chloride abstraction from methanolic solutions of [RhCl(aa)Cp*] by AgBF₄.⁸³ The room temperature ¹H NMR spectra in d₄-MeOH contained a single set of signals, on cooling the sample to -90°C the resonances did broaden. The authors suggested that this observation was due to the rate of epimerisation being comparable to the NMR timescale at -90°C, however, more recently Carmona *et al.* have postulated that trimeric species may be present.⁸⁴

The size of the monodentate ligand can substantially affect the diastereoselectivity. Thus, the diastereomer ratios of complexes [RhCl(L)Cp*] are 50:50 for L = alanine and 95:5 for L = proline (**1.28/1.28'**), whereas reaction with PPh₃ generates [Rh(PPh₃)(L)Cp*]⁺ 95:5 for L = alanine (**1.30/1.30'**) and 62:38 for L = proline (**1.31/1.31'**).⁸³ Thus, the relative diastereoselectivity has reversed on substitution with PPh₃, the alanine complexes now showing much higher selectivity. The reversal in diastereoselectivity could be due to PPh₃ exerting an increased steric influence relative to Cl, such that the isomer where the R-substituent is orientated away from the PPh₃ might be thermodynamically favoured.

To summarise, simple amino-acidate complexes are formed in low diastereoselectivity (as 50:50 mixtures) and often co-crystallise. In D₂O or d₄-MeOH, mixtures of epimerising chloride and solvent-coordinated diastereomers are present thus, highlighting that the energy barrier to epimerisation is moderately low, hindering isolation of single diastereomers.

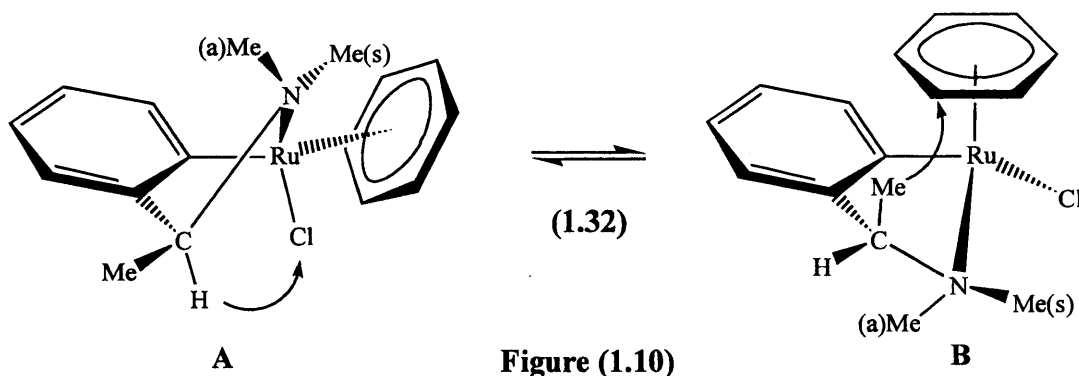
The research groups of Nelson,⁸⁵⁻⁸⁸ Pfeffer⁸⁹ and Brunner⁹⁰ have synthesised and investigated the chemistry of cyclometallated amine complexes $[\text{RuCl}(\text{L})(\text{arene})]$ {where L = the anion of H-TMBA or H-TMNA; arene = C_6H_6 , $\text{C}_6\text{H}_5\text{CH}_3$, *p*-cy}. The diastereomeric complexes (1.32/1.32') and (1.33/1.33') (Figure 1.9) were prepared in moderate chemical yield by the reaction between $[\text{RuCl}_2(\text{C}_6\text{H}_6)]_2$ and the transmetallating reagent $\text{HgCl}[(S)\text{-C}_6\text{H}_4\text{CH}(\text{Me})\text{NMe}_2]$ ⁸⁶ or $\text{HgCl}[(S)\text{-C}_{10}\text{H}_6\text{CH}(\text{Me})\text{NMe}_2]$,⁸⁷ respectively. Complexes (1.32/1.32') and (1.33/1.33') are obtained in almost identical diastereomer ratios (see Figure 1.9) but, despite initial reports to the contrary,^{86, 87} do not have configurationally stable metal centres.⁹⁰



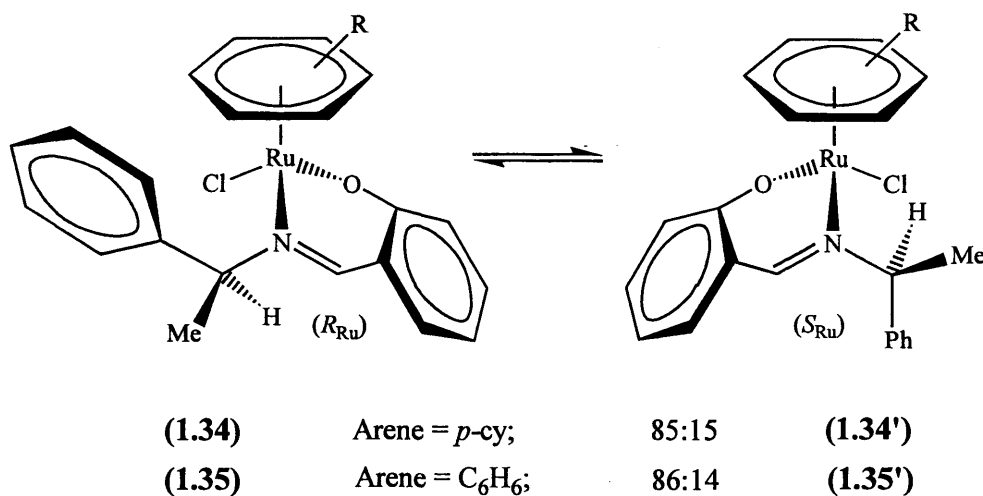
The ^1H NMR spectra of (1.32/1.32') obtained in CDCl_3 , d_6 -acetone and CD_3NO_2 are independent of time (days) and temperature (-20 to 50°C), leading the authors to conclude that the complex was configurationally stable. However, Brunner *et al.* recently showed this was not the case; the ^1H NMR spectrum of crystals dissolved and recorded at -80°C in CD_2Cl_2 showed only (1.32). Measuring the spectrum at -50 , 0 and $+20^\circ\text{C}$ revealed that (1.32') is only formed at higher temperatures, proving that (1.32/1.32') epimerise and the observed diastereomer ratio (95:5) is the thermodynamic equilibrium ratio.⁹⁰ The misinterpretation of the configurational stability signifies that previous conclusions regarding the stereochemistry of substitution at the metal in such complexes are unmerited.⁸⁵⁻⁸⁸ Thus, the diastereoselectivities of their substitution compounds only reflect the different stabilities of the diastereomers in the respective

diastereomer equilibria (*i.e.* the reactions are under thermodynamic control, not kinetic control). These problems arose because the rate of epimerisation was relatively fast on the chemical timescale ($k > 10^{-3} \text{ s}^{-1}$) but slow on the NMR timescale ($k < 10^{-1} \text{ s}^{-1}$), as described in Section (1.3.2).

Interestingly, the two types of ruthenacycle (with TMBA or TMNA) show different levels of conformational selectivity. In the TMBA complexes, the five-membered chelate ring interconverts in solution between two limiting conformations wherein the C-Me bond is either pseudoequatorial or pseudoaxial (**Figure 1.10**); X-ray diffraction showed conformer A was preferred in the solid-state due to loss of the unfavourable 1,3-diaxial η^6 -arene \cdots Me interaction. In the TMNA complexes, the five-membered chelate ring is rigid with the C-Me bond in the pseudoequatorial position. This is most probably due to the naphthyl ring being bigger than phenyl, thus more solvent would be displaced by the motion required to interconvert the conformers in the naphthyl diastereomers.



In addition to chiral amine-containing ligands, half-sandwich complexes of chiral Schiff-base (imine-containing) ligands have received much study. The ligands are readily synthesised by condensation of a carbonyl group and a chiral amine. Complexes $[\text{RuCl}(\text{salaldimine})(\text{arene})]$ {salaldimine = the anion of (*S*)-*N*-(1-phenylethyl)-salicylaldimine} and numerous derivatives have been prepared by the groups of Brunner,^{91, 92} and Mandal and Chakravarty.^{93, 94} The diastereomeric complexes (1.34/1.34') and (1.35/1.35') were formed by reaction of $[\text{RuCl}_2(\text{arene})]_2$ with NaL.



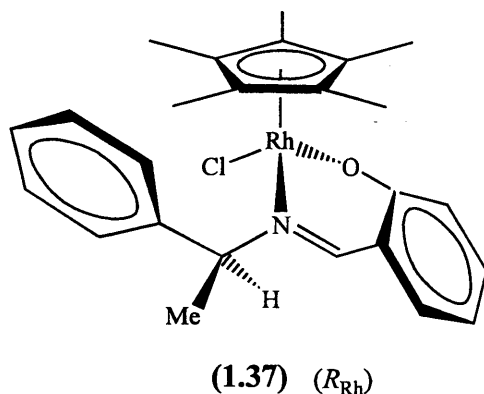
Complexes **(1.34/1.34')** and **(1.35/1.35')** are obtained in very similar diastereomer ratios (86:14 and 85:15, respectively). Crystallisation of the crude reaction mixture **(1.34/1.34')** gave only isomer **(1.34)**, shown by X-ray diffraction studies to have (R_{Ru}, S_C) configuration.⁹¹ A selection of crystals were examined and found to have the same unit cell and crystal morphology, implying an absence of **(1.34')**. However, dissolution and recording the ¹H NMR spectrum of these crystals at -80°C in CD₂Cl₂ gave an isomer ratio 86:14 (identical to that observed at room temperature), indicating that epimerisation at ruthenium was fast on the chemical timescale, even at -80°C. Similar rapid equilibration was observed for **(1.35/1.35')**,⁹¹ which was erroneously reported to be configurationally stable in solution, even at 70°C.⁹³ The problem arose because the equilibrium position was reached quickly, in the short period of time between making up the sample and running it, as described previously for cyclometallated amine complexes.^{93, 94}

Complexes **(1.34/1.34')** and **(1.35/1.35')** are formed with high diastereoselectivity, the R_{Ru} **(1.34/1.35)** isomer being thermodynamically favoured. There are several important steric and electronic interactions which result in the (R_{Ru}) isomer being favoured, which also apply in other complexes containing a Schiff-base ligand derived from (*S*)-*N*-(1-phenylethyl)-amine. X-ray structures indicate that there is an attractive interaction caused by the edge-to-face orientation of the phenyl ring to the η^6 -arene. This interaction is known as the 'β-phenyl-effect' and is believed to be retained in solution as demonstrated by 'high-field' shifts of the ¹H NMR signals of the arene ligand (due to the magnetic anisotropy of the phenyl substituent). Thus, in the major isomer the phenyl is orientated towards the arene with the hydrogen substituent on the chiral carbon orientated towards the chloride ligand. To retain a 'β-phenyl-effect'

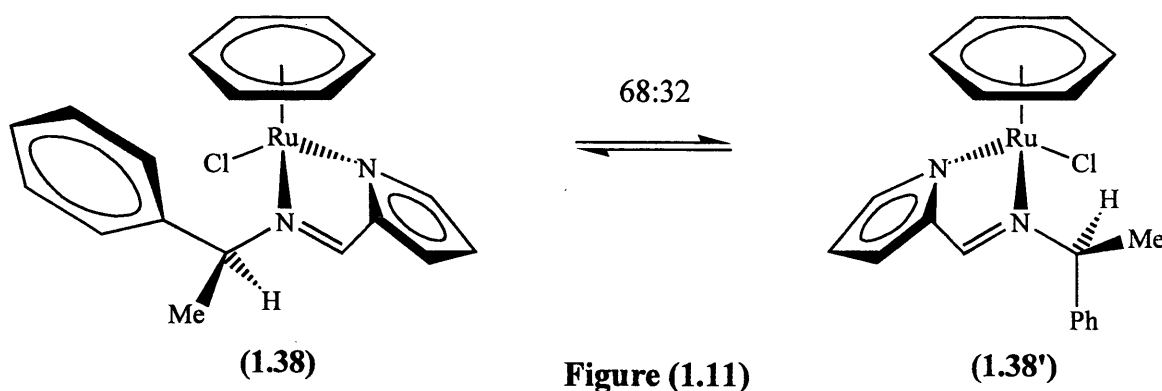
in the minor isomer requires the methyl substituent on the chiral carbon to be orientated towards the chloride, which would be sterically disfavoured. This unfavourable interaction in the minor isomer outweighs any stabilisation that might have been gained from the attractive 'β-phenyl-effect'; thus in the minor isomer, the phenyl is oriented away from the arene.

The chloride complexes **(1.34)** and **(1.35)** react with Ag^+ followed by monodentate ligands L ($L = \text{PPh}_3, 2\text{-Me-py}, 4\text{-Me-py}$) to form $[\text{RuL}(\text{salaldimine})(\text{arene})]^+$.⁹¹ Many of these derivatives have been shown to undergo epimerisation at the metal centre as found for **(1.34/1.35)**. For example, $[\text{Ru}(4\text{-Me-py})(\text{salaldimine})(p\text{-cy})]\text{PF}_6$ (**1.36/1.36'**) exists as a 74:24 mixture of diastereomers at RT in d_6 -acetone, as shown by ^1H NMR. Crystallisation of the crude reaction mixture gave a single isomer product in 90% yield. This indicates that substantial epimerisation at ruthenium must have occurred during crystallisation (referred to as an asymmetric transformation of the second kind).⁹¹ The ^1H NMR spectrum of crystallised **(1.36)**, both dissolved and recorded at -80°C , confirmed that only one diastereomer was present and the rate of epimerisation was slow on the chemical timescale at -80°C , in contrast to **(1.34)**. Warming the sample to room temperature and recording the spectrum gave an identical 76:24 diastereomer ratio confirming that the system is at the thermodynamic equilibrium. The authors concluded that the ruthenium configuration was unstable under the reaction conditions, which meant the stereochemistry of substitution (whether the complex was formed with retention or inversion of configuration) could not be determined.⁹²

Recently, Parr *et al.* reported that the rhodium analogue of **(1.34/1.35)**, *i.e.* $[\text{RhCl}(\text{salaldimine})\text{Cp}^*]$ (**1.37**), was formed as a single diastereomer, shown by X-ray diffraction studies to be the (R_{Rh}) isomer.⁹⁵ Evidence of the (S_{Rh}) diastereomer was not found in the room temperature ^1H NMR spectra of either the crude or crystallised samples. However, since the reported NMR data were obtained at room temperature (and at only 100 MHz) it is possible that the spectra were time-averaged, due to rapid epimerisation in solution. The process would be expected to be faster for rhodium (**1.37**) than for the corresponding ruthenium complexes **(1.34/1.35)**,⁹¹ for which epimerisation was rapid on a chemical timescale even at -80°C .



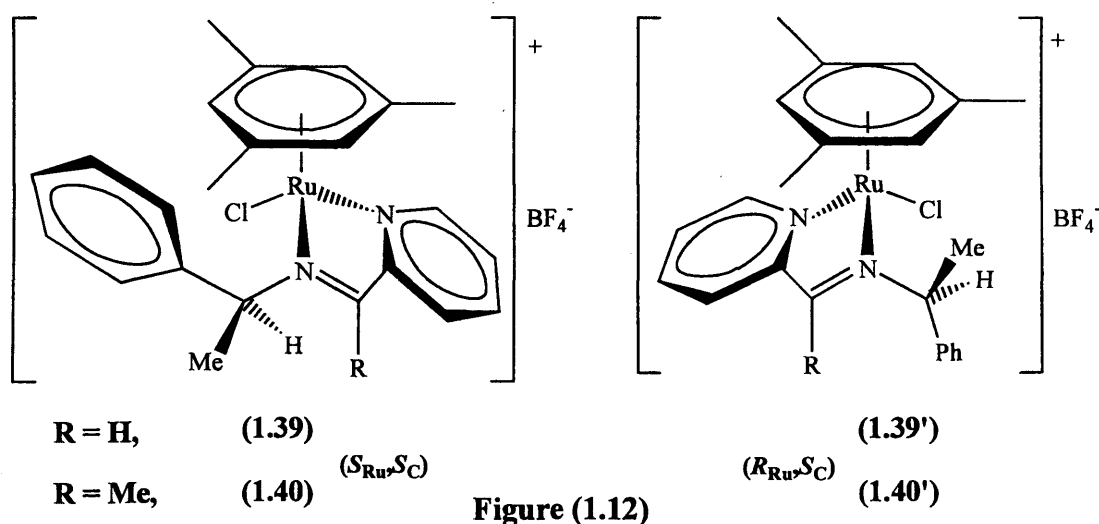
Having determined that complexes (1.34–1.36) of anionic Schiff-base *N,O*-donor ligand salaldimine,^{91, 92} have a low energy barrier to interconversion, Brunner *et al.* investigated the stability and diastereoselectivity of the analogous compounds with anionic *N,N*-donor Schiff-base ligand pyrrolealdimine. The complex [RuCl(pyrrolealdimine)(C₆H₆)] (1.38) {pyrrolealdimine = the anion of (*S*)-*N*-(1-phenylethyl)-pyrrolecarbalimine} was formed by reacting [RuCl₂(C₆H₆)₂] with two equivalents of NaL (Figure 1.11).⁹⁶



The room temperature ¹H NMR spectrum of the crude reaction mixture (1.38/1.38') contained signals for two diastereomers in a ratio of 68:32. This ratio did not change over time, indicating the sample may have reached the equilibrium position. Crystallisation from this mixture gave only (1.38), as shown by X-ray diffraction and ¹H NMR spectroscopy at -25°C, in approximately 91% yield (based on 1.38/1.38') indicating that epimerisation must have occurred during crystallisation to account for the increased yield of (1.38). In the X-ray structure a 'β-phenyl-effect' interaction is observed between the phenyl and C₆H₆, whilst the methyl of the (*S*)-phenyl-ethyl substituent is orientated away from the chloride, reducing unfavourable steric interactions, as observed in the X-ray structures of (1.34/1.35). On warming the sample

from -25°C to room temperature, signals for the minor isomer (**1.38'**) were observed in the ^1H NMR spectrum; at above 0°C the equilibrium position (68:32) had been established. The half-life for the approach to equilibrium (**1.38** \rightleftharpoons **1.38'**) is much slower than for the analogous salicylaldehyde complexes (**1.34/1.35**), which interconvert rapidly, even at -80°C .⁹¹

In the series of related arene-ruthenium Schiff-base complexes, the configurational stability has increased on moving from an anionic *N,O*-donor ligand (salaldimine) to an anionic *N,N'*-donor (pyrrolealdimine). It would be logical, therefore, that a *neutral N,N'*-donor would form similar complexes that are even more stable to epimerisation, since these would be cationic, rather than neutral compounds and loss of the chloride ligand from a cation should be less favoured. Davies *et al.* have studied such complexes $[\text{RuCl}(\text{pyaldimine})(\text{mes})]\text{BF}_4$ {**1.39/1.39'** pyaldimine = Schiff-base formed by treatment of (*S*)-1-phenylethylamine with pyridine-2-carboxaldehyde} and $[\text{RuCl}(\text{pyketimine})(\text{mes})]\text{BF}_4$ {**1.40/1.40'**, pyketimine = the Schiff-base formed by treatment of (*S*)-1-phenylethylamine with 2-acetyl pyridine} that were formed by reacting $[\text{RuCl}_2(\text{mes})]_2$ with two equivalents of the appropriate ligand in the presence of NaBF_4 (Figure 1.12).⁷⁵



The ^1H NMR spectra of crude samples of **1.39/1.39'** and **1.40/1.40'** in CDCl_3 contained mixtures of diastereomers in a ratio of 73:27 or 67:33, respectively. The major diastereomer from each complex crystallised selectively, leaving the mother liquor enriched in the more soluble isomer. The X-ray crystal structures of (**1.39**) and (**1.40**), both (S_{Ru})-configuration, have significant differences to those of the analogous Schiff-base complexes (**1.34/1.35**)^{91, 93} and (**1.38**).⁹⁶ Complexes (**1.39**) and (**1.40**) do

not exhibit a ‘ β -phenyl-effect’, possibly due to increased steric bulk of the mesitylene ligand compared to C₆H₆. In addition, the C-Me bond of the (*S*)-phenyl-ethyl substituent in both structures is orientated towards the chloride. This might be due to a reduction in steric hindrance between the methyl and the chloride in a five-membered chelate ring compared to a six-membered ring, as found in salicylaldimine complexes,^{91, 92} and/or it might be to put the C–H bond eclipsing the arene. These factors might explain the lower diastereoselectivity of (1.38–1.40), as opposed to (1.34/1.35). There was no evidence of a characteristic high-field shift in the room temperature CDCl₃ ¹H NMR spectra of crystallised (1.39) and (1.40), consistent with the absence of a ‘ β -phenyl-effect’ in solution as was also observed in the solid-state. Integration of the signals for the two isomers indicated the presence of the major isomer in >95:5, in both cases. This ratio did not change over 2-3 days indicating interconversion of diastereomers is relatively slow, even on the chemical timescale, in CDCl₃. However, in keeping with the previously discussed Schiff-base complexes, the rate and ease of interconversion is solvent dependent. In D₂O, epimerisation of crystallised (1.39) occurred reaching a final equilibrium ratio of 55:45. In addition to the change in stability, signals due to four species were observed, assigned to diastereomeric pairs of chloro- and D₂O-coordinated complexes (similar to those observed in amino-acidate complexes discussed previously). Addition of excess NaCl led to a disappearance of the signals for the D₂O-coordinated diastereomers. These observations suggest that epimerisation is likely to proceed via exchange in the labile aqua complexes, as found for amino-acidate complexes.^{73, 76}

As expected, the charge on the ligand/complex has a dramatic effect on the rate of epimerisation. Epimerisation is generally faster in neutral complexes [RuCl(L)(arene)]ⁿ⁺ (n = 0), which incorporate an anionic chelate rather than in cationic complexes (n = 1) containing neutral bidentate ligands (L). Dissociation of a chloride ion from a neutral complex will generate a mono-cationic species, whereas dissociation from a cationic complex will be more difficult because it will form a dicationic species.

On this basis, complexes of neutral *N-N'* donor pyridyloxazolines (R-pymox) would be expected to be configurationally stable at the metal. Such complexes [MCl(R-pymox)(ring)]SbF₆ (1.41, M = Ru, ring = mes; 1.42, M = Rh, ring = Cp*) were formed by heating to reflux solutions of [RuCl₂(mes)]₂ or [RhCl₂Cp*]₂ in methanol with two equivalents of R-pymox in the presence of NaSbF₆ (Figure 1.13).^{97, 98}

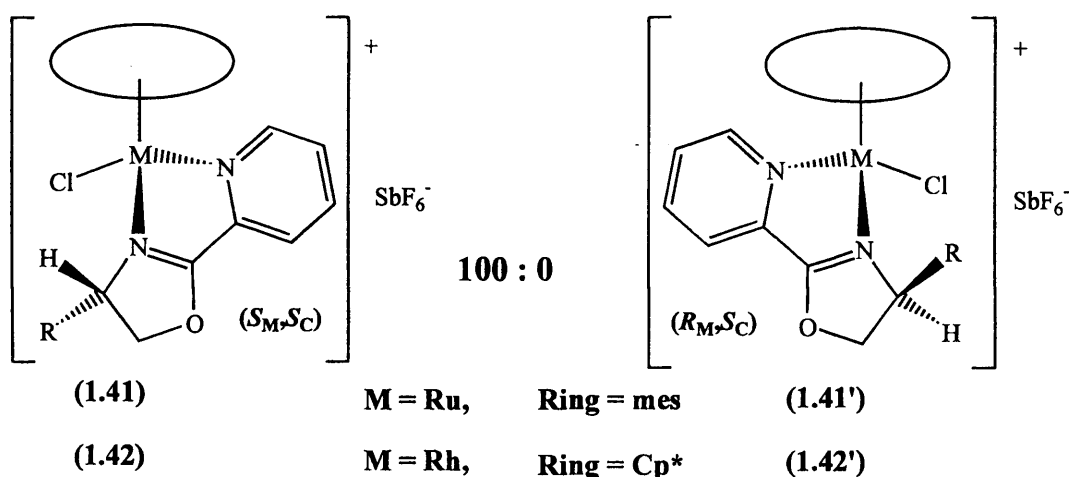


Figure (1.13)

The ^1H NMR spectra of crude samples of (1.41, R = ^iPr) and (1.42, R = ^iPr) in CDCl_3 each contained only one set of signals, indicating either their formation was highly diastereoselective or that epimerisation was fast on the NMR timescale, such that time-averaged signals were observed. The latter explanation is unlikely given the cationic nature of the half-sandwich moiety. The X-ray crystal structures of (1.41, R = ^iPr) and (1.42, R = ^iPr) adopt the geometry with the isopropyl substituent orientated more towards the chloride rather than the polyhaptoc ring, (S_M, S_C)-configuration, presumably to minimise unfavourable steric interactions.

Unpublished work in our group has shown that, in contrast to (1.41, R = ^iPr), the analogous Ph-substituted complex (1.41, R = Ph) was formed as a 71:29 mixture of diastereomers, as shown by ^1H NMR spectroscopy in CDCl_3 .⁹⁹ Crystallisation gave exclusively the major diastereomer, leaving the mother liquor enriched in the more soluble isomer. The X-ray crystal structure of (1.41, R = Ph),¹⁰⁰ (S_{Ru})-configuration, is similar to those of (1.39) and (1.40).⁷⁵ The phenyl is orientated towards the chloride rather than the mesitylene. The resulting absence of a ‘ β -phenyl-effect’ is possibly due to increased steric bulk of the mesitylene compared to C_6H_6 (the methyl groups create additional steric repulsion with the phenyl) as found for (1.39/1.40).⁷⁵ The ^1H NMR spectrum of crystallised (1.41, R = Ph) showed no trace of the minor isomer even after 1 week in CD_2Cl_2 , consistent with the ruthenium centre being configurationally stable under these conditions, as observed previously for related pyridylimine Schiff-base complexes (1.39/1.40).⁷⁵ The NOESY spectrum showed a cross peak between the $\text{NC}(H)\text{R}$ proton and those of the mesitylene ring (shown in Figure 1.14), showing that the structure in solution is the same as that in the solid state.

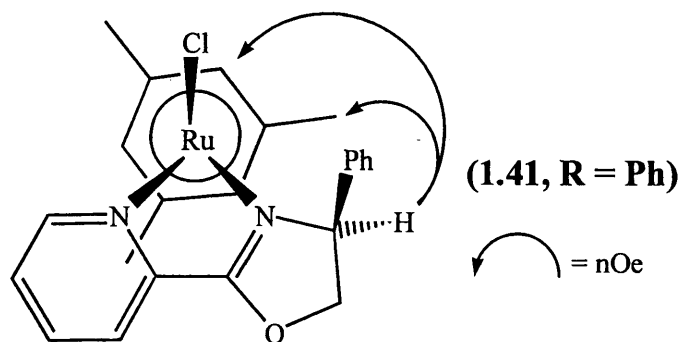
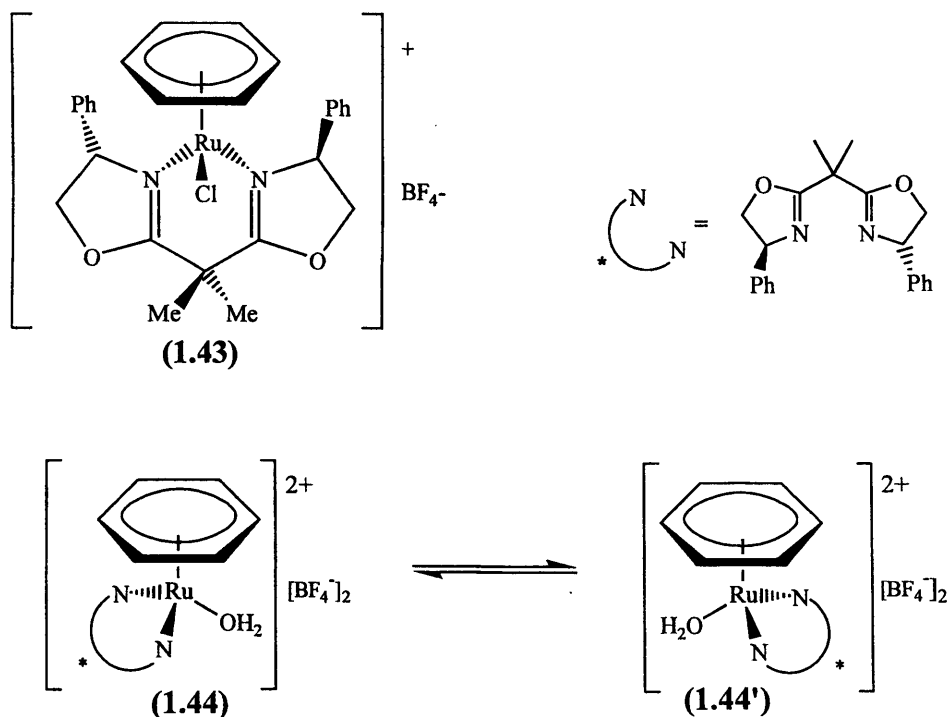


Figure (1.14)

The fluxional behaviour (pseudo epimerisation) of an enantiomeric **type 2** (chiral centre{s} on one ligand) complex **(1.43)** has been probed by variable-temperature NMR.²⁴ Kurosawa *et al.* showed that **(1.43)** is not fluxional at room temperature. However, upon chloride abstraction with AgBF_4 (in “wet” solvent) the aqua complex formed **(1.44/1.44')** was found to undergo pseudoepimerisation rapidly at room temperature (**Scheme 1.15**). Low temperature NMR studies proved that the mechanism of interconversion between **1.44** and **1.44'** proceeds through a dissociative (unimolecular) mechanism involving the 16-electron species $[\text{Ru}(\{\text{R}\}\text{-bop})(\text{C}_6\text{H}_6)]^{2+}$, rather than through an associative (bimolecular) H_2O exchange process.²⁴



Scheme (1.15)

From these studies three key factors (1 to 3) can be identified as being important in controlling the diastereoselectivity of $[\text{MCl}(\text{L})(\text{ring})]^{n+}$ ($\{n = 0, 1\}$ L = bidentate

ligand) complexes and four important interactions (4 to 7) have also been shown to have a dramatic effect on the rate of epimerisation, these are: (1) intramolecular hydrogen bonding; (2) conformational effects; (3) 'β-phenyl-effect'; (4) nature of other L; (5) choice of M(ring); (6) charge on ligand/complex and, finally, (7) donor atoms/π-donor properties.

Intramolecular H-bonding has been reported to preferentially stabilise one diastereomer of an amino-acidate complex,¹⁰¹ however, this interaction is probably significant in only a few cases.⁸¹ The presence of conformational effects, in contrast, leads to high diastereoselectivity in numerous complexes. For example, the presence of a tertiary nitrogen donor atom in *N*Me₂-amino-acidate,^{76, 82} TMBA⁸⁶ and TMNA⁸⁷ containing complexes and the additional chiral centre in proline containing complexes,⁷⁶ results in high diastereomer ratios ranging from 90:10 to 100:0. The 'β-phenyl-effect' was also shown to be an important interaction, contributing to the high diastereoselectivity observed in arene ruthenium complexes, most significantly when the arene is C₆H₆ and the Schiff-base ligands are salaldimine^{91, 93, 102} and pyrrolealdimine.^{96, 103}

The observed diastereoselectivity is not great for some of the ligands discussed in the section, which might limit their application in asymmetric catalysis. Some of the most diastereoselective complexes were formed with *N*-donor atom ligands, *e.g.* *N*Me₂-amino-acidate, TMBA, TMNA, salicylaldimine and pymox. However, the use of conformationally rigid ligands (after complexation) might be important for their use in asymmetric catalysis; the ligands derived from (*S*)-*N*-(1-phenylethyl)amine might give inherently low enantioselectivity, due to the free rotation about the N—CH(Me)Ph bond. Therefore, complexes of ligands where the stereogenic centre(s) are fixed within a ring system, such as an oxazoline, might achieve greater asymmetric induction in catalytic (or stoichiometric) reactions.

The effect on the rate of epimerisation of substitution of the chloride by an alternative donor such as halide (Br⁻ or I⁻), phosphine or amine is not readily predictable. This is evident in the pyrrolecarbaldimine complexes when comparing [RuCl(pyrrolealdimine)(C₆H₆)] with [Ru(PPh₃)(pyrrolealdimine)(C₆H₆)]PF₆ (see **Figure 1.15**). The Cl⁻ complex epimerises at room temperature in CDCl₃ whereas the PPh₃ complex doesn't epimerise until 85°C in d₃-nitromethane.⁹⁶ This can be

rationalised by a different ligand needing to dissociate to allow epimerisation (assuming a dissociative mechanism rather than an opening of the bidentate chelate).

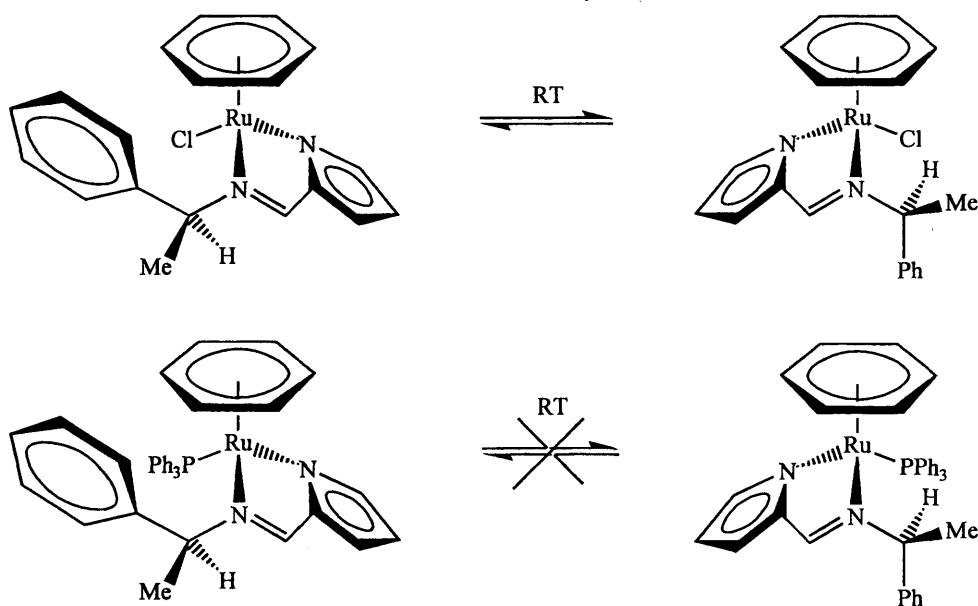


Figure (1.15)

The rate of epimerisation is dependent on the M(ring) combination. Merbach *et al.* found that the rates of water exchange in $[M(H_2O)(bpy)Cp^*]^{2+}$ ($M = Rh$ or Ir) were nearly the same, whereas the rates for the analogous complexes $[Ru(H_2O)(bpy)(arene)]^{2+}$ (arene = C_6H_6 ; *p*-*cy*; C_6Me_6 , respectively) (which were all similar) were all slower by approximately four orders of magnitude.⁶³ This marked difference between (arene)Ru vs. Cp^*Rh/Ir combinations was ascribed to the larger *trans* labilising effect of anionic Cp^* compared to that of the neutral arene ligands. Also, the rate of water exchange in $[Rh(H_2O)_3Cp^*]^{2+}$ was found to be much faster than in $[Rh(H_2O)(bpy)Cp^*]^{2+}$ consistent with stabilisation of the latter complex.⁶³ These findings support the general observations of reduced stability for the metal configuration for $[RhCl(L)Cp^*]$ as opposed to $[RuCl(L)(arene)]$ described in this section.

For arene ruthenium Schiff-base complexes, it is clear that epimerisation at the metal becomes less rapid moving from anionic *N,O* and *N,N'* donor ligands to neutral *N,N'* donor ligands, due to increased difficulty of chloride dissociation. The donor atoms (particularly the π -donor properties) of the chelating ligand also have an affect on the configurational stability of half-sandwich complexes.^{85, 104} The more electron density that the ligand donates to the metal centre, the greater the stabilisation of the 16-electron intermediate, hence the smaller the energy barrier to epimerisation and, consequently,

the faster the rate of interconversion. Comparing the bonding components of the two anionic ligands salicylaldimine (N,O^-) and pyrrolocarbaldimine (N,N^-), the imine nitrogen is similar in each case but the O^- and N^- have different donor properties, particularly their π -donor properties. The O^- has two lone pairs of electrons available, whilst the N^- has only one π -lone pair which is involved in delocalisation with the pyrrole ring π -system; consequently, some of its π electron density cannot be utilised for bonding so weakening the π -donor properties. Furthermore, the phenolic O^- of salicylaldimine is not contained in a ring system, thus allowing greater conformational freedom to adopt favourable molecular orbital overlap in order to donate its π electron density. Hence, the greater π -donor ability of the salicylaldimine ligand contributes to a faster rate of epimerisation than in the analogous pyrrolocarbaldimine complex.

This section has discussed the factors controlling diastereoselectivity and epimerisation for a range of (arene)Ru and Cp*Rh complexes. When using diastereomeric chiral-at-metal complexes as asymmetric catalysts, it would be desirable to form *either* a single diastereomer which does not epimerise in solution, *or* to form a complex with very high diastereoselectivity, even if it is configurationally unstable since the minor isomer may not contribute significantly to the reaction. Complexes which have low diastereoselectivity and fast epimerisation are least useful. The well-defined geometry of half-sandwich complexes also allows the possibility of probing in more detail the mechanism of reactions and hence investigating the basis of enantioselection at a molecular level. As illustrated above, nitrogen-containing ligands have proved to be capable of generating high diastereoselectivity. The rest of this thesis will describe the synthesis of some new oxazoline, imidazoline and Schiff-base half-sandwich complexes (Chapter Two and Three) and their evaluation as asymmetric Lewis-acid catalysts is described in Chapter Four.

Chapter Two:

Chiral (Arene)Ru & (Cp*)Rh Complexes with Nitrogen-Donor Ligands

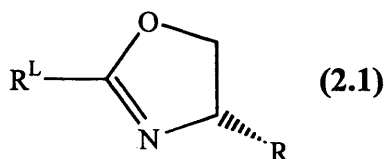
Chapter Two : Chiral (Arene)Ru & (Cp*)Rh Complexes with Nitrogen-Donor Ligands

The most impressive examples of using chiral half-sandwich complexes in asymmetric catalysis are Noyori's transfer hydrogenation catalysts.⁸¹ The precursors [RuCl(*p*-TsDPEN)(arene)] (arene = *p*-cy, mes) promote the reaction of prochiral aryl ketones into chiral aryl alcohols with high enantioselectivity (up to 100% *e.e.* being obtained).⁸⁰ Noyori's catalysts illustrate that combining the half-sandwich structure with *N*-donor ligands can give highly asymmetric catalytic systems. This chapter will describe the synthesis, characterisation and coordination chemistry of chiral arene-ruthenium and Cp*-rhodium complexes formed from oxazoline, imidazoline or Schiff-base ligands. At the commencement of this work very few half-sandwich complexes of oxazolines were known,⁹⁷ none with imidazolines and none with the particular Schiff-bases we have examined. Previous work on arene-ruthenium and Cp*-rhodium complexes with *N*-donor ligands were summarised in Section 1.4.3.

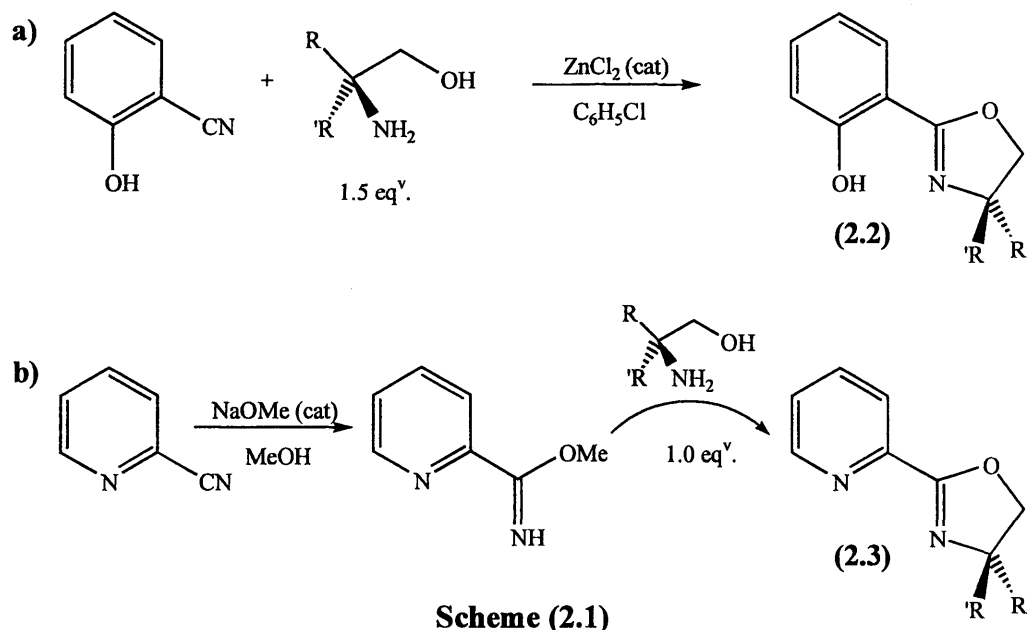
(2.1) – Introduction

Over the last decade, chiral oxazoline containing ligands have been extensively studied and have proven to be highly successful at inducing enantioselectivity in a variety of catalysed organic transformations.¹⁰⁵⁻¹⁰⁸ These applications will be discussed in greater detail in Chapter Four.

The positioning of the chiral centre next to the nitrogen atom is significant (see 2.1); on coordination of the nitrogen to a metal, the sterically bulky groups (*e.g.* ^{*i*}Pr, ^{*t*}Bu) attached to the chiral carbon are in close proximity to the metal. Hence, the substituents should have a notable effect on the enantioselectivity of a reaction proceeding at the metal. The oxazoline compounds discussed in the remainder of this section incorporate either the deprotonated phenol monoxazolines (phenmox) (2.2) or the pyridine monoxazolines (2.3).



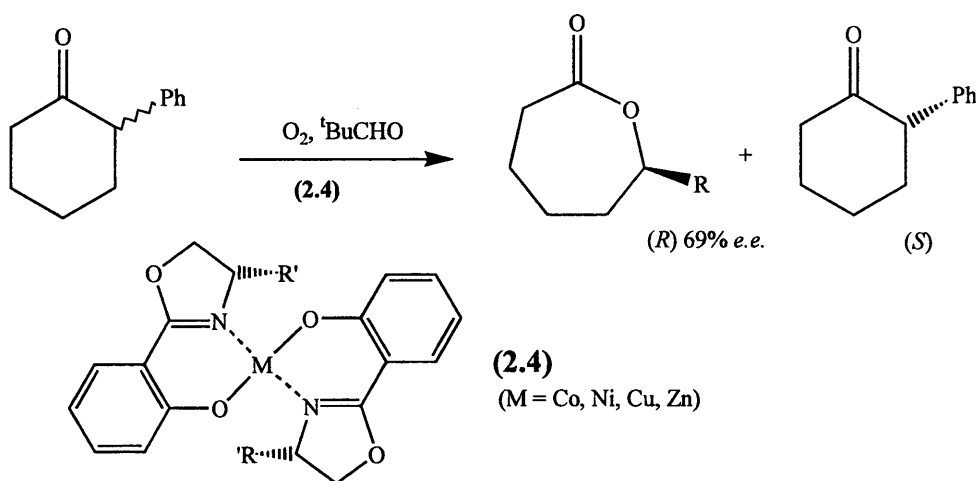
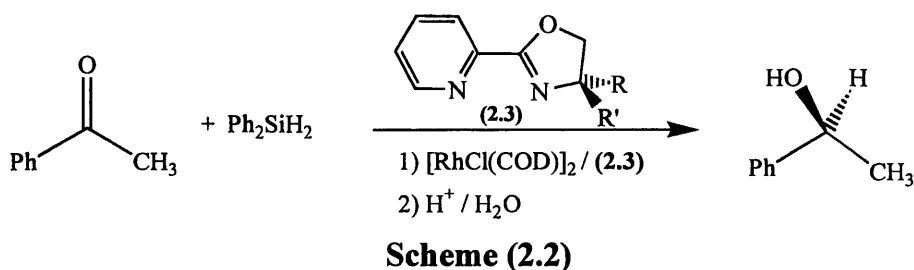
In contrast with many chiral phosphines, enantiopure oxazolines are inexpensively and conveniently prepared by reacting chiral amino alcohols (obtained by the reduction of amino-acids) with a suitable carbonyl or nitrile precursor (**Scheme 2.1**). The use of amino-acids as the source of chirality gives the potential for a wide variety of R-substituents allowing variation of the steric requirements in the oxazoline, and readily provides enantiopure ligands without the need for resolution of a racemate (as is often required with chiral phosphine ligands).



The syntheses of oxazoline ligands are well documented.¹⁰⁹⁻¹¹³ Phenmox ligands (**2.2**) have been prepared by heating 2-cyanophenol with the required amino alcohol in chlorobenzene to reflux with ZnCl_2 as catalyst (method **a**, **Scheme 2.1**).¹¹¹ This method gives high (overall) yields for phenmox ligands (based on 2-cyanophenol) but the work-up involves lengthy column chromatography and excess chiral amino alcohol (1.5 equivalents) is needed. Unfortunately, method **b** via an imidate (**Scheme 2.1**),¹⁰⁹ which requires only one equivalent of chiral amino alcohol, only works well when an electron withdrawing group is adjacent to the nitrile group and hence fails in the phenmox case. However, method **b** works well for pymox (**2.3**) because the nitrogen atom activates the nitrile towards base catalysed imidate formation.

The pymox ligands (**2.3**) were used *in situ* by Brunner *et al.* in 1989 for the Rh(I)-catalysed enantioselective hydrosilylation of ketones, to give chiral alcohols, in up to 83% *e.e.* ($\text{R} = \text{tBu}$, $\text{R}' = \text{H}$) (**Scheme 2.2**).¹¹⁴ Previous work in our group shows that pymox can be complexed to arene ruthenium⁹⁷,¹¹⁵ and Cp^* rhodium however,

comparable complexes of phenmox were not known at the start of this work. Complexes (2.4), were synthesised as metal-salen analogues by Bolm *et al.*¹¹⁶ The copper complexes were found to be asymmetric catalysts for the Baeyer-Villiger oxidation of racemic cyclic ketones to lactones **Scheme (2.3)**.¹¹⁷



As mentioned above, the application of chiral oxazoline-containing ligands is varied and has met with great success. Imidazolines (2.5) are five-membered heterocycles analogous to oxazolines (**Figure 2.1**). Since both heterocycles coordinate through the imine, if the substituent (R) is the same they should have similar steric requirements; consequently, imidazolines might express similar asymmetric induction properties to oxazolines. However, electronically, imidazolines should be more electron rich due to the decreased electronegativity of nitrogen relative to oxygen. In addition, changing the substituent on the amine nitrogen (R'') can alter the electronic properties whilst leaving the steric requirements almost unaltered, especially if there is delocalisation through the amidine (NCN) fragment. Imidazolines, therefore, are ideal ligands to probe electronic effects on enantioselectivity.



Figure (2.1): Structural comparison of oxazolines and imidazolines

Furthermore, imidazolines offer potential advantages over oxazolines in asymmetric catalysis. Firstly, the R'' substituent could be used to attach the complex to a polymer support, allowing easier separation of products from catalyst and facilitating easier recycling of ligand if dissociation from the metal occurs. Secondly, if the R'' substituent was bulky it might be possible to synthesise ligands containing a chiral carbon and a stereogenic axis along the imidazoline aryl bond (Figure 2.2).

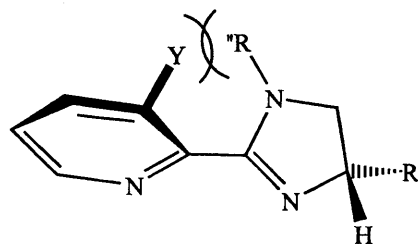
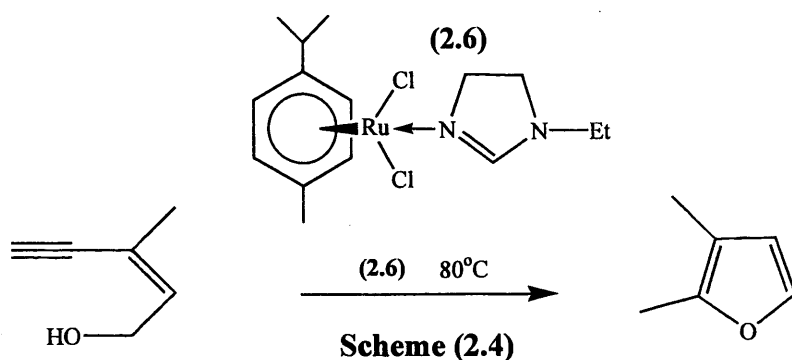
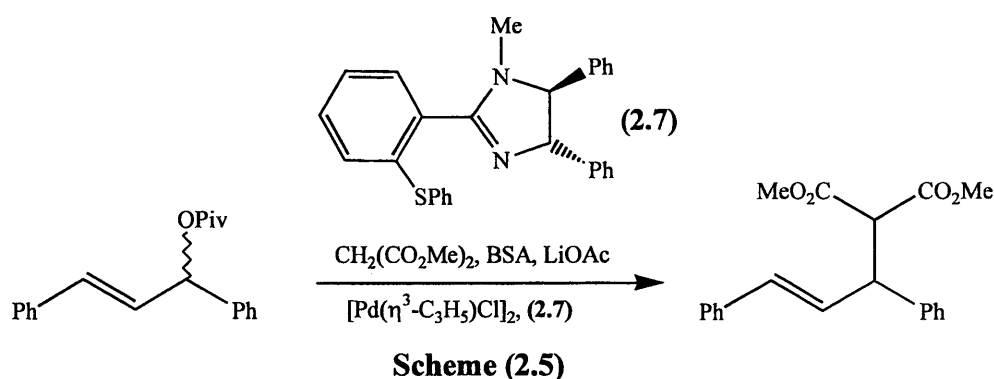


Figure (2.2): Potential rotamer formation.

The earliest reports of imidazoline syntheses involved reaction of ethylenediamine with either methanoates¹¹⁸ or isonitriles catalysed by silver cyanide,¹¹⁹ forming the achiral products in variable yield. The convenient preparation of chiral imidazoline ligands is therefore limited by ready availability of enantiopure ethylenediamines. Imidazoline and ethylenediamine synthesis will be discussed in more detail in (Section 2.2.3). Imidazolines have received comparatively little study as ligands to metals, notably an arene ruthenium complex (2.6) was reported during the course of our work¹²⁰ and (2.6) was employed as a precatalyst for intramolecular cyclisation of *Z*-enyols into furans (Scheme 2.4).

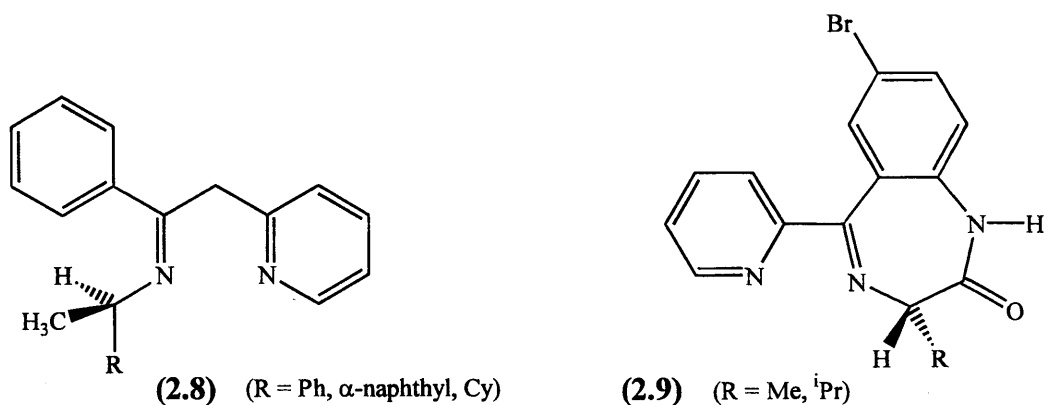


To date, only two metal complexes with achiral imidazolines have been structurally characterised¹²¹ and no chiral imidazoline complexes have even been isolated and characterised. The synthesis of chiral imidazolines has been reported,¹²² however, these were limited to those prepared from just two C₂-symmetric ethylenediamines. More recently, the bidentate thioimidazoline ligand (**2.7**) was reported to give high enantiomeric excess (up to 96% *e.e.*) for palladium catalysed allylic alkylation (**Scheme 2.5**) though the catalyst was prepared *in situ*.¹²³



Schiff-base ligands, first prepared in 1864,¹²⁴ are formed from condensation of amines with aldehydes or ketones to give an imine, which must have one or more aryl groups attached to either nitrogen or carbon for stability. The synthesis allows facile variation of electronic and steric properties, resulting in a number of structurally related ligands that have been well-reviewed.¹²⁵⁻¹²⁷ Schiff-bases were the first successful *N*-donor ligands used as cocatalysts with [RhCl(COD)]₂ for asymmetric hydrosilylation reactions.¹²⁸ Recently, the success of bis-imine-pyridyl ligands in olefin polymerisation catalysis^{129, 130} has led to a resurgence of interest in applications of Schiff-bases.

The remainder of this section will focus on bidentate ketimine Schiff-base ligands (**2.8**, R = Ph, Nap, Cy)^{131, 132} and (**2.9**, R = Me, ⁱPr)¹³³; synthesised by the research group of V. Sunjic (Ruder Boskovic Institute, HR-Zagreb, Croatia).

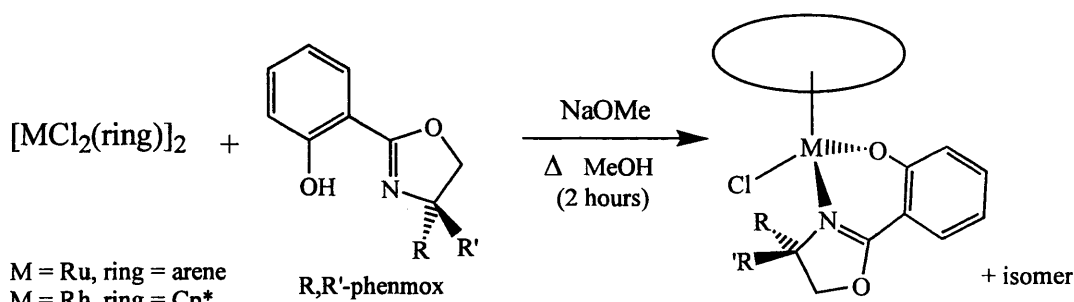


Copper(I) complexes of **(2.8 R = Ph)** and **(2.9)** have been reported.^{131, 133} The former, generated *in situ*, has been evaluated as an enantioselective cyclopropanation catalyst.¹³¹ However no half-sandwich complexes of **(2.8)** or **(2.9)** are known.

(2.2) – Results and Discussion

(2.2.1) – Half-Sandwich Complexes of Unsymmetrical Oxazoline Ligands

The ligands *R,R'*-phenmox (**2.2**)¹¹¹ and (**2.3**, *R* = ^{*i*}Pr)¹¹⁴ were prepared by literature methods (Scheme 2.1) using (*S*)-amino-alcohols prepared by reduction of L-amino acids. Half-sandwich complexes [MCl(*R,R'*-phenmox)(ring)] (**2.10** - **2.15**) were prepared in high isolated yield (65–83%) by treating the relevant dimer [MCl₂(ring)]₂ (M = Ru, ring = arene; M = Rh, ring = Cp*) with two equivalents of the phenmox ligand (**2.2**) and sodium methoxide in refluxing MeOH (Scheme 2.6).



(2.10 - 2.15): Table (2.1)

Scheme (2.6)

Table (2.1): Complexes [MCl(*R,R'*-phenmox)(ring)]

Code Number	M	ring	R	R'
2.10	Ru	mes	Me	Me
2.11	Rh	Cp*	Me	Me
2.12	Ru	mes	^{<i>t</i>} Bu, ^{<i>i</i>} Pr, Bn, Ph	H
2.13	Ru	<i>p</i> -cy	^{<i>t</i>} Bu, ^{<i>i</i>} Pr	H
2.14	Ru	C ₆ H ₆	^{<i>i</i>} Pr	H
2.15	Rh	Cp*	^{<i>t</i>} Bu, ^{<i>i</i>} Pr, Bn, Ph	H

Complexes (**2.10–2.15**) were characterised by a combination of X-ray crystallography; mass spectrometry; microanalysis; ¹H NMR; ¹H-¹H COSY; ¹H-¹H NOESY and ¹³C DEPT-135 NMR spectroscopy (Tables 2C.2 – 2C.6, p 128). In all the complexes (**2.10–2.15**), the metal is chiral because of the C₁ symmetry of the phenmox ligand. Hence, complexes [RuCl(Me₂-phenmox)(mes)] (**2.10**) and [RhCl(Me₂-phenmox)(Cp*)] (**2.11**) (containing the achiral Me₂-phenmox ligand) exist as racemates whilst (**2.12 – 2.15**) may, theoretically exist as mixtures of diastereomers. The ¹H NMR

spectrum of (2.10) showed two doublets at δ 4.10 and 4.30 and two singlets at δ 1.41 and 1.62 due to the two inequivalent OCH_2 protons and CMe_2 group, respectively. However, the corresponding signals in the ^1H NMR spectrum of (2.11) were rather broad, broad singlets at δ 3.93 and 4.19 for OCH_2 , and two inequivalent NCMe groups also broad singlets at δ 1.33 and 1.45. Cooling this sample to 273 K caused the broad singlets for the OCH protons to resolve into sharp doublets. These experiments indicate that chloride exchange and fluxionality of (2.11) (*i.e.* racemisation) is occurring at a rate similar to the NMR timescale at room temperature (see Scheme 2.7); whereas, at 273 K interconversion is slow on the NMR timescale. The well resolved signals for (2.10) indicate chloride exchange is slow on the NMR timescale at RT and interconversion in the ruthenium phenmox complex is *slower* than for the comparable rhodium complex. These findings are consistent with the relative rates of water exchange found for $[\text{Rh}(\text{OH}_2)(\text{bpy})\text{Cp}^*]^{2+}$ and $[\text{Ru}(\text{OH}_2)(\text{bpy})(\text{mes})]^{2+}$ (see section 1.4.2).⁶³ The X-ray structure of (2.11) has been determined and is discussed later.

In complexes (2.12–2.15) the phenmox ligand itself is chiral and so, theoretically, mixtures of diastereomers can be obtained (Figure 2.3) (discussed in section 1.2.2, p 6).

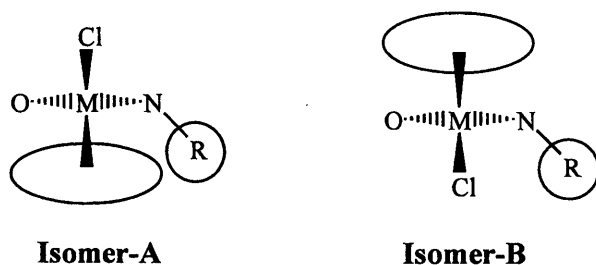


Figure (2.3): Illustration of isomer A and B

In both isomers, the configuration about the stereogenic carbon of the oxazoline ligand is (*S*) so the isomer-A ($S_M S_C$) and isomer-B ($R_M S_C$) diastereomers correspond to switching the positions of the ring and chloride ligands. The diastereoselectivity is expected to depend on the sizes of the substituents on the arene and the oxazoline. If both are large, significant steric repulsions are expected in isomer-A; thus isomer-B, in which the oxazoline-substituent(s) is(are) directed towards the chloride, would be energetically favoured. The ratios of diastereomers formed for (2.12–2.15) were determined by ^1H NMR spectroscopy (both from the crude reaction mixture and after recrystallisation) from the relative integration of either the η^6 -arene and/or the Ar-6-*H*

signals of the two isomers, with X-ray diffraction and nOe experiments, being used to determine the configuration at the metal.

Some general observations can be made regarding the ^1H NMR spectra (Tables 2C.2 – 2C.6, p 128). The chemical shifts of the complexed ligands were significantly different to those of the free ligands. The coordinated phenoxy ring signals were observed at higher-field (lower frequency) by up to 0.5 ppm, probably due to deprotonation of the OH group. In contrast, the signals due to the NCH and the OCH₂ protons of the oxazoline ring were moved downfield upon coordination due to donation of electron density to the metal. Surprisingly, the CHMe₂ proton in complexes (2.12, R = ⁱPr) and (2.15, R = ⁱPr), is deshielded compared to that of the free ligand by almost 1 ppm from δ 1.80 to *ca.* δ 2.80, whereas, the signals due to the CHMe₂ protons are essentially unchanged (*ca.* δ 0.9). The coordinated arenes give rise to singlets at *ca.* δ 5.6 due to C₆H₆ in (2.14) and at between δ 1.90 and 2.25 (C₆H₃Me₃) and δ 4.20 to 4.95 (C₆H₃Me₃) for complexes (2.12). Similarly, singlets due to the Cp* methyl groups occur between δ 1.26 and 1.80 for rhodium complexes (2.11/2.15). Complex (2.13, R = ^tBu) exhibits two doublets at *ca.* δ 1.20 (ArCHMe₂), with a singlet at δ 2.32 (Ar-Me), a septet at δ 2.76 (CHMe₂), and four doublets between δ 4.93 and 5.49 (Ar-H) as expected for a chiral complex.

The ^1H NMR spectra of the ruthenium complex (2.12, R = ⁱPr) contains a single set of well-resolved signals. The most likely explanation is that the complex was formed with high diastereoselectivity (*ca.* 100% *d.e.*) *i.e.* as one diastereomer. Alternatively, epimerisation of the diastereomers is fast on the NMR timescale, hence time-averaged signals are observed in the ^1H NMR spectrum. To investigate this the ^1H NMR spectrum was recorded at 233 K; signals for a second diastereomer were not observed, suggesting diastereoselective formation (\sim 100% *d.e.*), or that the rate of exchange is still fast at 233 K. The latter suggestion is unlikely since the rate of epimerisation of [RuCl(Me₂-phenmox)(mes)] (2.10) is slow on the NMR timescale at room temperature. Furthermore, epimerisation of the analogous salicylaldimine Schiff-base complex [RuCl(L⁴)(C₆H₆)]⁹¹ (see section 1.4.3) was also slow on the NMR timescale, supporting the inference of very high diastereoselectivity for the ruthenium complex (2.12, R = ⁱPr).

Crystallisation from CH₂Cl₂/ether gave X-ray quality crystals of (2.12, R = ⁱPr). The crystal structure (Figure 2.11, p 59) showed the presence of only one diastereomer,

with the isopropyl group pointing towards the chloride (isomer-B). The observation of only one isomer of (2.12, R = ⁱPr) by ¹H NMR spectroscopy suggests that the solid state structure (isomer-B) is maintained in solution. To confirm this a phase-sensitive NOESY experiment was performed. Isomer-B would be expected to show nOes between the NCH proton (δ 4.44) and either of the mesitylene proton signals (δ 2.21 and δ 4.89), whilst isomer-A might show nOes between the mesitylene signals and those of the ⁱPr (δ 0.74, 0.99 and 2.82). These predicted structure-determining nOes are shown in Figure (2.4). The NOESY spectrum (Figure 2.5) contains nOes consistent with the isomer-B and the absence of those expected for isomer-A, confirming that the ⁱPr group is orientated away from the mesitylene ring and towards the chloride ligand and that the solid-state isomer is indeed the same as that found in solution.

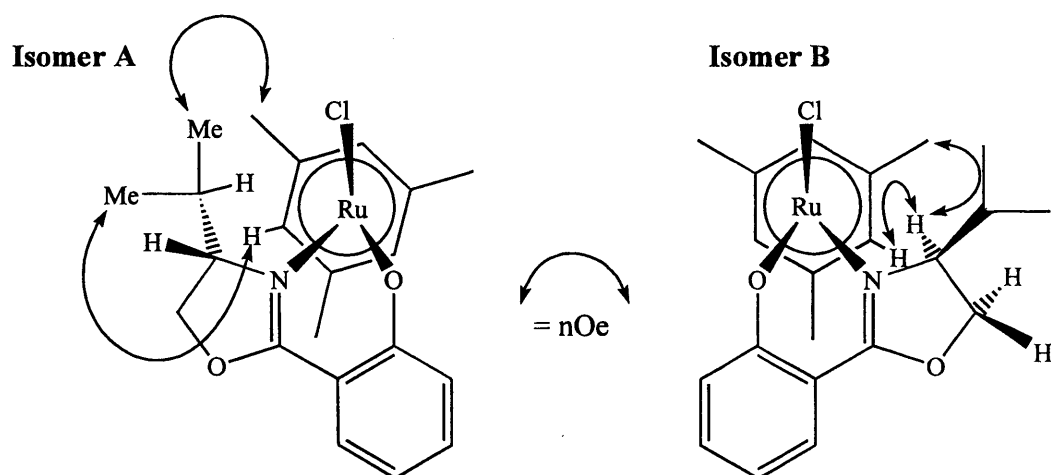
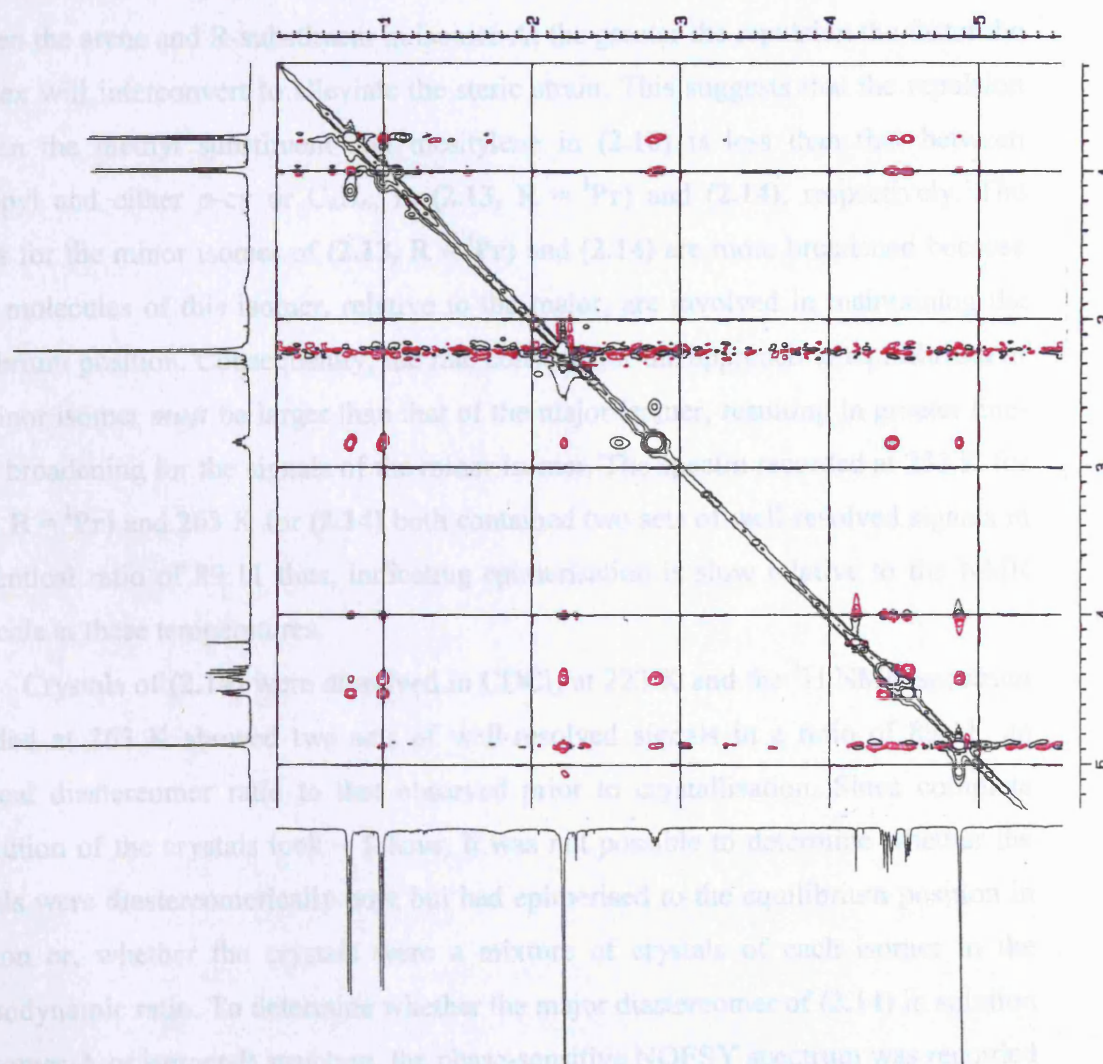


Figure (2.4): Predicted nOes for isomer A and B of (2.12, R = ⁱPr)

Figure (2.5): ^1H - ^1H NOESY spectrum of (2.12, R = ^iPr) recorded in CDCl_3 at 300 K and 400 MHz.



In order to investigate the effect of arene ring size on diastereoselectivity the *p*-cy (**2.13**, **R** = ^{*i*}Pr) and C₆H₆ (**2.14**) analogues of (**2.12**, **R** = ^{*i*}Pr) were synthesised. The ¹H NMR spectrum of each complex contained two sets of broad nearly overlapping signals in an approximate 89:11 ratio, which did not change over time; signals for the minor isomer were broader than those of the major. These observations indicate that both (**2.13**, **R** = ^{*i*}Pr) and (**2.14**) exist as two diastereomers that are epimerising at a rate similar to the NMR timescale such that the thermodynamic equilibrium has been established. Thus, epimerisation of these diastereomers is faster than racemisation in [RuCl(Me₂-phenmox)(mes)] (**2.10**), which was slow on the NMR timescale at room temperature. This may be rationalised by considering the degree of steric repulsion between the arene and R-substituent in isomer-A; the greater the repulsion the faster the complex will interconvert to alleviate the steric strain. This suggests that the repulsion between the methyl substituent and mesitylene in (**2.10**) is less than that between isopropyl and either *p*-cy or C₆H₆, in (**2.13**, **R** = ^{*i*}Pr) and (**2.14**), respectively. The signals for the minor isomer of (**2.13**, **R** = ^{*i*}Pr) and (**2.14**) are more broadened because fewer molecules of this isomer, relative to the major, are involved in maintaining the equilibrium position. Consequently, the rate constant for the approach to equilibrium of the minor isomer *must* be larger than that of the major isomer, resulting in greater line-width broadening for the signals of the minor isomer. The spectra recorded at 233 K for (**2.13**, **R** = ^{*i*}Pr) and 263 K for (**2.14**) both contained two sets of well-resolved signals in an identical ratio of 89:11 thus, indicating epimerisation is slow relative to the NMR timescale at these temperatures.

Crystals of (**2.14**) were dissolved in CDCl₃ at 223 K and the ¹H NMR spectrum recorded at 263 K showed two sets of well-resolved signals in a ratio of 89:11, an identical diastereomer ratio to that observed prior to crystallisation. Since complete dissolution of the crystals took ~ 1 hour, it was not possible to determine whether the crystals were diastereomerically pure but had epimerised to the equilibrium position in solution or, whether the crystals were a mixture of crystals of each isomer in the thermodynamic ratio. To determine whether the major diastereomer of (**2.14**) in solution has isomer-A or isomer-B structure, the phase-sensitive NOESY spectrum was recorded at 263 K. The NOESY spectrum contains nOes between the NCH proton (δ 4.60) and the C₆H₆ protons (δ 5.60) consistent with the major isomer possessing isomer-B structure (*R*_{Ru}, *S*_C) with the ^{*i*}Pr group orientated towards the chloride rather than the

C₆H₆ ring (as found for **2.12**, **R** = ⁱ**Pr**). No nOe signals were observed for the minor isomer, possibly due to its low concentration (only 11% of the sample).

Attempts to determine the solution structure for the isomers of (**2.13**, **R** = ⁱ**Pr**) failed due to unfortunate overlap of NMR signals (in particular, the phenmox NCH δ 4.65 signal overlaps with an OCH peak). However, since *p*-cy is larger than C₆H₆ and similar to mesitylene it is not unreasonable to predict that the major diastereomer of (**2.13**, **R** = ⁱ**Pr**) adopts the same geometry as both (**2.14**) and (**2.12**, **R** = ⁱ**Pr**). The increased diastereoselectivity with mesitylene is probably due to increased steric interaction between the η^6 -ring and the R-substituent in isomer-A of (**2.12**, **R** = ⁱ**Pr**). A similar increase in diastereoselectivity was observed for [RuCl(ⁱPr-pymox)(arene)]⁺ (arene = mes, *p*-cy, C₆H₆); the *p*-cy and C₆H₆ complexes are 50:50 mixtures of diastereomers whilst the mesitylene complex is a single diastereomer.¹⁰⁰

In order to investigate the effect of the size of oxazoline substituent (R) on diastereoselectivity, the complexes [RuCl(R-phenmox)(arene)] (**2.12**, **R** = ^t**Bu**, ⁱ**Pr**, **Bn**, **Ph**) were prepared. The ¹H NMR spectrum of (**2.12**, **R** = ^t**Bu**) contained a single set of well-resolved signals, similar to that found for (**2.12**, **R** = ⁱ**Pr**), suggesting that this complex is also formed with high diastereoselectivity (> 98:2 isomer ratio). In contrast to (**2.12**, **R** = ⁱ**Pr**, ^t**Bu**), the ¹H NMR spectra of complexes (**2.12**, **R** = **Bn**, **Ph**), in dry CDCl₃, each contained two sets of well-resolved signals that were assigned to two isomers in ratios of 79:21 and 24:76, respectively. The observation of sharp signals shows that the rate of epimerisation is slow on the NMR timescale. This observation adds further support to the earlier suggestion that complexes (**2.12**, **R** = ⁱ**Pr**, ^t**Bu**) were formed with very high diastereoselectivity.

In complex (**2.12**, **R** = **Bn**), the absence of a highfield shift for the mesitylene C₆H₃Me₃ protons { δ 4.94 (major) and 4.89 (minor)} suggests a ' β -phenyl-effect' is not present in either isomer; this is consistent with the related diastereomeric complex [RuCl(**Bn**-pymox)(mes)]SbF₆.¹⁰⁰ In order to determine which is the major diastereomer a NOESY spectrum was recorded. The spectrum showed nOe cross-peaks for the major isomer between the NCH δ 4.71 and both mesitylene signals (δ 2.24 and 4.94), as expected for isomer-B. In addition, chemical exchange correlations were observed between diastereotopic PhCH₂ protons (at δ 2.79_{major} and δ 2.64_{minor}) and the OCH₂ signals (at δ 4.35_{major} and δ 4.16_{minor}) of the major and minor isomers. This type of correlation arises because the two protons are interchanged rapidly compared to the

NOESY timescale; indicating that epimerisation is occurring in solution, such that $k > 10^{-3} \text{ s}^{-1}$ hence the observed isomer ratio (79:21) corresponds to the equilibrium ratio.

As mentioned above, (**2.12**, **R = Ph**) also exists as a mixture of diastereomers (24:76). In this case crystallisation from $\text{CH}_2\text{Cl}_2/\text{ether}$ gave X-ray quality crystals and the structure (discussed later-**Figure 2.12**, p 59) showed only the presence of the diastereomer with the phenyl group pointing towards the mesitylene ring (isomer-A). Crystals from the same batch were dissolved in CD_2Cl_2 at -80°C and the ^1H NMR spectrum recorded at this temperature showed the presence of both isomers in a ratio of 40:60. The mesitylene ($\text{C}_6\text{H}_3\text{Me}_3$) signal of the minor isomer was observed at δ 4.56 compared to δ 4.07 for the major isomer, the shift to higher field may be due to a ‘ β -phenyl-effect’ (see later). On warming the solution, the ratio of the two diastereomers did not change proving the system had already reached the equilibrium diastereomer ratio in dichloromethane. Alternatively, the observation of only one diastereomer in the X-ray structure but two in the low temperature ^1H NMR spectrum may be because the single crystal selected for X-ray diffraction did not represent the diastereomer ratio in the bulk sample (*i.e.* 60 % of crystals possessed S_{Ru} , S_{C} and 40 % R_{Ru} , S_{C} configurations). However, this explanation can be ruled out since the diastereomer ratio changes when crystals from the same batch are dissolved in different solvents (24:76 in CDCl_3 compared to 40:60 in CD_2Cl_2) indicating that epimerisation has taken place. Since the NMR spectra in either solvent contained sharp signals the ratios of which do not change with time, even at -80°C , the rate of epimerisation must be fast on the chemical timescale even at -80°C ($k > 10^{-3} \text{ s}^{-1}$) but slow on the NMR timescale ($k < 10^{-1} \text{ s}^{-1}$). A ^1H NMR spectrum recorded at 323 K (in CDCl_3) showed line-width broadening of the signals proving further confirmation that epimerisation is occurring, though coalescence had not occurred by this temperature.

In order to confirm the solution structures of the two diastereomers a NOESY spectrum was recorded. Unfortunately, resonances assigned to the oxazoline and mesitylene ring protons overlapped in the ^1H NMR spectra (in CDCl_3 and CD_2Cl_2 at 400 MHz) recorded at room temperature. However, at 203 K the mesitylene ring proton resonance (δ 4.07 *c.f.* δ 4.16 at RT) no longer overlapped the OCH proton signal of the minor isomer, thus allowing full characterisation of complex (**2.12**, **R = Ph**). Based on the crystal structure (isomer-A), the most likely nOes are between the phenyl substituent protons (δ 7.42 –7.60) and either of the mesitylene signals (δ 1.91 for $\text{C}_6\text{H}_3\text{Me}_3$ and δ

4.22 for $C_6H_3Me_3$), however, the Ph-substituent protons for the major and minor isomers overlap, nullifying characterisation from this isomer. For isomer-B, nOes would be expected between the NCH proton (δ 5.73) and either of the mesitylene signals (δ 2.02 for $C_6H_3Me_3$ and δ 4.64 for $C_6H_3Me_3$) (**Figure 2.6**). An nOe was observed for the minor isomer between the NCH proton and the $C_6H_3Me_3$ methyls indicating that this is isomer-B hence the major isomer has isomer-A structure as found in the solid-state structure (**Figure 2.12**).

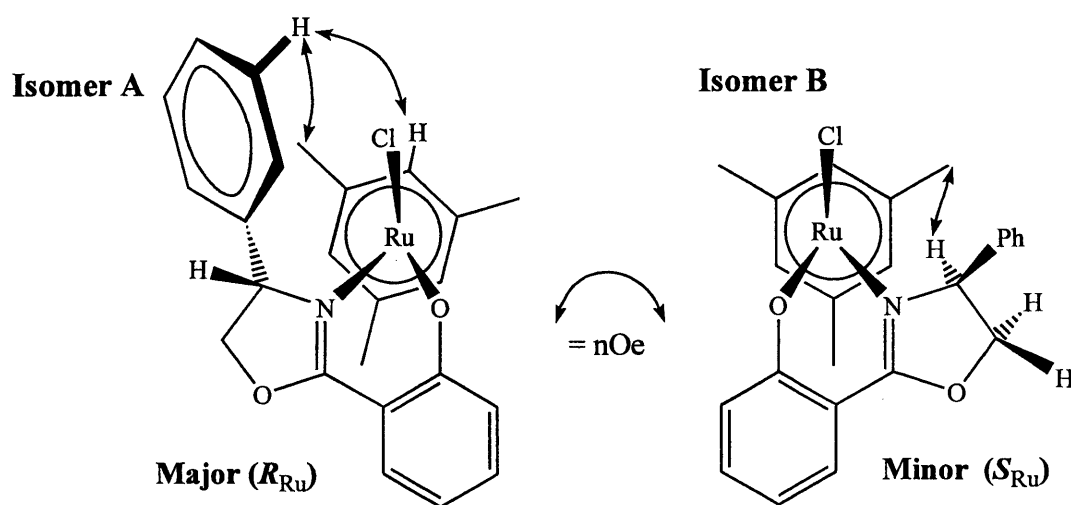
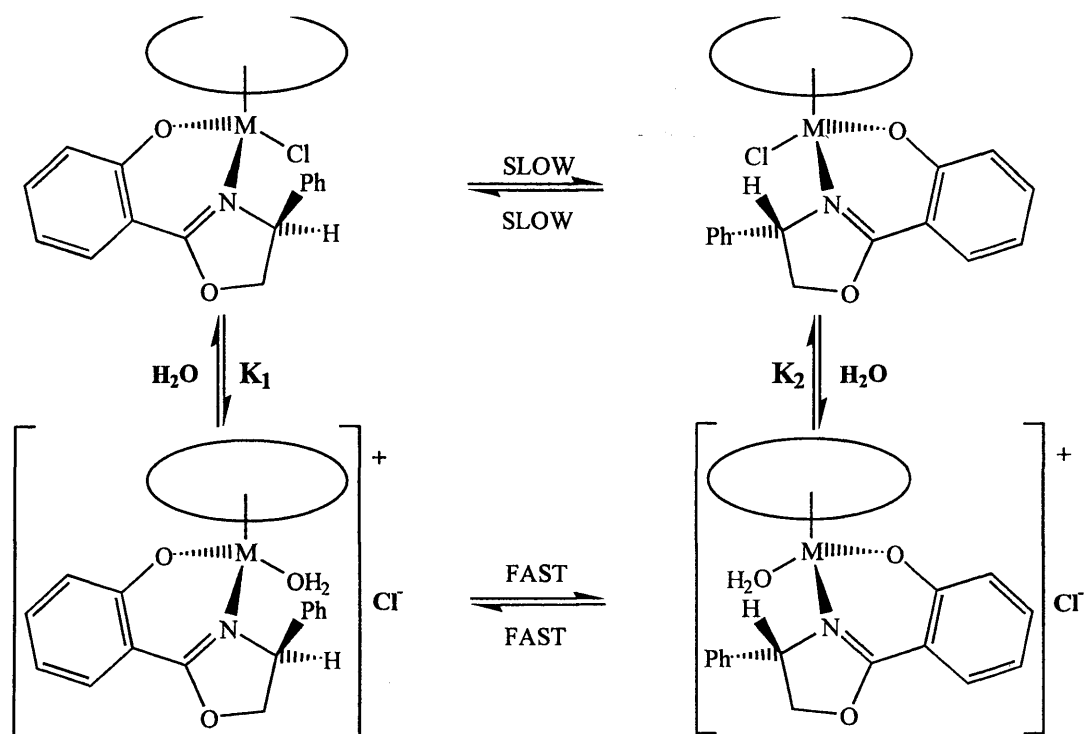


Figure (2.6): Predicted nOes for (2.12, R = Ph)

When complex (2.12, R = Ph) was dissolved in CD_2Cl_2 (not pre-dried) the signals observed in the 1H NMR spectrum (400 MHz) were broad, especially those of the minor isomer, suggesting that the rate of epimerisation had increased. This may be due to the presence of some water (observed in the spectrum at δ 1.62). The increased polarity of the solvent, could in principle effect the rate of epimerisation. In addition, water will aid solvation of dissociating chloride ligands and will stabilise the $16e^-$ intermediate by forming a cationic water complex (which may epimerise faster than the chloride complex) see **Scheme (2.8)**.¹⁰¹



Scheme (2.8)

The effect of water on the rate of exchange was tested by dissolving crystals of **(2.12, R = Ph)** in dry CD_2Cl_2 and recording the ^1H NMR spectrum. The signals, which were in the expected 40:60 ratio, were well-resolved indicating that epimerisation must be slower than the NMR timescale. Re-recording the spectrum after the addition of 2 drops of D_2O yielded signals with very broad line-widths, indicating that water does increase the rate of exchange. On cooling this sample to 233 K, the resulting spectrum contained well-resolved signals with an unchanged diastereomer ratio of 40:60, indicating that the equilibrium ratio had been reached and confirming it is unaffected by small amounts of water. This also suggests that the equilibrium between chloride and aqua-coordinated species is heavily in favour of chloride coordinated.

Complex **(2.13, R = ^tBu)** was synthesised to determine whether increasing the steric bulk of the R-substituent, from ⁱPr to ^tBu, will result in increased diastereoselectivity; *p*-cy complex **(2.13, R = ⁱPr)** is a mixture of diastereomers in ratio 89:11. The ^1H NMR spectrum of **(2.13, R = ^tBu)** contains only one set of sharp signals, indicating that it is formed with very high diastereoselectivity, as was found for **(2.12, R = ⁱPr, ^tBu)**. Recrystallisation from $\text{CH}_2\text{Cl}_2/\text{ether}$ gave crystals that were suitable for X-ray crystallography; the structure (discussed later-**Figure 2.13**, p 60) shows only one isomer (B) with the ^tBu-substituent towards the chloride, rather than towards the *p*-cy

ring. The observation of only one isomer by ^1H NMR suggests that the solid-state structure is retained in solution, as was found for (**2.12**, $\text{R} = \text{}^i\text{Pr}$, $\text{}^t\text{Bu}$).

The diastereoselectivity of ruthenium-phenmox complexes does depend on the size of the arene ring and the R-substituent, as predicted. For example, the C_6H_6 and *p*-cymene complexes (**2.13/2.14**, $\text{R} = \text{}^i\text{Pr}$) were present as *ca.* 89:11 mixtures of diastereomers, whilst with the bulkier arene mesitylene, only one isomer was observed by ^1H NMR, indicating very high diastereoselectivity. All other ruthenium-phenmox complexes were obtained, under the reaction conditions, with high diastereoselectivity except for (**2.12**, $\text{R} = \text{Bn}$, Ph), which were shown by ^1H NMR to be mixtures of isomers in ratio 79:21 and 24:76, respectively.

The ^1H NMR spectrum of the rhodium complex (**2.15**, $\text{R} = \text{}^i\text{Pr}$) recorded at RT in CDCl_3 contained one set of well-resolved signals suggesting that the complex was formed with very high diastereoselectivity ($\sim 100\%$ *d.e.*) or, that two diastereomers were interconverting quickly on the NMR timescale. Crystallisation from CH_2Cl_2 /ether gave X-ray quality crystals of (**2.15**, $\text{R} = \text{}^i\text{Pr}$). The crystal structure (discussed later-**Figure 2.10**, p 58) is similar to the arene-ruthenium complex (**2.12**, $\text{R} = \text{}^i\text{Pr}$) (isomer-B), with the isopropyl pointing towards the chloride, rather than the Cp^* , thus minimising unfavourable steric interactions. Since only one set of signals is observed by ^1H NMR spectroscopy it is assumed that the isomer-B structure of (**2.15**, $\text{R} = \text{}^i\text{Pr}$) is retained in solution.

The ^1H NMR spectra of the rhodium complexes (**2.15**, $\text{R} = \text{Bn}$, Ph) contain two sets of broad signals at room temperature, suggesting that both isomers, A and B, exist in solution and that epimerisation occurs on the NMR timescale. Confirmation of this was obtained by recording the ^1H NMR spectrum of (**2.15**, $\text{R} = \text{Ph}$) at 233 K; the broad signals resolved into two sets of sharp signals (one for each isomer) in an approximate ratio 76:24. Even at 233 K the signals for both isomers were still slightly broad {see **Figure (2.8)**}, suggesting that the epimerisation had not been 'frozen-out'. Thus, epimerisation of diastereomers of (**2.15**, $\text{R} = \text{Ph}$) is faster than racemisation of $[\text{RhCl}(\text{Me}_2\text{-phenmox})(\text{Cp}^*)]$ which can be frozen-out at 273 K as observed for related ruthenium complexes [(**2.13**, $\text{R} = \text{}^i\text{Pr}$) and (**2.14**) are faster than (**2.10**)].

To determine the configuration of the major diastereomer of (**2.15**, $\text{R} = \text{Ph}$) a phase-sensitive NOESY experiment was performed at 243 K in CDCl_3 (**Figure 2.8**). The presence of an nOe response in the major isomer between the NCH proton signal at δ 5.75 and the Cp^* signal at δ 1.23, and the absence of this nOe for the minor isomer,

suggests that the phenyl substituent is orientated towards the chloride (isomer-B) and not towards the ring. Hence the configuration of the rhodium centre is (*R*), while the Ph-phenmox chiral centre has an (*S*)-configuration. In addition to nOes, a chemical exchange cross-peak was observed between, the *OCH'* signal of isomer-B at δ 4.62 and the *OCH* signal of isomer-A at δ 4.17 (**Figure 2.7**). This cross-peak arises because the two protons are interchanging rapidly *i.e.* with a rate constant $k > 10^{-3} \text{ s}^{-1}$. The fast rate of the process, relative to the NMR timescale, is further exemplified by observation of an nOe between the *OCH* (pointing towards the Cp* in isomer-A) at δ 4.17 and the *OCH* (pointing towards the Cp* in isomer-B) at δ 4.80 (shown in **Figure 2.7**), *i.e.* between two non-interchangeable protons. This arises because the magnetisation energy carried through the chemical exchange process has not subsided before relaxation time T_1 has passed, and so can still give rise to a further nOe.

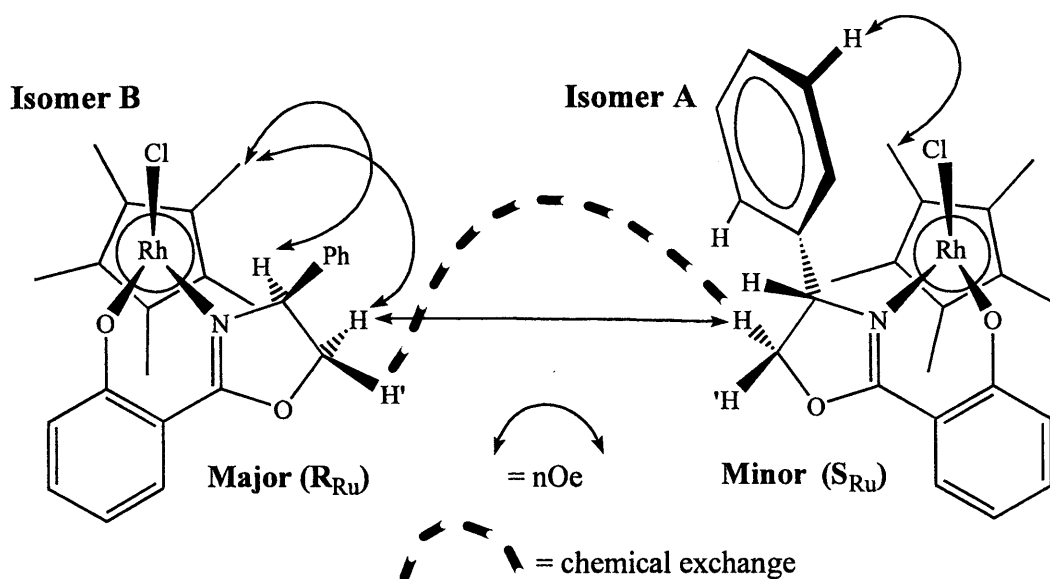
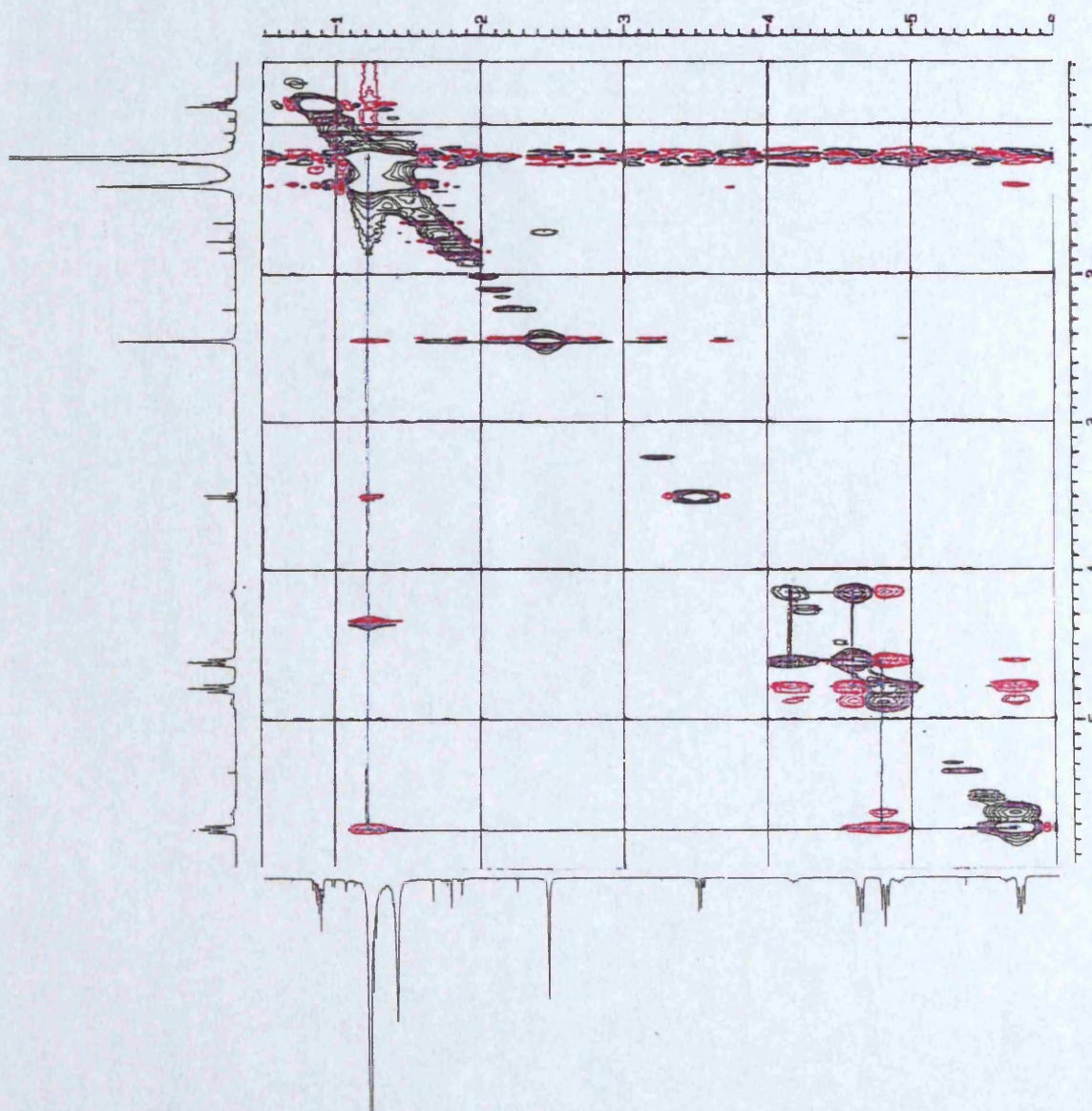


Figure (2.7): Observed cross-peaks in NOESY spectrum of (2.15, R = Ph)

Figure (2.8): ^1H - ^1H NOESY spectrum of (2.15, R = Ph) recorded in CDCl_3 at 243 K and 400 MHz.



As mentioned previously, recrystallisation from $\text{CH}_2\text{Cl}_2/\text{ether}$ gave X-ray quality crystals of rhodium complexes (**2.11**) and (**2.15**, $\text{R} = \text{}^i\text{Pr}$). The crystal structures of these complexes are shown in **Figures (2.9)** and (**2.10**), respectively, with selected bond lengths and angles in **Table (2.2)**. The complexes adopt the expected pseudo-octahedral structure, with the Cp^* ligand occupying three facial coordination sites of the rhodium. The crystal of (**2.11**) contained both enantiomers as expected for a racemate, (only the R_{Rh} enantiomer is shown in **Figure 2.9**). The crystal structure of (**2.15**, $\text{R} = \text{}^i\text{Pr}$) contains a single diastereomer, with the phenmox ligand coordinated such that the isopropyl group is pointing towards the Cl (isomer-B), instead of towards the Cp^* ring (isomer-A), thus minimising unfavourable steric interactions. The configuration at rhodium is (*R*) based on the priority sequence $\eta^5\text{-ring} > \text{Cl} > \text{O}_{\text{Ar.}} > \text{N}_{\text{ox.}}$ ^{104, 134} {the configuration at the chiral carbon is (*S*)}. The length of the Ru-N(1) bonds [2.105(4) and 2.097(4) Å] and the Ru-O(1) distances [2.092(3) and 2.084(4) Å] in (**2.11**) and (**2.15**, $\text{R} = \text{}^i\text{Pr}$), respectively, are statistically the same in each complex suggesting the rhodium isomer structural requirements are the same regardless of the ligand substituent. In contrast, the bite angle O-Rh-N(1) in (**2.15**, $\text{R} = \text{}^i\text{Pr}$), 87.1(2)°, is considerably larger than that 82.98(14)° for complex (**2.11**). This is evidence that the smaller bite angle is observed for complexes where a substituent (Ph or Me) is orientated towards the polyhapto-ring (isomer-A structure).

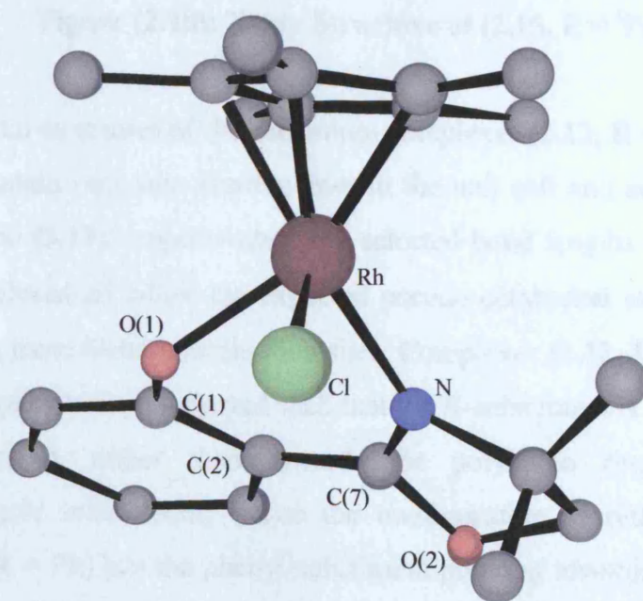
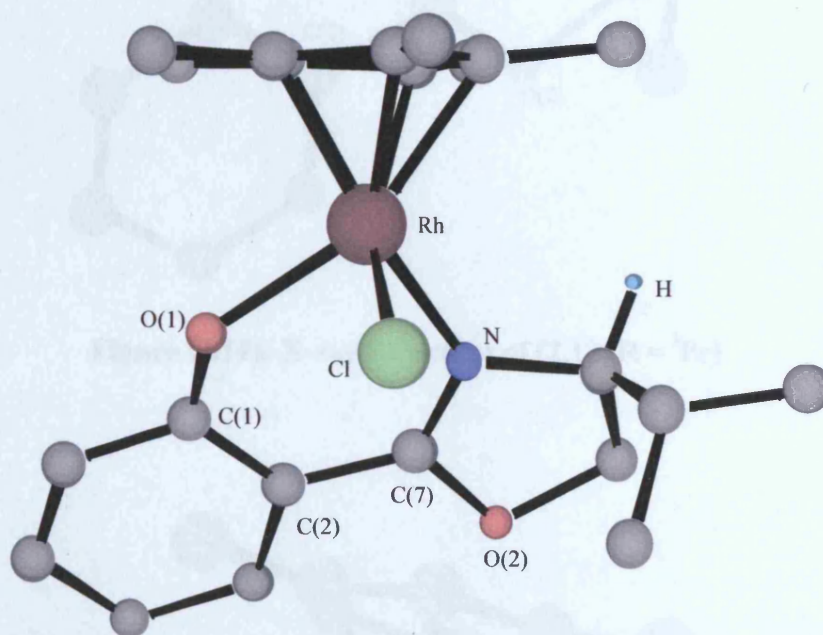


Figure (2.9): X-ray Structure of (R_{Rh} 2.11)

Table (2.2): Selected Bond Distances (Å) and Angles (°) of (2.11) and (2.15, R = ⁱPr)

	(2.11)	(2.15, R = ⁱ Pr)		(2.11)	(2.15, R = ⁱ Pr)
Rh – N(1)	2.105(4)	2.097(4)	O(1)–C(1)	1.311(6)	1.291(7)
Rh – O(1)	2.092(3)	2.084(4)	C(1)–C(2)	1.419(7)	1.431(7)
Rh – Cl(1)	2.4210(13)	2.414(2)	C(2)– (7)	1.450(7)	1.437(8)
N(1)-Rh-O(1)	82.98(14)	87.1(2)	N(1)–C(7)	1.295(6)	1.310(7)
N-C(7)-C(2)-C(1)	15.8(6)	3.5(9)	-	-	-

**Figure (2.10): X-ray Structure of (2.15, R = ⁱPr)**

The crystal structures of the ruthenium complexes (**2.12**, R = ⁱPr, Ph) and (**2.13**, R = ^tBu) all contain only one diastereomer in the unit cell and are shown in **Figures (2.11), (2.12) and (2.13)**, respectively, with selected bond lengths and angles in **Table (2.3)**. The complexes all adopt the expected pseudo-octahedral structure with the η^6 -arene occupying three facial coordination sites. Complexes (**2.12**, R = ⁱPr) and (**2.13**, R = ^tBu) have the phenmox coordinated such that the R-substituent is pointing towards the chloride (isomer-B), rather than towards the polyhapto ring, thus minimising unfavourable steric interactions; hence the configuration at ruthenium is (R_{Ru}). In contrast, (**2.12**, R = Ph) has the phenyl substituent pointing towards the mesitylene ring (isomer-A), rather than towards the chloride, giving an (S_{Ru}) configuration.

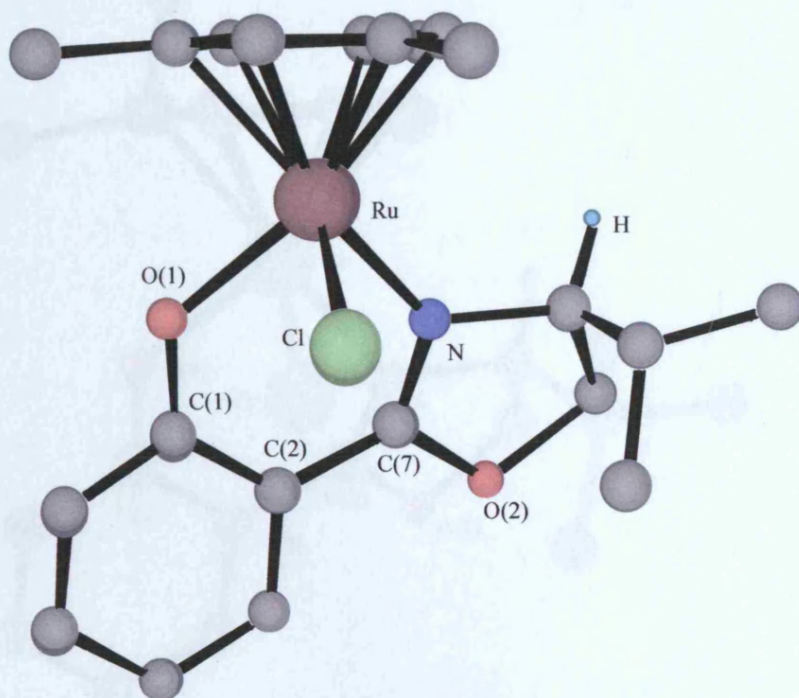


Figure (2.11): X-ray Structure of (2.12, R = ⁱPr)

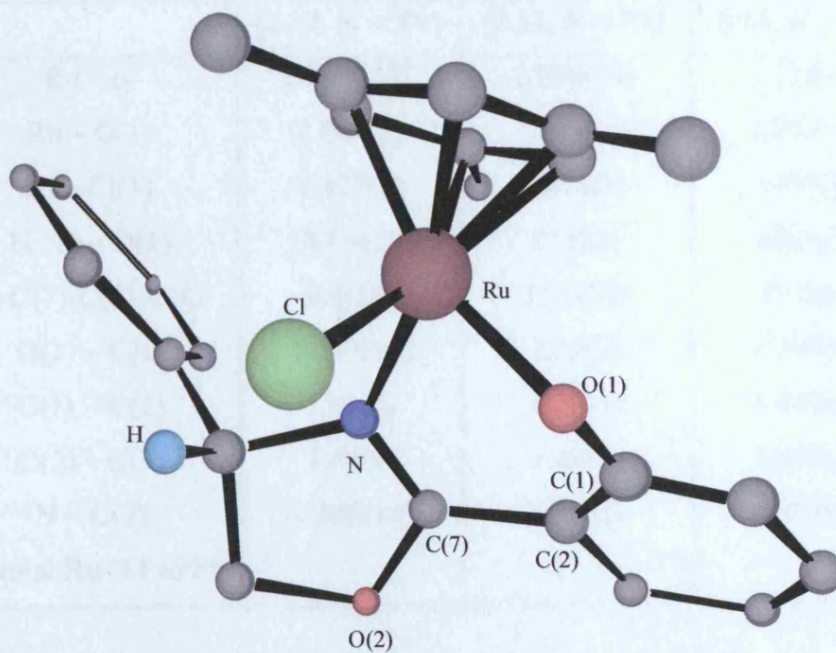


Figure (2.12): X-ray Structure of (2.12, R = Ph)

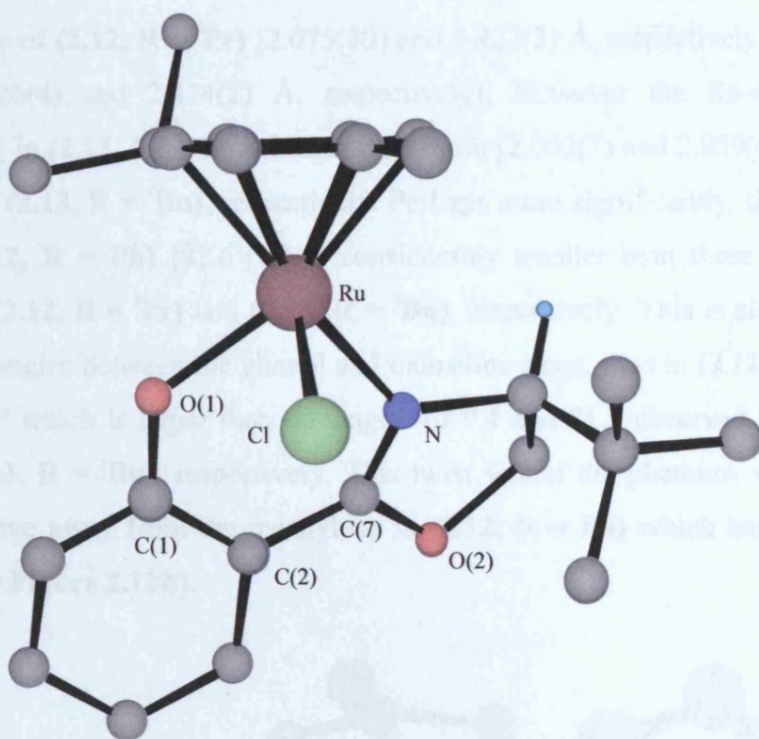


Figure (2.13): X-ray Structure of (2.13, R = ^tBu)

Table (2.3): Selected Bond Distances (Å) and Angles (°) of (2.12, R = ⁱPr, Ph) and (2.13, R = ^tBu)

	(2.12, R = ⁱ Pr)	(2.12, R = Ph)	(2.13, R = ^t Bu)
Ru – N	2.075(10)	2.098(14)	2.126(4)
Ru – O(1)	2.062(7)	2.106(12)	2.059(4)
Ru– Cl(1)	2.427(3)	2.418(5)	2.414(2)
N–Ru– O(1)	87.0(3)	82.6(5)	88.3(2)
N–C(7)–C(2)–C(1)	9.4(18)	31.3(24)	21.5(9)
O(1) – C(1)	1.299(13)	1.32(2)	1.309(6)
C(1) – C(2)	1.41(2)	1.39(3)	1.410(8)
C(2) – C(7)	1.44(2)	1.48(3)	1.444(7)
N – C(7)	1.295(14)	1.28(2)	1.294(6)
Normal Ru-X1 to Ph	-	41.7	-

It is interesting to consider whether there are significant differences in the structures for those adopting an isomer-B structure (2.12, R = ⁱPr) and (2.13, R = ^tBu), and (2.12, R = Ph) which adopts an isomer-A structure. The Ru–N and Ru–Cl(1) distances [2.098(14) and 2.418(5) Å, respectively] for (2.12, R = Ph) are intermediate

between those of (**2.12**, **R** = ^{*i*}**Pr**) [2.075(10) and 2.427(3) Å, respectively] and (**2.13**, **R** = ^{*t*}**Bu**) [2.126(4) and 2.414(2) Å, respectively]. However the Ru–O(1) distance [2.106(12) Å] in (**2.12**, **R** = **Ph**) is longer than those [2.062(7) and 2.059(4) Å] in (**2.12**, **R** = ^{*i*}**Pr**) and (**2.13**, **R** = ^{*t*}**Bu**), respectively. Perhaps more significantly, the chelate bite angle of (**2.12**, **R** = **Ph**) [82.6°(5)] is considerably smaller than those [87.0°(3) and 88.3°(2)] of (**2.12**, **R** = ^{*i*}**Pr**) and (**2.13**, **R** = ^{*t*}**Bu**), respectively. This is also reflected in the dihedral angles between the phenol and oxazoline rings, thus in (**2.12**, **R** = **Ph**) this angle is 31.3° which is larger than the angles of 9.4 and 21.5 observed for (**2.12**, **R** = ^{*i*}**Pr**) and (**2.13**, **R** = ^{*t*}**Bu**), respectively. This twist within the phenmox may allow the phenyl to move away from the mesitylene in (**2.12**, **R** = **Ph**) which has an isomer-A structure (see **Figure 2.12b**).

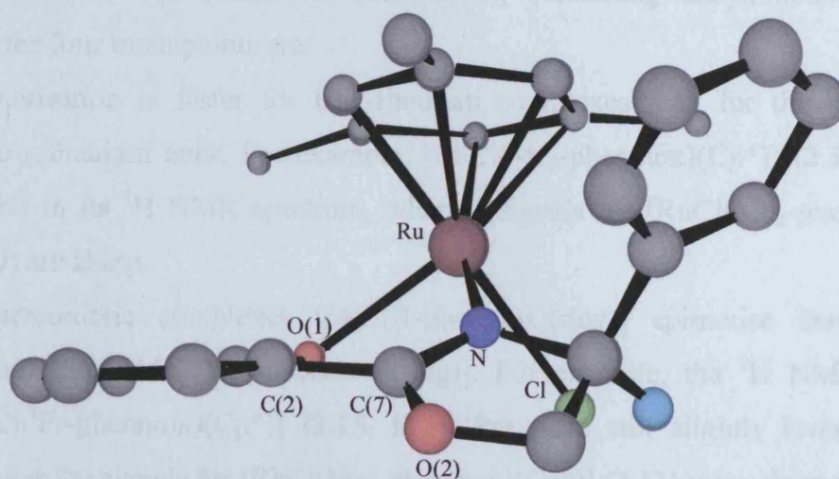


Figure (2.12b): X-ray Structure of (2.12, R = Ph)

The reason(s) for the differences in structure between the major isomers when **R** = **Ph** compared to **R** = **Bn**, ^{*i*}**Pr** and ^{*t*}**Bu** is (are) not clear. The interactions that are likely to be the most critical are those between the **R**-substituent and chloride (in isomer-B) *and* those between the **R**-substituent and mesitylene (in isomer-A). When **R** = ^{*t*}**Bu** or ^{*i*}**Pr** only isomer-B is observed, yet when **R** = **Bn** or **Ph** a mixture of isomers-(A + B) is formed. A possible explanation is that since ^{*t*}**Bu** and ^{*i*}**Pr** groups are bulky in 3-dimensions isomer-A is particularly unfavourable; whereas, with **Ph** and **Bn** either the more planar nature of the substituents allows them to orient to reduce interactions or, some π – π interactions may even stabilise isomer-A (see below).

The distances between the centroids of the mesitylene and the **Ph** rings is 5.101 Å in (**2.12**, **R** = **Ph**) which is slightly larger than the distance, 4.74 Å, for related Schiff-

base complex $[\text{RuCl}(\text{pyrrolealdimine})(\text{C}_6\text{H}_6)]$ (**1.38**), which exhibits a ‘ β -phenyl-effect’.⁹⁶ Also, the angle between the ring normals was smaller in (**2.12**, **R = Ph**), 41.7° , compared to 51.3° for Brunner’s complex, this indicates that less of an edge-to-face interaction exists and that it is far from ideal (90.0°) in (**2.12**, **R = Ph**). The presence of a “ β -Ph-effect” in (**1.35 – 1.39**) is also apparent from high field shifts of the η^6 -arene in the ^1H NMR spectra. The signals for mesitylene in (**2.12**, **R = Ph**) are observed at δ 4.22 (isomer-A) and δ 4.64 (isomer-B), a rather larger separation (0.42 ppm) than is found for $[\text{RuCl}(\text{Ph-pymox})(\text{mes})]^+$ (**1.42**, **R = Ph**) [δ 5.25 (isomer-A) and δ 5.08 (isomer-B)] with no “ β -Ph-effect”, with isomer-A to higher field consistent with a “ β -Ph-effect” in this isomer of (**2.12**, **R = Ph**).

Thus for the complexes (**2.10–2.15**), containing unsymmetrical phenmox ligands, the four main points are:

1. Epimerisation is faster for Cp^* -rhodium complexes than for the corresponding arene-ruthenium ones. For example, $[\text{RhCl}(\text{Me}_2\text{-phenmox})(\text{Cp}^*)]$ (**2.11**) has broad signals in its ^1H NMR spectrum, whereas signals for $[\text{RuCl}(\text{Me}_2\text{-phenmox})(\text{mes})]$ (**2.10**) are sharp.
2. Diastereomeric complexes $[\text{MCl}(\text{R-phenmox})(\text{ring})]$ epimerise faster than the enantiomeric $[\text{MCl}(\text{Me}_2\text{-phenmox})(\text{ring})]$. For example, the ^1H NMR signals of $[\text{RhCl}(\text{}^i\text{Pr-phenmox})(\text{Cp}^*)]$ (**2.15**, **R = ${}^i\text{Pr}$**) were still slightly broad at 233 K, whereas the signals for $[\text{RhCl}(\text{Me}_2\text{-phenmox})(\text{Cp}^*)]$ (**2.11**) were sharp at 273 K.
3. The diastereoselectivity depends on the oxazoline-substituent (R) and, for ruthenium complexes, on the arene. Using large alkyl groups (${}^t\text{Bu}$, ${}^i\text{Pr}$) and bulky arenes, a single diastereomer can be formed with complete selectivity. For example mesitylene complexes (**2.12**, **R = ${}^i\text{Pr}$, ${}^t\text{Bu}$**), *p*-cy complex (**2.13**, **R = ${}^t\text{Bu}$**) and Cp^* -rhodium complexes (**2.15**, **R = ${}^i\text{Pr}$, ${}^t\text{Bu}$**).
4. Where mixtures of diastereomers are formed isomer-B is usually preferred except when **R = Ph** when isomer-A may be more favourable.

It is useful to compare the results with phenmox complexes with previous work on Schiff bases (see Chapter One): i) epimerisation and ii) diastereoselectivity.

The Schiff-base complexes (**1.34/1.35**, **1.36-1.38** and **1.39-1.41**) discussed in Section (1.4.3) were all found to epimerise, for Schiff-base complexes (**1.34-6**, **1.38-1.41**) the rates depended on the donor-atom type, overall charge and solvent. The

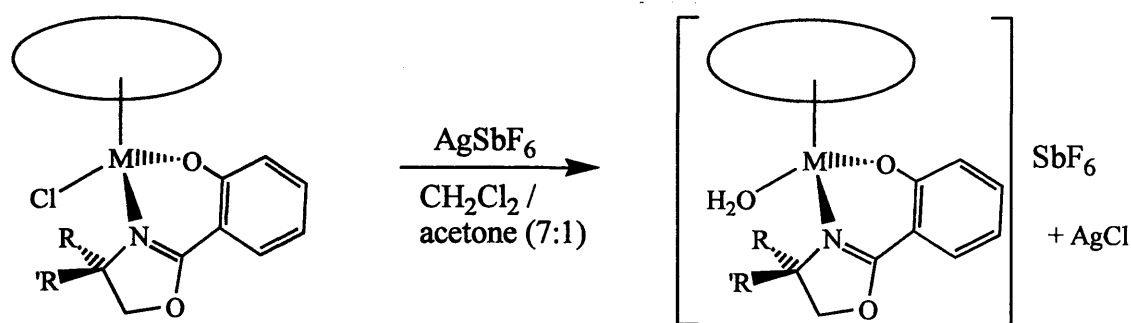
diastereomers of (1.34/1.35), containing anionic salicylalimine Schiff-base ligand (L^4), were found to exchange rapidly on the chemical timescale, even at $-80\text{ }^\circ\text{C}$.^{91, 92} In addition, the chloride ligands of Schiff-bases (1.39/1.40) and amino-acidate complexes were displaced by treatment with D_2O , providing a low energy route to epimerisation.^{73, 75, 78} Likewise, for phenmox complexes (2.12-2.14) epimerisation was fast on the chemical timescale and addition of D_2O increased the rate of exchange, however, the thermodynamic equilibrium position favours isomer-B (with a notable exception of 2.12, $R = Ph$); thus, the lack of configurational stability should not affect their application in asymmetric catalysis.

The diastereoselectivity of the phenmox complexes compare favourably with those of many ruthenium half-sandwich complexes. For example, the arene-ruthenium Schiff-base complexes discussed earlier (1.34-6, 1.38-1.40), which were all formed as mixtures of diastereomers with equilibrium diastereomer ratios ranging from 67:33⁷⁵ to 86:14.^{91, 92, 96} The lower diastereoselectivity exhibited by pyrrolocarbaldimine and pyridylimine complexes is controlled by rotation of the $N-CH(Me)Ph$ bond in the Schiff-base ligands, which are all derived from (*S*)-1-phenylethylamine. Even though certain orientations of the imine substituent are favoured in some instances (resulting from the ' β -phenyl-effect'), the energy difference between the two isomers is insufficient to give exclusively one diastereomer. However, for (2.13-2.15) the oxazoline-substituents (R) are only able to rotate about the $C-C$ bonds not the $C-N$ bond, hence they are orientated either towards the η -ring (isomer-A) or towards the chloride ligand (isomer-B). As a result changing these substituents and those on the arene allow a means to control the diastereoselectivity.

Changing the chloride ligand should alter the diastereoselectivity and may also effect the rate of epimerisation. Hence, this section, will describe the substitution of phenmox complexes with OH_2 , Me, *N*-donor, *P*-donor or larger halide ligands at the sixth coordination site of the metal. The effect on the diastereoselectivity when increasing the steric bulk and/or altering the electronic properties of the unidentate ligand will be assessed. These ligands may also give an indication of the effect of size and nature (of ligand) on the rate of diastereomer exchange with implications for the selectivity of a catalysed reaction.

Aqua complexes, $[M(OH_2)(R,R'-phenmox)(ring)](SbF_6)$, (2.16-2.18) were synthesised from the chloride precursors by abstraction of chloride with $AgSbF_6$ in

CH₂Cl₂/acetone (8:1) **Scheme (2.9)**, the aqua ligand being provided by traces of water in the acetone (not pre-dried).



2.11 M = Rh R = Me R' = Me Ring = Cp* **2.16**

2.12 M = Ru R = ⁱPr, Ph R' = H Ring = mes **2.17**

2.15 M = Rh R = ⁱPr R' = H Ring = Cp* **2.18**

Scheme (2.9)

Pure complexes were isolated by filtration of the crude reaction mixture through celite, to remove the AgCl by-product. The cationic aqua complexes were moderately hygroscopic and recrystallisations usually resulted in oily products, consequently characterisation has relied on NMR, mass spectrometry and elemental analyses (where possible) (**Tables 2D.1 - 2D.3**, p 126; see Experimental Section), though an X-ray structure was determined for (**2.16**). The water ligands of the analogous pymox,¹⁰⁰ salicylaldehyde (**L**⁴)⁹⁴ and bis-oxazoline-propane (**1.9**)²⁴ aqua complexes are more labile than the chloride ligand of the respective precursor complexes. As a result, exchange/epimerisation is expected to be more rapid with the aqua complexes. Complexes (**2.16–2.18**) were all only sparingly soluble in CDCl₃ so their ¹H NMR spectra were recorded in CD₂Cl₂.

Rhodium complex (**2.16**), containing the achiral Me₂-phenmox ligand exists as a racemate. The prochiral methyl groups make it an ideal complex to examine water exchange and racemisation, without the added complication of having two possible diastereomers (as discussed in Section 1.3.2). The ¹H NMR signals due to the phenmox and Cp* ligands of (**2.16**) are all deshielded (by 0.3–0.6 ppm) compared to the neutral chloride precursor (**2.11**), as expected for a cationic complex. The protons of the NCM₂ and OCH₂ groups were both observed as singlets, suggesting that epimerisation at the metal is fast on the NMR timescale making each group of protons appear

equivalent (see **Scheme 2.7**). At room temperature a signal for coordinated water was not observed most probably due to rapid exchange between free and coordinated water and/or fast proton/deuterium exchange. Even at 223 K and 400MHz the rate of interconversion had not slowed sufficiently for the NCMe_2 , OCH_2 and OH_2 signals to be resolved. This indicates that the rate of interconversion is faster than in the analogous dicationic $[\text{Rh}(\text{OH}_2)(\text{Me}_2\text{-pymox})\text{Cp}^*][\text{SbF}_6]_2$ complex, for which, the signals due to the NCMe_2 and OCH_2 protons resolved into sharp singlets and doublets, respectively.¹⁰⁰ Neither FAB nor electrospray (MeOH/water) mass spectrometry revealed the molecular ion peak expected at m/z 446, the major ion being observed at m/z 428, attributed to $[\text{Rh}(\text{Me}_2\text{-phenmox})\text{Cp}^*]^+$.

Crystallisation of **(2.16)** from $\text{CH}_2\text{Cl}_2/\text{ether}$ gave X-ray quality crystals. The X-ray structure shown in **Figure (2.13)**, with selected bond lengths and an angle given in **Table (2.4)**, confirms that water is coordinated to the metal. The Rh–N [2.114(4) Å] and Rh–O(2) [2.098(3) Å] bond lengths and the O(2)–Rh–N(1) bond angle [82.1(2)°] are similar to those of the corresponding neutral chloride complex **(2.11)** [2.105(4), 2.092(3) Å and 82.98(14)°, respectively]. Indicating that the geometry of the $\text{Rh}(\text{Me}_2\text{-phenmox})\text{Cp}^*$ fragment is relatively unperturbed by substitution of chloride by water.

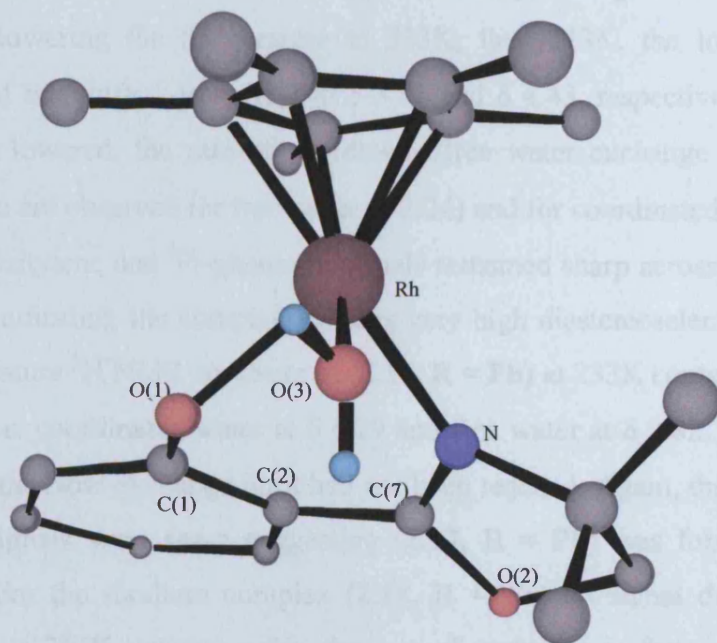


Figure (2.14): X-ray Structure of the cation (2.16)

Table (2.4): Selected Bond Distances (Å) and Angles (°) of (2.16)

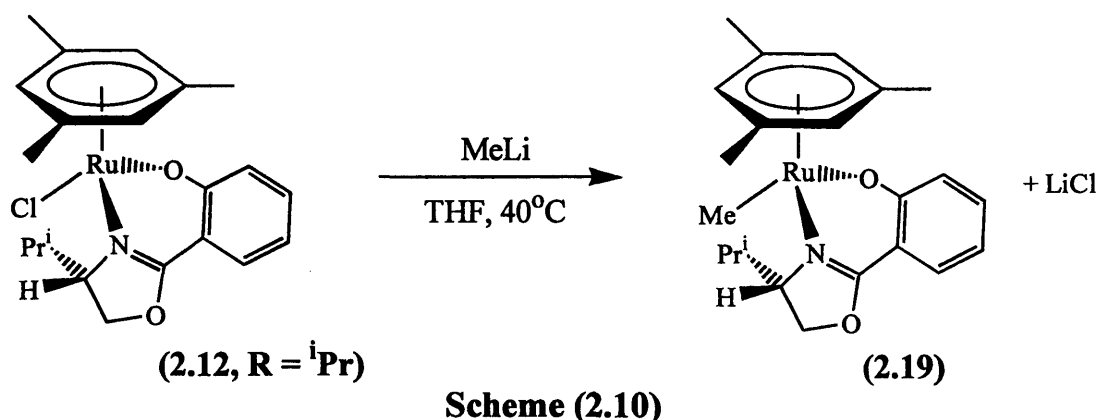
Rh(1) – N(1)	2.114 (4)	O(1) – C(1)	1.334 (6)
Rh(1) – O(1)	2.098 (3)	C(1) – C(2)	1.411 (7)
Rh(1) – O(3)	2.89 (4)	C(2) – C(7)	1.443 (7)
O(1) -Rh- N(1)	82.1 (2)	N(1) – C(7)	1.304 (7)

The ^1H NMR spectra of the diastereomeric complexes (2.17–2.18) each show the presence of only one isomer [including that of (2.17, R = Ph), for which the chloride precursor showed two isomers]. The signals for the aryl protons of the phenmox ligand and the polyhapto ring are deshielded (by 0.3–0.5 ppm), as found for (2.16). At room temperature no signal is observed for coordinated water or free water, suggesting that exchange of coordinated/free water (alternatively proton/deuterium exchange) is occurring rapidly on the NMR timescale. Thus interconversion of the two possible diastereomers may be occurring rapidly on the NMR timescale leading to only one set of time-averaged signals in the ^1H NMR spectra. To investigate this, the spectrum of (2.17, R = ^iPr) was recorded at lower temperatures. At 253 K a broad singlet at δ 3.16 and a very broad signal at δ 2.24 (partially masked by the signal for $\text{C}_6\text{H}_3\text{Me}_3$) were observed; on lowering the temperature to 233K, then 213K, the lower-field signal remained broad but shifted downfield to δ 3.81 and δ 4.43, respectively. Thus, as the temperature is lowered, the rate of coordinated/free water exchange slows such that separate signals are observed for free water (δ 2.24) and for coordinated water (δ 4.43 at 213K). The mesitylene and ^iPr -phenmox signals remained sharp across the temperature range studied indicating the complex exhibits very high diastereoselectivity. Similarly, the low temperature ^1H NMR spectrum of (2.17, R = Ph) at 233K contained two signals due to water, *i.e.* coordinated water at δ 6.29 and free water at δ 2.82, which were still broad because the slow exchange limit had not been reached. Again, the mesitylene and Ph-phenmox signals were sharp suggesting (2.17, R = Ph) was formed as a single diastereomer. For the rhodium complex (2.18, R = ^iPr) no signal due to water was observed even at 233K indicating that the rate of exchange is faster for the rhodium complex than for the ruthenium-mesitylene derivative as found for the chloride complexes described earlier. For rhodium, the Cp* and ^iPr -phenmox signals remained sharp, suggesting high diastereoselectivity, but the possibility of time-averaged spectra cannot be ruled out. The ruthenium complex (2.17, R = ^iPr) also contained a sharp

singlet at δ 2.21 (6H), which was assigned to free acetone. This signal integrated to precisely one equivalent of acetone relative to the rest of the spectrum, possibly indicating that acetone was coordinated in the solid state and then exchanged for water in solution (*i.e.* from the NMR solvent).

The electrospray (recorded in MeOH/water) and FAB mass spectra of complexes (2.17–2.18) (Table 2D.3; see Experimental Section) contain a single ion pattern, due to $[M(R\text{-phenmox})(\text{ring})]^+$ ($M = \text{Ru}$, ring = mes, $R = {}^i\text{Pr}$, Ph; $M = \text{Rh}$, ring = Cp*, $R = {}^i\text{Pr}$). As for (2.16), coordinated water is not sufficiently strongly bound to be observed in the molecular ion.

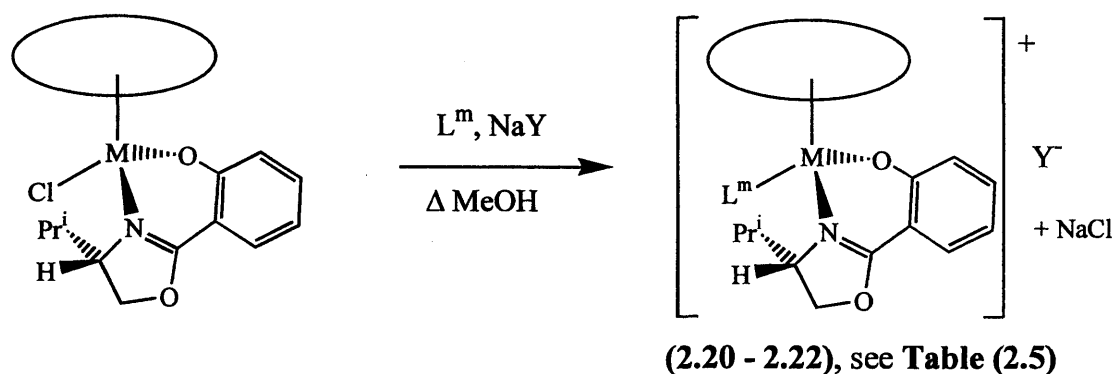
The complex $[\text{RuMe}({}^i\text{Pr}\text{-phenmox})(\text{mes})]$ (2.19) was prepared by treating the chloride precursor (2.12, $R = {}^i\text{Pr}$) with one equivalent of MeLi in THF at 40 °C (Scheme 2.10). The reaction was monitored by electrospray mass spectrometry; the observation of ions m/z 440 indicates the presence of $[\text{RuMe}({}^i\text{Pr}\text{-phenmox})(\text{mes})]^+$ whilst ions at m/z 426 $[\text{Ru}({}^i\text{Pr}\text{-phenmox})(\text{mes})]^+$ could arise from (2.19) or chloride starting complex.



Complex (2.19) was characterised by a combination of mass spectrometry, ${}^1\text{H}$ NMR and ${}^1\text{H}$ - ${}^1\text{H}$ -NOESY NMR spectroscopy (see Experimental Section). The ${}^1\text{H}$ NMR spectrum showed a 3H singlet at δ 0.87 for the Ru–Me. Only one isomer is observed both at room temperature and at 233K; suggesting (2.19) was formed with high diastereoselectivity. In this case rapid epimerisation by loss of Me^- would not be expected. The chemical shifts of (2.19) are similar to those of the chloride precursor, with the exception of the isopropyl proton at δ 2.02, which is observed at δ 2.80 in the chloride precursor and at δ 1.80 in the free ligand. The large downfield shift in the chloride complex may be due to the electronegativity of the Cl^- atom in close proximity. Crystallisation failed to yield X-ray quality crystals so identification of the preferred

diastereomer was achieved by a phase-sensitive NOESY experiment. An nOe was observed between the mesitylene $C_6H_3Me_3$ singlet at δ 4.42 and the NCH proton at δ 3.96, indicating that isomer-B is formed with the isopropyl group directed towards the methyl ligand, rather than towards the mesitylene ring. Interestingly, an nOe was observed between the Ru–Me singlet at δ 0.87 and the mesitylene $C_6H_3Me_3$ singlet at δ 4.42.

The complexes $[ML^m(\text{Pr-phenmox})(\text{ring})]Y$ (**2.20–2.22**) were prepared by treating the appropriate chloride precursor with ligand L^m and NaY ($Y^- = SbF_6$ or BPh_4) in methanol at reflux (**Scheme 2.11**).



Scheme (2.11)
Table (2.5)

Code	M	L^m	Ring	Y^-
2.20	Ru	4-Me-py, 2-Me-py, Py	mes	SbF_6
2.21	Ru	PPh_3	mes	BPh_4
2.22	Rh	4-Me-py, Py	Cp^*	SbF_6

Complexes (**2.20–2.22**) are all soluble in $CDCl_3$ except for (**2.20**, $L^m = PPh_3$), which is soluble in CD_2Cl_2 . The complexes were characterised by a combination of X-ray crystallography; mass spectrometry; microanalyses; 1H NMR; 1H - 1H COSY and 1H - 1H NOESY NMR spectroscopy (**Tables 2E.2 - 2E.4**, p 134). The 1H NMR spectra of (**2.20–2.22**) all contain two sets of signals, except for (**2.20**, $L^m = 2\text{-Me-py}$), indicating that in each case two diastereomers are formed.

The 1H NMR signals of (**2.20**, $L^m = py$) are reasonably broad at RT, though a diastereomer ratio of 84:16 could be measured from the integrals of the 1H NMR signals of the Ar-6-H at δ 7.91(7.69) or the mesitylene methyls at δ 2.06(2.17), minor isomer shifts in parentheses, suggesting that the two isomers are interconverting at a similar rate to the NMR timescale. This ratio didn't change with time indicating the equilibrium

position had been reached. Hence the spectrum was recorded at low temperature (253K), sharp signals for two isomers were observed in an 84:16 ratio, identical to that at room temperature, indicating that the rate of epimerisation was slow compared to the NMR timescale at 253K. The isopropyl signals of the major isomer at δ -0.09, 0.87 (*CHMeMe'*) and 1.36 (*CHMeMe'*) are at higher frequency than those of the minor isomer (δ 0.76, 1.11 and 2.41, respectively). These shifts to higher field (up to 1.05 ppm) for the major isomer are thought to be due to the localised 'ring-current' of the pyridine ring, indicating that the isopropyl group is in close proximity. The signals for the coordinated pyridine overlapped with those of the phenmox ligand at room temperature and at low temperature making the ^1H NMR and 2-D NMR spectra difficult to interpret fully. To overcome this problem, and to try and obtain X-ray quality crystals the structurally related complex (**2.20**, $\text{L}^{\text{m}} = 4\text{-Me-py}$) was synthesised. The ^1H NMR spectrum of this complex at room temperature also contained two sets of broad signals in a ratio of 85:15. As found for (**2.20**, $\text{L}^{\text{m}} = \text{py}$), the isopropyl signals of the major isomer were shifted to higher field and the remaining signals were at similar chemical shifts to those of the pyridine derivative. To determine whether the major species in the NMR spectrum exhibits an isomer-A or -B structure the phase-sensitive ^1H - ^1H NOESY NMR spectrum was recorded at 273 K in CD_2Cl_2 . The most important structural determining nOes are shown in **Figure (2.15)**. Cross-peaks are observed for the major isomer between all the ^iPr signals (δ 0.1, 0.85 and 1.32) and the 4-*Me*-py protons at δ 2.48. These nOes are consistent with the major diastereomer having isomer-B structure in solution and they also support the suggestion that the highfield shifts of the isopropyl protons is due to a ring-current effect of the 4-*Me*-py. When the NOESY spectrum was recorded at room temperature, additional cross-peaks due to chemical exchange between isomer A and B were observed, for example, between the protons at δ 0.1 (*Me'*CHMe isomer-B) and δ 0.8 (*Me'*CHMe isomer-A) and between the signals at δ 7.54 (*Ar-6-H* isomer-B) with δ 7.02 (*Ar-6-H* isomer-A). On cooling this sample to 273 K the broad singlet at δ 0.73 for the *Me'*CHMe protons (of the minor isomer) resolved in to a doublet.

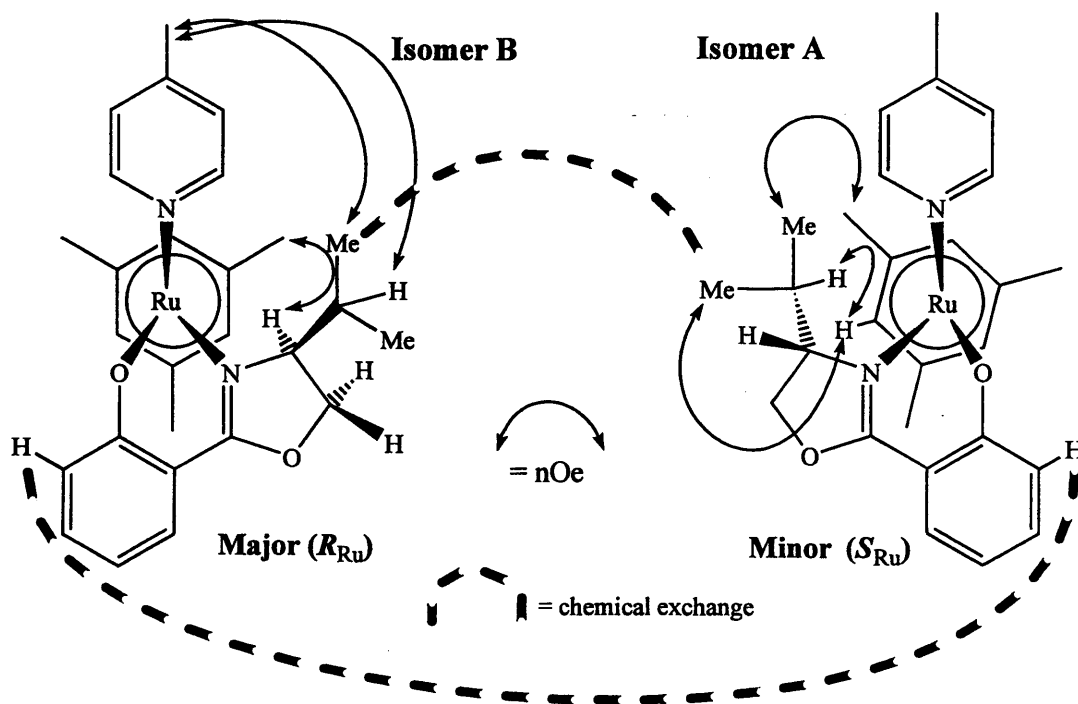


Figure (2.15): Observed nOes for (2.20, $L^m = 4\text{-Me-py}$)

Crystallisation from $\text{CH}_2\text{Cl}_2/\text{ether}$ gave X-ray quality crystals that had uniform morphology. The X-ray crystal structure is shown in (Figure 2.16), with selected bond lengths and angles in (Table 2.6). The crystals are of a single diastereomer with the $i\text{Pr}$ group directed towards the 4-Me-pyridine, which means the configuration of the Ru centre, can be assigned as (R_{Ru}) ($\text{mes} > \text{O} > \text{N}_{(\text{ox})} > \text{N}_{(4\text{-Me-py})}$).

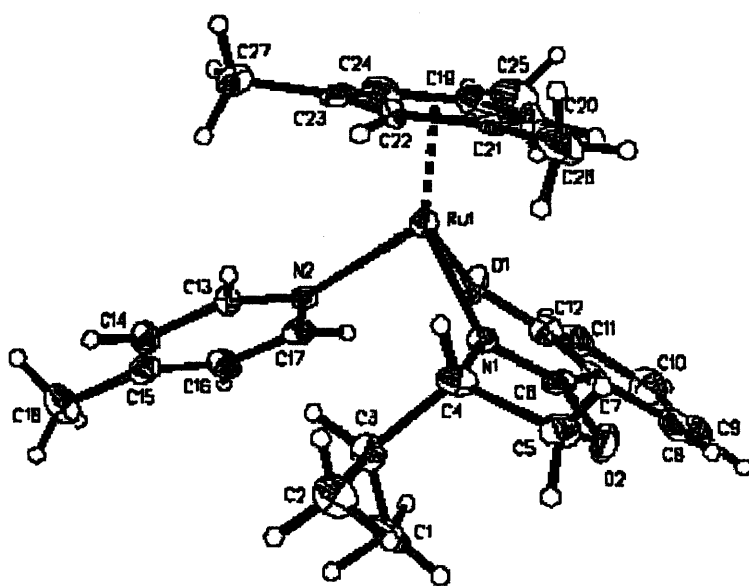


Figure (2.16): X-ray Structure of the cation (2.20, $L^m = 4\text{-Me-py}$)

Table (2.6): Selected Bond Distances (Å) and Angles (°) of (2.20, L^m = 4-Me-py)

Ru - N(1)	2.108 (9)	O(1) - C(12)	1.31 (2)
Ru - O(1)	2.037 (9)	C(12) - C(7)	1.40 (2)
Ru - N(2)	2.152 (10)	C(7) - C(6)	1.49 (2)
O(1) - Ru - N(1)	84.2 (4)	C(6) - N(1)	1.29 (2)

Comparing (2.20, L^m = 4-Me-py) with the precursor chloride (2.12, R = ⁱPr), the Ru–O bond lengths are similar [2.037(9) and 2.062(7) Å, respectively], whilst the Ru–N(1)_{ox} bond is slightly longer in (2.20, L^m = 4-Me-py), 2.108(9) Å compared to 2.075(10) Å. The length of the Ru–N(2)_{4-Me-py} bond for (2.20, L^m = 4-Me-py) [2.152(10) Å] is similar to that of the related salicylaldimine (L⁴) complex [Ru(4-Me-py)(L⁴)(C₆H₆)]PF₆ [2.138(5) Å].⁹¹ Dissolution of the X-ray crystal sample at approximately 193K and then recording the ¹H NMR spectrum at 203K gave a spectrum that contained two sets of well-resolved signals. The diastereomer ratio (93:7), calculated from the integrals, was different to the ratio at room temperature (85:15). On warming to 213K, then 233K, the diastereomer ratio changed to 92:8, then 90:10 and finally reached equilibrium (85:15) at 253K, after which there was no further change with time. These observations show that epimerisation occurs even at 203K over 1-2 hrs. The ¹H NMR spectrum of the mother liquor showed two isomers in 85:15 ratio, confirming that epimerisation had occurred to restore the equilibrium. These findings are consistent with those for [Ru(4-Me-py)(L⁴)(C₆H₆)]PF₆,⁹¹ for which dissolution of crystals in d₆-acetone at –80 °C showed the complex to be one diastereomer by ¹H NMR, which on warming to –35 °C, epimerised to reach equilibrium after several hours.⁹¹ From the low temperature dissolution and NOESY ¹H NMR experiments it can be inferred that the solid state structure (isomer-B) of (2.20, L^m = 4-Me-py) is retained in solution as the major diastereomer.

The complex [Ru(2-Me-py)(ⁱPr-phenmox)(mes)]SbF₆ (2.20, L^m = 2-Me-py) was synthesised to evaluate the steric effect of 2-Me-py compared to 4-Me-py. In contrast to (2.20, L^m = 4-Me-py), the ¹H NMR spectrum of (2.20, L^m = 2-Me-py) at room temperature contains only one set of slightly broad signals. At 233K in CD₂Cl₂, the spectrum contained two sets of well-resolved signals in an equilibrium ratio of 61:39 (which didn't change further with time). The analogous Schiff-base complex [Ru(2-Me-py)(L⁴)(C₆H₆)]PF₆⁹¹ was reportedly formed with high diastereoselectivity, though

additional NMR signals were attributed to rotamers of the complex, due to restricted rotation about the Ru—N_{2-Me-py} bond. To determine whether the same conclusion holds true for (2.20, L^m = 2-Me-py) or whether two diastereomers are present, NMR spectra of related complexes were compared. The very highfield shift observed (δ -0.08 and δ 0.00) for one isopropyl methyl in (2.20, L^m = 4-Me-py and Py, respectively), do not occur in the spectrum of (2.20, L^m = 2-Me-py), the four isopropyl methyl signals being observed between δ 0.52 and δ 1.04. The absence of a high-field shift is consistent with two rotamers of isomer-A structure where the isopropyl substituent is orientated towards the mesitylene ring such that shielding by the aromatic ring current of 2-Me-py is not possible. Crystallisation was attempted but X-ray quality crystals were not obtained before the solution of (2.20, L^m = 2-Me-py) decomposed. Instead, the geometry of the major isomer was determined by a phase-sensitive NOESY experiment in CD₂Cl₂ at 233K. Even at this temperature the isomers were interconverting, as evidenced by a chemical exchange cross-peak between the Ar-4-H signals, δ 6.14 and 6.49, of the major and minor isomers, respectively. A structure-confirming nOe was observed in the major isomer between the CHMeMe' signal (at δ 2.43) and the C₆H₃Me₃ singlet (at δ 5.02) (Figure 2.17) indicating the ⁱPr group is orientated towards the mesitylene (isomer-A), rather than towards the 2-Me-py. This is expected, since steric clashes between the ⁱPr and the *ortho*-methyl of the py ligand are likely to be severe.

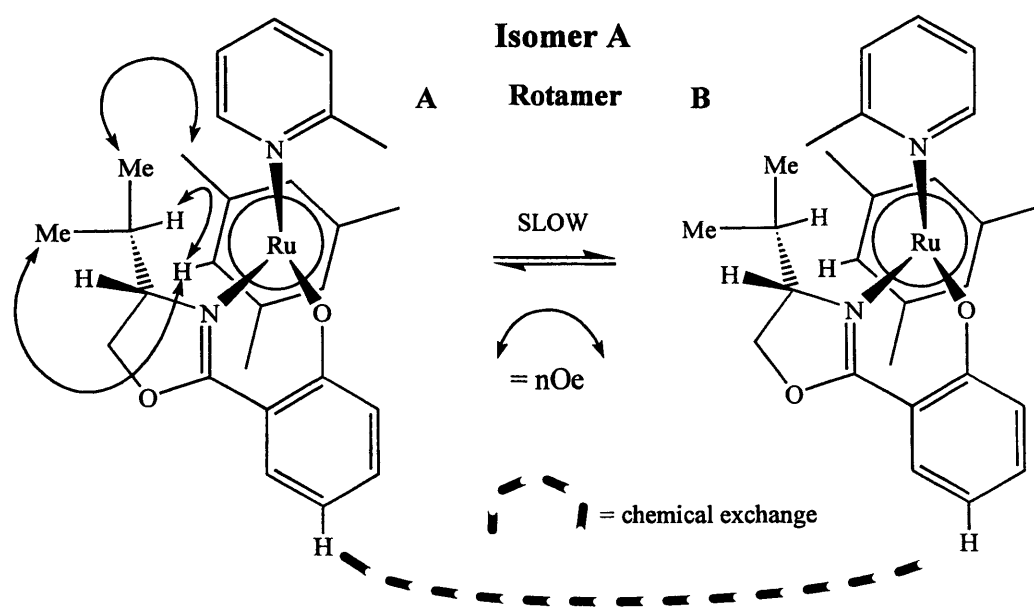


Figure (2.17): Observed nOes for (2.20, L^m = 2-Me-py)

Unfortunately, nOes between the ^1Pr signals and either the mesitylene or 2-Me-py signals were not observed in the spectrum of the minor isomer; as such, the structure of the minor isomer cannot be confirmed from this experiment. However, comparison of the ^1H NMR chemical shifts for both sets of signals in (**2.20**, $\text{L}^{\text{m}} = 2\text{-Me-py}$) with those of (**2.20**, $\text{L}^{\text{m}} = 4\text{-Me-py}$) indicates that (**2.20**, $\text{L}^{\text{m}} = 2\text{-Me-py}$) exists as two rotamers in a 61:39 ratio.

In contrast to complexes (**2.20**), the ^1H NMR spectrum of (**2.21**, $\text{L}^{\text{m}} = \text{PPh}_3$) showed sharp signals for two isomers at room temperature. The diastereomer ratio was 50:50, measured from the relative integration of the multiplets at δ 1.21 and 2.08 for MeCHMe', and from the triplets at δ 6.51 and 6.61 for Ar-5-H in the two isomers. The absence of diastereoselectivity is most probably as a result of the PPh_3 ligand being so sterically bulky that interactions between the isopropyl and PPh_3 in isomer-B balance any unfavourable interactions between the isopropyl and mesitylene in isomer-A. The $^{31}\text{P}\{^1\text{H}\}$ NMR spectrum contained two signals at δ 30.13 and δ 30.89 typical for PPh_3 coordinated to arene ruthenium.¹³⁵ To fully assign the peaks in the ^1H NMR spectrum to the particular diastereomer, A or B, combinations of ^1H - ^1H COSY, ^1H -decoupling and ^1H - ^1H NOESY experiments were carried out. The ^1H - ^1H COSY experiment determined the connectivity between protons on adjacent carbons, for example the isopropyl signals at δ 0.00, 0.58 and 1.21 arise from one isomer whilst those at δ 0.92, 0.98 and 2.08 are due to the other. The decoupling experiments helped to distinguish between the NCH and OCH protons of each isomer. Thus, irradiation at δ 1.21 MeCHMe' led to the collapse in coupling for the NCH signal at δ 3.73, whilst irradiation at δ 4.14 OCH in the other isomer led to a collapse in coupling at δ 3.19 (NCH) and δ 2.87 (OCH).

To identify which set of signals originated from isomer-A and which from isomer-B a ^1H - ^1H NOESY NMR experiment was performed (the most important structural determining nOes are shown in **Figure 2.18**). The NOESY spectrum was recorded at 233 K, to minimise any problems from chemical exchange. The spectrum of (**2.21**, $\text{L}^{\text{m}} = \text{PPh}_3$) contained an nOe between the mesitylene signal at δ 5.06 and the isopropyl hydrogen at δ 2.08 and nOes between the two isopropyl methyls at δ 0.98 and 0.92 with the mesitylene signal at δ 1.72, indicating that these signals originated from the diastereomer where the isopropyl group is orientated towards the mesitylene (isomer-A). Consequently, the other signals should correspond to isomer-B. This is

supported by the observation of a doublet at δ 0.00 (MeCHMe'), a methyl experiencing a ring current from the PPh₃.

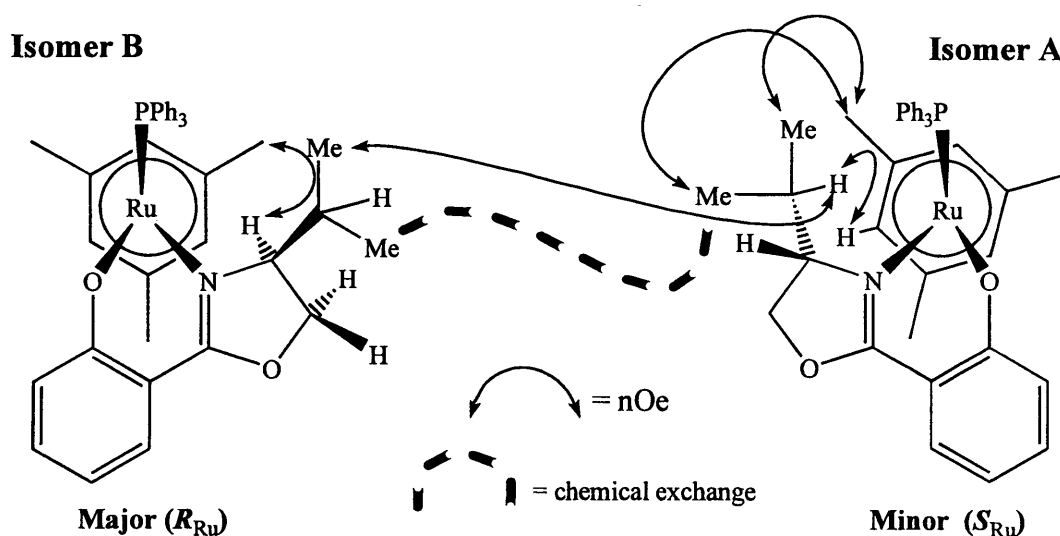


Figure (2.18): Observed cross-peaks for (2.21, $L^m = PPh_3$)

In order to confirm whether epimerisation occurs at higher temperatures the phase-sensitive NOESY spectrum on this sample was also recorded at room temperature. The spectrum showed chemical exchange cross-peaks, *e.g.* the Me'CHMe at δ 0.00 (isomer-B) and δ 0.98 (isomer-A) and additional nOes between signals in one isomer and signals in the other isomer that are non-interchangeable, for example, between δ 2.08 for MeCHMe' isomer-A and δ 0.58 for Me'CHMe isomer-B (as discussed for 2.20, $L^m = 4\text{-Me-py}$). The observation of chemical exchange cross-peaks shows that the rate of epimerisation is fast compared to the timescale of the NOESY experiment.

Complex (2.21, $L^m = PPh_3$) was crystallised from CH_2Cl_2 /ether. Dissolution of these crystals at approximately 193 K (over 1-2 hrs) and recording the 1H NMR spectrum at this temperature gave an isomer ratio (B:A) of 86:14 (at 193 K), calculated from the relative integration of the signals (Me'CHMe) at δ 0.58 and δ 0.98. The equilibration process was followed by 1H NMR spectroscopy by warming the sample until the final equilibrium diastereomer ratio of 1:1 was observed at 300 K. Thus crystallisation of (2.21, $L^m = PPh_3$) can occur diastereoselectively, but the sample epimerises to the equilibrium ratio in solution, as found for (2.20, $L^m = 4\text{-Me-py}$).

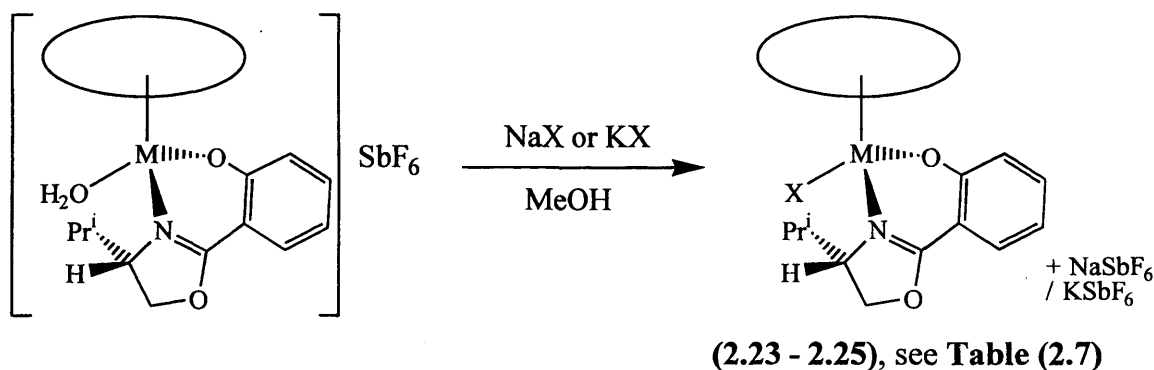
These results reveal that epimerisation of (2.20, $L^m = 4\text{-Me-py}$) and (2.21, $L^m = PPh_3$) is fast on a chemical timescale, consequently determination of the

stereochemistry of their formation (retention or inversion) is impossible. Failure to recognise this has led to erroneous reports in the literature (discussed in Chapter One). For example, it led Mandal and Chakravarty to incorrectly assume that $[\text{Ru}(4\text{-Me-py})(\text{L}^4)(p\text{-cy})][\text{PF}_6]$ was configurationally stable in solution because the isomer ratio did not change over time, *i.e.* they failed to recognise it had already reached equilibrium. Therefore, they erroneously reported that it was formed with retention of configuration at ruthenium.⁹³

The ^1H NMR spectra of the rhodium complexes (**2.22**, $\text{L}^m = \text{py}$ and **4-Me-py**) each contain only one set of moderately broad signals at room temperature. However, the low temperature spectra (273 K to 213 K) of (**2.22**, $\text{L}^m = \text{4-Me-py}$) showed two isomers in a ratio of 95:5 (at 213 K), calculated from the relative integration of the methyl signals (MeCHMe') of the major ($\delta -0.05$) and minor isomers ($\delta 0.83$). The highfield shift ($\delta -0.05$) of one methyl in the major isomer is consistent with this experiencing a ring-current effect, hence the isopropyl group is pointing towards the pyridine (isomer-B). When the spectra were recorded at higher temperatures extreme broadening of the signal at $\delta -0.05$ for $\text{Me}'\text{CHMe}$ and disappearance of the signal at $\delta 0.83$ was observed. At room temperature, the high-field methyl signal in (**2.22**, $\text{L}^m = \text{4-Me-py}$) is very broad in contrast to a well-resolved doublet at $\delta 0.93$ ($\text{Me}'\text{CHMe}$) of (**2.22**, $\text{L}^m = \text{4-Me-py}$). The difference in line widths is because the broad methyl signal is averaged over 0.78 ppm whilst the sharp doublet arises from doublets averaging over 0.16 ppm. Similar observations are assumed for (**2.22**, $\text{L}^m = \text{Py}$) at low temperature.

The fact that time-averaged signals were observed for the Cp^* -rhodium complex (**2.22**, $\text{L}^m = \text{4-Me-py}$) whilst two isomers were observed for arene-ruthenium complexes (**2.20**, $\text{L}^m = \text{py}$, **4-Me-py**) shows, as found previously for aqua complexes, that the rate of epimerisation is faster in rhodium complexes than in the related ruthenium complexes. Notably, the cationic substitution complexes (**2.20-2.21**) were found to epimerise faster than the analogous chloride complexes. From these observations it could be inferred that an ionic ligand (Cl^-) will dissociate less readily than a neutral ligand (PPh_3 or Py , etc.). Alternatively, the increased steric size of PPh_3/Py might nullify the extra donating ability of the phosphorus/nitrogen, thus they dissociate more readily than chloride. To further evaluate the steric and electronic effects on the diastereoselectivity and rate of exchange, the bromide and iodide analogues of (**2.12** and **2.15**, $\text{R} = \text{}^i\text{Pr}$) were prepared.

Halide complexes $[MX(^i\text{Pr-phenmox})(\text{mes})]$ ($M = \text{Ru}$, $X = \text{Br}^-$ **2.23**; $M = \text{Ru}$, $X = \text{I}^-$ **2.24**; $M = \text{Rh}$, $X = \text{I}^-$ **2.25**) were synthesised by treating the appropriate aqua complex with 1.2 equivalents of KBr or NaI in methanol at room temperature (**Tables 2F.1**, p 127; see Experimental Section). The reactions appeared to be instantaneous, an immediate colour change being observed, giving a methanolic solution of the desired bromide or iodide complex (**Scheme 2.12**).



Scheme (2.12)

Table (2.7): Complexes $[MX(^i\text{Pr-phenmox})(\text{mes})]$

Code	M	X	Ring
2.23	Ru	Br	mes
2.24	Ru	I	mes
2.25	Rh	I	Cp*

The complexes were characterised by combinations of ^1H NMR, ^1H - ^1H NOESY, mass spectrometry and microanalyses (**Tables 2F.2** and **2D.3**, p 137/146). The complexes were only partially soluble (5 mg in 1 ml) in CDCl_3 but were very soluble in CD_2Cl_2 . The crude reaction mixture of bromide complex (**2.23**) contained a single isomer by ^1H NMR (**Table 2F.2**) with chemical shifts similar to those of the analogous chloride complex (**2.12**, $\text{R} = ^i\text{Pr}$). For example, in (**2.23**) signals for the isopropyl occur at δ 0.74, 1.02 and 2.70, and the Ar-5-*H* of phenmox at δ 6.45, compared to δ 0.74, 0.99 and 2.82, and δ 6.39, respectively, for (**2.12**, $\text{R} = ^i\text{Pr}$). Thus, (**2.23**) is presumed to exist as a single diastereomer, with the same structure as (**2.12**, $\text{R} = ^i\text{Pr}$) (*i.e.* isomer-B). The FAB mass spectrum of (**2.23**) showed a minor ion ($\sim 7\%$) due to $[\text{M}]^+$ m/z 505 (^{79}Br), with the major ion due to $[\text{M} - \text{Br}]^+$ m/z 426.

The ^1H NMR spectrum (in CDCl_3) of the crude reaction mixture of the iodide complex (**2.24**), contained two species in a ratio of 96:4 based on mesitylene signals.

However, examination of the chemical shifts for the minor set of signals revealed they were due to free ligand (ⁱPr-phenmox) and a species that gives singlets at δ 2.36 and 5.43, and not a second diastereomer. Crystallisation in air from CH₂Cl₂/ether (2-3 days) lead to partial decomposition of the complex (signal ratio 62:38) and formation of a dark green solution. The solvent was evaporated and the solid residue was washed with chloroform to remove ⁱPr-phenmox and (2.24), leaving behind a dark black residue, which was soluble in CD₂Cl₂. The ¹H NMR spectrum of the latter contained resonances at δ 2.36 and 5.43, suggesting a “(mes)Ru” species. The FAB mass spectrum contained a minor peak at m/z 952 M⁺ attributed to [Ru₂I₄(mes)₂]⁺, the major ion due to [M-I]⁺ m/z 824 and minor ions at both m/z 697 and 577 as a result of further loss of I and then mesitylene. These results indicate that decomposition of (2.24) has occurred with dissociation of ⁱPr-phenmox and the formation of [RuI₂(mes)]₂ possibly aided by the presence of excess iodide.

The reaction was repeated using one equivalent of NaI. The ¹H NMR spectrum recorded straight after dissolution in CD₂Cl₂ only showed signals for (2.24). Hence, either it is formed highly diastereoselectively or two diastereomers are epimerising faster than the NMR timescale such that the time averaged spectrum is observed. The latter is unlikely since neither a second set of signals nor line-width broadening was observed in the ¹H NMR spectrum at 253K. The chemical shifts for the signals of (2.24) are similar to those of the analogous chloride (2.12, R = ⁱPr) and bromide (2.23) complexes. This suggests that an isomer-B structure with ⁱPr next to halide is still favoured even for the more sterically bulky iodide. The NOESY NMR spectrum showed nOes between the NCH proton (δ 4.51) and the mesitylene signals (δ 2.28 and 5.09, for C₆H₃Me₃ and C₆H₃Me₃, respectively) as expected for isomer-B. Whilst those expected for an isomer-A structure *i.e.* between the mesitylene ring and either of the ⁱPr methyls (δ 0.80 and 1.10), were not observed (**Figure 2.19**). This confirms that even for the iodide, the ⁱPr-substituent is orientated towards the halide, rather than towards the mesitylene ring, presumably to minimise unfavourable steric interactions.

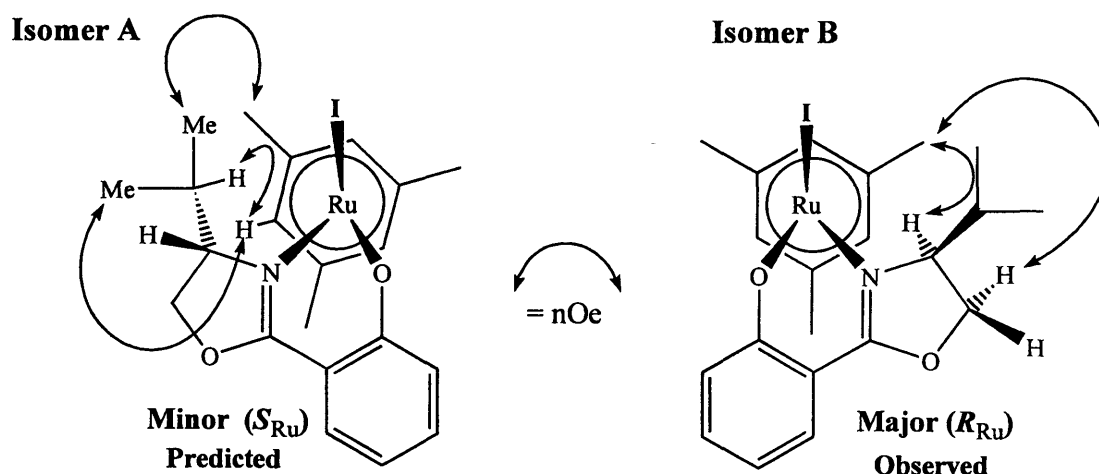


Figure (2.19): Structure determining nOes for $[\text{RuI}(\text{}^i\text{Pr-phenmox})(\text{mes})]$ (2.24)

The rhodium iodide complex (2.25) was formed similarly, its ^1H NMR spectrum contained one set of well-resolved signals, suggesting that the complex was formed with high diastereoselectivity. From comparison of the chemical shifts with those of the analogous chloride complex (2.15, $\text{R} = \text{}^i\text{Pr}$), it was inferred that (2.25) has the same structure as the chloride complex (isomer-B). This indicates that the increased steric bulk of iodide compared to chloride has no effect on diastereomer formation for the Cp^* -rhodium complex, as found for (2.24) described above. Attempts to monitor the iodide reaction by ^1H NMR spectroscopy failed to observe any intermediate species.

In conclusion, the relatively fast epimerisation of (2.20 – 2.22) at room temperature implies that these half-sandwich phenmox complexes could be active Lewis-acid catalysts with potentially high turnover frequencies. The high diastereoselectivity observed in most cases suggests that in catalytic applications the presence of a second diastereomer is only likely with very large substrates hence catalysis should proceed through a single chiral catalyst and high enantioselectivity may be possible. Results on the application of these complexes as asymmetric catalysts for Diels-Alder reactions will be discussed in Chapter Four.

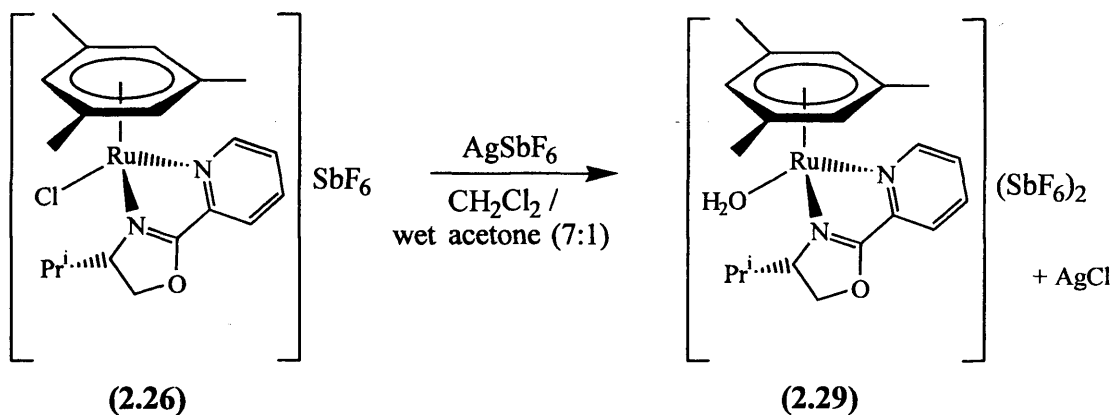
As noted above, the configurational instability at the metal for these ${}^i\text{Pr}$ -phenmox complexes prevents conclusions regarding the stereochemistry of substitution at the metal. As discussed in Chapter One, the use of a neutral N,N' -donor ligand gave greater configurational stability than O,N or N,N anionic ligands for arene-ruthenium Schiff-base complexes. Indeed, diastereomers of $[\text{RuCl}(\text{Ph-pymox})(\text{mes})]\text{SbF}_6$ (1.41) do not epimerise at room temperature (see Chapter One).¹⁰⁰ Thus, complexes $[\text{RuX}(\text{}^i\text{Pr-phenmox})(\text{mes})]$

pymox)(mes)]SbF₆ (X = Cl, Br, I) were employed to investigate the stereoselectivity of halide substitution at the metal, and the results are described below.

(2.2.2) – Mechanism of Substitution

The complex [RuCl(ⁱPr-pymox)(mes)]SbF₆ (**2.26**) is formed as a single diastereomer when prepared in refluxing methanol.⁹⁷ It was shown by X-ray crystallography to adopt isomer-B structure (**2.26 B**), with the ⁱPr group pointing towards the chloride rather than the π -bound mesitylene.⁹⁷ Previous work in our group showed that abstraction of the chloride ligand with a silver-salt (AgSbF₆) followed by addition of a bromide or iodide source (KBr or NaI) resulted in mixtures of diastereomers for each complex, 45:55 for (**2.27**) and 60:40 for (**2.28**); the diastereomer ratios of both (**2.27/2.28**) didn't change over days in d₆-acetone at room temperature.¹⁰⁰ X-ray crystallography showed (**2.28**) to possess isomer-A structure (ⁱPr-substituent towards mesitylene) in the solid-state. In addition, selective crystallisations gave different ratios in the mother liquors showing that equilibrium was not being established quickly in solution. Both these observations indicate that the configuration at the metal is stable under these conditions. The NOESY spectrum recorded on the 60:40 sample, confirmed that the major diastereomer in solution has isomer-A structure, as found in the solid-state. Monitoring the synthesis of (**2.28**) by *in situ* NMR led Garratt to conclude that (**2.28**) was formed predominantly by S_N2-type attack of halide on the aqua complex, *i.e.* giving mostly inversion of configuration at the metal.¹⁰⁰ In order to fully investigate the configurational stabilities, kinetic and thermodynamic selectivities and to determine the stereochemistry of substitution at the metal, these halide substitution experiments with Cl⁻, Br⁻ and I⁻ have been re-examined in more detail and the results are discussed below.

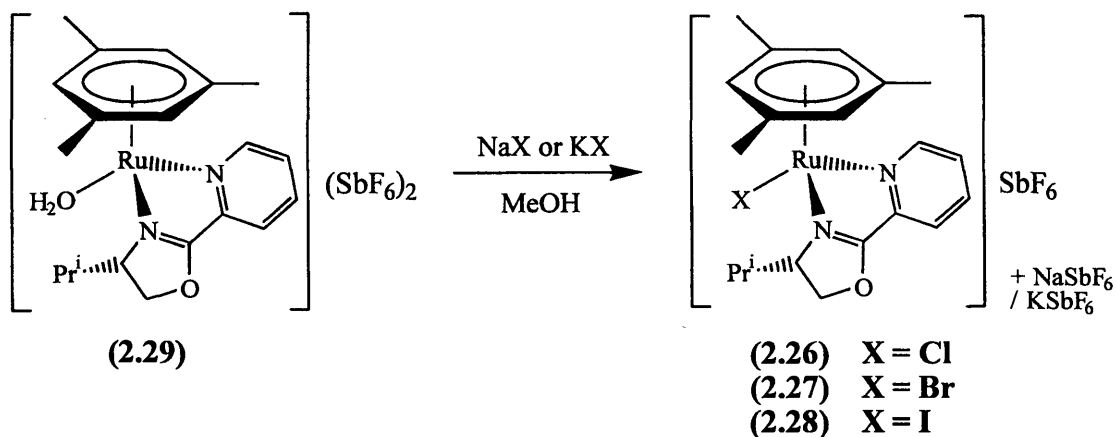
Complex [Ru(OH₂)(ⁱPr-pymox)(mes)][SbF₆]₂ (**2.29**) was prepared by the literature method (**Scheme 2.13**), traces of water in the acetone providing the aqua ligand.



Scheme (2.13)

Pure **(2.29)** was isolated by filtration of the crude reaction mixture through celite, to remove AgCl by-product, followed by recrystallisation from acetone/ether yielding a yellow powder that was moderately hygroscopic, forming an oil under atmospheric conditions. The complex was characterised by comparison of the ^1H NMR spectrum to published data.¹³⁶ The observation of two different signals for coordinated δ 5.40 and free H_2O δ 1.80 demonstrates that water (or proton) exchange is slow on the NMR timescale in 10:1 $\text{CD}_2\text{Cl}_2/\text{d}_6\text{-acetone}$.

The halide complexes $[\text{RuX}(\text{}^i\text{Pr-pymox})(\text{mes})]\text{SbF}_6$ ($\text{X} = \text{Cl, Br, I}$; **2.26–2.28**) were synthesised by treatment of **(2.29)** with 1.2 equivalents of KCl, KBr or NaI in methanol, at room temperature. The reactions appeared to be instantaneous, an immediate colour change being observed, quantitatively giving the desired chloride, bromide or iodide complex (**Scheme 2.14**).



Scheme (2.14)

The data for complexes **(2.26 – 2.28)** are in agreement with previous work except for **(2.26A)** which is characterised for the first time (^1H NMR, mass

spectrometry and microanalyses are in **Tables 2H.1 – 2H.4** and **2G.5**, p 142). NMR spectra were recorded from both crude and recrystallised products in order to determine the diastereomer ratios. The ^1H NMR spectrum (in CD_2Cl_2) of the crude reaction mixture of chloride complex (**2.26 A/B**) contained two distinct sets of arene and pymox signals in a ratio of 79:21. The minor set of resonances are identical to those of the product obtained from synthesis in refluxing methanol, previously characterised by X-ray crystallography as isomer-B, namely the ^iPr group pointing towards the chloride rather than towards mesitylene.⁹⁷ By deduction, therefore, the major set of NMR signals are assigned to the isomer-A structure, with the ^iPr group pointing towards the mesitylene rather than towards the chloride. The ^1H NMR signals for the ^iPr -substituent, the pyridine ring and mesitylene of isomer-A are all shifted downfield (by up to 0.43 ppm) compared to the comparable signals of isomer-B, whereas, the oxazoline ring protons are all shifted upfield (by up to 0.4 ppm) relative to isomer-B. Isomer-A was selectively crystallised from CH_2Cl_2 /ether but the crystals were not of X-ray quality. The ^1H NMR spectrum showed only isomer-A, no trace of isomer-B was seen, even after days at RT. Similarly, the ratio of the 79:21 mixture did not change within a few days in CD_2Cl_2 . Hence, the configuration at the metal is stable in this solvent.

The ^1H NMR spectrum of a crude sample of bromide complex (**2.27**) showed the presence of two diastereomers in a ratio of 73:27. The chemical shifts for the major and minor isomers are very similar to those of isomer-A and -B, respectively, of the chloride analogue (**2.26 A/B**). Careful recrystallisation of the mixture (**2.27 A/B**) allowed separation of the two diastereomers and the structure of (**2.27 A**) was determined by X-ray diffraction. A crystal of (**2.27 B**) (obtained by S. Garratt) was also analysed by X-ray diffraction; the X-ray structures of the cations of (**2.27 A**) and (**2.27 B**) are shown in **Figures (2.20)** and **(2.21)**, respectively, with selected bond distances and bond angles in **Table (2.8)**. The structure of (**2.27 A**) is much like that of the iodide analogue,¹⁰⁰ with the isopropyl-group orientated away from the sterically large bromide ligand, such that the configuration at ruthenium is (*R*) {mes > Br > N(ox) > N(py)}.^{104, 134} As expected, the structure of (**2.27 B**) is similar to that found previously for (**2.26B**),¹¹⁵ with the isopropyl-group orientated towards the bromide ligand rather than towards the mesitylene ring, such that the configuration at ruthenium is (*S*).

Table (2.8): Selected Bond Distances (Å) and Angles (°) of (2.27 A) and (2.27 B)

	(2.27 A)	(2.27 B)		(2.27 A)	(2.27 B)
Ru – N(1)	2.096(10)	2.122(11)	N(2)-Ru-Br	85.6(4)	82.1(3)
Ru – N(2)	2.097(13)	2.103(10)	N(1)-C(6)	1.227(18)	1.28(2)
Ru – Br(1)	2.522(2)	2.532(2)	C(5)-C(6)	1.441(19)	1.41(2)
N(1)-Ru-N(2)	76.4(5)	76.3(4)	N(2)-C(5)	1.338(19)	1.34(2)
N(1)-Ru-Br	82.9(3)	89.3(3)	-	-	-

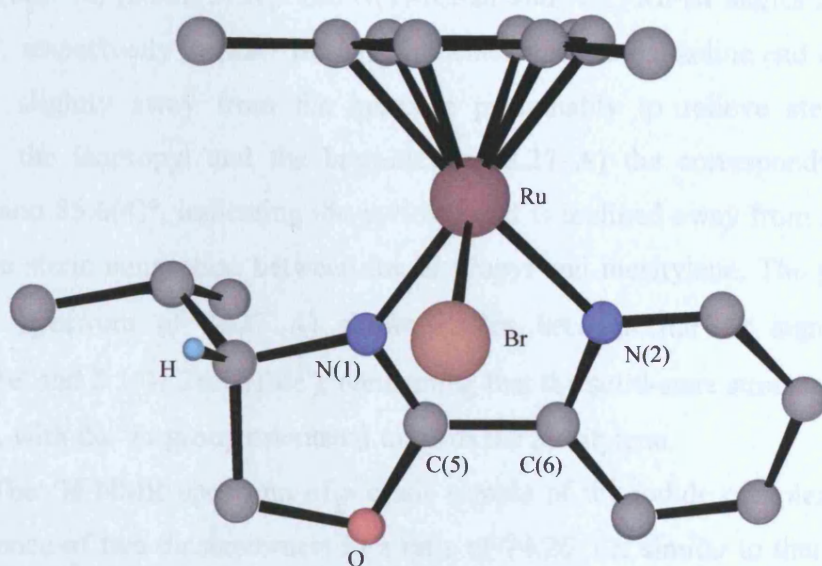


Figure (2.20): X-ray Structure of the cation (2.27 A)

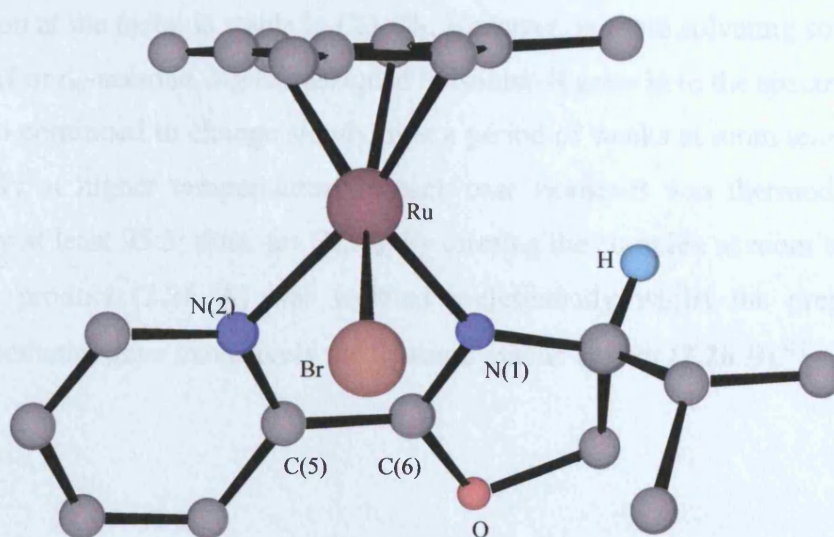


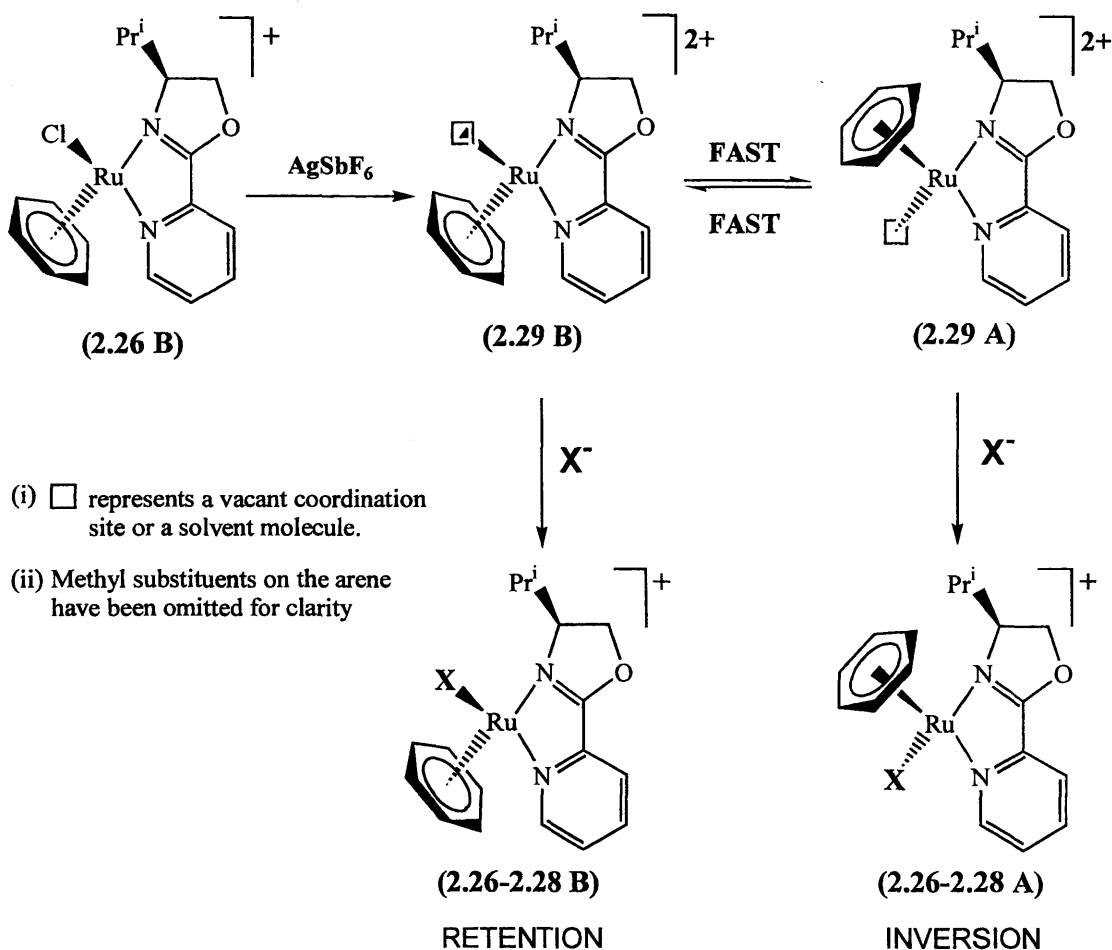
Figure (2.21): X-ray Structure of the cation (2.27 B)

Complexes (**2.27 A/B**) possess opposite structural arrangements (ⁱPr pointing at mesitylene or bromide, respectively), however, their X-ray structures share many similarities. The length of the Ru-N(1) bonds [2.096(10) and 2.122(11) Å], the Ru-N(2) bonds [2.097(13) Å and 2.103(10) Å] and the N(1)-Ru-N(2) angles [76.4(5) and 76.3(4)°] in (**2.27A**) and (**2.27B**), respectively, are statistically the same in each isomer and the same as the chloride (**2.26B**) [2.118(4), 2.117(4) Å and 76.4(2)°, respectively].⁹⁷ The length of the Ru-Br bond is slightly longer in (**2.27 B**) [2.532(2) Å] than in (**2.27 A**) [2.522(2) Å]. The N(1)-Ru-Br and N(2)-Ru-Br angles are 89.3(3) and 82.1(3)°, respectively in (**2.27 B**). This indicates that the oxazoline end of the ligand is inclined slightly away from the bromide presumably to relieve steric congestion between the isopropyl and the bromide. In (**2.27 A**) the corresponding angles are 82.9(3) and 85.6(4)°, indicating the pyridine end is inclined away from the bromide to minimise steric congestion between the isopropyl and mesitylene. The phase-sensitive NOESY spectrum of (**2.27 A**) showed nOes between the ⁱPr signals (at δ 2.65 MeCHMe' and δ 1.01 MeCHMe'); confirming that the solid-state structure is retained in solution, with the ⁱPr group orientated towards the mesitylene.

The ¹H NMR spectrum of a crude sample of the iodide complex (**2.28**) shows the presence of two diastereomers in a ratio of 74:26, *i.e.* similar to that of both (**2.26**) and (**2.27**). Slow recrystallisation gave a sample of pure (**2.28A**).

The ¹H NMR spectra of crystals of (**2.26-2.28 A**) in CD₂Cl₂ showed only the presence of isomer-A; no trace of isomer-B was seen after several days at RT, hence the configuration at the metal is stable in CD₂Cl₂. However, in more solvating solvents such as d₄-MeOH or d₆-acetone, signals assigned to isomer-B grew in to the spectrum and the isomer ratio continued to change slowly over a period of weeks at room temperature or more rapidly at higher temperatures. In each case isomer-B was thermodynamically preferred by at least 95:5; thus, for (**2.26**), by forming the complex at room temperature the kinetic product (**2.26 A**) was isolated preferentially whilst the preparation in refluxing methanol gave exclusively the thermodynamic isomer (**2.26 B**).⁹⁷

These experiments lead to the conclusion that the two-step halide substitution reactions are unambiguous examples of kinetic control of stereoselectivity with the favoured pathway being a rare case of formal inversion at the metal.¹³⁷ The proposed mechanism is shown in **Scheme (2.15)**.



Scheme (2.15)

Abstraction of halide by Ag^+ provides the aqua/solvent species **(2.29 A/B)**, epimerisation of which will be much faster than for the halide coordinated species. Species **(2.29 A)** is expected to react faster since attack of the halide occurs preferentially from the side opposite the oxazoline substituent, *i.e.* the least sterically hindered approach, giving **(2.26-2.28 A)** with the isopropyl pointing towards the π -bound arene rather than the halide. The rate of epimerisation of **(2.26-2.28)** in methanol is sufficiently slow (weeks at room temperature) that it cannot account for the amount of isomer-B formed, *i.e.* the reaction is not forming exclusively isomer-A followed by epimerisation to isomer-B.

At room temperature, in CD₂Cl₂, the configuration at ruthenium in (2.26-2.28) is stable, at least over a period of weeks. Epimerisation, therefore, was monitored by ¹H NMR spectroscopy in d₆-acetone at thermostatted temperatures between 313 and 333K. In the range of temperatures measured for (2.26-2.28), the epimerisation obeyed a first-order rate law (Figures 5.1-5.5, see Appendix, p 214) with derived rate constants (Table 2.9) ranging from $(1.13 \pm 0.04) \times 10^{-6} \text{ s}^{-1}$ ($\tau_{1/2} = 170.9 \text{ h}$, 313K) to $(5.70 \pm 0.05) \times 10^{-6} \text{ s}^{-1}$ ($\tau_{1/2} = 33.8 \text{ h}$, 333K). At 313K, the rate of epimerisation increases slightly [$(1.13 \pm 0.04) \times 10^{-6} \text{ s}^{-1}$ to $(5.0 \pm 0.4) \times 10^{-6} \text{ s}^{-1}$] as the ligand required to dissociate changes from chloride to bromide to iodide, consistent with a weaker bond for iodide. For complexes [RuX(TMBA)(*p*-cy)] (X = Cl, I) iodide epimerises faster than chloride.⁹⁰ Electronic and steric factors will determine the ‘ease’ of halide dissociation, but these results do indicate that greater steric repulsion with increasing size of halide results in faster halide dissociation and consequent epimerisation. Epimerisation of bromide complex (2.27) was monitored at three temperatures with derived rate constants ranging from $(1.39 \pm 0.1) \times 10^{-6} \text{ s}^{-1}$ ($\tau_{1/2} = 135.35 \text{ h}$, 313K) to $(5.70 \pm 0.05) \times 10^{-6} \text{ s}^{-1}$ ($\tau_{1/2} = 33.8 \text{ h}$, 333K) see Table (2.9). From the temperature dependence of the rate constant, the activation parameters $\Delta H^\ddagger = 55 \pm 10 \text{ kJ mol}^{-1}$ and $\Delta S^\ddagger = -183 \pm 30 \text{ J K}^{-1} \text{ mol}^{-1}$ were extracted by least-squares (Figure 5.11, see Appendix, p 219).¹³⁸ The magnitude of ΔH^\ddagger suggests that a bond is broken during the epimerisation process, with the values being similar to that [$\Delta H^\ddagger = 91.4 \pm 3.4 \text{ KJ mol}^{-1}$] reported for amino-acidate complex [Ir(C≡CBu¹)(proline)(Cp^{*})]^[145] and [$\Delta H^\ddagger = 98.1 \text{ KJ mol}^{-1}$] for [RuCl(TMBA)(*p*-cy)].⁹⁰ Note, an alternative mechanism involving opening of the chelate ring is feasible and can not be discounted from our data.

Table (2.9): Rate Data for (2.26 – 2.28)

Code	T (K)	$k_{\text{eq}} (\times 10^{-6} \text{ s}^{-1})$	$\tau_{1/2}$ (hrs)	K_{eq}
2.26	313	1.13 (± 0.04)	170.89	51.67
2.27	313	1.39 (± 0.1)	138.16	57.82
2.27	327	2.83 (± 0.15)	67.96	65.65
2.27	333	5.70 (± 0.05)	33.78	70.35
2.28	313	5.0 (± 0.4)	38.51	14.39

The circular dichroism (CD) spectra for both kinetically and thermodynamically favoured mixtures of complexes (2.26-2.28) have been measured to establish whether it is a reliable indicator of the configuration of the metal. The spectra for selected complexes are shown in Figures (2.22-2.25). The free ligand, ⁱPr-pymox (2.9, R = ⁱPr), shows very little absorption in the CD spectra in the range 230-600 nm thus these absorptions are arising from the metal environment. The CD curve for diastereomerically pure complex (2.26 B) (dashed line in Figure 2.22) consisted of four peaks centred at (-)225, (+)281, (-)380 and (+)438 nm, with the sign of the Cotton effect in parenthesis, the peak at ~380 being rather broad. The CD spectrum of a kinetically favoured sample of (2.26 A:B) in ratio 79:21 (dotted line in Figure 2.22) is the approximate mirror image of the thermodynamic isomer (2.26 B), as expected (see Section 1.3.2). The bromide (2.27) shows similar features (Figure 2.23). However the iodide (2.28) (Figure 2.24), shows differences in the region 290 to 410 nm compared to that of (2.26) and (2.27); with more maxima and minima but a lower CD. The CD spectra of thermodynamically enriched halide complexes: chloride 100:0 (continuous line), bromide 96:4 (dashed line) and iodide 99:1 (dotted line) are shown in Figure (2.25). The signs of the first band above 250 nm and the band between 420 and 550 nm may be a reasonable guide to the configuration at the metal for these [RuX(ⁱPr-pymox)(mes)]⁺ cations.

Figure (2.22): CD Spectra of [RuCl(ⁱPr-pymox)(mes)]SbF₆ (2.26)

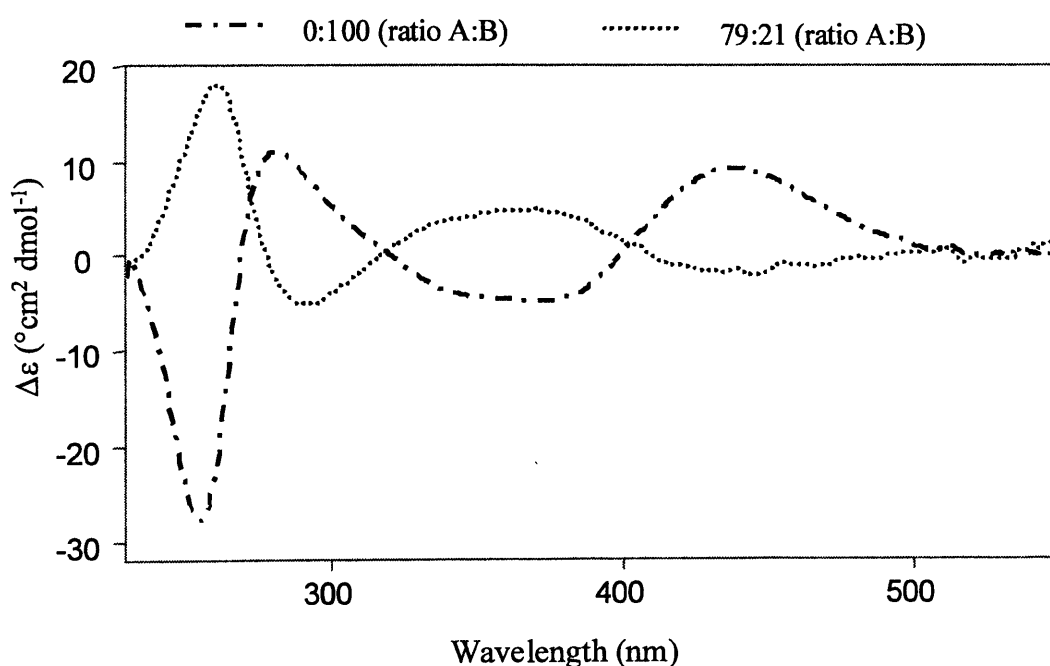


Figure (2.23): CD Spectra of [RuBr(¹Pr-pymox)(mes)]SbF₆ (2.27)

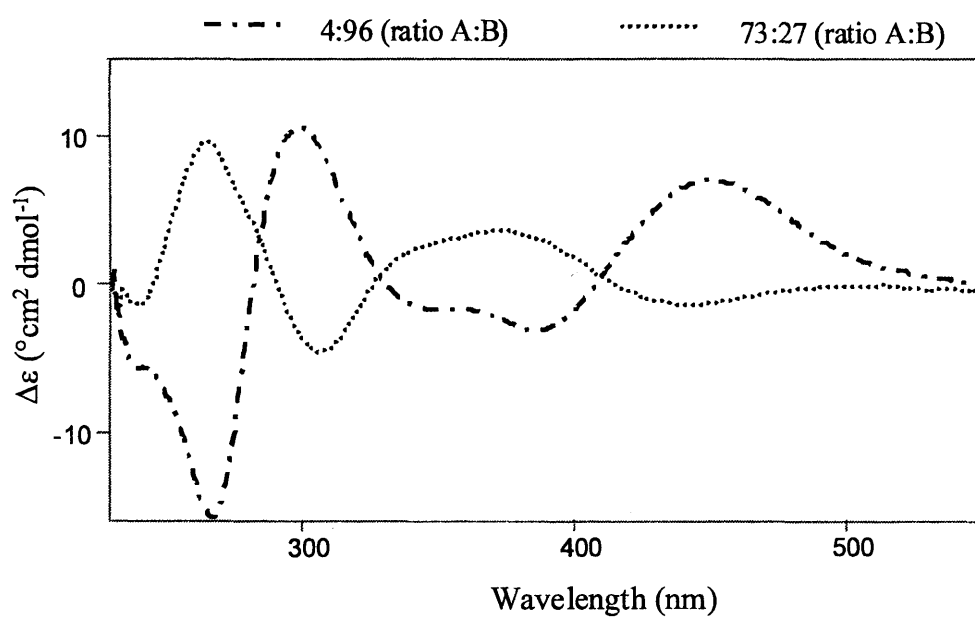


Figure (2.24): CD Spectra of [RuI(¹Pr-pymox)(mes)]SbF₆ (2.28)

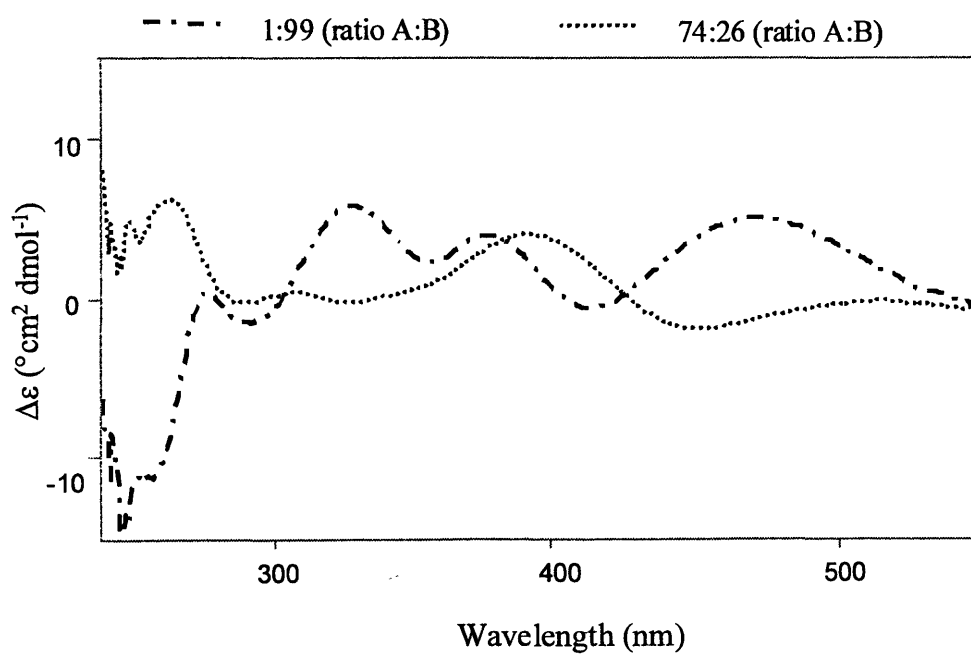
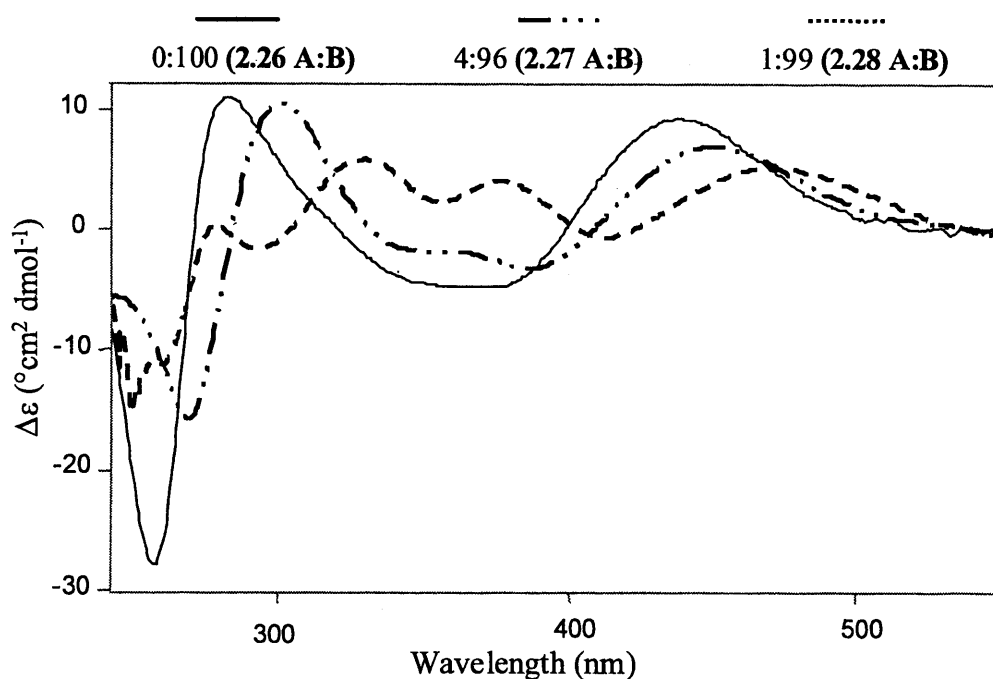


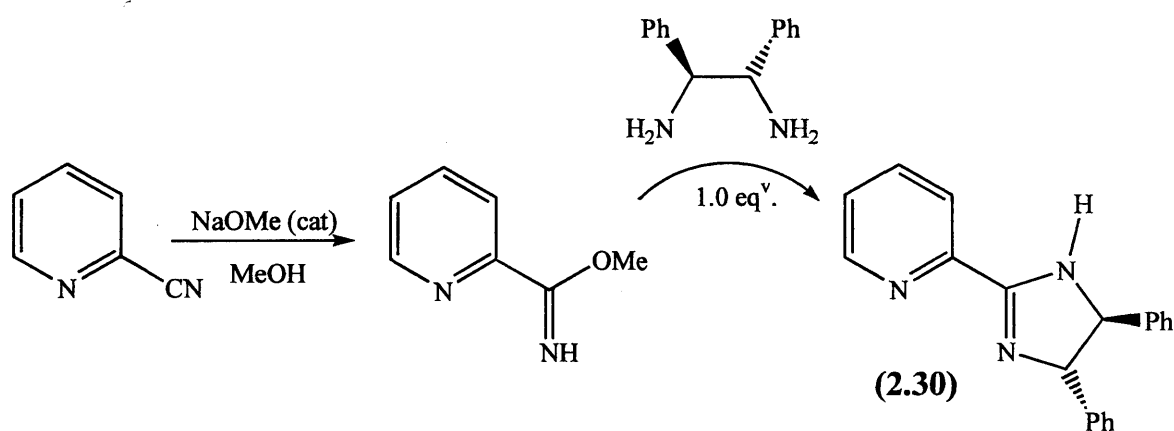
Figure (2.25): CD Spectra of $[\text{RuX}(\text{}^i\text{Pr-pymox})(\text{mes})]\text{SbF}_6$ (2.26-2.28 B)



In conclusion, manipulation of the conditions of synthesis of $[\text{RuX}(\text{}^i\text{Pr-pymox})(\text{mes})][\text{SbF}_6]$ allow preferential formation of isomer-A (kinetic) or exclusive formation of isomer-B (thermodynamic). Regardless of which halide is used, isomer-B with the isopropyl-substituent orientated towards the halide, rather than towards the π -bound mesitylene, is thermodynamically preferred. The first-order rate constants for (2.26-2.28) and activation parameters for epimerisation of (2.27 A) to (2.27 B) are consistent with a bond breaking rate-determining step, which may be solvent assisted. The two-step substitution reactions to form complexes $[\text{RuX}(\text{R-pymox})(\text{arene})]^+\text{SbF}_6^-$ are unambiguous examples of kinetic control of stereoselectivity with the favoured pathway being a rare case of formal inversion at the metal.

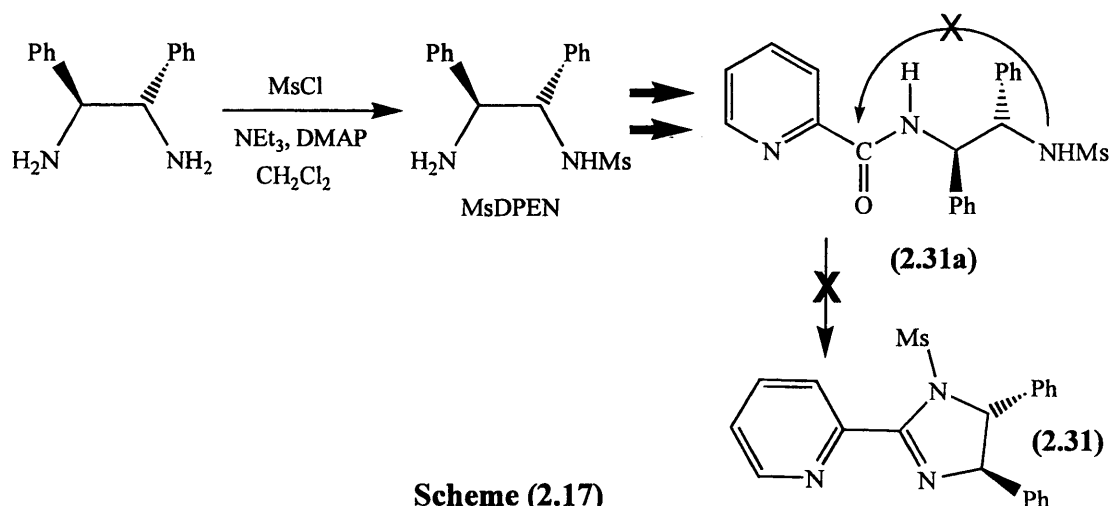
(2.2.3) – Half-Sandwich Complexes of Chiral Imidazoline Ligands

The previously unreported imidazoline ligand Ph₂-pymimH (**2.30**), containing two chiral centres, was synthesised in 99% yield from (1*S*,2*S*)-diphenylethylenediamine (DPEN) and 2-cyanopyridine via the imidate (**Scheme 2.16**). The ¹H NMR spectrum of (**2.30**) at room temperature shows two broad singlets at δ 4.8 and δ 5.1 for the imidazoline ring; cooling to 243 K causes the two signals to sharpen into well resolved doublets at δ 4.86 (*CH^aPh*) and δ 5.13 (*CH^bPh*), respectively. These observations are consistent with solvent assisted tautomerism, which has been observed previously for achiral imidazolines.^{122, 139, 140}

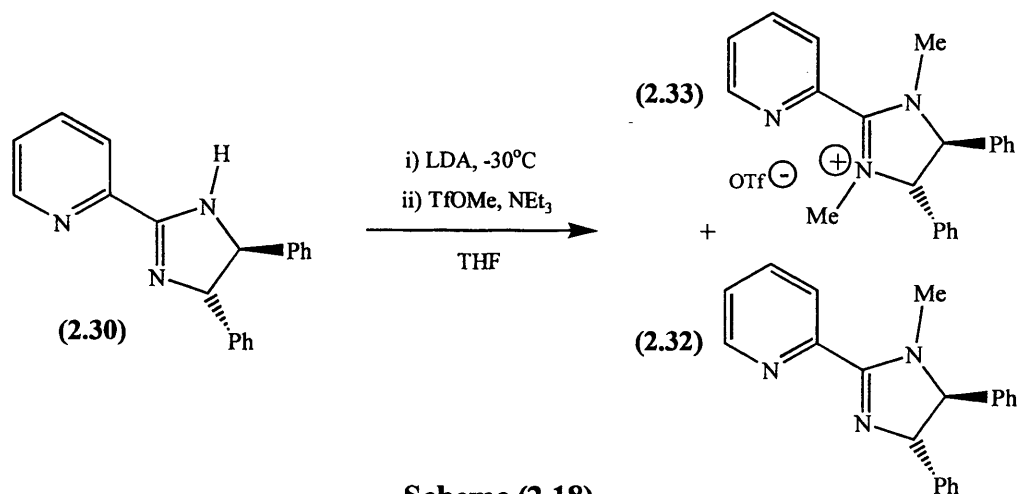


Scheme (2.16)

Preparation of the *N*-substituted derivatives Ph₂-pymimMs (**2.31**) and Ph₂-pymimMe (**2.32**) were attempted via several different methods. The first attempt to make (**2.31**) involved selective mono-mesylation of (1*S*, 2*S*)-DPEN with MsCl (**Scheme 2.17**) to form (1*S*, 2*S*)-MsDPEN, according to the method of Fujisawa *et al.*¹⁴¹ The (1*S*, 2*S*)-MsDPEN produced was then reacted with the imidate from 2-cyanopyridine (*c.f.* **Scheme 2.16**). The ¹H NMR spectrum of the product contained a broad 1H singlet at δ 11.0 (assigned to an amide proton) as well as additional signals consistent with formation of an NMs-amide intermediate (**2.31a**). However, even following heating to reflux in chloroform, ring closure was not achieved, probably due to a reduction in nucleophilicity of -NHMs compared to -NH₂, thus inhibiting attack at the carbonyl carbon and hence preventing cyclisation. It was hypothesised that this route might work for (**2.32**) since the methylated-nitrogen would be more nucleophilic. Unfortunately, preparation of (1*S*, 2*S*)-MeDPEN by a similar method was not selective, giving mixtures of mono, di, tri and tetra-methylated DPEN, which proved to be resistant to separation.

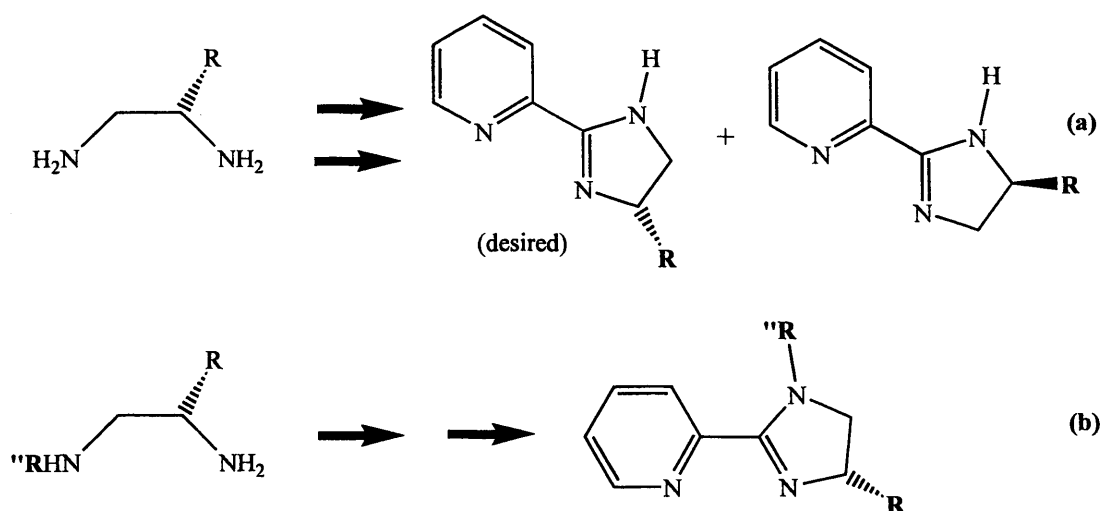


Preparation of **(2.32)** was attempted by deprotonation of **(2.30)**, using LDA at -30°C , followed by addition of methyl triflate. The ^1H NMR spectrum of the crude reaction mixture, showed signals corresponding **(2.30)**, **(2.32)** and a third species that possessed a 6H singlet, possibly two equivalent N-Me groups. The reaction was repeated using dry methyl iodide instead of methyl triflate as the methylating agent. This allowed isolation of **(2.32)** in 81% yield after purification by chromatography. The ^1H NMR spectrum of **(2.32)** contained a singlet at δ 2.99 (3H, NMe) and two well resolved doublets at δ 4.36 ($\text{CH}^{\text{a}}\text{Ph}$) and δ 4.99 ($\text{CH}^{\text{b}}\text{Ph}$) indicating that tautomerism is not occurring, as expected after substituting hydrogen by methyl. The electrospray mass spectrum contains the molecular ion $[\text{M}+\text{H}]^+$ m/z 314, as the largest peak. To identify the third product from the methyl triflate reaction, the conditions were adjusted to favour this product. To a CH_2Cl_2 solution of **(2.30)** at -78°C was added methyl triflate and NEt_3 , this yielded **(2.30)**, **(2.32)** and **(2.33)** (**Scheme 2.18**) in the ratio 0.9:1.0:2.0, respectively, as shown by NMR. Chromatography afforded pure **(2.33)**, which was characterised by ^1H NMR and mass spectrometry (see Experimental Section). The ^1H NMR spectrum shows a singlet 6H for two equivalent N-Me groups (δ 2.94) and a singlet 2H (δ 5.24), for two equivalent CHPh protons, which is downfield compared to the inequivalent $\text{NCH}^{\text{a/b}}\text{Ph}$ protons of **(2.30)** or **(2.32)**. The pyridine ring protons are also deshielded by up to 0.38 ppm compared to **(2.32)**; these observations are indicative of cationic $[\text{Ph}_2\text{-pymimMe}_2]^+[\text{OTf}]^-$ **(2.33)**. The electrospray mass spectrum showed the molecular ion at m/z 328 (100%) $[\text{Ph}_2\text{-pymimMe}_2]^+$.



Scheme (2.18)

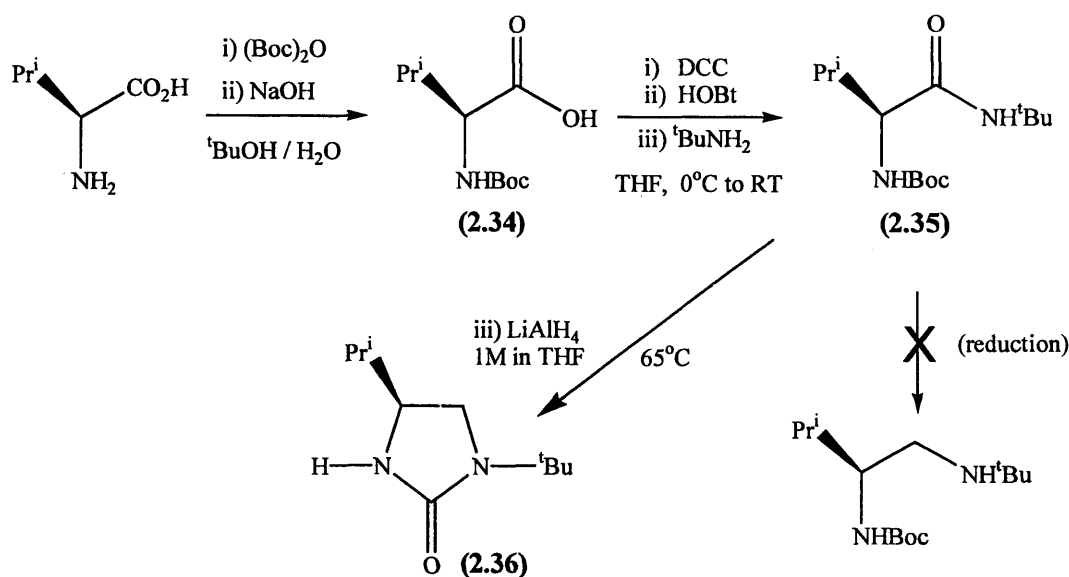
The imidazoline ligands discussed so far originate from C₂-symmetric enantiopure ethylenediamines and hence contain two chiral centres; thus in their syntheses, if either primary amine terminus ‘attacks’ the imidate carbon an identical product is formed **Scheme (2.16)**. However, if C₁-symmetric enantiopure ethylenediamines are used a mixture of two isomers would be expected {see **(a) Scheme 2.19**}, with the chiral centre adjacent to the imine nitrogen (desired) or adjacent to the amino nitrogen (expected to give less chiral induction). To overcome, this problem the necessary precursor would be a C₁-symmetric mono *N*-protected ethylenediamine with the stereogenic centre adjacent to the primary nitrogen {see **(b) in Scheme 2.19**}.



Scheme (2.19)

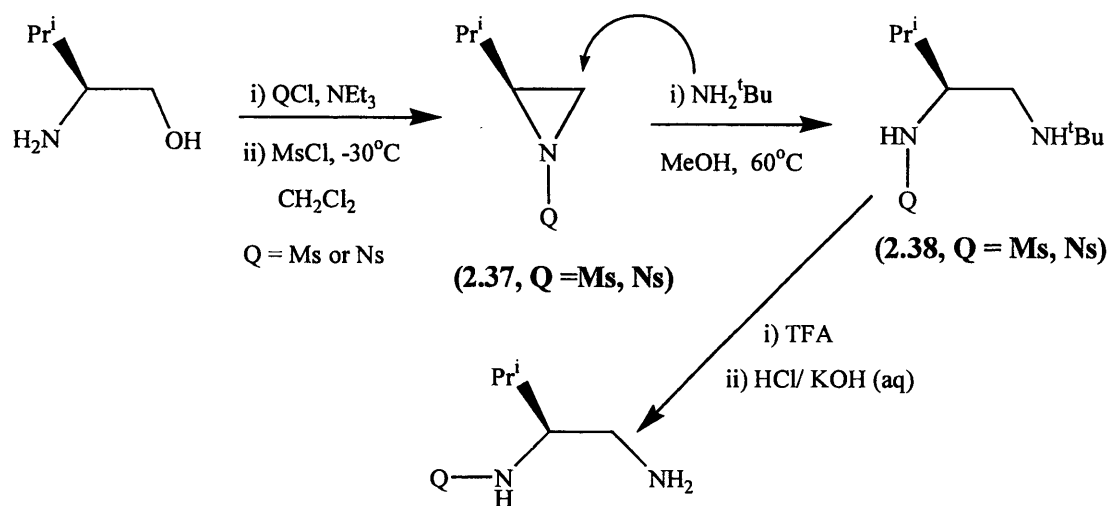
The first approach to the target enantiopure ethylenediamines involved the use of amino acid peptide chemistry (**Scheme 2.20**). (*N*)-Boc-(*L*)-valine (2.34) was prepared

by standard methods¹⁴² and then coupled with ^tBuNH₂ (using DCC and HOBT)¹⁴³ to give (*N*)-Boc-(*L*)-valamide (**2.35**) in 94% overall yield. Reduction of (**2.35**) was expected to give the desired (*N*)-Boc protected ethylenediamine. However, the carbonyl of (**2.35**) proved to be surprisingly resistant to reduction; heating to reflux with NaBH₄-I₂ in THF; LiBH₄/Me₃SiCl in THF; or LiAlH₄(s) in THF returned unreacted (**2.35**) in each case. Under more forcing conditions, reaction of (**2.35**) with LiAlH₄(solⁿ) in THF at reflux, a product was formed. The ¹H NMR spectrum contained only one ^tBu signal (δ 1.38) compared to two for (**2.35**) (δ 1.36 N- ^tBu and δ 1.47 O- ^tBu), suggesting the removal of the Boc group. The ¹³C (DEPT 135) NMR spectrum confirmed the presence of only one C(CH₃)₃ group (δ 26.59), an NCH₂ group and a single carbonyl carbon (δ 161.56) in addition to the other expected signals. The IR spectrum contains strong absorptions at 1456 (C–N) and 1685 cm⁻¹ (C=O), which are indicative of a cyclic urea; Thus the product is formulated as the cyclic urea (**2.36**) (see **Scheme 2.20**). The ES mass spectrum, shows the molecular ion at *m/z* 259 [MH]⁺, and the elemental analysis confirm the identification of (**2.36**).



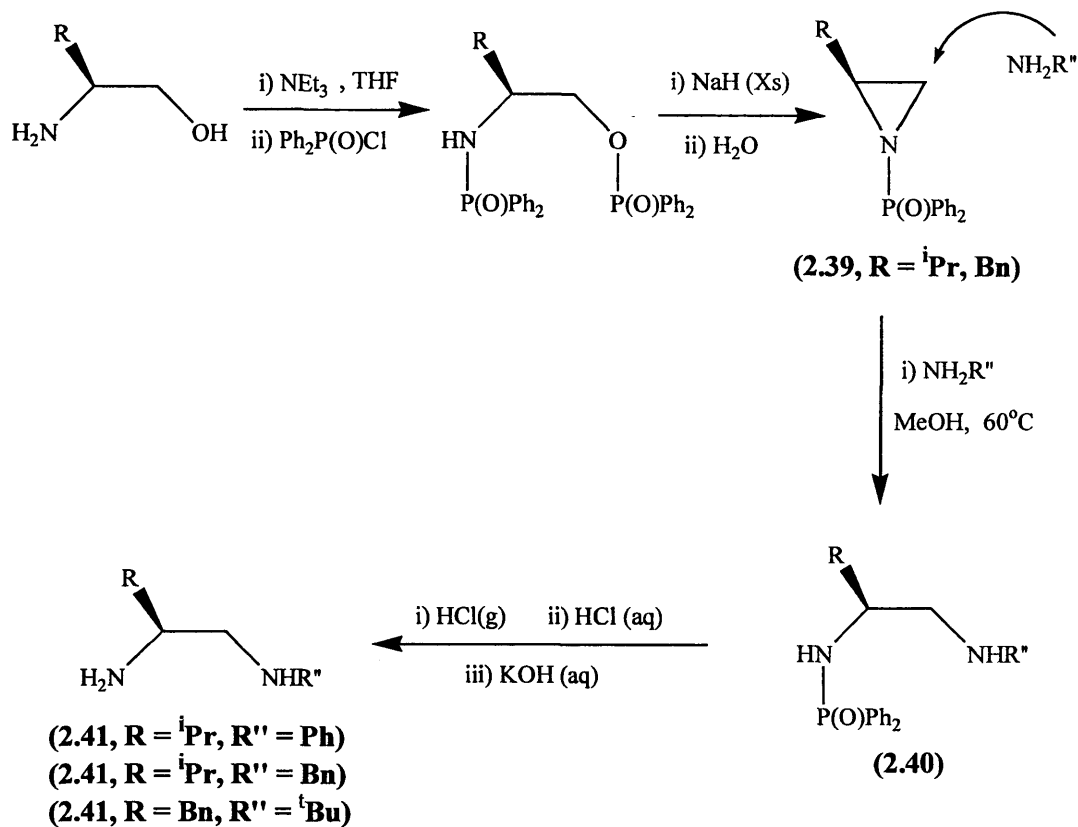
The second method envisaged for synthesis of the target ethylenediamine was via chiral aziridine formation followed by regioselective ring opening with primary amines, such an approach having been used to produce C₃-symmetric tripodal tetraamines.¹⁴⁴ Chiral aziridines (**2.37**, Q = Ms, Ns) were made from L-valinol with either mesyl or nosyl chloride followed by reaction with sodium carbonate in accord with the literature methods of Moberg *et al.*¹⁴⁴ Nucleophilic ring opening of (**2.37**, Q = Ms, Ns)

by ^tBuNH₂ in refluxing methanol produced single isomer, *N*-Ms- or *N*-Ns-protected, enantiopure ethylenediamines (**2.38**, Q = Ms, Ns) as oils in high yield (91-99%) **Scheme (2.21)**. The ¹H-¹H-NOESY spectrum of (**2.38**, Q = Ns) contained a correlation between δ 3.23 (NCHⁱPr) and δ 8.12 (Ns-NH), confirming the desired regioselectivity of aziridine ring opening. Deprotection of (**2.38**, Q = Ms) was attempted using, 5M HCl, LiAlH₄ in THF or Na(s)/NH₃(l), however only unreacted (**2.38**) was recovered.



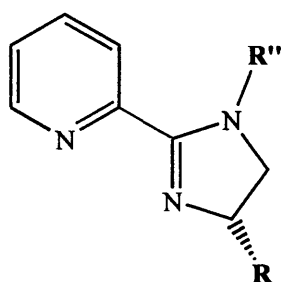
Scheme (2.21)

When trifluoroacetic acid was used the ^tBu group (N-C bond) was cleaved instead of the mesyl group (N-S bond), as shown by ¹H NMR and mass spectrometry. To solve this problem, the use of a protecting group that will be more readily cleaved *i.e.* diphenylphosphonyl was investigated (**Scheme 2.22**). Chiral aziridines (**2.39**, R = ⁱPr, Bn; Q = P{O}Ph₂) analogous to (**2.37**) were synthesised following the method of Sweeney *et al.*¹⁴⁵ Regioselective nucleophilic ring opening of (**2.39**) was achieved with R''NH₂ (R'' = ^tBu, ⁿBu, Bn, Ph), by heating to reflux in methanol, to form (**2.40**), which were deprotected by bubbling dry HCl (g) through CH₂Cl₂/ether solutions of (**2.40**) to yield (**2.41**).



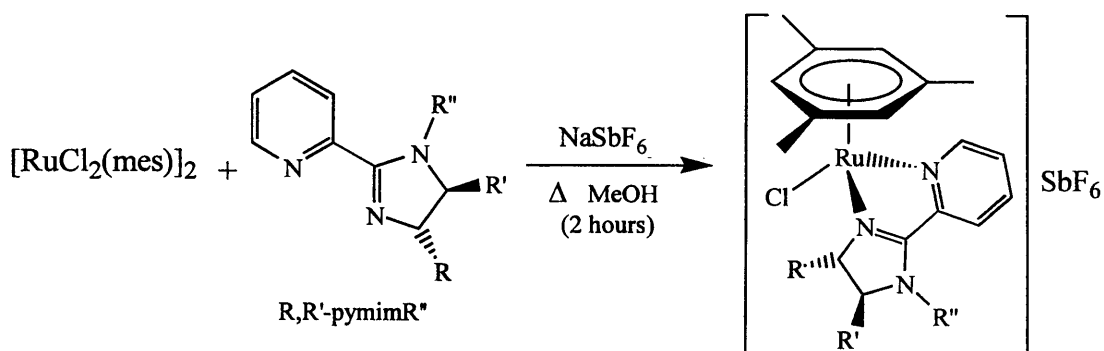
Scheme (2.22)

The new ligands, (*S*)-1R-pymimR'' (2.42), were synthesised from (2.41) and 2-cyanopyridine in 86-93% yield by an analogous method to the preparation of (2.30) shown in **Scheme (2.16)**.



- (2.42, R = ^iPr , $\text{R}'' = \text{Ph}$)**
(2.42, R = ^iPr , $\text{R}'' = ^n\text{Bu}$)
(2.42, R = Bn , $\text{R}'' = ^t\text{Bu}$)

Half-sandwich complexes $[\text{RuCl}(\text{1R,2R}'\text{-pymimR}'')(\text{mes})]\text{SbF}_6$ (2.43–2.47) were synthesised in high yield (94-99%) from $[\text{RuCl}_2(\text{mes})]_2$ by treatment with two equivalents of ligand (2.30/2.32/2.42) and NaSbF_6 , in refluxing MeOH (**Scheme 2.23**).



(2.43 - 2.47): Table (2.10)

Scheme (2.23)

Table (2.10): Complexes $[\text{RuCl}(\text{R},\text{R}'\text{-pymimR}'')(\text{mes})]\text{SbF}_6$

Code	R	R'	R''
(2.43)	Ph	Ph	H
(2.44)	Ph	Ph	Me
(2.45)	ⁱ Pr	H	Ph
(2.46)	ⁱ Pr	H	ⁿ Bu
(2.47)	Bn	H	^t Bu

Complexes (2.43-2.47) were characterised by ¹H NMR, ¹H-¹H NOESY, mass spectrometry and microanalysis (Tables 2G.1 –2G.5) and by X-ray diffraction where possible. In all the complexes (2.43-2.47), both the metal centre and the imidazoline ligands are chiral so a mixture of diastereomers is possible (Figure 2.26) (as found for analogous phenmox and pymox complexes 2.12 – 2.25 and 2.26 - 2.29, respectively).

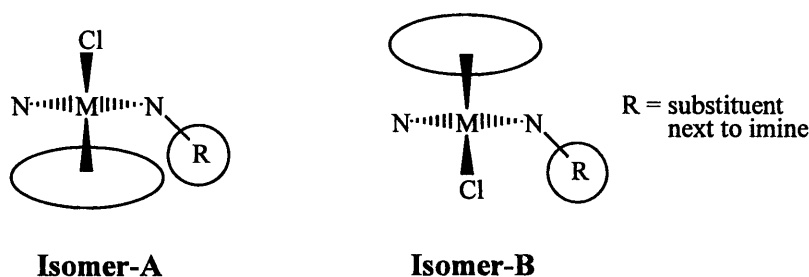


Figure (2.26): Illustration of Isomers A and B

The diastereoselectivity will depend primarily on the size of the R-substituent, since this is closest to the metal. If R is large, the steric interaction with mesitylene in isomer-A is expected to be significant; thus isomer-B, in which the R-substituent points at the chloride, would be energetically favoured. The diastereomer ratios were determined by

^1H NMR (see below) with X-ray crystallography and phase-sensitive NOESY experiments, used to confirm the identity of individual isomers.

Pymim complexes (**2.45**) and (**2.46**) are soluble in CDCl_3 , (**2.47**) is soluble in CD_2Cl_2 , whilst (**2.43**) and (**2.44**) are only sparingly soluble in CD_2Cl_2 , but completely soluble in d_6 -acetone. The ^1H NMR spectra of the complexed ligands are significantly different from those of the free ligands. The signals due to the pyridine and imidazoline ring protons of (**2.43-2.47**) are mostly shifted downfield (by 0.15–0.8 ppm) due to the ligand donating electron density to the metal. The mesitylene signals are observed at δ 2.32–2.07 ($\text{C}_6\text{H}_3\text{Me}_3$) and δ 5.51–5.30 ($\text{C}_6\text{H}_3\text{Me}_3$). The signals of the imidazoline complexes are at very similar chemical shifts to those of the related pymox complexes,¹³⁶ indicating that the ligands have similar steric and electronic requirements. Epimerisation of diastereomeric pymox complexes (**2.26-2.28**) was shown to be very slow on the chemical timescale at room temperature, even in d_6 -acetone, therefore it is likely that any epimerisation of (**2.43-2.47**) will not be fast on the chemical timescale.

Signals due to the pairs of diastereomers can readily be distinguished by ^1H NMR spectroscopy, particularly those due to mesitylene or the py-6-*H*. The relative integration of the two gives the diastereomer ratio. The ^1H NMR spectra of crude reaction mixtures containing (**2.43**) or (**2.44**) both contain two signals for the $\text{C}_6\text{H}_3\text{Me}_3$ protons, *i.e.* singlets at δ 5.40(5.52) for (**2.43**) and δ 5.43(5.51) for (**2.44**) with diastereomer ratios 53:47 and 47:53, respectively. The isomer ratios did not change over a month in d_6 -acetone, indicating that either the ruthenium configuration of (**2.43**) and (**2.44**) is stable under these conditions, or that the complexes have already reached the equilibrium diastereomer ratio and the rate of epimerisation is much slower than that of the NMR timescale.

Careful recrystallisation from mixtures of acetone/ether gave crystals suitable for X-ray diffraction. The X-ray structures of the cations are shown in **Figures (2.27)** and **(2.28)** respectively, with selected bond distances and angles in **Table (2.11)**. The complexes adopt the expected pseudo-octahedral structure, with the $\text{Ph}_2\text{-pymimR}''$ ligands coordinated such that the phenyl substituent adjacent to the imine nitrogen [C(8) for both complexes] is pointing towards the Cl (isomer-B), instead of towards the mesitylene ring (isomer-A). The configuration at the ruthenium centre is (*S*) ($\text{mes} > \text{Cl} > \text{N}_{\text{im}} > \text{N}_{\text{py}}$); the configurations at the chiral carbons are also both (*S*), as (1*S*,2*S*)-DPEN

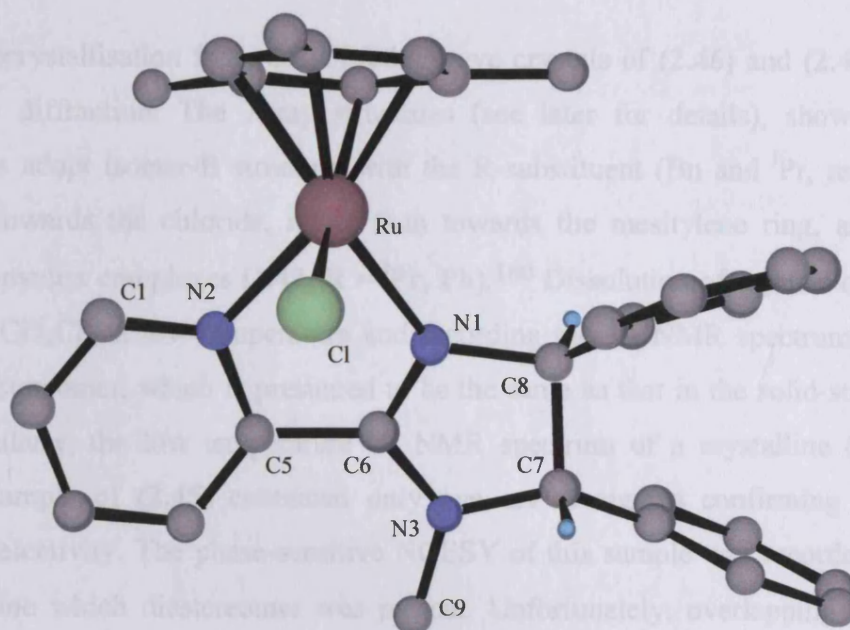


Figure (2.28): X-ray Structure of the cation (2.44)

In each case, dissolution of crystals of **(2.43)** or **(2.44)** in CD_2Cl_2 at -80°C and recording the ^1H NMR spectrum showed a single diastereomer which is assumed to be the same as that found in the solid state. In acetone solution the single diastereomers undergo epimerisation at the metal reaching equilibrium (*ca.* 45:55 mixture of diastereomers) over a period of 2-3 days at room temperature compared with about 40 days at 40°C for the pymox complex **(1.42, R = Ph)**.¹⁰⁰ The increased rate of epimerisation is consistent with the increased electron donor properties of the imidazoline, providing greater stabilisation of the presumed 16-electron intermediate than with the oxazoline. The phase-sensitive NOESY spectrum of **(2.43)** at equilibrium contained a structure determining nOe correlation between the signals at δ 2.08 ($\text{C}_6\text{H}_3\text{Me}_3$) and δ 5.77 (CH^bPh) for the major isomer; confirming that this diastereomer has isomer-B structure, which is the same as that found in the solid-state and directly after low temperature dissolution.

The ^1H NMR spectra in CD_2Cl_2 of crude reaction mixtures containing **(2.45-2.47)** each contained a single set of well-resolved signals, with no trace of a second isomer. This indicates that either **(2.45-2.47)** were formed in greater than 98:2 diastereomer ratio, or that epimerisation is fast on the NMR timescale such that time-averaged signals are observed. The latter suggestion is unlikely considering epimerisation of **(2.43)** and **(2.44)** took 2-3 days in (more solvating) acetone.

Recrystallisation from CH_2Cl_2 /ether gave crystals of (2.46) and (2.47) suitable for X-ray diffraction. The X-ray structures (see later for details), show that both complexes adopt isomer-B structure with the R-substituent (Bn and $i\text{Pr}$, respectively) pointing towards the chloride, rather than towards the mesitylene ring, as found in related R-pymox complexes (1.42, $\text{R} = i\text{Pr}, \text{Ph}$).¹⁰⁰ Dissolution of crystals of (2.46) or (2.47) in CD_2Cl_2 at low temperature and recording the ^1H NMR spectrum showed a single diastereomer, which is presumed to be the same as that in the solid-state in each case. Similarly, the low temperature ^1H NMR spectrum of a crystalline (non-X-ray quality) sample of (2.45) contained only one set of signals confirming very high diastereoselectivity. The phase-sensitive NOESY of this sample was recorded at 253K to determine which diastereomer was present. Unfortunately, overlapping CHMe_2 (δ 2.27) and $\text{C}_6\text{H}_3\text{Me}_3$ (δ 2.27) signals hinder unambiguous structure determination. However, the signals at δ 3.96 and 4.54 can be assigned to imidazoline ring protons H^{A} and H^{B} respectively since only H^{B} shows an nOe to the $\text{C}_6\text{H}_3\text{Me}_3$ signal at δ 5.38. Another nOe correlation was observed between CH^{A} (δ 3.96) and both CHMe_2 signals (δ 0.90 and 1.00) (see Figure 2.29), indicating the isopropyl group is on the same side as H^{A} *i.e.* towards the chloride ligand (isomer-B). In addition, nOes that would indicate isomer-A structure (shown in Figure 2.29, isomer-A) were absent. The NOESY spectrum thus confirms isomer-B structure for (2.45) as found in the solid-state structures of (2.46) and (2.47).

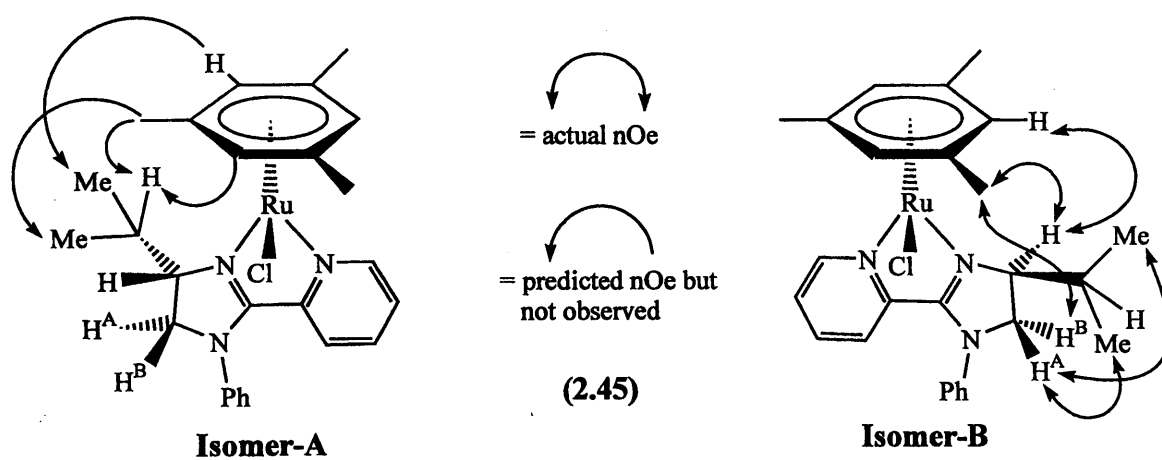


Figure (2.29): Hypothetical nOes for (2.45)

The X-ray structures of the cations of (2.46) and (2.47) are shown in Figures (2.30) and (2.31), respectively, with selected bond distances and angles in Table (2.12). As mentioned previously, both complexes adopt isomer-B structure with the R-

substituent pointing towards chloride. In the case of **(2.47)** the phenyl ring of the benzyl substituent is orientated anti and perpendicular to the mesitylene ring, reducing unfavourable interactions with both the mesitylene and chloride ligand. In contrast to **(2.43)**, **(2.44)** and **(1.42, R = ⁱPr**; [2.117(4) and 2.118(4) Å, respectively]) the Ru-N(2) and Ru-N(1) distances, to pyridine and imine, respectively, are statistically different within each complex **(2.46)** and **(2.47)**; the Ru-N(1)_{im} distances being shorter than Ru-N(2)_{py}, possibly due to greater electron donating ability of the imidazoline ring. However, the Ru-N(2)_{py} distances in **(2.46)** 2.112(5) Å, and **(2.47)** 2.098(8) Å, are statistically the same as the corresponding distances in **(2.43)**, **(2.44)** and **(1.42, R = ⁱPr)**¹⁰⁰ [2.115(7), 2.096(6) and 2.117(4) Å, respectively]. The Ru–Cl distances and chelate bite angles for **(2.46)** [2.406(2) Å, 75.55(18)°] and **(2.47)** [2.394(3) Å, 74.9(3)°] are similar to each other, and to those of the analogous complex **(1.42, R = ⁱPr)** [2.402(2) and 76.4(2) Å, respectively]. Thus **(2.46)** and **(2.47)** are structurally similar to **(1.42, R = ⁱPr)**, showing once again that the steric requirements of imidazolines are similar to those of the related oxazolines. This is also consistent with the similar diastereoselectivity observed for R-pymox complexes.

	(2.46)	(2.47)
Ru(1)–N(1)	2.097(8)	2.077(9)
Ru(1)–N(2)	2.112(5)	2.098(8)
Ru(1)–Cl	2.406(2)	2.394(3)
N(1)–Ru–N(2)	75.55(18)	74.9(3)
N(2)–C(1)–C(5)	120.9(3)	120.9(3)
N(1)–Ru–Cl	75.5(2)	74.9(3)

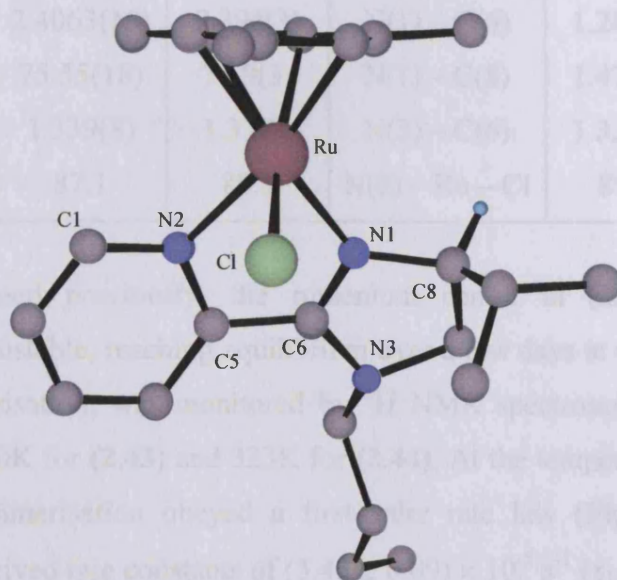


Figure (2.30): X-ray Structure of the cation (2.46)

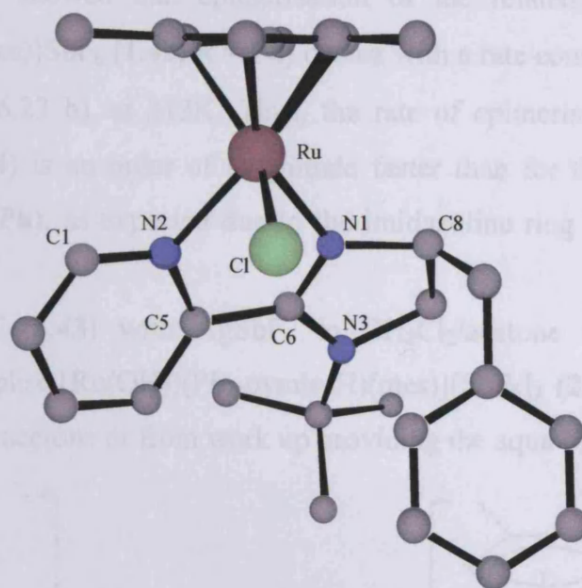


Figure (2.31): X-ray Structure of the cation (2.47)

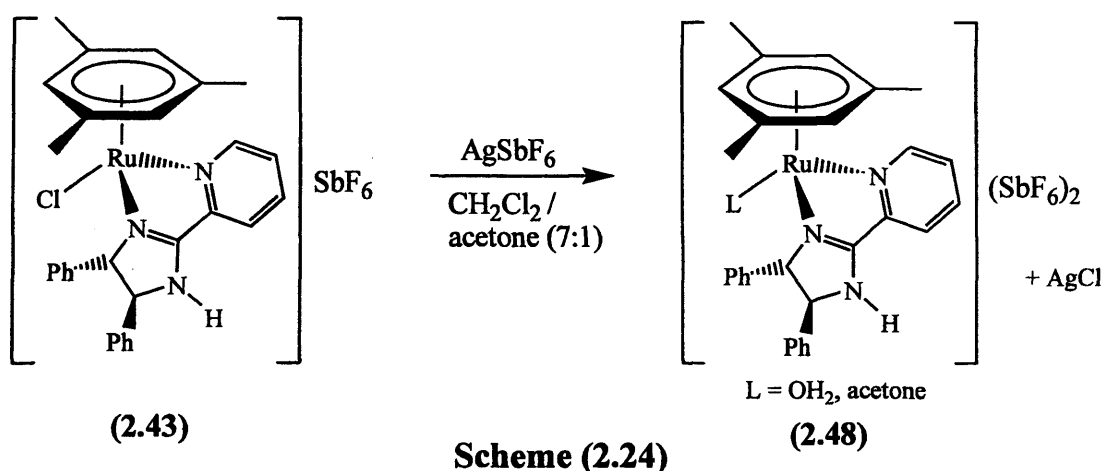
Table (2.12): Selected Bond Distances (Å) and Bond Angles (°) of (2.46) and (2.47)

	(2.46)	(2.47)		(2.46)	(2.47)
Ru(1) – N(1)	2.073(6)	2.057(9)	N(2) – C(5)	1.356(8)	1.373(14)
Ru(1) – N(2)	2.112(5)	2.098(8)	C(5) – C(6)	1.468(8)	1.481(15)
Ru(1) – Cl	2.4063(15)	2.394(3)	N(1) – C(6)	1.282(7)	1.306(13)
N(1) – Ru – N(2)	75.55(18)	74.9(3)	N(1) – C(8)	1.473(7)	1.471(13)
N(2) – C(1)	1.339(8)	1.33(2)	N(3) – C(6)	1.359(8)	1.362(14)
N(1) – Ru – Cl	87.1	88.3	N(2) – Ru – Cl	81.2	82.9

As mentioned previously, the ruthenium centre in (2.43) and (2.44) is configurationally unstable, reaching equilibrium over a few days at room temperature in d_6 -acetone. Epimerisation, was monitored by ^1H NMR spectroscopy at thermostated temperatures of 320K for (2.43) and 323K for (2.44). At the temperatures measured for (2.43-2.44) the epimerisation obeyed a first-order rate law (Figures 5.6-5.10, see Appendix) with derived rate constants of $(3.43 \pm 0.09) \times 10^{-5} \text{ s}^{-1}$ ($\tau_{1/2} = 5.61 \text{ h}$), at 323K for (2.43) and $(7.33 \pm 0.5) \times 10^{-5} \text{ s}^{-1}$ ($\tau_{1/2} = 2.63 \text{ h}$), at 320K for (2.44). The slightly faster rate of epimerisation for (2.43) may be due to deprotonation of the N–H group of the imidazoline, resulting in a neutral complex that is predicted to epimerise faster, as found for related pyrrolocarbaldimine⁹⁶ and phenmox complexes (see Section 2.1).

Similar experiments showed that epimerisation of the related oxazoline complex $[\text{RuCl}(\text{Ph-pymox})(\text{mes})]\text{SbF}_6$ (**1.42**, $\text{R} = \text{Ph}$) occurs with a rate constant of $(1.32 \pm 0.16) \times 10^{-6} \text{ s}^{-1}$ ($\tau_{1/2} = 146.23 \text{ h}$), at 313K. Thus, the rate of epimerisation in imidazoline complexes (**2.43/2.44**) is an order of magnitude faster than for the related oxazoline complex (**1.42**, $\text{R} = \text{Ph}$), as expected due to the imidazoline ring being more electron rich.

Treatment of (**2.43**) with AgSbF_6 in $\text{CH}_2\text{Cl}_2/\text{acetone}$ (7:1) generates the dicationic aqua complex $[\text{Ru}(\text{OH}_2)(\text{Ph}_2\text{-pymimH})(\text{mes})][\text{SbF}_6]_2$ (**2.48**) (Scheme 2.24), traces of water in the acetone or from work up providing the aqua ligand.



The pure complex was isolated by filtration of the crude reaction mixture through celite, to remove AgCl by-product, followed by recrystallisation from acetone/ether to yield a somewhat hygroscopic powder. Consequently, the X-ray crystal structure could not be obtained so characterisation has relied on NMR and mass spectrometry (Tables 2H.1 – 2H.2 and 2G.5). The H_2O ligand is expected to be easily lost in solution, as was found for the aqua complexes of phenmox and pymox, discussed earlier (Section 2.2.1 and 2.2.2). As a result, epimerisation is likely to be faster than with the corresponding chloride precursor (**2.43**). There are possible complications of competing acetone or water coordination in solution as well as the possibility of two diastereomers, so the NMR spectra may be more complicated. Complex (**2.48**) is only sparingly soluble in CD_2Cl_2 but very soluble in the more polar acetone or methanol. The ^1H NMR spectrum recorded in CD_2Cl_2 contains two species $[\text{RuL}(\text{Ph}_2\text{-pymimH})(\text{mes})]^{n+}$ with sharp signals in a ratio 19:81 and a singlet at δ 2.00 assigned to acetone, no signals being observed for water (coordinated or free water). Addition of d_6 -acetone to the NMR sample, to make an $\sim 10:1$ mixture of $\text{CD}_2\text{Cl}_2/\text{d}_6$ -acetone resulted

in the ratio of the minor set of signals increasing to $\sim 45:55$, providing evidence to suggest this species has acetone-coordinated, whilst the major has water-coordinated. The NMR signals for both species in CD_2Cl_2 , were very similar to those of the chloride precursor, except that the pymim and mesitylene signals are deshielded compared to the chloride precursor, consistent with them being dications. Thus, it is proposed that the two species are single diastereomers of (2.48) (one with acetone and one with water coordinated). Hence the diastereomer ratio is very different to those of the chloride precursors (2.43) and (2.44) and they may therefore be suitable for use as asymmetric catalysts (see Chapter Four).

In summary, we have demonstrated that imidazolines are sterically very similar to the corresponding oxazolines, giving comparable diastereoselectivities in arene ruthenium complexes. The rates of epimerisation of imidazoline complexes are faster than corresponding oxazoline complexes consistent with imidazolines being more electron-donating than oxazolines.

(2.2.4) - Half-Sandwich Complexes of Chiral Schiff-base Ligands

As outlined in Section 2.1, ketimine Schiff-base ligands (2.8, $\text{R} = \text{Ph}$, Nap, Cy) and (2.9, $\text{R} = \text{Me}$, ^iPr) were obtained from the research group of Vitimir Sunjic (Ruder Boskovic Institute, HR-Zagreb, Croatia). The ligands (2.8) exist as two tautomers (see Figure 2.32). The equilibrium position in the free ligands lies to the right, favouring the enamine tautomer.

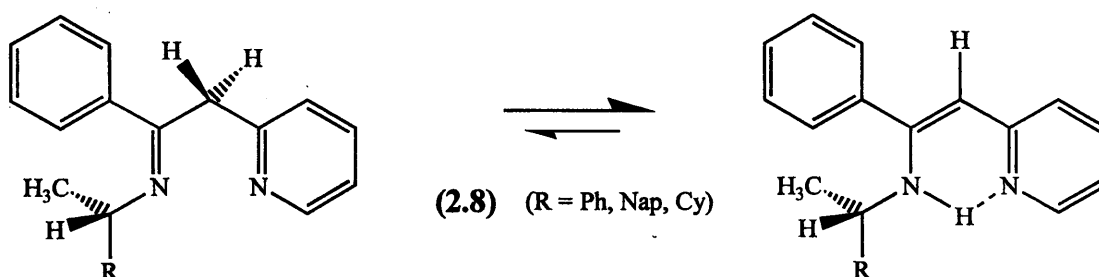


Figure (2.32): Tautomerism in ketimine ligands (2.8)

Reaction of $[\text{RuCl}_2(\text{mes})]_2$, two equivalents of ligand (2.8, $\text{R} = \text{Ph}$, Nap, Cy) and NaSbF_6 in refluxing MeOH gave yellow/orange solids in high yields. The electrospray mass spectra of the products contained negative ion patterns at $m/z - 235/237$ (100%) $[\text{M}]$ due to SbF_6^- . The elemental analyses were also consistent with the presence of SbF_6^- hence the products are formulated as salts (2.49-2.51) with the ligands

acting as neutral ketimines rather than deprotonated enamines and in all the complexes the metal centre is chiral hence two diastereomers are possible (see Figure 2.33).

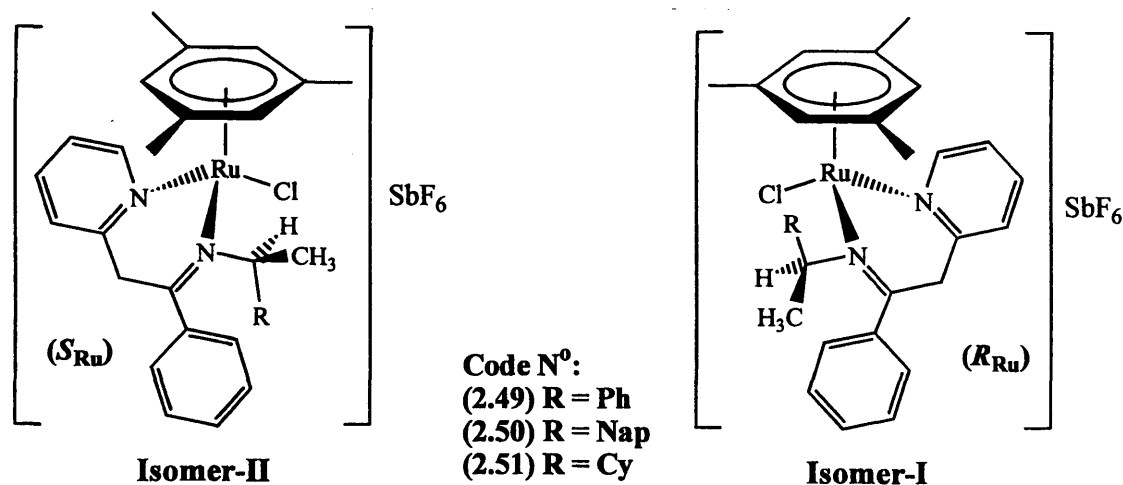


Figure (2.33): Diastereomers of (2.49 - 2.51)

Complexes (2.49 - 2.51) were fully characterised by ^1H NMR, mass spectrometry and microanalysis (Tables 2G.1 - 2G.5) and by X-ray diffraction (2.49). Two inequivalent ^1H doublet signals are observed in the ^1H NMR spectrum of each complex between δ 4.39 and 4.92 consistent with the ketimine tautomer of the ligand. The signals due to the coordinated ketimine ligand back-bone in (2.49-2.51) are mostly shifted downfield (by up to 1.8 ppm) compared to free ligand, due to donation of electron density to the metal. The signals due to mesitylene are observed between δ 2.02-2.27 ($\text{C}_6\text{H}_3\text{Me}_3$) and δ 5.11-5.64 ($\text{C}_6\text{H}_3\text{Me}_3$), at similar shifts to the pymox (2.26) and pymim (2.43 - 2.47) complexes containing neutral N,N -donor ligands. The ^1H NMR spectra of complexes (2.49 - 2.51) each show sharp signals corresponding to two diastereomers in ratios 8:92 (2.49), 34:66 (2.50) and 65:35 (2.51). Careful recrystallisation of (2.49) gave crystals suitable for X-ray diffraction; the X-ray structure of the cation is shown in Figure (2.34), with selected bond distances and angles given in Table (2.13). In the solid-state, complex (2.49) adopts the expected pseudo-octahedral structure and exists as a single diastereomer with (S_{Ru}) configuration, (arene > Cl > N_{im} > N_{py})^{104, 134} {the configuration at the chiral carbon is (S), as (S)-1-phenylethylamine was used in its synthesis^{131, 132}}.

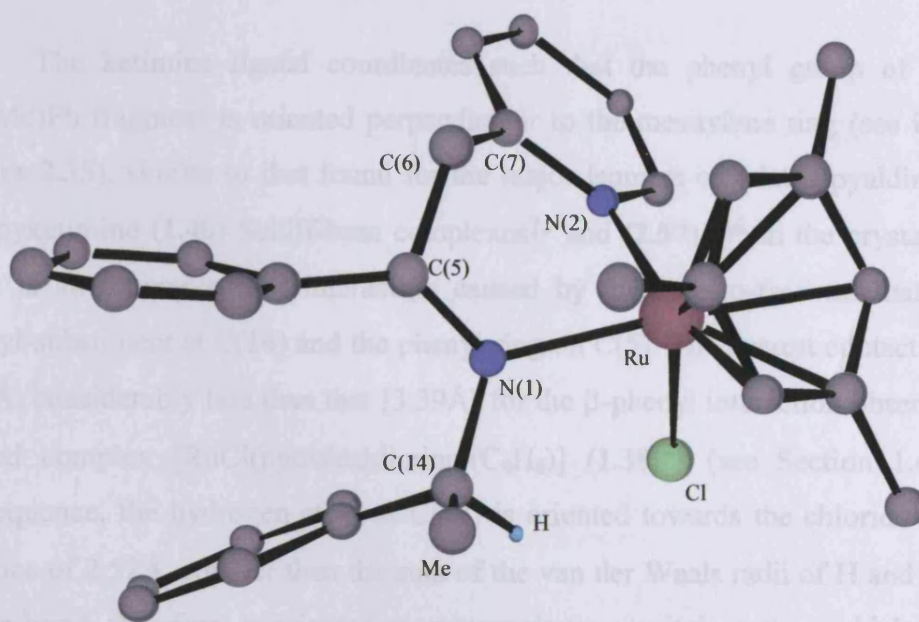
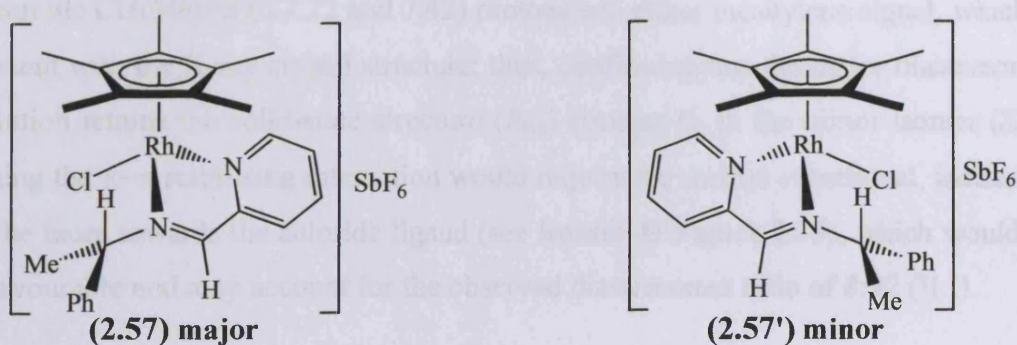


Figure (2.34): X-ray Structure of the cation (2.49)

Table (2.13): Selected Bond Distances (Å) and Bond Angles (°) of (2.49)

Ru(1) – N(1)	2.142 (3)	N(2) – C(5)	1.355 (5)
Ru(1) – N(2)	2.086 (3)	C(5) – C(6)	1.476 (7)
Ru(1)– Cl(1)	2.3886 (8)	C(6) – C(7)	1.516 (5)
N(1) –Ru- N(2)	83.15 (12)	N(1) – C(7)	1.282 (4)

The Ru–N(1) (imine) bond [2.142(3) Å] is much longer than the Ru–N(2) (pyridine) bond [2.086(3) Å], a similar though less pronounced difference is seen in related complexes (2.57) [2.131(4) and 2.113(4) Å, respectively]¹⁴⁶ and [RuCl(pyketimine)(mes)]BF₄ (1.40) [2.086(5) and 2.066(5) Å, respectively].⁷⁵ The pyridine and imine fragments in (2.49) are not conjugated, which is apparent from the puckered conformation of the six-membered chelate, with C(6) most out of the plane, unlike the essentially planar five-membered chelate rings observed for (1.40)⁷⁵ and (2.57).¹⁴⁶



The ketimine ligand coordinates such that the phenyl group of the $N_{\text{imine}}\text{-CH(Me)Ph}$ fragment is oriented perpendicular to the mesitylene ring (see **isomer-I** in **Figure 2.35**), similar to that found for the major isomers of related pyaldimine (**1.39**) and pyketimine (**1.40**) Schiff-base complexes⁷⁵ and (**2.57**).¹⁴⁶ In the crystal structure, there is an attractive $\pi\text{-}\pi$ interaction caused by the face-to-face orientation of the phenyl-substituent at C(14) and the phenyl ring on C(5). The nearest contact distance is 2.91 Å, considerably less than that [3.39 Å] for the β -phenyl interaction observed for the related complex [RuCl(pyrrolealdimine)(C₆H₆)] (**1.38**)⁹⁶ (see Section 1.4.3). As a consequence, the hydrogen atom at C(14) is oriented towards the chloride ligand at a distance of 2.52 Å, smaller than the sum of the van der Waals radii of H and Cl.¹⁴⁷ The C–Me bond, therefore, is oriented most towards the mesitylene ring, which is different to that in the major isomer of (**2.57**).¹⁴⁶ Interestingly, the edge-to-face β -phenyl interaction found in [RuCl(salaldimine)(arene)] (arene = C₆H₆, *p*-cy) complexes (**1.34/1.35**)^{91, 93} (see Section 1.4.3) is not present in this diastereomer nor related complexes (**1.39/1.40**)⁷⁵; perhaps because in these cases the arene is mesitylene for which the methyl substituents might inhibit the β -phenyl interaction.

Recording the ¹H NMR spectrum of the X-ray crystal sample showed two diastereomers in a ratio of 8:92. The ratio was independent of time, indicating that either the complex had epimerised to the equilibrium position or the X-ray sample was a mixture of diastereomerically pure crystals in a ratio of 8:92. To determine whether the solid-state structure corresponds to the major diastereomer in solution, a phase-sensitive NOESY experiment was performed (in d₆-acetone at 400 MHz). NOe correlations were observed between the CH(*Me*)Ph (δ 1.77) protons and both mesitylene signals (δ 2.19 for C₆H₃Me₃ and δ 5.23 for C₆H₃Me₃) but not between the CH(*Me*)Ph (δ 5.94) proton and the mesitylene signals, suggesting that this proton is not pointing towards the η^6 -arene as found in the major isomer of (**2.57**). In addition, NOes were not observed between the CH(*Me*)Ph (δ 7.22 and 7.42) protons and either mesitylene signal, which is consistent with the X-ray crystal structure; thus, confirming that the major diastereomer in solution retains the solid-state structure (*R*_{Ru}) (**isomer-I**). In the minor isomer (*S*_{Ru}), retaining the $\pi\text{-}\pi$ stabilising interaction would require the methyl substituent, instead of H, to be more towards the chloride ligand (see **isomer-II** **Figure 2.35**), which would be less favourable and may account for the observed diastereomer ratio of 8:92 (II:I).

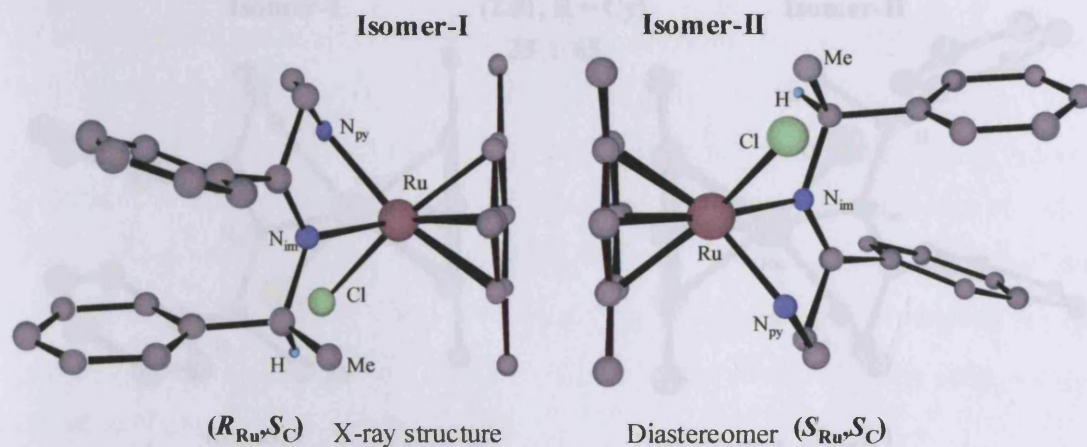


Figure (2.35): Favoured Conformations of (2.49)

The ^1H NMR spectrum of (2.50 *i.e.* $\text{R} = \text{Nap}$) shows two isomers (34:66) with signals of the major isomer being similar to those for the major isomer of (2.49), hence we assign this as the same diastereomer (R_{Ru} – isomer I). In contrast, the chemical shifts for the major isomer of (2.51, $\text{R} = \text{Cy}$) are similar to the minor isomer of (2.49, $\text{R} = \text{Ph}$); suggesting that with the sterically bulky (and non-aryl) cyclohexyl substituent at the chiral carbon the major diastereomer has the (S_{Ru}) configuration rather than (R_{Ru}) for both phenyl and naphthyl. In an attempt to fully characterise the rotamer structure of the major and minor diastereomers of (2.51), a phase-sensitive NOESY spectrum was recorded in CD_2Cl_2 . NOe correlations were observed between the $\text{CH}(\text{Me})\text{Cy}$ protons (δ 1.50 major and δ 1.36 minor) and both mesitylene signals in each isomer (δ 2.06 and 5.11 major, δ 2.12 and 5.22 minor), whilst nOes were not observed between the $\text{CH}(\text{Me})\text{Cy}$ quartet or any of the cyclohexyl protons with either of the mesitylene signals in either isomer. The nOe information is consistent with the C–Me bond, in each isomer being moderately close to the mesitylene however, an eclipsed conformation is unlikely, since this would also require the bulky cyclohexyl group to eclipse the C(7) phenyl, which would be sterically disfavoured; clearly no stabilising π - π interaction is possible with cyclohexyl. Possible structures are illustrated below (see **Figure 2.36**), isomer-I is generated from the X-ray structure of (2.49) by rotation about the $\text{N}_{\text{imine}}\text{--CH}(\text{Me})\text{Cy}$ bond of 60° , putting the Me closer to mesitylene and Cy away from the C(7) phenyl; isomer-II is generated in a similar manner.

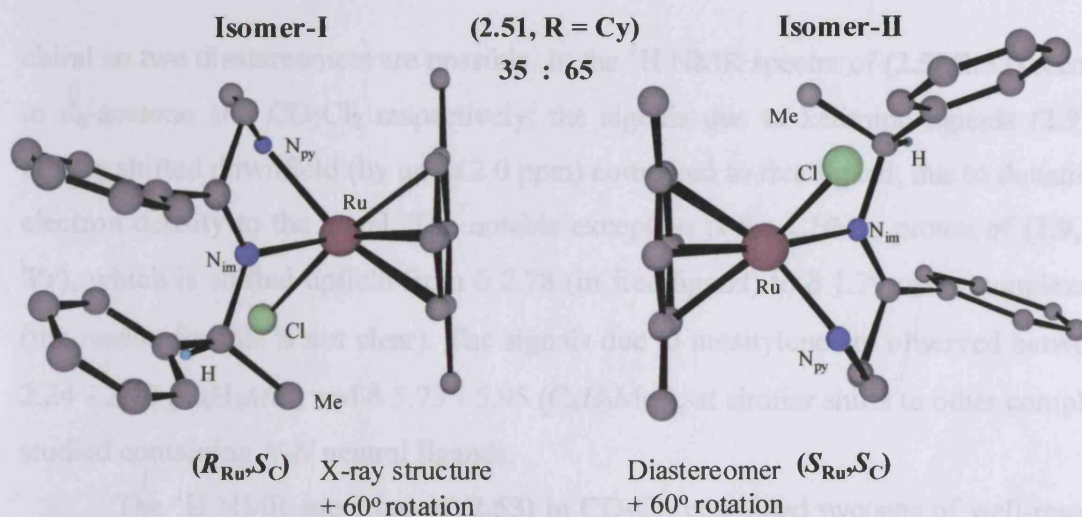
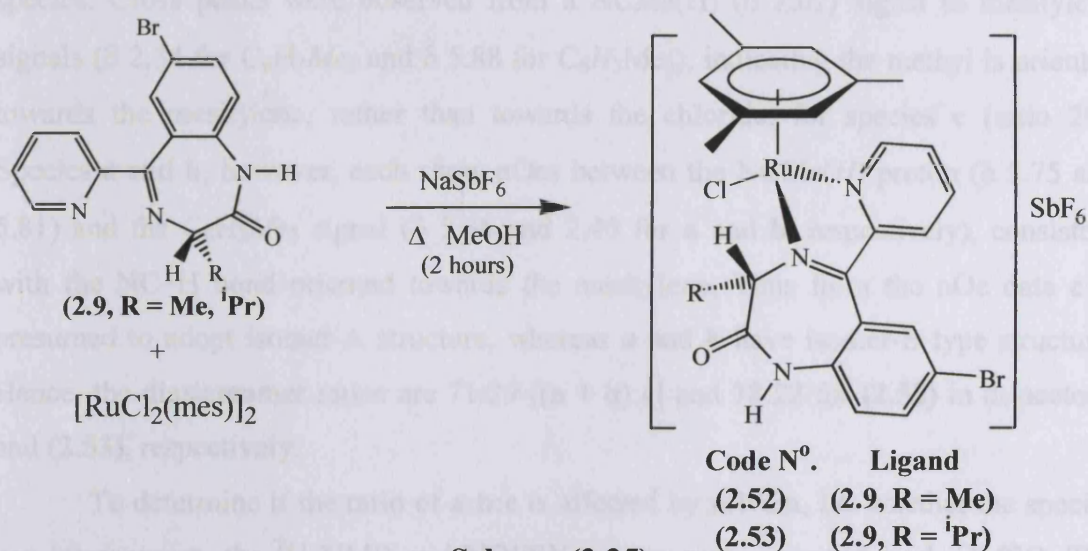


Figure (2.36): Representations for the most likely conformations of (2.51, R = Cy).

Note (For simplicity Cy is represented as planar)

Full verification of this assignment would require an X-ray structure of a single diastereomer, followed by ^1H NMR spectroscopy on the dissolved crystal sample.

Half-sandwich complexes $[\text{RuCl}(\text{R-ketimine})(\text{mes})]\text{SbF}_6$ ($\text{R} = \text{Me}, \text{}^i\text{Pr}$) (2.52/2.53), were synthesised in high yield (98-99%) from $[\text{RuCl}_2(\text{mes})]_2$, by treatment of the dimer with two equivalents of ligand (2.9, $\text{R} = \text{Me}, \text{}^i\text{Pr}$) and NaSbF_6 , in refluxing MeOH (Scheme 2.25).



Scheme (2.25)

Complexes (2.52/2.53) were characterised by ^1H NMR, mass spectrometry and microanalysis (Tables 2G.1 – 2G.5). In both complexes (2.52/2.53), the metal centre is chiral because the ketimine ligands are C_1 -symmetric, and the ligands themselves are

chiral so two diastereomers are possible. In the ^1H NMR spectra of (**2.52/2.53**) recorded in d_6 -acetone and CD_2Cl_2 respectively, the signals due to ketimine ligands (**2.9**) are mostly shifted downfield (by up to 2.0 ppm) compared to free ligand, due to donation of electron density to the metal. The notable exception is the CHMe_2 proton of (**2.9**, $\text{R} = \text{Pr}$), which is shifted upfield from δ 2.78 (in free ligand) to δ 1.79 upon complexation (the reason for this is not clear). The signals due to mesitylene are observed between δ 2.24 - 2.40 ($\text{C}_6\text{H}_3\text{Me}_3$) and δ 5.73 - 5.95 ($\text{C}_6\text{H}_3\text{Me}_3$), at similar shifts to other complexes studied containing *N-N* neutral ligands.

The ^1H NMR spectrum of (**2.53**) in CD_2Cl_2 contained two sets of well-resolved signals (for example, signals for two mesitylene rings and two isopropyl groups were observed) that did not change in ratio (72:28) over time, indicating the presence of two diastereomers. In contrast, the ^1H NMR spectrum of (**2.52**) in d_6 -acetone contained three “Ru(Me-ketimine)(mes)” species (*e.g.* signals at δ 5.95, 5.83 and 5.88 for $\text{C}_6\text{H}_3\text{Me}_3$) in a ratio of 36:35:29, these will be referred to as **a**, **b** and **c**, respectively. The ratio of signals did not change over time at room temperature or after heating at 40°C for 6 hours, suggesting that either the three species were not interconverting or that the equilibrium position had already been reached in d_6 -acetone. A phase-sensitive NOESY experiment was performed on this sample to aid structural determination of the three species. Cross peaks were observed from a NCMe(H) (δ 2.02) signal to mesitylene signals (δ 2.34 for $\text{C}_6\text{H}_3\text{Me}_3$ and δ 5.88 for $\text{C}_6\text{H}_3\text{Me}_3$), indicating the methyl is oriented towards the mesitylene, rather than towards the chloride, for species **c** (ratio 29). Species **a** and **b**, however, each show nOes between the NCMe(H) proton (δ 5.75 and 5.81) and the $\text{C}_6\text{H}_3\text{Me}_3$ signal (δ 2.36 and 2.40 for **a** and **b**, respectively), consistent with the NC-H bond oriented towards the mesitylene. Thus from the nOe data **c** is presumed to adopt isomer-A structure, whereas **a** and **b** have isomer-B type structure. Hence, the diastereomer ratios are 71:29 [(**a** + **b**):**c**] and 78:22 for (**2.52**) in d_6 -acetone and (**2.53**), respectively.

To determine if the ratio of **a:b:c** is affected by solvent, *i.e.* whether the species can interconvert, the ^1H NMR and NOESY spectra were recorded in d_6 -DMSO. The ratio of **a:b:c** was 76:12:12 (as evidenced by similar NOESY spectra in d_6 -DMSO and d_6 -acetone). A second spectrum, recorded after 17 hours, showed the ratios had further changed to 65:12:23. After heating for 2 hours at 50°C the equilibrium position of 63:12:25 (**a:b:c**) was reached. These experiments suggest that species **a/b** and **c**, which

have opposite ruthenium configurations (as determined by nOes), are diastereomers that have epimerised to the equilibrium ratio. The observation can be rationalised by the isomer-B diastereomer existing as two rotamers (species **a** and **b**) see **Figure (2.36)** where the seven-membered heterocycle can adopt both conformer **a** and **b**, similar to that found for related TMBA complex (**1.32**) (Section 1.4.3, p 27).

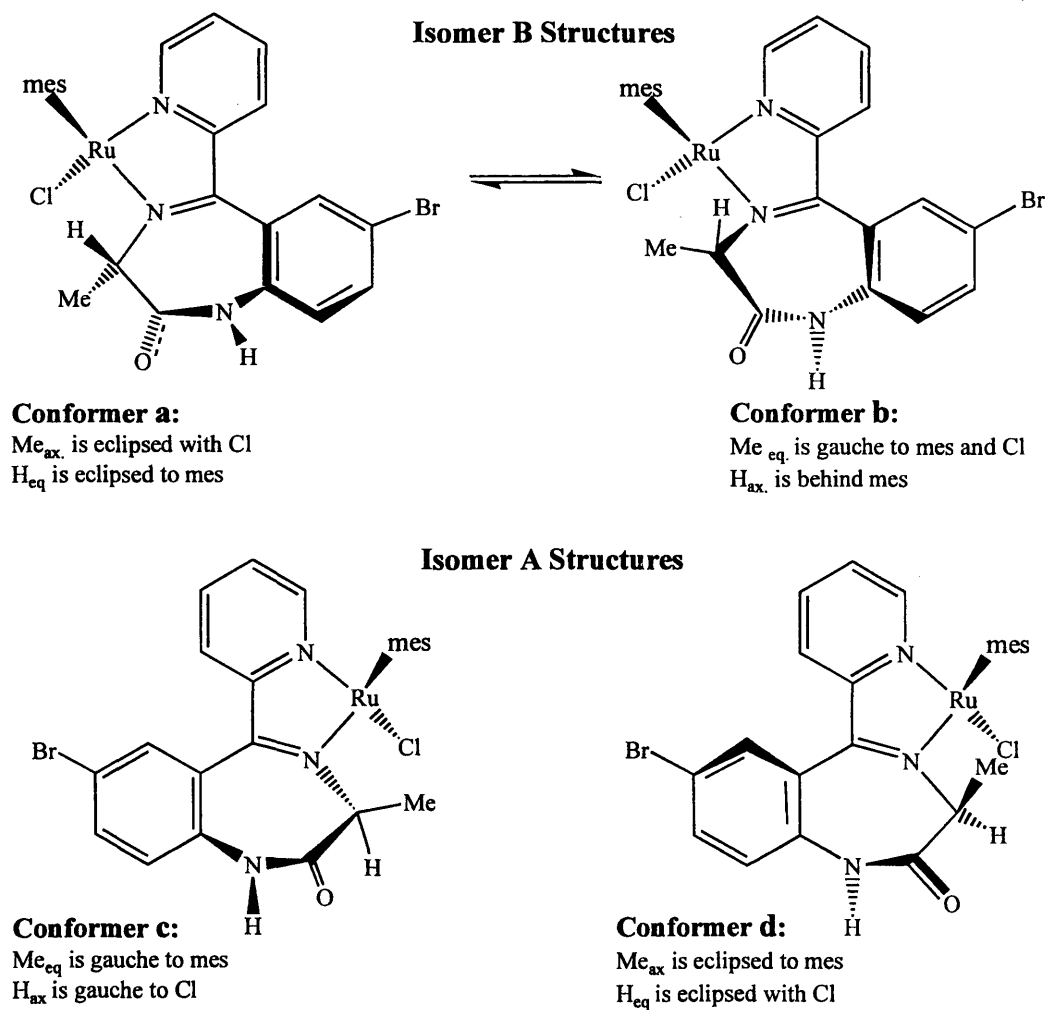
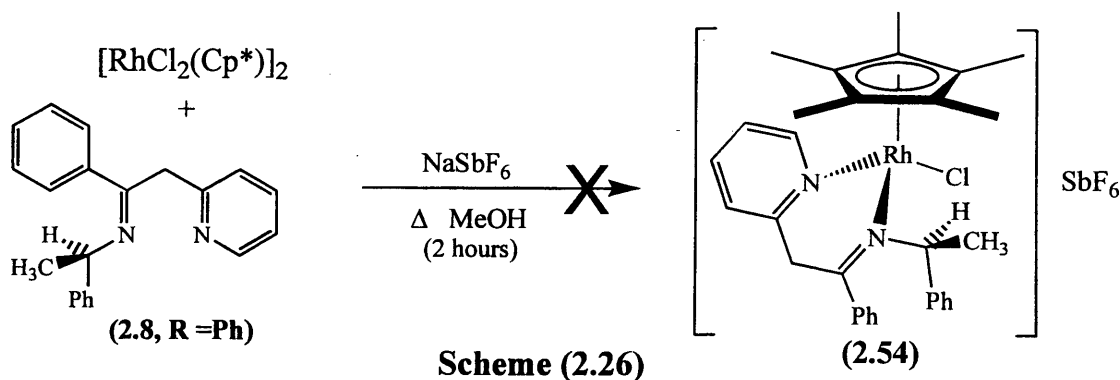


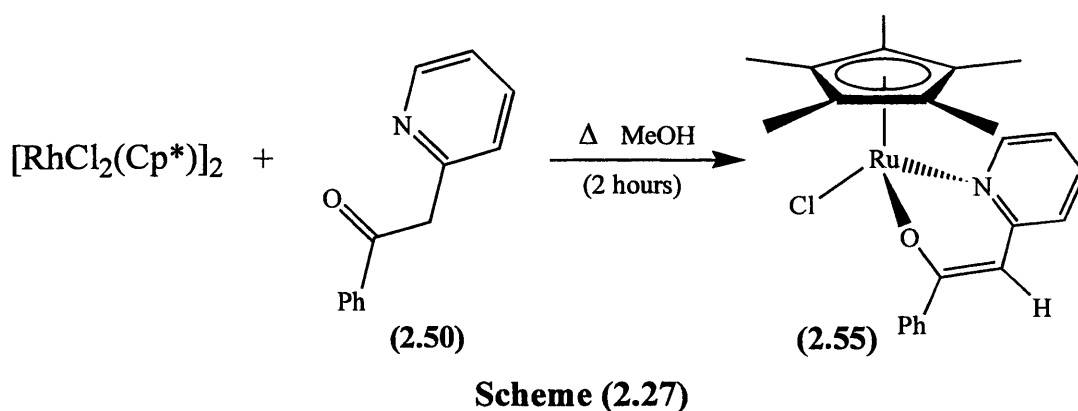
Figure (2.36): Hypothetical Conformers of (2.52)

In the isomer-A structure, the theoretical conformer **d** is disfavoured due to strong 1,3-diaxial mesitylene...Me interactions. In the isomer-B structure, the comparable interaction (see conformer **a**) is between mesitylene and H; thus less steric repulsion is expected.

Synthesis of $[\text{RhCl}(\text{Ph-ketimine})(\text{Cp}^*)]\text{SbF}_6$ (Ph-ketimine = **2.8**, **R = Ph**) (**2.54**), was attempted using identical conditions to those for analogous complexes (**2.49-2.51**) (**Scheme 2.26**).



The ^1H NMR spectrum (in CDCl_3) of the product showed the presence of a Cp^*Rh complex but no signals for the chiral $\text{N}_{(\text{imine})}\text{-CH}(\text{Me})\text{Ph}$ fragment were observed. Signals for a monosubstituted pyridyl, a phenyl and a singlet at δ 5.77 are observed indicating the product has part of the ligand coordinated. However, the chemical shifts are quite different to those of (2.49), the pyridyl signals being only *ca.* 0.1 ppm downfield from those in (2.8, R = Ph), hence it might be a neutral complex, which is supported by the high solubility in CDCl_3 . In addition, the two characteristic (1H) doublets due to PhC-CHH observed between (δ 4.5 – 4.7) in (2.49 – 2.51) were not present, instead a singlet (1H) (δ 5.77) was observed which is assigned to an olefinic proton. The electrospray mass spectrum contained a peak at m/z 434 (100%) $[\text{RhC}_{23}\text{H}_{25}\text{ON}]^+$ and no ion for SbF_6^- in the negative ion spectrum. These data are consistent with hydrolysis of ketimine (2.8, R = Ph) and formation of (2.55); microanalysis of the product also corresponded to (2.55). To confirm the identity of the product, $[\text{RhCl}_2(\text{Cp}^*)]_2$ was reacted with two equivalents of enaminone ligand (2.56) in refluxing MeOH (Scheme 2.27) forming (2.55) in 92% yield.



The ^1H NMR and mass spectra of (2.55) are identical to those of the product from the reaction shown in (Scheme 2.26), confirming, hydrolysis of ketimine (2.8, R =

Ph) to form enaminone ligand (**2.56**) must have occurred under the reaction conditions, *i.e.* the products from the syntheses in **Schemes (2.26/2.27)** are both $[\text{RhCl}(\text{enaminone})(\text{Cp}^*)]$ (**2.55**).

To summarise the coordination chemistry of the Schiff-base ligands described above, there are three main conclusions:

1. Schiff-base ligands (**2.8**) preferentially form half-sandwich complexes as neutral, rather than anionic ligands.
2. Increasing the size of the R-substituent affects the complex diastereoselectivity; however formation of single diastereomers was not achieved with either of the ligand types.
3. Formation of cationic complex $[\text{RhCl}(\text{Ph-ketimine})\text{Cp}^*]\text{SbF}_6$ (**2.54**) is disfavoured relative to ligand hydrolysis followed by complexation to form neutral $[\text{RhCl}(\text{enaminone})\text{Cp}^*]$ (**2.55**), deprotonation occurring easily in the ketone case but not for the imine.

(2.3) - Experimental

All reactions were carried out under an atmosphere of nitrogen, except for some purely organic reactions, or unless otherwise stated. The reactions were worked up in air hence precautions for storage of the isolated products are unnecessary. Solvents were dried by heating to reflux with the appropriate drying agents: dichloromethane from calcium hydride; diethyl ether, hexane, pentane and THF from sodium / benzophenone; chloroform and acetone from calcium sulphate; and ethanol and methanol from magnesium / iodine.

^1H , ^{13}C and $^{31}\text{P}\{^1\text{H}\}$ NMR spectra were recorded on a Bruker AM300 or DX400 (variable-temperature) spectrometers, in CDCl_3 unless otherwise indicated. When necessary, CDCl_3 and CD_2Cl_2 were dried over P_2O_5 , and d_6 -acetone and d_6 -DMSO over anhydrous calcium sulphate. Chemical shifts were recorded in ppm (on a δ scale for ^1H NMR, with tetramethylsilane or protonated solvent as internal reference). Microanalyses were performed by Butterworth Laboratories Ltd., Middlesex. The FAB mass spectra were recorded on a Kratos Concept mass spectrometer using a 3-nitrobenzyl alcohol matrix. Electrospray mass spectra were obtained on a Micromass Quattro LC using MeOH or MeCN. Circular dichroism spectra were run on a JASCO J-715 spectropolarimeter, polarimetric measurements on a Perkin-Elmer 341 instrument at ambient temperature at 589 nm, concentration in g per 100 ml solution. Crystal structure determinations were carried out by Dr. J. Fawcett using a Bruker P4 diffractometer and refinements were using SHELXL97, crystal details are given in **Tables (5.1 – 5.18; see Appendix, p 220)**.

Preparation of chiral ligands and precursors

The chiral amino alcohol (*S*)-2-phenylalaninol was a gift from Monsanto as >99% *e.e.* (*S*)-valinol, (*S*)-*tert*-leucinol and (*S*)-phenylglycinol were synthesised by NaBH_4/I_2 reduction of the relevant amino acid, according to the method of Meyers *et al.*¹⁴⁸. Pyridine-carboxyimide was prepared from cyanopyridine according to the literature procedure.¹⁰⁹ All other chemicals were obtained from Aldrich and Lancaster synthesis.

Preparation of Oxazoline ligands

The ligands R,R'-phenmox (R = ^tBu, ⁱPr or Ph, R' = H; R = R' = Me)^{111, 116} and ⁱPr-pymox^{111, 114} were synthesised by literature methods, or modifications thereof. The zinc dichloride catalyst was melted (293 °C) under high vacuum and then cooled under nitrogen.

Preparation of (S)-Bn-phenmox (2.2, R = Bn)

Using the general method of Bolm,¹¹¹ anhydrous ZnCl₂ (57.5 mg, 0.422 mmol), 2-hydroxybenzotrile (1.0 g, 8.40 mmol) and (S)-phenylalaninol (1.904 g, 12.6 mmol) were heated to reflux in chlorobenzene (45 ml) for 24 hours, then evaporated. The crude residue was dissolved in dichloromethane (45 ml) and the solution was extracted three times with water (3 x 25 ml). The aqueous layers were extracted with dichloromethane (40 ml) and the combined organic layers were dried over MgSO₄. The solvent was evaporated, leaving an off-white residue that was purified by column chromatography eluting with CH₂Cl₂/petrol 40-60°C (1:1) to give 1.38 g (68.7% yield) of a clear yellow oil, that was shown to be pure by ¹H NMR: δ 2.81 (1H, dd, PhCH), 3.11 (1H, dd, PhCH'), 4.13 (1H, dd, OCH), 4.20 (1H, dd, OCH'), 4.62 (1H, m, NCH), 6.87 (1H, m, Ar-5-H), 7.01 (1H, m, Ar-3-H), 7.30 (1H, m, Ar-4-H), 7.63 (1H, m, Ar-6-H), 12.23 (1H, s, OH).

Preparation of chiral Imidazoline ligands and precursors

The enantiopure (N)-sulfonyl-aziridines (**2.38**, R = ⁱPr; Q = Ms, Ns),¹⁴⁴ (N)-diphenylphosphinoyl-aziridines (**2.40**, R = ⁱPr, Bn)¹⁴⁵ and (N)-Boc-(L)-valine (**2.34**),¹⁴² were synthesised by literature methods, or modifications thereof.

Preparation of (1S,2S)-Ph₂-pymimH (2.30)

A mixture of pyridine-carboxyimide (303 mg, 2.22 mmol), (1S,2S)-1,2-diphenylethylenediamine (471 mg, 2.22 mmol) and CHCl₃ (1 ml) was stirred overnight at 60°C. The resulting pale yellow paste was evaporated, dissolved in CH₂Cl₂ and then washed with three 15 ml portions of water. The aqueous layers were extracted with dichloromethane (40 ml) and the combined organic layers were dried over MgSO₄ and evaporated to give an off-white solid. Recrystallisation from CH₂Cl₂/hexane afforded a white crystalline solid. Yield = 627 mg (85%).

^1H NMR (400MHz, CDCl_3 , 243 K): δ 4.86 (dd, 1H, $\{J = 1, 9 \text{ Hz}\}$, CH^aPh), 5.13 (d, 1H, $\{J = 9 \text{ Hz}\}$, CH^bPh), 6.62 (br s, 1H, NH), 7.36 (m, 10H, 2^*Ph), 7.48 (ddd, 1H, $\{J = 1, 5, 7.5 \text{ Hz}\}$, py 5-*H*), 7.88 (dt, 1H, $\{J = 2, 7.5 \text{ Hz}\}$, py 4-*H*), 8.34 (td, 1H, $\{J = 1, 8 \text{ Hz}\}$, py 3-*H*), 8.66 (ddd, 1H, $\{J = 1, 2, 5 \text{ Hz}\}$, py 6-*H*). FAB-MS: m/z 300 $[\text{M} + \text{H}]^+$. Microanalysis: $\text{C}_{20}\text{H}_{17}\text{N}_3$ found (calculated) C: 80.06 % (80.24 %), H: 5.84 % (5.72 %), N: 14.54 % (14.04 %).

Preparation of (1S,2S)-Ph₂-pymimMe (2.32)

To a dry degassed colourless solution of (1S,2S)-Ph₂-pymimH (**2.30**) (319 mg, 1.06 mmol) in THF (24 ml) at 243K was added a cyclohexane solution of LDA (1.5M, 2.13 ml, 2.44 mmol), the solution immediately turned dark purple. After stirring for four hours dry MeI (73 μl , 1.17 mmol) was added and the reaction mixture allowed to slowly warm to room temperature over two hours, which was accompanied by a colour change to pale yellow/brown. Evaporation gave a brown crude residue which was dissolved in CH_2Cl_2 and then washed with three 20 ml portions of water. The aqueous layers were extracted with dichloromethane (40 ml) and the combined organic layers were dried over MgSO_4 and evaporated to give a pale brown oily residue. The oil was chromatographed on silica, with $\text{CHCl}_3/\text{MeOH}/\text{NEt}_3$ (80:15:5) as eluents. Evaporation of the fore-run gave an oil; recrystallisation from various laboratory solvents failed to give a solid product, however the resultant pale brown oil (**2.32**) (247 mg, 74%) was pure by ^1H NMR.

^1H NMR: δ 2.99 (s, 3H, NMe), 4.36 (d, 1H, $\{J = 10.5 \text{ Hz}\}$, CH^aPh), 4.99 (d, 1H, $\{J = 10.5 \text{ Hz}\}$, CH^bPh), 7.32 (m, 11H, $2^*\text{Ph} + \text{py } 5\text{-H}$), 7.81 (dt, 1H, $\{J = 2, 8 \text{ Hz}\}$, py 4-*H*), 8.10 (td, 1H, $\{J = 1, 7.5 \text{ Hz}\}$, py 3-*H*), 8.71 (ddd, 1H, $\{J = 1, 2, 5 \text{ Hz}\}$, py 6-*H*). FAB-MS: m/z 314 $[\text{M} + \text{H}]^+$.

Preparation of [(1S,2S)-Ph₂-pymimMe₂]OTf (2.33)

To a dry degassed colourless solution of (1S,2S)-Ph₂-pymimH (**2.30**) (82 mg, 0.274 mmol) in CH_2Cl_2 (3 ml) at 195K was added TfOMe (0.062 ml, 0.568 mmol). After stirring for 2 hours, dry NEt_3 (0.042 ml, 0.301 mmol) was added and the reaction mixture allowed to slowly warm to room temperature over two hours, which was accompanied by a colour change to pale brown. Evaporation gave a light brown crude residue which was dissolved in CH_2Cl_2 and then washed with three 20 ml portions of

water. The aqueous layers were extracted with dichloromethane (40 ml) and the combined organic layers were dried over MgSO₄ and evaporated to give a pale brown oily residue. The oil was chromatographed on silica, with CHCl₃/MeOH/NEt₃ (80:15:5) as eluents. Evaporation of the fore-run gave an oil; recrystallisation from various laboratory solvents failed to give a solid product, however the resultant pale brown oil (**2.33**) (53 mg, 39%) was pure by ¹H NMR.

¹H NMR: δ 2.94 (s, 6H, 2*N-Me), 5.24 (s, 2H, 2*MeNCHPh), 7.50 (m, 10H, 2*Ph), 7.68 (m, 1H, Py-5-H), 8.14 (t, 1H, {J = 8.5 Hz}, Py-4-H), 8.48 (d, 1H, {J = 8.5 Hz}, Py-3-H), 8.86 (d, 1H, {J = 6.5 Hz}, Py-6-H). ES-MS: *m/z* 328 (100%) [M]⁺, *m/z* 149 (100%) [M]⁻.

Preparation of (N)-Boc-(L)-valamide (**2.35**)

Using a method similar to that of Miyazawa *et al.*,¹⁴³ to a stirred solution of (N)-Boc-(L)-valine (8.52 g, 39.3 mmol), HOBT (530 mg, 3.93 mmol) and DCC (8.91 g, 43.2 mmol) in THF (200 ml) at 273K was slowly added ^tBuNH₂ (4.13 ml, 39.3 mmol). After stirring for 5 minutes a white precipitate (DCU) formed and the suspension was warmed to room temperature and stirred for 72 hours. The white precipitate was removed by filtration through celite and the filtrate was evaporated to give a yellow/white residue. The crude product was chromatographed on silica, with hexane/ethyl acetate (2:1) as eluent. Evaporation of the fore-run gave (**2.35**) (4.790 g, 45%).

¹H NMR: δ 0.92 (d, 3H, {J = 6.5 Hz}, CHMe'Me), 0.98 (d, 3H, {J = 6.5 Hz}, Me'CHMe), 1.36 (s, 9H, HN-^tBu), 1.47 (s, 9H, O-^tBu), 2.08 (m, 1H, CHMe'Me), 3.73 (m, 1H, Me'CH), 5.11 (m, 1H, HN^tBu), 5.70 (m, 1H, ^tBuO(CO)NH); ¹³C Dept 135: δ 17.01 (Me'CHMe), 18.21 (Me'CHMe), 27.26 (N-CMe₃), 27.68 (O-CMe₃), 30.22 (CHMe'Me), 49.11 {47.84} (ⁱPrCH), 152.53 (NCMe₃), 154.91 (OCMe₃), 155.71 (OC)NH^tBu), 169.82 (OC-O^tBu). FAB-MS: *m/z* 273 [M + H]⁺. Microanalysis: C₁₄H₂₈N₂O₃ found (calculated) C: 61.08 % (61.73 %), H: 10.00 % (10.36 %), N: 10.08 % (10.28 %).

Reduction of (N)-Boc-(L)-valamide (**2.35**)

A solution of (**2.35**) (1.00 g, 3.67 mmol), 1M LiAlH₄(sol.) (5.14 ml, 5.14 mmol) in THF (40 ml) was heated to reflux for 4 days. Water (3 ml) was slowly added (to destroy excess LiAlH₄) producing a white precipitate that was removed by filtration.

Evaporation gave an off-white residue which was dissolved in CH₂Cl₂ (40 ml) and washed with water (3 x 20 ml). The aqueous layers were extracted with dichloromethane (40 ml) and the combined organic layers were dried over MgSO₄ and evaporated to give 1-^tBu,5-ⁱPr-imidazolidin-2-one (**2.36**) as a white semi-crystalline solid. Yield = 460 mg (49%).

¹H NMR: δ 0.90 (d, 3H, {J = 6.5 Hz}, MeCHMe'), 0.94 (d, 3H, {J = 6.5 Hz}, MeCHMe'), 1.38 (s, 9H, Me₃C-N), 1.62 (m, 1H, MeCHMe'), 3.10 (t, 1H, {J = 8 Hz}, NCHH'), 3.25 (dd, 1H, {J = 8.5, 1.5 Hz}, NCHⁱPr), 3.50 (t, 1H, {J = 8.5 Hz}, NCHH'), 4.59 (br.s, 1H, N-H); ¹³C: δ 16.99 (MeCHMe'), 17.47 (MeCHMe'), 26.59 (N-CMe₃), 32.06 (MeCHMe'), 46.47 (NCH₂), 51.68 (N-CMe₃), 54.35 (NCHⁱPr), 161.56 (C=O). ES-MS: *m/z* 259 [M + H]⁺. IR: 1456.3 cm⁻¹ (C-N), 1685.6 cm⁻¹ (C=O).

General Method A: Chiral Aziridine Ring Opening

A solution of *N*-protected chiral aziridine (1 equivalent) and primary amine (10 equivalents) in MeOH (2 ml) were heated to reflux for 2-10 days, then evaporated. The crude oil was purified by dissolving in CH₂Cl₂ and adding hexane causing separation of the product as a pale-yellow oil that was pure by NMR. Quantities of reagents used, yields obtained, NMR data and mass spectrometry results are given in lists below.

Preparation of (2*S*)-ⁱPr-(*N*)-Ms-(*N*)-^tBu-ethylenediamine (**2.38**, Q = Ms)

Following general method A, using (1*S*)-ⁱPr-(*N*)-Ms-aziridine (**2.37**, Q = Ms) (908 mg, 5.56 mmol) and ^tBuNH₂ (5.84 ml, 55.6 mmol) gave (**2.38**, Q = Ms) as an oil (1.206 g, 92 %).

¹H NMR: δ 0.96 (d, 3H, {J = 6.5 Hz}, MeCHMe'), 0.98 (d, 3H, {J = 6 Hz}, MeCHMe'), 1.10 (s, 9H, N-CMe₃), 1.86 (m, 1H, MeCHMe'), 2.70 (m, 2H, CH₂NCMe₃), 3.02 (s, 3H, MeSO₂), 3.14 (m, 1H, CHCHMeMe'). FAB-MS: *m/z* 237 (100%) [M + H]⁺, *m/z* 473 (5%) [2M + H]⁺.

Preparation of (2*S*)-ⁱPr-(*N*)-Ns-(*N*)-^tBu-ethylenediamine (**2.38**, Q = Ns)

Following general method A, using (1*S*)-ⁱPr-(*N*)-Ns-aziridine (**2.37**, Q = Ns) (420 mg, 1.55 mmol) and ^tBuNH₂ (0.96 ml, 15.5 mmol) gave (**2.38**, Q = Ns) as an oil (530 mg, 99 %).

¹H NMR: δ 0.91 (s, 9H, N-^tBu), 0.91 (d, 3H, {J = 6.5 Hz}, MeCHMe'), 0.95 (d, 3H, {J = 6.5 Hz}, MeCHMe'), 1.88 (octet, 1H, {J = 6.5 Hz}, MeCHMe'), 2.49 (dd, 1H, {J = 12.0, 4.5 Hz}, N-CHH'), 2.58 (dd, 1H, {J = 12, 6.5 Hz}, N-CHH'), 3.23 (ddd, 1H, {J = 6.5, 6.5, 4.5 Hz}, NsHN-CH), 7.72 (m, 2H, Ns), 7.95 (m, 1H, Ns), 8.14 (m, 1H, Ns). ES-MS: *m/z* 345 [M + H]⁺.

Preparation of (2S)-Bn-(N)-^tBu-(N)-POPh₂-ethylenediamine (2.40 R=Bn, R''=^tBu)

Following general method A, using (1S)-Bn-(N)-POPh₂-aziridine (**2.39**, R = Bn) (997 mg, 2.79 mmol) and ^tBuNH₂ (2.93 ml, 27.9 mmol) gave (**2.40 R=Bn, R''=^tBu**) as an oil (1.012 g, 83 %).

³¹P{¹H} NMR C₆D₆/MeOH: δ 23.59 (N-P{O}Ph₂); ¹H NMR 250 MHz: δ 1.07 (s, 9H, N-^tBu), 2.71 (m, 1H, CHPh), 2.77 (br.s, 1H, ^tBuN-H), 2.84 (m, 1H, CHPh), 3.30 (br.s, 1H, P(O)N-H), 3.30 (m, 2H, ^tBuNH-CH₂), 3.99 (m, 1H, NCHBn), 7.05 (m, 2H, Ph), 7.22 (m, 6H, Ph), 7.37 (m, 3H, Ph), 7.52 (m, 2H, Ph), 7.80 (m, 2H, Ph); ¹³C Dept 135 CDCl₃: δ 29.01 (CMe₃), 41.77 (PhCH₂), 47.59 (^tBuNHCH₂), 51.49 (CMe₃), 54.07 (NCH^tPr), [3°] 126.78, 128.77, 128.84, 128.91, 130.06, 131.33, 131.90, 132.28, 132.71, 132.86 (P-C 4°), 139.08 (P-C 4°).

Preparation of (2S)-ⁱPr-(N)-ⁿBu-(N)-POPh₂-ethylenediamine (2.40 R=ⁱPr, R''=ⁿBu)

Following general method A, using (1S)-ⁱPr-(N)-POPh₂-aziridine (**2.39**, R = ⁱPr) (616 mg, 2.04 mmol) and ⁿBuNH₂ (6.90 ml, 70.0 mmol) gave (**2.40 R=ⁱPr, R''=ⁿBu**) as an oil (760 mg, 99 %).

³¹P{¹H} NMR: δ 24.19 (N-P(O)Ph₂); ¹H NMR: δ 0.90 (m, 6H, MeCHMe' + MeCHMe'), 0.90 (m, 3H, ⁿPr-CH₃), 1.37 (m, 2H, -CH₂-CH₃), 1.49 (m, 2H, -CH₂-Et), 1.88 (m, 1H, MeCHMe'), 2.41 (br.s, 1H, N-H), 2.55 (m, 2H, N-CH₂-ⁿPr), 2.70 (d, 2H, {J = 6 Hz}, OCH₂), 2.99 (m, 1H, NCH), 3.20 (br.s, 1H, Ph₂P{O}N-H), 7.45 (m, 6H, 2*Ph), 7.92 (m, 4H, 2*Ph).

Preparation of (2S)-ⁱPr-(N)-Ph-(N)-POPh₂-ethylenediamine (2.40 R=ⁱPr, R''= Ph)

Following general method A, using (1S)-ⁱPr-(N)-POPh₂-aziridine (**2.39**, R = ⁱPr) (994 mg, 3.49 mmol) and PhNH₂ (10.20 ml, 12.0 mmol) gave (**2.40 R=ⁱPr, R''= Ph**) as an oil (1.12 g, 90 %).

$^{31}\text{P}\{^1\text{H}\}$ NMR: δ 25.50 (N-*P*(O)Ph₂); ^1H NMR: δ 0.96 (t, 6H, {*J* = 6.5 Hz}, CHMeMe'), 1.90 (m, 1H, MeCHMe'), 2.84 (m, 1H, NCHⁱPr), 2.97 (m, 1H, PhNCH^b), 3.32 (dd, 1H, {*J* = 12, 3 Hz}, PhNCH^c), 3.67 (br.s, 2H, PhN-*H* + Ph₂P(O)N-*H*), 6.68 (m, 3H, *Ph*-N), 7.20 (m, 2H, *Ph*-N), 7.45 (m, 4H, *P-Ph*₂), 7.71 (m, 2H, *P-Ph*₂), 7.90 (m, 4H, *P-Ph*₂). ES-MS: *m/z* 379 (100%) [M + H]⁺, *m/z* 401 (70%) [M + Na]⁺.

Preparation of (2*S*)-ⁱPr-(*N*)-Bn-(*N*)-POPh₂-ethylenediamine (**2.40** R = ⁱPr, R'' = Bn)

Following general method A, using (1*S*)-ⁱPr-(*N*)-POPh₂-aziridine (**2.39**, R = ⁱPr) (50 mg, 0.165 mmol) and BnNH₂ (1.53 ml, 14.0 mmol) gave (**2.40** R = ⁱPr, R'' = Bn) as an oil (71 mg, 104 %).

$^{31}\text{P}\{^1\text{H}\}$ NMR: δ 24.47 (N-*P*(O)Ph₂). This compound was not isolated but was deprotected to give (**2.41** R = ⁱPr, R'' = Bn) see below.

General Method B: Chiral Ethylenediamine Deprotection

Dry HCl_(g) was bubbled through a solution of *N*-POPh₂ protected chiral ethylenediamine (**2.40**) in 1:1 CH₂Cl₂/ether (20 ml) dry for 10 minutes, resulting in precipitation of an off-white residue. This residue was collected by filtration, dissolved in 2M HCl (20 ml) and washed with CH₂Cl₂ (2 x 25 ml). The organic layers were extracted with water, the acidic aqueous layers were combined and then treated with KOH_(s) to pH 11. The resulting alkali solution was extracted with CH₂Cl₂ (3 x 40 ml), dried over MgSO₄ and evaporated to afford pale yellow/brown oils. Recrystallisations failed to yield solids, returning oils that were pure by NMR. Quantities of reagents used, yields obtained, NMR data and mass spectrometry results are given in lists below.

Preparation of (1*S*)-Bn-(*N*)-^tBu-ethylenediamine (**2.41**, R = Bn, R'' = ^tBu)

Following general method B, with (**2.40** R = Bn, R'' = ^tBu) (1.012 g, 2.49 mmol). Yield = 250 mg (49 %).

^1H NMR: δ 1.07 (s, 9H, CMe₃), 1.07 (br.s, 3H, NH₂ + ^tBuNH), 2.34 (dd, 1H, {*J* = 10.5, 8.5 Hz}, CHPh), 2.45 (dd, 1H, {*J* = 11, 10 Hz}, CHPh), 2.63 (dd, 1H, {*J* = 11.5, 3.5 Hz}, Bu^tNCH^t), 2.77 (dd, 1H, {*J* = 12, 3.5 Hz}, Bu^tNCH), 2.93 (m, 1H, NCH-Bn), 7.17 (m, 3H, CH₂Ph), 7.27 (m, 2H, CH₂Ph). ES-MS: *m/z* 207 (100%) [M + H]⁺, *m/z* 190 [M - NH₂]⁺.

Preparation of (1*S*)-ⁱPr-(*N*)-ⁿBu-ethylenediamine (2.41, R = ⁱPr, R'' = ⁿBu)

Following general method **B**, with (2.40, R = ⁱPr, R'' = ⁿBu) (760 mg, 2.02 mmol). Yield = 246 mg (77 %).

¹H NMR 250 MHz: δ 0.91 (m, 6H, MeCHMe'), 0.91 (m, 3H, ⁿPrCH₃), 1.35 (m, 2H, -CH₂CH₃), 1.52 (m, 2H, -CH₂C₂H₅), 1.52 (m, 1H, MeCHMe'), 1.93 (br.s, 3H, NH₂ + ⁿBnN-H), 2.39 (dd, 1H, {J = 10.5, 9.5 Hz}, ⁿBuNCH^b), 2.62 (m, 2H, N-CH₂ⁿPr), 2.62 (m, 1H, ⁱPr-CH^a-N), 2.75 (dd, 1H, {J = 10.5, 3 Hz}, ⁿBuN-CH^c). ES-MS: *m/z* 159 (100%) [M + H]⁺, *m/z* 142 (90%) [M - NH₂]⁺, *m/z* 181 (10%) [M + Na]⁺.

Preparation of (1*S*)-ⁱPr-(*N*)-Ph-ethylenediamine (2.41, R = ⁱPr, R'' = Ph)

Following general method **B**, with (2.40, R = ⁱPr, R'' = Ph) (1.12 g, 2.96 mmol). Yield = 366 mg (69 %).

¹H NMR: δ 0.95 (d, 3H, {J = 7.5 Hz}, MeCHMe'), 0.99 (d, 3H, {J = 7.5 Hz}, MeCHMe'), 1.33 (br.s, 2H, -NH₂), 1.68 (m, 1H, MeCHMe'), 2.77 (m, 1H, NCH^a-ⁱPr), 2.82 (dd, 1H, {J = 10.5, 10 Hz}, PhNCH^b), 3.26 (dd, 1H, {J = 10.5, 3 Hz}, PhNCH^c), 4.15 (br.s, 1H, -NHPh), 6.65 (m, 3H, *m,p*-Ph), 7.17 (m, 2H, *o*-Ph). ES: *m/z* 179 (60%) [M + H]⁺, *m/z* 162 (65%) [M - NH₂]⁺.

Preparation of (1*S*)-ⁱPr-(*N*)-Bn-ethylenediamine (2.41, R = ⁱPr, R'' = Bn)

Following general method **B**, with (2.40, R = ⁱPr, R'' = Bn) (71 g, 0.17 mmol). Yield = 22 mg (67 %).

¹H NMR: δ 0.87 (d, 3H, {J = 6.5 Hz}, MeCHMe'), 1.00 (d, 3H, {J = 7 Hz}, MeCHMe'), 1.57 (m, 1H, MeCHMe'), 2.06 (br.s, 3H, -NH₂ + BnN-H), 2.91 (m, 1H, BnNCH^a), 3.01 (m, 1H, BnNCH^b), 3.12 (m, 1H, NCHⁱPr), 3.41 (d, 1H, {J = 7 Hz}, PhCH^a-N), 3.66 (d, 1H, {J = 7 Hz}, PhCH^b-N), 7.32 (m, 5H, NCH₂Ph). ES: *m/z* 193 (100%) [M + H]⁺, *m/z* 176 (70%) [M - NH₂]⁺, *m/z* 215 (15%) [M + Na]⁺.

Preparation of half-sandwich complexes

The dimers [RuCl₂(mes)]₂,³⁹ [RuCl₂(*p*-cy)]₂,⁴² [RuCl₂(C₆H₆)]₂⁴² and [RhCl₂(Cp*)]₂⁴⁰, and complex [Ru(OH₂)(ⁱPr-pymox)(mes)](SbF₆)₂ (2.29)¹⁰⁰ were prepared by literature methods. NaSbF₆ was obtained from Fluorochem, NaOMe from Aldrich and AgSbF₆ from Lancaster.

General Method C: Synthesis of [MCl(R,R'-phenmox)(ring)] (2.10 – 2.15)

A solution of ligand R,R'-phenmox (2.2 equivalents) and NaOMe (2.5 equivalents) in MeOH (10 ml) was added to [MCl₂(ring)]₂ (M = Ru, ring = arene; M = Rh, ring = Cp*) (1.0 equivalents) and the resulting suspension was heated to reflux for two hours, giving a dark red/brown coloured solution, which was then evaporated. The crude residue was dissolved in CH₂Cl₂ and the solution was filtered through celite, to give a red solution, which was evaporated afford the crude product. Recrystallisation from CH₂Cl₂/ether resulted in crystalline product, which was shown to be pure by NMR. Quantities of reagents used and yields obtained are in **Table (2C.1)**, with ¹H NMR data in **Tables (2C.2 – 2C.6)** and microanalysis and mass spectrometry results in **Table (2C.7)**.

General Method D: Synthesis of [M(OH₂)(R,R'-phenmox)(ring)]SbF₆ (2.16 – 2.18)

To a solution of AgSbF₆ (1.05 equivalents) in acetone (0.5 ml) was added a solution of [MCl(R,R'-phenmox)(ring)] (M = Ru, ring = arene; M = Rh, ring = Cp*) (1.0 equivalents) in CH₂Cl₂ (4 ml), giving a yellow/orange solution and an immediate AgCl precipitate. The solution was stirred for one hour at room temperature (protected from light) and was then filtered through celite (to remove AgCl). The solvent was evaporated, and the solid was washed with chloroform to give the aqua complexes (**2.16 – 2.18**) as orange hygroscopic solids. In some cases, the products could be recrystallised from CH₂Cl₂/ether, affording crystals or powders. Quantities of reagents used and yields obtained are in **Table (2D.1)**, with ¹H NMR data in **Table (2D.2)** and elemental microanalysis (in some cases) and mass spectrometry results in **Table (2D.3)**.

General Method E: Synthesis of [ML^m(ⁱPr-phenmox)(ring)]SbF₆ (2.19 – 2.22)

To a solution of [MCl(ⁱPr-phenmox)(ring)] (**2.12** – M = Ru, ring = mes; **2.15** – M = Rh, ring = Cp*) (1.0 equivalents) in MeOH (10 ml) was added NaSbF₆ (1.2 equivalents) and ligand L^m (L^m = py, 4-Me-py, 2-Me-py, PPh₃) (3.0 equivalents). The mixture was heated to reflux temperature for two hours with continuous stirring. On cooling a white precipitate was observed, to remove this the solvent was evaporated and the residue re-dissolved in CH₂Cl₂ prior to filtering through celite. The resulting red solution was evaporated to afford the crude complex. Recrystallisation from CH₂Cl₂/ether (or different common laboratory solvents) gave (**2.19 - 2.22**) as crystalline red/orange solids. Quantities of reagents used and yields obtained are in **Table (2E.1)**,

with ^1H NMR data in **Tables (2E.2 – 2E.4)** and elemental microanalysis and mass spectrometry results in **Table (2D.3)**.

General Method F: Synthesis of $[\text{MX}(\text{}^i\text{Pr-phenmox})(\text{ring})]\text{SbF}_6$ (2.23 – 2.25)

To a solution of the corresponding aqua complex $[\text{M}(\text{OH}_2)(\text{}^i\text{Pr-phenmox})(\text{ring})]\text{SbF}_6$ (**2.17**, $\text{R} = \text{}^i\text{Pr}$ or **2.18**, $\text{R} = \text{}^i\text{Pr}$) (1.0 equivalents) in MeOH (3 ml) was added KBr or NaI (1.2 equivalents) and the mixture was stirred at room temperature for one hour, during which time the solution changed colour from orange to red. The methanol was removed *in vacuo*, the residue dissolved in CH_2Cl_2 prior to filtering through celite (to remove unreacted KBr/NaI and by-product) and evaporated to afford crude product. Recrystallisation from CH_2Cl_2 /ether gave (**2.23 – 2.25**) as red powders. Quantities of reagents used and yields obtained are in **Table (2F.1)**, with ^1H NMR data in **Table (2F.2)** and mass spectrometry and elemental microanalysis results in **Tables (2D.3)**.

General Method G: Synthesis of $[\text{RuCl}(\text{N-N})(\text{mes})]\text{SbF}_6$ (2.43-2.47, 2.49-2.53)

A solution of ligand N-N (N-N = R,R'-pymimR'' or ketimines) (2.0 equivalents) and NaSbF_6 (2.0 equivalents) in MeOH (10 ml) was added to $[\text{RuCl}_2(\text{mes})]_2$ (1.0 equivalents) and the resulting suspension was heated to reflux for two hours. An orange/brown coloured solution was obtained, which was evaporated and the crude residue was dissolved in CH_2Cl_2 . Filtration through celite gave a red solution, which was evaporated to afford the crude product. Recrystallisation from CH_2Cl_2 /ether gave (**2.43-2.47, 2.49-2.53**) as crystalline solids. Quantities of reagents used and yields obtained are in **Table (2G.1)**, ^1H NMR data in **Tables (2G.2 – 2G.4)** and microanalysis and mass spectrometry results in **Table (2G.5)**.

Synthesis of $[\text{MX}(\text{}^i\text{Pr-pymox})(\text{mes})](\text{SbF}_6)$ (X = Cl, 2.26)

To a solution of the aqua complex $[\text{Ru}(\text{OH}_2)(\text{}^i\text{Pr-pymox})(\text{mes})](\text{SbF}_6)_2$ (**2.29**) (125 mg, 0.139 mmol) in MeOH (3 ml) was added KCl (8.1 mg, 0.068 mmol) and the mixture was stirred at room temperature for one hour, during which time the solution changed colour from orange to red. The methanol was removed *in vacuo*, the residue dissolved in CH_2Cl_2 prior to filtering through celite (to remove unreacted KCl and by-product) and evaporated to afford crude product. Recrystallisation from CH_2Cl_2 /ether gave (**2.26**) as a red powder (83 mg, 87%). The known complexes¹⁰⁰ (X = Br, I) were

prepared similarly and ^1H NMR data for all complexes is included in **Tables (2H.1 – 2H.3)**.

General Procedure for Kinetic Measurements: $[\text{RuX}(\text{N-N})(\text{mes})](\text{SbF}_6)$

A Young's tap NMR tube was charged with $[\text{RuX}(\text{N-N})(\text{mes})](\text{SbF}_6)$ (0.011 mmol) and degassed using a Schlenk line. Under N_2 , dry d_6 -acetone (0.5 ml) was added and the resultant yellow/orange solutions degassed using 'freeze-pump-thaw' techniques. The ^1H NMR spectrum was recorded immediately to establish the initial isomer ratio, the NMR tube was then thermostatted at the desired temperature and the NMR spectrum re-recorded at suitable time-intervals. The ratio of isomer A:B was calculated from the relative integration of the $\text{C}_6\text{H}_3\text{Me}_3$ singlets and corroborated by the integration of the py-6-*H* signals. Concentration $\{\ln([A]_t/[A]_e)\}$ vs time data were fitted by conventional linear regression methods (**Figures 5.1 – 5.10**; see Appendix).¹⁴⁹ The activation parameters ($\Delta H^\ddagger = 55 \pm 10 \text{ KJ mol}^{-1}$ and $\Delta S^\ddagger = -183 \pm 30 \text{ J K}^{-1} \text{ mol}^{-1}$) were obtained by a least-squares fit of the Eyring plot.¹³⁸

Preparation of $[\text{RuMe}(\text{}^i\text{Pr-phenmox})(\text{mes})]$ (2.19**)**

To a degassed solution of $[\text{RuCl}(\text{}^i\text{Pr-phenmox})(\text{mes})]$ (**2.12**, $\text{R} = \text{}^i\text{Pr}$) (200 mg, 0.43 mmol) in THF (15 ml) was added MeLi (0.27 ml, 0.43 mmol). The mixture was heated to 40°C for four hours with continuous stirring. On cooling a white precipitate was observed. The solvent was evaporated and the residue re-dissolved in CH_2Cl_2 prior to filtering through celite. The crude product was chromatographed on silica, with hexane/ethyl acetate (3:1) as eluent. Evaporation of the fore-run gave (**2.19**) as a dark red solid (82 mg, 43 %), which was pure by ^1H NMR spectroscopy. However, attempts at recrystallisation failed hence elemental analysis has not been obtained.

^1H NMR: δ 0.69 (d, 3H, *MeCHMe'*), 0.87 (s, 3H, Ru-*Me*), 0.89 (d, 3H, *MeCHMe'*), 1.96-2.10 (m, 1H, *MeCHMe'*), 2.02 (s, 9H, $\text{C}_6\text{H}_3\text{Me}_3$), 3.96 (m, 1H, NCH), 4.22 (m, 1H, OCH), 4.35 (m, 1H, OCH'), 4.42 (s, 3H, $\text{C}_6\text{H}_3\text{Me}_3$), 6.33 (t, 1H, $\{J = 6.5 \text{ Hz}\}$, Ar-*H*), 6.76 (d, 1H, $\{J = 6.5\}$, Ar-3-*H*), 7.09 (t, 1H, $\{J = 6 \text{ Hz}\}$, Ar-*H*), 7.48 (d, 1H, $\{J = 6 \text{ Hz}\}$, Ar-6-*H*). ES-MS: m/z 440 (15%) $[\text{M}]^+$ and m/z 426 (70%) $[\text{M} - \text{Cl}]^+$.

Preparation of [Ru(OH₂)(Ph₂-pymimH)(mes)](SbF₆)₂ (2.48)

To a solution of AgSbF₆ (45 mg, 0.13 mmol) in acetone (0.5 ml) was added a solution of [RuCl(Ph₂-pymimH)(mes)](SbF₆) (2.43) (100 mg, 0.133 mmol) in CH₂Cl₂ (4 ml), giving a yellow/orange solution and an immediate AgCl precipitate. The solution was stirred for one hour at room temperature (protected from light) and was then filtered through celite (to remove AgCl). Evaporation, followed by washing with chloroform gave the aqua complex (2.48) as a yellow oily residue, which was recrystallised from acetone/ether, affording a yellow hygroscopic powder (125 mg, 97%), which was shown to be pure by ¹H NMR spectroscopy.

¹H NMR CD₂Cl₂: δ 2.00 [2.03] (s, 9H, C₆H₃Me₃), 5.17 [5.28] (s, 3H, C₆H₃Me₃), 5.31 (m, 1H, PhCH^b), 5.47 [5.50] (m, 1H, PhCH^a), 7.17 (br.s, 1H, N-H), 7.32 (m, 4H, PhCH^{a,b}), 7.45 (m, 3H, PhCH^{a,b}), 7.55 (m, 3H, PhCH^{a,b}), 7.88 (7.87) (t, 1H, {J = 7 Hz}, Py-5-H), 8.02 (8.10) (d, 1H, {J = 7.5 Hz}, Py-3-H), 8.21 (t, 1H, {J = 7.5 Hz}, Py-4-H), 9.37 (9.17) (d, 1H, {J = 6 Hz}, Py-6-H). Signals for free / coordinated water were not observed.

Preparation of [RhCl(enaminone)(Cp)] (2.55)*

This was prepared following method (G), with enaminone ligand (2.56) (21 mg, 0.11 mmol), NaSbF₆ (29 mg, 0.11 mmol) and [RhCl₂(Cp*)]₂ (33 mg, 0.05 mmol), giving (2.55) as a red powder (46 mg, 92%).

¹H NMR: δ 1.54 (s, 15H, C₅Me₅), 5.77 (s, 1H, C=CH), 6.76 (ddd, 1H, {J = 7, 6, 1.5 Hz}, Py-4-H), 6.84 (br.d, 1H, Py-3-H), 7.31-7.42 (m, 3H, Ph + 1H Py-5-H), 7.97 (m, 2H, Ph), 8.34 (dd, 1H, {J = 6, 1 Hz}, Py-6-H). FAB-MS: *m/z* 434 [M - Cl]⁺. Microanalysis: C₂₃H₂₅ClNORh found (calculated) C: 57.40 % (58.80 %), H: 5.39 % (5.36 %), N: 3.11 % (2.88 %).

Table (2C.1): Preparation of complexes [MCl(O⁻N)(ring)]

Compound	Code	Quantity of dimer (mg / mmol)	Quantity of ligand O ⁻ -N (mg / mmol)	Quantity of NaOMe (mg / mmol)	Final Yield (mg / %)
[RuCl(^t Pr-phenmox)(mes)]	(2.12, R = ^t Pr)	320 / 0.55	247 / 1.21	74 / 1.37	405 / 80
[RuCl(^t Bu-phenmox)(mes)]	(2.12, R = ^t Bu)	100 / 0.17	75 / 0.34	25 / 0.47	46 / 28
[RuCl(Bn-phenmox)(mes)]	(2.12, R = Bn)	115 / 0.20	109 / 0.43	27 / 0.49	141 / 71
[RuCl(Ph-phenmox)(mes)]	(2.12, R = Ph)	147 / 0.25	133 / 0.56	34 / 0.63	185 / 76
[RuCl(^t Pr-phenmox)(<i>p</i> -cy)]	(2.13, R = ^t Pr)	64 / 0.11	45 / 0.22	13 / 0.24	74 / 74
[RuCl(^t Bu-phenmox)(<i>p</i> -cy)]	(2.13, R = ^t Bu)	125 / 0.21	94 / 0.43	28 / 0.51	139 / 70
[RuCl(^t Pr-phenmox)(C ₆ H ₆)]	(2.14)	136 / 0.27	112 / 0.55	37 / 0.68	207 / 90
[RhCl(^t Pr-phenmox)(Cp*)]	(2.15, R = ^t Pr)	323 / 0.52	236 / 1.15	71 / 1.31	380 / 76
[RhCl(Bn-phenmox)(mes)]	(2.15, R = Bn)	70 / 0.11	63 / 0.25	15 / 0.28	99 / 83
[RhCl(Ph-phenmox)(Cp*)]	(2.15, R = Ph)	70 / 0.11	60 / 0.25	15 / 0.28	87 / 75
[RhCl(Me ₂ -phenmox)(Cp*)]	(2.11)	150 / 0.24	102 / 0.53	33 / 0.61	161 / 71
[RuCl(Me ₂ -phenmox)(mes)]	(2.10)	103 / 0.14	74 / 0.30	20 / 0.30	69 / 69

Table (2D.1): Preparation of complexes [M(OH₂)(O⁻-N)(ring)]SbF₆

Complex	Code	Precursor Complex	Quantity of Precursor (mg / mmol)	Quantity of AgSbF ₆ (mg / mmol)	Final Yield (mg / %)
[Ru(OH ₂)(¹ Pr-phenmox)(mes)]SbF ₆	(2.17, R = ¹ Pr)	[RuCl(O ⁻ -N)(mes)]	78 / 0.17	59 / 0.17	116 / 96
[Ru(OH ₂)(Ph-phenmox)(mes)]SbF ₆	(2.17, R = Ph)	[RuCl(O ⁻ -N)(mes)]	65 / 0.13	45 / 0.13	92 / 98
[Rh(OH ₂)(¹ Pr-phenmox)(Cp*)]SbF ₆	(2.18)	[RhCl(O ⁻ -N)(Cp*)]	65 / 0.14	47 / 0.14	99 / 99
[Rh(OH ₂)(Me ₂ -phenmox)(Cp*)]SbF ₆	(2.16)	[RhCl(O ⁻ -N)(Cp*)]	88 / 0.19	65 / 0.19	127 / 98

Table (2E.1): Preparation of complexes [M(L^m)(O⁻-N)(ring)]Y

Compound	Code	Quantity of Precursor (mg / mmol)	Quantity of NaSbF ₆ (mg / mmol)	Quantity of L ^m (mg / mmol)	Final Yield (mg / %)
[Ru(4-Me-py)(¹ Pr-phenmox)(mes)]SbF ₆	(2.20, R = ¹ Pr)	57 / 0.12	39 / 0.15	35 / 0.37	80 / 86
[Ru(2-Me-py)(¹ Pr-phenmox)(mes)]SbF ₆	(2.20, R = ¹ Pr)	61 / 0.13	41 / 0.16	37 / 0.40	72 / 72
[Ru(Py)(¹ Pr-phenmox)(mes)]SbF ₆	(2.20, R = ¹ Pr)	60 / 0.13	38 / 0.15	43 / 0.54	66 / 70
[Ru(PPh ₃)(¹ Pr-phenmox)(mes)] BPh ₄	(2.21, R = ¹ Pr)	51 / 0.11	45 / 0.13 ^A	35 / 0.13	104 / 94
[Rh(4-Me-py)(¹ Pr-phenmox)(Cp*)]SbF ₆	(2.22, R = ¹ Pr)	62 / 0.13	40 / 0.16	36 / 0.40	82 / 82
[Rh(Py)(¹ Pr-phenmox)(Cp*)]SbF ₆	(2.22, R = ¹ Pr)	62 / 0.13	40 / 0.16	31 / 0.40	74 / 76

^A NaBPh₄ used instead of NaSbF₆.

Table (2F.1): Preparation of complexes [MX(O⁻-N)(ring)]

Complex	Code	Precursor Complex	Quantity of Precursor (mg / mmol)	Quantity of NaX (mg / mmol)	Final Yield (mg / %)
[RuBr(¹ Pr-phenmox)(mes)]	(2.23)	(2.17, R = ¹ Pr)	44 / 0.06	8.1 / 0.06	59 / 84
[RuI(¹ Pr-phenmox)(mes)]	(2.24)	(2.17, R = ¹ Pr)	44 / 0.07	10.0 / 0.07	29 / 85
[RhI(¹ Pr-phenmox)(Cp*)]	(2.25)	(2.18)	16 / 0.03	4.0 / 0.03	11 / 85

Table (2G.1): Preparation of complexes [RuCl(N-N)(mes)](SbF₆)

Compound	Code	Quantity of [RuCl ₂ (mes)] ₂ (mg / mmol)	Quantity of ligand N-N (mg / mmol)	Quantity of NaSbF ₆ (mg / mmol)	Final Yield (mg / %)
[RuCl(¹ Pr-pymox)(mes)](SbF ₆)	(2.26 B)	100 / 0.17	72 / 0.38	93 / 0.36	215 / 92
[RuCl(Ph ₂ -pymimH)(mes)](SbF ₆)	(2.43)	37 / 0.06	38 / 0.13	33 / 0.13	99 / 99
[RuCl(¹ Pr-pymimPh)(mes)](SbF ₆)	(2.45)	22 / 0.04	20 / 0.08	20 / 0.08	54 / 95
[RuCl(¹ Pr-pymim ⁿ Bu)(mes)](SbF ₆)	(2.46)	78 / 0.27	66 / 0.27	70 / 0.27	181 / 91
[RuCl(Bn-pymim ^t Bu)(mes)](SbF ₆)	(2.47)	50 / 0.09	50 / 0.17	46 / 0.17	127 / 94
[RuCl(Ph-Ketimine)(mes)](SbF ₆)	(2.49)	54 / 0.09	58 / 0.19	50 / 0.19	148 / 96
[RuCl(Nap-Ketimine)(mes)](SbF ₆)	(2.50)	40 / 0.07	50 / 0.14	37 / 0.14	95 / 83
[RuCl(Cy-Ketimine)(mes)](SbF ₆)	(2.51)	53 / 0.09	58 / 0.19	49 / 0.19	137 / 95
[RuCl(Me-Ketimine)(mes)](SbF ₆)	(2.52)	71 / 0.12	84 / 0.26	66 / 0.26	196 / 98
[RuCl(¹ Pr-pymim)(mes)](SbF ₆)	(2.53)	52 / 0.09	66 / 0.19	48 / 0.19	148 / 99

Table (2C.2): NMR spectroscopic data (300 MHz) for complexes [RuCl(R,R'-phenmox) (ring)] in CDCl₃ (δ / ppm)

Compound	π-Ring	Substituent R	Phenoxy ring	Oxazoline ring
[RuCl(Me ₂ -O ⁻ -N)(mes)] (2.10, R = R' = Me)	2.10, 4.82	1.41 (s, 3H, NCM <i>e</i>), 1.62 (s, 3H, NCM <i>e</i>)	6.48 (1H, ddd {J = 8, 7, 1 Hz} Ar-5- <i>H</i>), 7.02 (1H, dd {J = 8.5, 1 Hz} Ar-3- <i>H</i>), 7.21 (1H, ddd {J = 8.5, 7, 2 Hz} Ar-4- <i>H</i>), 7.48 (1H, dd {J = 8, 2 Hz} Ar-6- <i>H</i>)	4.10 (2H, d {J = 8 Hz} OCH), 4.29 (1H, d {J = 8 Hz} OCH)
[RuCl(^t Pr-O ⁻ -N)(mes)] (2.12, R = ^t Pr)	2.21, 4.89	0.74 (d, 3H, MeCHMe'), 0.99 (d, 3H, MeCHMe'), 2.82 (m, 1H, MeCHMe')	6.39 (m, 1H, Ar-5- <i>H</i>), 6.97 (m, 1H, Ar-3- <i>H</i>), 7.17 (m, 1H, Ar-4- <i>H</i>), 7.45 (m, 1H, Ar-6- <i>H</i>)	4.40 (m, 2H, OCH + OCH'), 4.52 (m, 1H, NCH)
[RuCl(^t Bu-O ⁻ -N)(mes)] (2.12, R = ^t Bu)	2.19, 4.89	1.18 (s, 9H, CMe ₃)	6.38 (m, 1H, Ar-5- <i>H</i>), 6.98 (m, 1H, Ar-3- <i>H</i>), 7.15 (m, 1H, Ar-4- <i>H</i>), 7.47 (m, 1H, Ar-6- <i>H</i>)	4.33 (m, 2H, OCH + OCH'), 4.65 (m, 1H, NCH)
[RuCl(Bn-O ⁻ -N)(mes)] (2.12, R = Bn)	2.19 [2.16], 4.95 [4.89]	2.78 [2.63](dd, {J = 11, 14 Hz} 1H, CHPh), 4 [3.96] (dd, {J = 3.5, 14 Hz} 1H, CHPh), 7.27 [7.27] (m, 5H, CH ₂ Ph)	6.41 [6.50] (m, 1H, Ar-5- <i>H</i>), 7.02 [7.02] (m, 1H, Ar-3- <i>H</i>), 7.27 [7.27] (m, 1H, Ar-4- <i>H</i>), 7.46 [7.27] (m, 1H, Ar-6- <i>H</i>)	4.35 [4.16 + 4.35] (m, 2H, OCH + OCH'), 4.71 [4.58] (m, 1H, NCH)

Table (2C.3): NMR spectroscopic data (300 MHz) for complexes [RuCl(R,R'-phenmox) (ring)] in CDCl₃ (δ / ppm)

Compound	π -Ring	Substituent R	Phenoxy ring	Oxazoline ring
[RuCl(Ph-O ⁻ -N (mes)) (2.12, R = Ph)	1.91 [2.02] (s, 9H, C ₆ H ₃ Me ₃), 4.22 [4.64] (s, 3H, C ₆ H ₃ Me ₃)	7.51 [7.51] (m, 3H, Ph), 7.73 [7.73] (m, 2H, Ph)	6.53 [6.41] (m, 1H, Ar-5- H), 7.03 [6.94] (m, 1H, Ar- 3-H), 7.22 [7.16] (m, 1H, Ar-4-H), 7.51 [7.51] (m, 1H, Ar-6-H)	4.81 [4.81] (m, 2H, OCH + OCH'), 5.59 [5.73] (m, 1H, NCH)
[RuCl(Ph-O ⁻ -N (mes)) (2.12, R = Ph) (400 MHz, 233K)	1.89 [2.01] (s, 9H, C ₆ H ₃ Me ₃), 4.10 [4.60] (s, 3H, C ₆ H ₃ Me ₃)	7.50 [7.50] (m, 1H, Ph), 7.55 [7.60] (m, 2H, Ph), 7.72 [7.74] (m, 2H, Ph)	6.60 [6.43] (m, 1H, Ar-5- H), 6.99 [6.80] (m, 1H, Ar- 3-H), 7.17 [7.18] (m, 1H, Ar-4-H), 7.51 [7.51] (m, 1H, Ar-6-H)	4.82 [4.92] (m, 1H, OCH), 4.82 [4.20] (m, 1H OCH'), 5.51 [5.75] (m, 1H, NCH)
[RuCl(ⁱ Pr -O ⁻ -N) (p-cy)] (2.13, R = ⁱ Pr)	1.17 (d, 3H, MeCHMe'), 1.27 (d, 3H, MeCHMe'), 2.25 (s, 3H, Me), 2.81(m, 1H, CHMe ₂) 5.35/4.97 (AB, 2H, H2/H3-cy) 5.43 (br. s, 2H, H4/H5-cy)	0.81 (d, 3H, MeCHMe'), 1.00 (d, 3H, MeCHMe'), 2.68 (m, 1H, MeCHMe')	6.36 (m, 1H, Ar-5-H), 6.92 (m, 1H, Ar-3-H), 7.15 (m, 1H, Ar-4-H), 7.39 (m, 1H, Ar-6-H)	4.33 (m, 1H, OCH'), 4.65 (m, 2H, NCH + OCH)

Table (2C.4): NMR spectroscopic data (300 MHz) for complexes [RuCl(R,R'-phenmox) (ring)] in CDCl₃ (δ / ppm)

Compound	π -Ring	Substituent R	Phenoxy ring	Oxazoline ring
[RuCl(ⁱ Pr-O ⁻ -N) (<i>p</i> -cy)] (2.13, R = ⁱPr) (400 MHz, 233K)	1.13 [1.19] (d, 3H, MeCHMe'), 1.27 [1.30] (d, 3H, MeCHMe'), 2.22 [2.18] (s, 3H, Me), 2.76 [2.87] (m, 1H, CHMe ₂) 4.97 [5.23] (d, 1H, H ₂ /H ₃ -cy) 5.38 (d, 1H, Ar-H), 5.46 (m, 2H, 2*Ar-H)	0.74 [0.86] (d, 3H, MeCHMe'), 1.02 [1.09] (d, 3H, MeCHMe'), 2.56 [2.37] (m, 1H, MeCHMe')	6.38 [6.37] (m, 1H, Ar-5-H), 6.78 [6.77] (m, 1H, Ar-3-H), 7.14 (m, 1H, Ar-4-H), 7.36 [7.32] (m, 1H, Ar-6-H)	4.39 [4.37] (m, 1H, OCH), 4.52 (m, 2H, OCH' + NCH)
[RuCl(^t Bu-O ⁻ -N) (<i>p</i> -cy)] (2.13, R = ^tBu)	1.17 (d, 3H, MeCHMe'), 1.24 (d, 3H, MeCHMe'), 2.32 (s, 3H, Me), 2.77 (m, 1H, CHMe ₂)	1.17 (s, 9H, Cme ₃)	6.38 (m, 1H, Ar-5-H), 6.98 (m, 1H, Ar-3-H), 7.15 (m, 1H, Ar-4-H), 7.47 (m, 1H, Ar-6-H)	4.45-4.33 (m, 2H, OCH + OCH'), 4.65 (m, 1H, NCH)
[RuCl(ⁱ Pr-O ⁻ -N) (C ₆ H ₆)] (2.14, R = ⁱPr) (400 MHz, 263K)	5.60 [5.62] (s, 6H, C ₆ H ₆)	0.85 [0.99] (d, 3H, {J = 6.5 Hz}, MeCHMe'), 1.02 [1.08] (d, 3H, {J = 7 Hz}, MeCHMe'), 2.67 [2.41] (m, 1H, MeCHMe')	6.40 [6.45] (t, 1H, {J = 7.5 Hz}, Ar-5-H), 6.89 [6.93] (d, 1H, {J = 8.5}, Ar-3-H), 7.14 [7.18] (dt, 1H, {J = 8.5, 1.5 Hz}, Ar-4-H), 7.37 [7.37] (dd, 1H, {J = 8, 1.5 Hz}, Ar-6-H)	4.40 [4.40] (t, 1H, {J = 9.5 Hz}, OCH), 4.53 [4.48] (dd, 1H, {J = 9, 3.5 Hz}, OCH'), 4.60 [4.60] (m, 1H, NCH)

Table (2C.5): NMR spectroscopic data (300 MHz) for complexes [RhCl(R,R'-phenmox) (Cp*)] in CDCl₃ (δ / ppm)

Compound	C ₅ Me ₅	Substituent R	Phenoxy ring	Oxazoline ring
[RhCl(Me ₂ -O ⁻ -N)(Cp*)] (2.11, R = R' = Me)	1.33 (br.s, 9H,)	R = 1.34 (br.s, 3H, <i>Me</i>), R' = 1.45 (br.s, 3H, <i>Me'</i>)	6.37 (m, 1H, Ar-5- <i>H</i>), 6.80 (m, 1H, Ar-3- <i>H</i>), 7.12 (m, 1H, Ar-4- <i>H</i>), 7.37 (m, 1H, Ar-6- <i>H</i>)	3.93 (br.s, 1H, OCH), 4.19 (br.s, 1H, OCH')
[RhCl(Me ₂ -O ⁻ -N)(Cp*)] (2.11, R = R' = Me) (CD ₂ Cl ₂ , 273 K) (400 MHz)	1.34 (s, 9H,)	R = 1.34 (s, 3H, <i>Me</i>), R' = 1.45 (s, 3H, <i>Me'</i>)	6.37 (m, 1H, Ar-5- <i>H</i>), 6.80 (m, 1H, Ar-3- <i>H</i>), 7.12 (m, 1H, Ar-4- <i>H</i>), 7.37 (m, 1H, Ar-6- <i>H</i>)	3.93 (s, 1H, OCH), 4.19 (s, 1H, OCH')
[RhCl(^t Bu-O ⁻ -N)(Cp*)] (2.15, R = ^tBu)	1.60 (s, 15H)	1.21 (s, 9H, CMe ₃)	6.39 (m, 1H, Ar-5- <i>H</i>), 6.88 (m, 1H, Ar-3- <i>H</i>), 7.19 (m, 1H, Ar-4- <i>H</i>), 7.42 (m, 1H, Ar-6- <i>H</i>)	4.38 (m, 2H, OCH + NCH), 4.41 (m, 1H, OCH')
[RhCl(ⁱ Pr-O ⁻ -N)(Cp*)] (2.15, R = ⁱPr)	1.58 (s, 15H)	0.76 (d, {J=6.5 Hz}, 3H, <i>MeCHMe'</i>), 0.93 (d, {J=7.5 Hz}, 3H, <i>MeCHMe'</i>), 2.80 (m, 1H, <i>MeCHMe'</i>)	6.39 (ddd, {J=8, 7, 1 Hz}, 1H, Ar-5- <i>H</i>), 6.96 (dd, {J=8.5, 1 Hz}, 1H, Ar- 3- <i>H</i>), 7.17 (ddd, {J=8.5, 7, 2 Hz}, 1H, Ar-4- <i>H</i>), 7.48 (dd, {J=8, 2 Hz}, 1H, Ar-6- <i>H</i>)	4.32 (m, 2H, OCH + OCH'), 4.46 (m, 1H, NCH)

Table (2C.6): NMR spectroscopic data (300 MHz) for complexes [RhCl(R,R'-phenmox) (Cp*)] in CDCl₃ (δ / ppm)

Compound	¹ H C ₅ Me ₅	Substituent R	Phenoxy ring	Oxazoline ring
[RhCl(Bn-O ⁻ -N)(Cp*)] (2.15, R = Bn)	1.63 (s, 15H)	2.92 (m, 2H, CHPh + CHPh'), 7.26 (m, 5H, CH ₂ Ph)	6.41 (m, 1H, Ar-5- H), 7.00 (m, 1H, Ar- 3-H), 7.26 (m, 1H, Ar-4-H), 7.46 (m, 1H, Ar-6-H)	3.88 (m, 1H, OCH), 4.33 (m, 1H, OCH), 4.62 (m, 1H, NCH)
[RhCl(Ph-O ⁻ -N)(Cp*)] (2.15, R = Ph) (233K, 400 MHz)	1.26 (s, 9H,)	7.43 (m, 3H, Ph), 7.61 (m, 2H, Ph)	6.48 (m, 1H, Ar-5- H), 6.94 (m, 1H, Ar- 3-H), 7.20 (m, 1H, Ar-4-H), 7.43 (m, 1H, Ar-6-H)	4.49 (br.s, 1H, OCH), 4.78 (m, 1H, OCH'), 5.69 (m, 1H, NCH)

Table (2D.2): NMR spectroscopic data (300 MHz) for complexes [ML(R,R'-phenmox)(ring)](SbF₆) in CDCl₃ (δ / ppm)

Compound	π-Ring	Substituent R	Ligand L	Phenoxy ring	Oxazoline ring
[Ru(OH ₂)(ⁱ Pr-O ⁻ -N)(mes)] ⁺ (2.17 , R = ⁱ Pr) (295K unless stated) (400 MHz)	2.25, 5.51	0.57 (d, 3H, MeCHMe'), 1.20 (d, 3H, MeCHMe'), 2.66 (m, 1H, MeCHMe')	2.21 (s, 6H, Me ₂ CO-free), 2.24 (v.br.s, 2H, OH ₂ , @ 253K), 4.43 (br.s, 2H, OH ₂ , @ 213K)	6.83 (m, 1H, Ar-5-H), 7.28 (m, 1H, Ar-3-H), 7.44 (m, 1H, Ar-4-H), 7.59 (m, 1H, Ar-6-H)	4.69 (m, 2H, OCH + OCH'), 5.00 (m, 1H, NCH)
[Ru(OH ₂)(Ph-O ⁻ -N)(mes)] ⁺ (2.17 , R = Ph) (CD ₂ Cl ₂ , 223K) (400 MHz)	1.84, 4.17	7.48 (m, 2H, Ph), 7.62 (m, 3H, Ph)	3.10 (br.s, 2H, OH ₂ -free), 6.30 (br.s, 2H, OH ₂ -coord.)	6.90 (m, 1H, Ar-5-H), 7.17 (m, 1H, Ar-3-H), 7.44 (m, 1H, Ar-4-H), 7.62 (m, 1H, Ar-6-H)	3.54 (m, 1H, OCH), 4.31 (m, 1H, OCH') 4.48 (m, 1H, NCH)
[Rh(OH ₂)(ⁱ Pr-O ⁻ -N)(Cp*)] ⁺ (2.18 , R = ⁱ Pr)	1.83	0.62 (d, 3H, MeCHMe'), 1.16 (d, 3H, MeCHMe'), 2.31 (m, 1H, MeCHMe')	Not observed at 233K	6.92 (m, 1H, Ar-5-H), 7.23 (m, 1H, Ar-3-H), 7.51 (m, 1H, Ar-4-H), 7.72 (m, 1H, Ar-6-H)	4.69 (m, 2H, OCH + OCH'), 5.00 (m, 1H, NCH)
[Rh(OH ₂)(Me ₂ -ON)(Cp*)] ⁺ (2.16 , R = R' = Me)	1.88 (br.s)	R = R' = 1.82 (br.s, 6H, Me(Me')CN)	Not observed at 223K	6.98 (m, 1H, Ar-5-H), 7.30 (d, 1H, Ar-3-H), 7.59 (m, 1H, Ar-4-H), 7.80 (d, 1H, Ar-6-H)	4.50 (br.s, 2H, OCH + OCH')

Table (2E.2): NMR spectroscopic data for complexes [Ru(L^m)(R,R'-phenmox) (mes)]Y in CD₂Cl₂ (δ / ppm)

Compound	C ₆ H ₃ Me ₃	MeCHMe'	Ligand L ^m	Phenoxy ring	Oxazoline ring
[Ru(4-Me-py)(ⁱ Pr-O ⁻ -N)(mes)]SbF ₆ (2.20) (400 MHz) [Minor signals broad]	2.11 [2.18], 5.09 [5.13]	0.10 [0.81] (d, 3H), 0.97 [1.19] (d, 3H), 1.32 [~2.07] (m, 1H)	2.51 [2.56] (br. s, 3H, py-Me), 7.30 [7.30] (m, 2H, py-3,5-H), 8.72 [8.35] (d, 2H, py-2,6-H)	6.60 [6.32] (m, 1H, Ar-5-H), 7.09 [6.92] (m, 1H, Ar-3-H), 7.41 [7.41] (m, 1H, Ar-4-H), 7.50 [7.50] (m, 1H, Ar-6-H)	4.53 [4.53] (m, 3H, OCH + OCH' + NCH)
[Ru(4-Me-py)(ⁱ Pr-O ⁻ -N)(mes)]SbF ₆ (2.20) (233K, 400 MHz)	2.07 [2.09], 5.06 [5.08]	-0.05 [0.73] (d, 3H), 0.85 [1.11] (d, 3H), 1.32 [~2.07] (m, 1H)	2.49 [2.49] (s, 3H, py-Me), 7.32 [7.32] (m, 2H, py-3,5-H), 8.74 [8.37] (d, 2H, py-2,6-H)	6.57 [6.58] (m, 1H, Ar-5-H), 7.04 [7.06] (m, 1H, Ar-3-H), 7.32 [7.38] (m, 1H, Ar-4-H), 7.54 [7.56] (m, 1H, Ar-6-H)	4.45 [4.45] (m, 2H, OCH + OCH'), 4.54 [4.54] (m, 1H, NCH)
[Ru(2-Me-py)(ⁱ Pr-O ⁻ -N)(mes)]SbF ₆ (2.20) (300 MHz)	2.13, 5.25	0.65 (d, 3H), 1.10 (d, 3H), 2.50 (m, 1H)	2.84 (s, 3H, 2-Me-py), 7.30 (m, 2H, py-3,5-H), 7.99 (m, 1H, py-4-H), 8.58 (m, 1H, py-6-H)	6.50 (m, 1H, Ar-5-H), 7.05 (m, 1H, Ar-3-H), 7.30 (m, 1H, Ar-4-H), 7.49 (m, 1H, Ar-6-H)	4.51 (m, 1H, OCH), 4.61 (m, 1H, OCH'), 4.73 (m, 1H, NCH)
[Ru(2-Me-py)(ⁱ Pr-O ⁻ -N)(mes)]SbF ₆ (2.20) (233K, 400 MHz)	1.97 [2.13], 5.02 [4.98]	0.61 [0.52] (d, 3H), 1.03 [0.90] (d, 3H), 2.42 [2.42] (m, 1H)	2.75 [2.63] (s, 3H, 2-Me-py), 7.02 [7.05] (m, 2H, py-3,5-H), 7.25 [7.20] (m, 1H, py-4-H), 8.48 [8.61] (m, 1H, py-6-H)	6.13 [6.49] (m, 1H, Ar-5-H), 6.85 [6.85] (m, 1H, Ar-3-H), 7.31 [7.27] (m, 1H, Ar-4-H), 7.55 [7.51] (m, 1H, Ar-6-H)	4.24 [4.38] (m, 1H, OCH), 4.42 (m, 1H, OCH'), 4.49 [4.50] (m, 1H, NCH)

Table (2E.3): NMR spectroscopic data for complexes [Ru(L^m)(R,R'-phenmox)(mes)]Y in CD₂Cl₂ (δ / ppm)

Compound	C ₆ H ₃ Me ₃	MeCHMe'	Ligand L ^m	Phenoxy ring	Oxazoline ring
[Ru(Py)(¹ Pr-O ⁻ -N)(mes)]SbF ₆ (2.20) (300 MHz)	2.06 [2.17], 5.10 [5.10]	-0.09 [0.76] (d, 3H), 0.87 [1.11] (d, 3H), 1.36 [2.41] (m, 1H)	7.32 [6.97] (m, 1H, py-4-H), 7.54 [7.54] (m, 2H, py-3,5-H), 8.91 [8.69] (m, 2H, py-1,6-H)	6.58 [6.22] (m, 1H, Ar-5-H), 7.06 [6.85] (m, 1H, Ar-3-H), 7.54 [7.32] (m, 1H, Ar-4-H), 7.91 [7.69] (m, 1H, Ar-6-H)	4.45 [4.45] (m, 2H, OCH + OCH'), 4.56 [4.72] (m, 1H, NCH)
[Ru(PPh ₃)(¹ Pr-O ⁻ -N)(mes)]BPh ₄ (2.21) (400 MHz)	1.81 [1.79], 4.48 [5.06]	0.00 [0.92] (d, 3H), 0.58 [0.98] (d, 3H), 1.21 [2.08] (m, 1H)	6.80-7.90 [6.80-7.90] (m, 35H, PPh ₃ + BPh ₄ ⁻)	6.51 [6.61] (m, 1H, Ar-5-H), 6.80-7.90 [6.80-7.90] (m, 3H, Ar-3,4,6-H),	3.74 [3.20] (m, 1H, NCH), 4.37 [2.87] (m, 1H, OCH), 4.53 [4.14] (m, 1H, OCH')
[Ru(PPh ₃)(¹ Pr-O ⁻ -N)(mes)]BPh ₄ (2.21) (233K, 400 MHz)	1.79 [1.79], 4.45 [5.08]	0.05 [0.97] (d, 3H), 0.60 [0.97] (d, 3H), 1.22 [2.11] (m, 1H)	6.75-7.90 [6.77-7.90] (m, 35H, PPh ₃ + BPh ₄ ⁻)	6.54 [6.62] (m, 1H, Ar-5-H), 6.75-7.90 [6.75-7.90] (m, 3H, Ar-3,4,6-H),	3.73 [3.24] (m, 1H, NCH), 4.46 [2.91] (m, 1H, OCH), 4.51 [4.20] (m, 1H, OCH')

Table (2E.4): NMR spectroscopic data (300 MHz) for complexes [Rh(L^m)(R,R'-phenmox)(Cp*)]SbF₆ in CD₂Cl₂ (δ / ppm)

Compound	C ₅ Me ₅	MeCHMe'	Ligand L ^m	Phenoxy ring	Oxazoline ring
[Rh(4-Me-py)(¹ Pr-O ⁻ -N)(Cp*)]SbF ₆ (2.22)	1.43 [1.71]	0.05 [0.05] (br. s, 3H), 0.93 [0.93] (d, 3H), 1.66 [~1.43] (m, 1H)	2.42 [2.42] (br. s, 3H, py-Me), 7.35 [7.35] (m, 2H, py-3,5-H), 8.76 [8.76] (d, 2H, py-2,6-H)	6.54 [6.54] (m, 1H, Ar-5-H), 7.03 [7.03] (m, 1H, Ar-3-H), 7.35 [7.35] (m, 1H, Ar-4-H), 7.54 [7.54] (m, 1H, Ar-6-H)	4.41 [4.41] (m, 3H, OCH + OCH' + NCH)
[Rh(4-Me-py)(¹ Pr-O ⁻ -N)(Cp*)]SbF ₆ (2.22) (213K, 400 MHz)	1.44 [1.38]	-0.20 [0.67] (d, 3H), 0.75 [1.00] (d, 3H), 1.48 [~1.36] (m, 1H)	2.37 [2.43] (s, 3H, py-Me), 7.25 [7.18] (m, 2H, py-3,5-H), 8.36 [8.19] (d, 2H, py-2,6-H)	6.52 [6.25] (m, 1H, Ar-5-H), 6.98 [6.82] (m, 1H, Ar-3-H), 7.25 [7.10] (m, 1H, Ar-4-H), 7.50 [7.42] (m, 1H, Ar-6-H)	4.21 [4.21] (m, 1H, OCH), 4.34 [4.34] (m, 2H, OCH' + NCH)
[Rh(Py)(¹ Pr-O ⁻ -N)(Cp*)]SbF ₆ (2.22)	1.58	0.01 (d, {J = 6.5 Hz}, 3H), 0.87 (d, {J = 6 Hz}, 3H), 1.99 (m, 1H)	7.65 (m, 2H, py-3,5-H), 8.06 (m, 1H, py-4-H), 8.87 (m, 2H, py-2,6-H)	6.49 (ddd {J=2, 7.5, 7.5 Hz} 1H, Ar-5-H), 7.01 (m, 1H, Ar-3-H), 7.26 (ddd {J=2, 7.5, 8.5 Hz} 1H, Ar-4-H), 7.46 (dd {J=2, 7.5 Hz} 1H, Ar-6-H)	4.52 (m, 2H, OCH + OCH'), 4.63 (m, 1H, NCH)

Table (2F.2): NMR spectroscopic data (300 MHz) for complexes [MX(¹Pr-phenmox)(ring)] in CD₂Cl₂ (δ / ppm)

Compound	π-Ring	MeCHMe'	Phenoxy ring	Oxazoline ring
[RuBr(¹ Pr-phenmox)(mes)] (2.23)	2.12, 4.98	0.74 (3H, d, {J = 6.5 Hz}, MeCHMe'), 1.02 (3H, d, {J = 6.5 Hz}, MeCHMe'), 2.70 (1H, m, MeCHMe')	6.45 (1H, m, Ar-5-H), 6.99 (1H, m, Ar-3-H), 7.21 (1H, m, Ar-4-H), 7.49 (1H, m, Ar-6-H)	4.36-4.58 (1H, m, OCH + 1H, m, OCH' + 1H, m, NCH)
[RuI(¹ Pr-phenmox)(mes)] (2.24)	2.31, 5.17	0.90 (3H, d, {J = 6 Hz}, MeCHMe'), 1.14 (3H, d, {J = 6.5 Hz}, MeCHMe'), 2.81 (1H, m, MeCHMe')	6.52 (1H, m, Ar-5-H), 6.98 (1H, m, Ar-3-H), 7.26 (1H, m, Ar-4-H), 7.55 (1H, m, Ar-6-H)	4.55 (1H, m, OCH + 1H, m, NCH), 4.69 (1H, m, OCH')
[RhI(¹ Pr-phenmox)(Cp*)] (2.25)	1.99	0.72 (3H, d, {J = 6.5 Hz}, MeCHMe'), 1.02 (3H, d, {J = 6.5 Hz}, MeCHMe'), 1.81 (1H, m, MeCHMe')	6.51 (1H, m, Ar-5-H), 6.88 (1H, m, Ar-3-H), 7.22 (1H, m, Ar-4-H), 7.54 (1H, m, Ar-6-H)	4.32 (1H, m, OCH + 1H, m, NCH), 4.44 (1H, m, OCH')
[RhI(¹ Pr-phenmox)(Cp*)] (2.25) (d ₄ -MeOH)	1.59	0.59 (3H, d, {J = 7 Hz}, MeCHMe'), 0.86 (3H, d, {J = 6.5 Hz}, MeCHMe'), 2.87 (1H, m, MeCHMe')	6.38 (1H, m, Ar-5-H), 6.77 (1H, m, Ar-3-H), 7.10 (1H, m, Ar-4-H), 7.43 (1H, m, Ar-6-H)	4.20 (1H, m, OCH + 1H, m, NCH), 4.34 (1H, m, OCH')

Table (2G.1): NMR spectroscopic data (300 MHz) for complexes [MCl(N-N)(mes)](SbF₆) in CD₂Cl₂ (δ / ppm)

Compound	π -Ring	Substituents R,R'	Pyridine ring	Heterocyclic ring
[RuCl(ⁱ Pr-pymox)(mes)] ⁺ (2.26) B) Thermodynamic Isomer	2.25, 5.34	0.77 (3H, d, {J = 7 Hz}, MeCHMe'), 1.02 (3H, d, {J = 7 Hz}, MeCHMe'), 2.23 (1H, m, MeCHMe')	7.73 (m, 1H, Py-5-H), 7.86 (d, 1H, {J = 7 Hz}, Py-3-H), 8.07 (dt, 1H, {J = 7.5, 1.5 Hz}, Py-4-H), 9.01 (d, 1H, {J = 5 Hz}, Py-6-H)	4.82 (1H, m, NCH), 4.82 (1H, m, OCH'), 5.00 (1H, t, {J = 11 Hz}, OCH)
[RuCl(Ph ₂ -pymimH)(mes)] ⁺ (2.43) (d ₆ -acetone)	2.08 [2.09], 5.40 [5.52]	7.35-7.47 (m, 10H, 2*Ph),	7.95 (t, 1H, {J = 6 Hz}, Py-H), 8.37 (m, 2H, Py-H), 9.02 [9.22] (br.s, 1H, NH), 9.44 [9.64] (d, 1H, {J = 5.5 Hz}, Py-6-H)	5.16 [5.10] (d, 1H, {J = 11.5, [6.5] Hz}, CH ^a Ph), 5.77 [5.19] (d, 1H, {J = 11.5, [6.5] Hz}, CH ^b Ph)
[RuCl(Ph ₂ -pymimMe)(mes)] ⁺ (2.44) (400 MHz), (d ₆ -acetone)	2.07 [2.10], 5.43 [5.51]	7.40-7.67 (m, 10H, 2*Ph),	7.96 (ddd, 1H, {J = 1, 5.5, 7 Hz}, Py-H), 8.35 [8.37] (dt, 1H, {J = 1.5, 8 Hz}, Py-H), 8.60 [8.58] (dt, 1H, {J = 1.5, 8 Hz}, Py-H), 9.49 [9.70] (ddd, 1H, {J = 0.5, 1.5, 5.5 Hz}, Py-6-H)	3.38 [3.35] (s, 3H, NMe), 5.00 [4.97] (d, 1H, {J = 12 [7.5] Hz}, CH ^a Ph), 5.69 [5.10] (d, 1H, {J = 12 [8] Hz}, CH ^b Ph)
[RuCl(ⁱ Pr-pymimPh)(mes)] ⁺ (2.45) (253K, 400 MHz)	2.27, 5.38	0.90 (d, 3H, {J = 6.5 Hz}, MeCHMe'), 1.00 (d, 3H, {J = 7 Hz}, MeCHMe'), 2.27 (m, 1H, MeCHMe')	6.88 (d, 1H, {J = 8 Hz}, Py-3-H), 7.51 (m, 1H, Py-5-H), 7.67 (dt, 1H, {J = 8, 1.5 Hz}, Py-4-H), 9.15 (d, 1H, {J = 5 Hz}, Py-6-H).	3.96 (dd, 1H, {J = 10, 5 Hz}, OCH'), 4.54 (t, 1H, {J = 10 Hz}, OCH), 4.78, m, 1H, NCH), 7.03 (m, 1H, N-Ph), 7.39 (m, 2H, N-Ph), 7.58 (m, 2H, N-Ph)

Table (2G.2): NMR spectroscopic data (300 MHz) for complexes [MCl(N-N)(mes)](SbF₆) in CD₂Cl₂ (δ / ppm)

Compound	π-Ring	Substituents R,R'	Pyridine ring	Imidazoline ring
[RuCl(ⁱ Pr-pymimPh)(mes)] ⁺ (2.45) (CDCl ₃)	2.30, 5.39	0.91 (d, 3H, {J = 7 Hz}, MeCHMe'), 1.03 (d, 3H, {J = 6.5 Hz}, MeCHMe'), 2.31 (m, 1H, MeCHMe')	6.89 (d, 1H, {J = 7.5 Hz}, Py-3-H), 7.52 (m, 1H, Py-5-H), 7.67 (m, 1H, Py-4-H), 9.13 (d, 1H, {J = 4.5 Hz}, Py-6-H).	3.96 (dd, 1H, {J = 10, 5 Hz}, OCH), 4.53 (t, 1H, {J = 10 Hz}, OCH), 4.79, m, 1H, NCH), 7.08 (br. s, 1H, N-Ph), 7.41 (br. s, 2H, N-Ph), 7.58 (m, 2H, N-Ph)
[RuCl(ⁱ Pr-pymim ⁿ Bu)(mes)] ⁺ (2.46) (CDCl ₃)	2.25, 5.30	0.73 (d, 3H, {J = 6.5 Hz}, MeCHMe'), 0.97 (d, 3H, {J = 7.5 Hz}, MeCHMe'), 2.24 (m, 1H, MeCHMe')	7.63, t, 1H, {J = 6.5 Hz}, Py-5-H), 7.78 (d, 1H, {J = 8 Hz}, Py-3-H), 8.00 (t, 1H, {J = 8 Hz}, Py-4-H), 9.17 (d, 1H, {J = 5.5 Hz}, Py-6-H)	0.98 (t, 3H, {J = 7.5 Hz}, ⁿ pr-CH ₃), 1.42 (m, 2H, -CH ₂ -CH ₃), 1.64 (m, 2H, -CH ₂ -C ₂ H ₅), 3.35 (m, 1H, OCH'), 3.81 (dd, 1H, {J = 10, 5.5 Hz}, OCH), 3.94 (m, 2H, N-CH ₂ -), 4.62 (m, 1H, NCH)
[RuCl(Bn-pymim ^t Bu)(mes)] ⁺ (2.47)	2.32, 5.37	2.67 (dd, 1H, {J = 14.5, 10.5 Hz}, CHH'Ph), 3.44 (dd, 1H, {J = 14.5, 4 Hz}, CHH'Ph)	7.32 (m, 5H, CH ₂ Ph), 7.68 (dt, 1H, {J = 6.0, 1.5 Hz}, Py-4-H), 8.01 (dt, 1H, {J = 7.0, 1.5 Hz}, Py-5-H), 8.15 (d, 1H, {J = 8.0 Hz}, Py-3-H), 9.18 (d, 1H, {J = 5.5 Hz}, Py-6-H)	1.48 (s, 9H, N-Bu ^t), 3.68 (dd, 1H, {J = 11, 7.5 Hz}, OCH'), 4.01 (dd, 1H, {J = 11, 10 Hz}, OCH), 4.79 (ddd, 1H, {J = 10.5, 10, 7.5 Hz}, NCH)

Table (2G.3): NMR spectroscopic data (300 MHz) for complexes [MCl(N-N)(mes)](SbF₆) in CD₂Cl₂ (δ / ppm)

Compound	π -Ring	N-CH(Me)R	Pyridine ring	Ketimine
[RuCl(Ph-ketimine)(mes)] ⁺ (2.49) (d ₆ -acetone)	2.19 [2.27], 5.23 [5.64]	1.77 [1.83] (d, 3H, {J = 8 Hz}, C-Me), 5.94 [5.62] (q, 1H, {J = 8 Hz}, C-H), 7.19 (7.19) (m, 2H, C-Ph), 7.22 (7.22) (m, 3H, C-Ph)	7.73 (t, 1H, {J = 8.5 Hz}, Py-5-H), 7.85 (d, 1H, {J = 8 Hz}, Py-3-H), 8.16 (t, 1H, {J = 7 Hz}, Py- 4-H), 9.29 (9.30) (d, 1H, {J = 7 Hz}, Py-6-H).	4.55 (d, 1H, {J = 13.5 Hz}, PhC-CH ^{down}), 4.67 (d, 1H, {J = 13.5 Hz}, PhC-CH ^{up}), 7.42 (br.s, 5H, N=C-Ph)
[RuCl(Nap-ketimine)(mes)] ⁺ (2.50)	2.02 [2.21], 5.20 [5.21]	1.30 [1.44] (d, 3H, {J = 8 Hz}, C-Me), 6.14 [5.88] (q, 1H, {J = 8 Hz}, C-H), 6.80 – 8.10 (m, 8H, Nap-H)	6.80 – 8.10 (m, 3H, Py-3,4,5-H), 9.17 [9.20] (d, 1H, {J = 6 Hz}, Py-6-H)	4.40 [4.57] (d, 1H, {J = 13 Hz}, PhC-CH ^{up}),
[RuCl(Cy-ketimine)(mes)] ⁺ (2.51)	2.06 [2.12], 5.11 [5.22]	0.62 [0.60] (m, 4H, C-Cy), 0.82 [0.70] (m, 4H, C-Cy), 0.96 [1.11] (m, 2H, C-Cy), 1.31 [1.31] (m, 1H, C-Cy), 1.50 [1.38] (d, 3H, {J = 6 Hz}, C-Me), 4.09 [4.09] (m, 1H, C-H)	7.62 [7.40] (d, 1H, {J = 8.5 Hz}, Py-3-H), 7.83 [7.83] (m, 2H, Py-4,5-H), 9.06 [8.99] (d, 1H, {J = 7 Hz}, Py-6-H)	4.39 [4.30] (d, 1H, {J = 12.5 Hz}, PhC-CH ^{up}), 4.92 [4.58] (d, 1H, {J = 12 Hz}, PhC-CH ^{down}), 7.49 [7.49] (m, 5H, N=C-Ph)

Table (2G.4): NMR spectroscopic data for complexes [MCl(N-N)(mes)](SbF₆) in CD₂Cl₂ (δ / ppm)

Compound	π -Ring	Substituent R	Pyridine ring	Ketimine
[RuCl(Me-ketimine)(mes)] ⁺ (2.50) (d ₆ -acetone, 400 MHz)	2.36 [2.40] [2.34], 5.95 [5.83] [5.88]	1.60 [1.32] [2.02] (d, 3H, {J = 6 Hz}, C-Me), 5.75 [5.81] [4.49] (q, 1H, {J = 7.5 Hz}, C-H)	7.50 [7.55] [7.44] (d, 1H, {J = 8.5 Hz}, Py-3-H), 7.94 [7.99] [7.94] (m, 1H, Py-5-H), 8.28 [8.39] [8.06] (m, 1H, Py-4-H), 9.58 [9.49] [9.65] (d, 1H, {J = 6 Hz}, Py-6-H)	7.73 (m, 1H, Ar-H), 7.95 (m, 2H, Ar-H), 9.83 [10.30] [10.43] (br.s, 1H, N-H)
[RuCl(Me-ketimine)(mes)] ⁺ (2.50) (d ₆ -DMSO, 400 MHz)	2.22 [2.19] [2.17], 5.93 [5.82] [5.78]	1.42 [1.12] [1.84] (d, 3H, {J = 7.5 Hz}, C-Me), 5.51 [5.62] [4.27] (q, 1H, {J = 7.5 Hz}, C-H)	7.24 [7.34] [7.36] (d, 1H, {J = 8.5 Hz}, Py-3-H), 7.84 [7.84] [7.86] (m, 1H, Py-5-H), 8.20 [8.31] [8.31] (m, 1H, Py-4-H), 9.49 [9.57] [9.39] (d, 1H, {J = 4.5 Hz}, Py-6-H)	7.84 (m, 1H, Ar-H), 7.92 [7.96] [7.96] (m, 1H, Ar-H), 8.04 (m, 1H, Ar-H-CBr), 10.91 [11.37] [11.46] (br. s, 1H, N-H)
[RuCl(¹ Pr-ketimine)(mes)] ⁺ (2.53) (300 MHz)	2.24 [2.29], 5.80 [5.73]	0.93 [1.06] (d, 3H, {J = 6.5 Hz}, CHMeMe'), 1.00 [1.12] (d, 3H, {J = 6.5 Hz}, CHMeMe'), 1.79 [1.71] (m, 1H, CHMeMe')	7.75 [7.75] (m, 1H, Py-3-H), 7.89 [7.89] (m, 1H, Py-5-H), 8.06 [8.06] (m, 1H, Py-4-H), 9.21 [9.29] (d, 1H, {J = 5.5 Hz}, Py-6-H)	5.25 [5.20] (d, 1H, {J = 10 Hz}, NCH ¹ Pr), 7.52 [7.54] (d, 1H, {J = 2 Hz}, Ar-H), 7.75 [7.75] (m, 1H, Ar-H), 7.87 [7.87] (s, 1H, Ar-H-CBr)

Table (2H.1): NMR spectroscopic data (300 MHz) for complexes [MCl(N-N)(mes)](SbF₆) in CD₂Cl₂ (δ / ppm)^A

Compound	π -Ring	Substituent R	Pyridine ring	Oxazoline ring
[RuCl(¹ Pr-pymox)(mes)] ⁺ (2.26 A) Kinetic Isomer	2.30, 5.77	0.97 (3H, d, {J = 6.5 Hz}, MeCHMe'), 1.15 (3H, d, {J = 7 Hz}, MeCHMe'), 2.64 (1H, m, MeCHMe')	7.73 (m, 1H, Py-5-H), 7.86 (m, 1H, Py-3-H), 8.11 (dd, 1H, {J = 8, 1.5 Hz}, Py-4-H), 9.22 (d, 1H, {J = 5.5 Hz}, Py-6-H)	4.39 (ddd, 1H {J = 9.5, 5, 3 Hz}, NCH), 4.72 (t, 1H, {J = 9.5 Hz}, OCH), 4.90 (t, 1H, {J = 11 Hz}, OCH')
[RuCl(¹ Pr-pymox)(mes)] ⁺ (2.26 B) Thermodynamic Isomer	2.25, 5.34	0.77 (3H, d, {J = 7 Hz}, MeCHMe'), 1.02 (3H, d, {J = 7 Hz}, MeCHMe'), 2.23 (1H, m, MeCHMe')	7.73 (m, 1H, Py-5-H), 7.86 (d, 1H, {J = 7 Hz}, Py-3-H), 8.07 (dt, 1H, {J = 7.5, 1.5 Hz}, Py-4-H), 9.01 (d, 1H, {J = 5 Hz}, Py-6-H)	4.82 (1H, m, NCH), 4.82 (1H, m, OCH'), 5.00 (1H, t, {J = 11 Hz}, OCH)
[RuBr(¹ Pr-pymox)(mes)] ⁺ (2.27 A) Kinetic Isomer	2.33, 5.86	1.01 (3H, d, {J = 6.5 Hz}, MeCHMe'), 1.16 (3H, d, {J = 7 Hz}, MeCHMe'), 2.65 (1H, m, MeCHMe')	7.85 (m, 1H, Py-5-H), 7.89 (m, 1H, Py-3-H), 8.12 (dt, 1H, {J = 7.5, 1 Hz}, Py-4-H), 9.21 (d, 1H, {J = 5.5 Hz}, Py-6-H)	4.37 (ddd, 1H {J = 10, 5, 3 Hz}, NCH), 4.73 (t, 1H, {J = 10 Hz}, OCH), 4.91 (dd, 1H, {J = 10, 5 Hz}, OCH')
[RuBr(¹ Pr-pymox)(mes)] ⁺ (2.27 B) Thermodynamic Isomer	2.30, 5.40	0.80 (3H, d, {J = 6.5 Hz}, MeCHMe'), 1.03 (3H, d, {J = 7 Hz}, MeCHMe'), 2.30 (1H, m, MeCHMe')	7.75 (dt, 1H, {J = 5.5, 1.5 Hz} Py- 5-H), 7.89 (m, 1H, Py-3-H), 8.10 (dt, 1H, {J = 7.5, 1 Hz}, Py-4-H), 9.05 (d, 1H, {J = 6 Hz}, Py-6-H)	4.87 (1H, m, NCH), 4.82 (1H, m, OCH'), 5.00 (1H, dd, {J = 9.5, 8 Hz}, OCH)

^A All data except that for **(2.26 A)** has been reported previously.¹⁰⁰

Table (2H.2): NMR spectroscopic data (300 MHz) for complexes [MCl(N-N)(mes)](SbF₆) in CD₂Cl₂ or d₆-acetone (δ / ppm)^A

Compound	π -Ring	Substituent R	Pyridine ring	Oxazoline ring
[RuI(¹ Pr-pymox)(mes)] ⁺ (2.28 A) (CD ₂ Cl ₂) Kinetic Isomer	2.33, 5.99	1.03 (3H, d, {J = 6.5 Hz}, MeCHMe'), 1.15 (3H, d, {J = 7 Hz}, MeCHMe'), 2.61 (1H, m, MeCHMe')	7.85 (dt, 1H, {J = 5, 1.5 Hz}, Py-5-H), 7.83 (m, 1H, Py-3- H), 8.11 (m, 1H, Py-4-H), 9.21 (d, 1H, {J = 5.5 Hz}, Py-6-H)	4.38 (ddd, 1H {J = 9.5, 5, 3 Hz}, NCH), 4.73 (m, 1H, OCH), 4.89 (m, 1H, OCH')
[RuI(¹ Pr-pymox)(mes)] ⁺ (2.28 B) (CD ₂ Cl ₂) Thermodynamic Isomer	2.37, 5.55	0.82 (3H, d, {J = 6.5 Hz}, MeCHMe'), 1.07 (3H, d, {J = 7 Hz}, MeCHMe'), 2.29 (1H, m, MeCHMe')	7.70 (dt, 1H, {J = 6, 2 Hz} Py- 5-H), 7.91 (dd, 1H, {J = 8, 0.5 Hz}, Py-3-H), 8.07 (dt, 1H, {J = 7.5, 0.5 Hz}, Py-4-H), 9.05 (d, 1H, {J = 6 Hz}, Py-6-H)	4.73 (m, 1H, NCH), 4.89 (m, 1H, OCH'), 5.10 (t, 1H, {J = 10 Hz}, OCH)
[RuCl(¹ Pr-pymox)(mes)] ⁺ (2.26 A) (d ₆ -acetone)	2.42, 6.36	1.09 (3H, d, {J = 7 Hz}, MeCHMe'), 1.21 (3H, d, {J = 7 Hz}, MeCHMe'), 2.89 (1H, m, MeCHMe')	7.93 (m, 1H, Py-5-H), 8.09 (m, 1H, Py-3-H), 8.33 (m, 1H, Py- 4-H), 9.60 (d, {J = 5.5 Hz}, 1H, Py-6-H)	4.50 (1H, ddd, {J = 10, 5, 3}, NCH), 4.85 (1H, t, {J = 10 Hz}, OCH'), 5.20 (1H, dd, {J = 5 Hz}, OCH)
[RuCl(¹ Pr-pymox)(mes)] ⁺ (2.26 B) (d ₆ -acetone)	2.42, 5.92	0.85 (3H, d, {J = 7 Hz}, MeCHMe'), 1.11 (3H, d, {J = 7 Hz}, MeCHMe'), 2.40 (1H, m, MeCHMe')	7.93 (m, 1H, Py-5-H), 8.09 (m, 1H, Py-3-H), 8.33 (m, 1H, Py- 4-H), 9.52 (d, {J = 6 Hz}, 1H, Py-6-H)	5.09 (3H, m, NCH + OCH + OCH')

^A All data except that for **(2.26 A)** has been reported previously.¹⁰⁰

Table (2H.3): NMR spectroscopic data (300 MHz) for complexes [MCl(N-N)(mes)](SbF₆) in d₆-acetone (δ / ppm)^A

Compound	π-Ring	Substituent R	Pyridine ring	Oxazoline ring
[RuBr(¹ Pr-pymox)(mes)] ⁺ (2.27 A) (d ₆ -acetone)	2.40, 6.23	1.06 (3H, d, {J = 7 Hz}, MeCHMe'), 1.22 (3H, d, {J = 7 Hz}, MeCHMe'), 2.89 (1H, m, MeCHMe')	7.96 (m, 1H, Py-5-H), 8.08 (m, 1H, Py-3-H), 8.34 (m, 1H, Py-4-H), 9.61 (d, {J = 5.5 Hz}, 1H, Py-6-H)	4.53 (1H, ddd, {J = 10, 5, 3}, NCH), 4.83 (1H, t, {J = 10 Hz}, OCH'), 5.20 (1H, dd, {J = 5 Hz}, OCH)
[RuBr(¹ Pr-pymox)(mes)] ⁺ (2.27 B) (d ₆ -acetone)	2.37, 5.78	0.83 (3H, d, {J = 7 Hz}, MeCHMe'), 1.09 (3H, d, {J = 7 Hz}, MeCHMe'), 2.37 (1H, m, MeCHMe')	7.96 (m, 1H, Py-5-H), 8.08 (m, 1H, Py-3-H), 8.34 (m, 1H, Py-4-H), 9.51 (d, {J = 5.5 Hz}, 1H, Py-6-H)	5.09 (3H, m, NCH + OCH + OCH')
[RuI(¹ Pr-pymox)(mes)] ⁺ (2.28 A) (d ₆ -acetone)	2.42, 6.36	1.09 (3H, d, {J = 7 Hz}, MeCHMe'), 1.21 (3H, d, {J = 7 Hz}, MeCHMe'), 2.89 (1H, m, MeCHMe')	7.93 (m, 1H, Py-5-H), 8.09 (m, 1H, Py-3-H), 8.33 (m, 1H, Py-4-H), 9.60 (d, {J = 5.5 Hz}, 1H, Py-6-H)	4.50 (1H, ddd, {J = 10, 5, 3}, NCH), 4.85 (1H, t, {J = 10 Hz}, OCH'), 5.20 (1H, dd, {J = 5 Hz}, OCH)
[RuI(¹ Pr-pymox)(mes)] ⁺ (2.28 B) (d ₆ -acetone)	2.42, 5.92	0.85 (3H, d, {J = 7 Hz}, MeCHMe'), 1.11 (3H, d, {J = 7 Hz}, MeCHMe'), 2.40 (1H, m, MeCHMe')	7.93 (m, 1H, Py-5-H), 8.09 (m, 1H, Py-3-H), 8.33 (m, 1H, Py-4-H), 9.52 (d, {J = 6 Hz}, 1H, Py-6-H)	5.09 (3H, m, NCH + OCH + OCH')

^A All data except that for (**2.26 A**) has been reported previously.¹⁰⁰

Table (2C.7): Analysis data for complexes [MCl(R,R'-phenmox)(ring)] in CDCl₃

Complex (code)	Elemental Analysis			Mass Spectrometry	
	Found (calculated)			Molecular ion M ⁺ (m/z)	Other ions (m/z)
	C %	H %	N %		
[RuCl(Me ₂ -phenmox)(mes)] (2.11)	56.45 (56.62)	5.46 (5.72)	3.02 (3.09)	448	[M-Cl] ⁺ = 413
[RuCl(^t Pr-phenmox)(mes)] (2.12)	54.47 (54.72)	5.55 (5.68)	2.96 (3.04)	461	[M-Cl] ⁺ = 426
[RuCl(^t Bu-phenmox)(mes)] (2.12)	47.94 (55.63)	5.88 (5.94)	1.79 (2.95)	-	[M-Cl] ⁺ = 441
[RuCl(Bn-phenmox)(mes)] (2.12)	55.90 (58.99)	4.91 (5.15)	2.47 (2.75)	509	[M-Cl] ⁺ = 474
[RuCl(Ph-phenmox)(mes)] (2.12)	58.27 (58.24)	4.76 (4.89)	2.92 (2.83)	495	[M-Cl] ⁺ = 460
[RuCl(^t Pr-phenmox)(<i>p</i> -cy)] (2.13)	51.98 (51.43)	5.53 (5.70)	2.40 (2.56)	-	[M-Cl] ⁺ = 440
[RuCl(^t Bu-phenmox)(<i>p</i> -cy)] (2.13)	-	-	-	489	[M-Cl] ⁺ = 454
[RuCl(^t Pr-phenmox)(C ₆ H ₆)] (2.14)	48.41 (48.25)	5.07 (4.50)	2.43 (3.13)	419	[M-Cl] ⁺ = 384
[RhCl(^t Pr-phenmox)(Cp [*])] (2.15)	55.05 (55.30)	5.92 (6.12)	2.88 (2.93)	477	[M-Cl] ⁺ = 442
[RhCl(Bn-phenmox)(mes)] (2.15)	57.13 (57.42)	5.39 (5.74)	2.47 (2.58)	-	[M-Cl]H ⁺ = 491
[RhCl(Ph-phenmox)(Cp [*])] (2.15)	58.57 (58.66)	5.65 (5.32)	2.72 (2.74)	511	[M-Cl] ⁺ = 476
[RhCl(Me ₂ -phenmox)(Cp [*])] (2.11)	53.43 (54.38)	5.79 (5.87)	3.12 (3.02)	463	[M-Cl] ⁺ = 428

Table (2D.3): Analysis data for complexes [M(L)(R,R'-phenmox)(ring)](Y)_n in CDCl₃

Complex (Code)	Elemental Analysis			Mass	Spectrometry
	Found (calculated)			Molecular ion	Other ions
	C %	H %	N %	M ⁺ (m/z)	(m/z)
[Ru(OH ₂)(¹ Pr-O ⁻ -N)(mes)]SbF ₆ (2.17)	38.84 (37.13)	4.55 (4.15)	2.08 (2.06)	-	[M-(OH ₂)] ⁺ = 426
[Ru(OH ₂)(Ph-O ⁻ -N)(mes)]SbF ₆ (2.17)	40.80 (40.41)	3.83 (3.67)	1.93 (1.96)	-	[M-(OH ₂)] ⁺ = 460
[Rh(OH ₂)(¹ Pr-O ⁻ -N)(Cp [*])]SbF ₆ (2.18)	36.75 (37.96)	3.98 (4.49)	1.66 (2.01)	-	[M-(OH ₂)] ⁺ = 442
[Rh(OH ₂)(Me ₂ -O ⁻ -N)(Cp [*])]SbF ₆ (2.16)	38.26 (36.98)	4.05 (4.29)	1.90 (2.05)	-	[M-(OH ₂)] ⁺ = 428
[Ru(4-Me-py)(¹ Pr-O ⁻ -N)(mes)]SbF ₆ (2.20)	42.94 (42.99)	4.43 (4.41)	3.81 (3.71)	519	[M-(Me-py)] ⁺ = 426
[Ru(2-Me-py)(¹ Pr-O ⁻ -N)(mes)]SbF ₆ (2.20)	42.60 (42.99)	4.18 (4.41)	3.46 (3.71)	-	[M-(Me-py)] ⁺ = 426
[Ru(Py)(¹ Pr-O ⁻ -N)(mes)]SbF ₆ ^A (2.20)	41.79 (42.18)	4.12 (4.22)	3.35 (3.78)	-	[M-Py] ⁺ = 426
[Ru(PPh ₃)(¹ Pr-O ⁻ -N)(mes)]BPh ₄ (2.21)	74.38 (75.14)	6.01 (6.11)	1.35 (1.39)	688	[M-PPh ₃] ⁺ = 426
[Rh(4-Me-py)(¹ Pr-O ⁻ -N)(Cp [*])]SbF ₆ (2.22)	35.91 (43.61)	3.67 (4.70)	2.32 (3.63)	535	[M-(Me-py)] ⁺ = 442
[Rh(Py)(¹ Pr-O ⁻ -N)(Cp [*])]SbF ₆ (2.22)	40.03 (39.93)	4.38 (4.31)	3.58 (3.33)	-	[M-py]H ⁺ = 443
[RuBr(¹ Pr-O ⁻ -N)(mes)] (2.23)	45.91 (49.91)	5.12 (5.18)	2.40 (2.77)	-	[M-Br] ⁺ = 426
[RuI(¹ Pr-O ⁻ -N)(mes)] (2.24)	39.37 (39.33)	4.23 (4.05)	2.29 (2.08)	554	[M-I] ⁺ = 426
[RhI(¹ Pr-O ⁻ -N)(Cp [*])] (2.25)	-	-	-	-	[M-I] ⁺ = 442

^A with 0.5 equivalents CH₂Cl₂.

Table (2G.5): Analysis data for complexes [RuX(N-N)(mes)](SbF₆)_n

Complex (Code)	Elemental Analysis			Mass	Spectrometry
	Found (calculated)			Molecular ion	Other ions
	C %	H %	N %	M ⁺ (m/z)	(m/z)
[RuCl(¹ Pr-pymox)(mes)]SbF ₆ (2.26)	40.80 (40.58)	4.18 (4.43)	3.94 (4.02)	447	[M - Cl] ⁺ = 412
[RuBr(¹ Pr-pymox)(mes)]SbF ₆ (2.27)	33.20 (33.04)	3.38 (3.60)	3.66 (3.85)	493	[M - Br] ⁺ = 412
[RuI(¹ Pr-pymox)(mes)]SbF ₆ (2.28)	31.57 (31.03)	3.28 (3.39)	3.61 (3.62)	539	[M - I] ⁺ = 412
[RuCl(Ph ₂ -pymimH)(mes)]SbF ₆ (2.43)	42.78 (41.61)	3.34 (3.49)	4.91 (4.93)	556	[M - Cl] ⁺ = 520
[RuCl(Ph ₂ -pymimMe)(mes)]SbF ₆ (2.44)	43.73 (43.74)	3.80 (4.03)	4.59 (5.10)	570	[M - Cl] ⁺ = 535
[RuCl(¹ Pr-pymimPh)(mes)]SbF ₆ (2.45)	40.04 (41.21)	4.00 (4.12)	5.24 (5.54)	522	[M - Cl] ⁺ = 487
[RuCl(¹ Pr-pymim ⁿ Bu)(mes)]SbF ₆ (2.46)	38.18 (39.07)	4.46 (4.78)	5.23 (5.70)	502	[M - Cl] ⁺ = 467
[RuCl(Bn-pymim ^t Bu)(mes)]SbF ₆ (2.47)	42.60 (42.79)	4.39 (4.49)	5.21 (5.35)	786	[M - Cl] ⁺ = 751
[Ru(OH ₂)(Ph ₂ -pymimH)(mes)](SbF ₆) ₂ (2.48)	-	-	-	-	[M - H] ⁺ = 538
[RuCl(Ph-ketimine)(mes)]SbF ₆ (2.49)	45.47 (45.45)	3.93 (4.07)	3.44 (3.53)	557	[M - Cl] ⁺ = 522
[RuCl(Nap-ketimine)(mes)]SbF ₆ (2.50)	-	-	-	607	[M - Cl] ⁺ = 570
[RuCl(Cy-ketimine)(mes)]SbF ₆ (2.51)	44.93 (45.10)	4.65 (4.79)	3.31 (3.51)	563	[M - Cl] ⁺ = 537
[RuCl(Me-ketimine)(mes)]SbF ₆ (2.52)	33.82 (35.04)	3.01 (2.94)	4.70 (5.11)	588	[M - Cl] ⁺ = 552
[RuCl(¹ Pr-ketimine)(mes)]SbF ₆ ^A (2.53)	38.02 (38.33)	3.68 (3.77)	4.37 (4.62)	616	[M - Cl] ⁺ = 581

^A with 1.0 equivalents acetone.

Chapter Three:

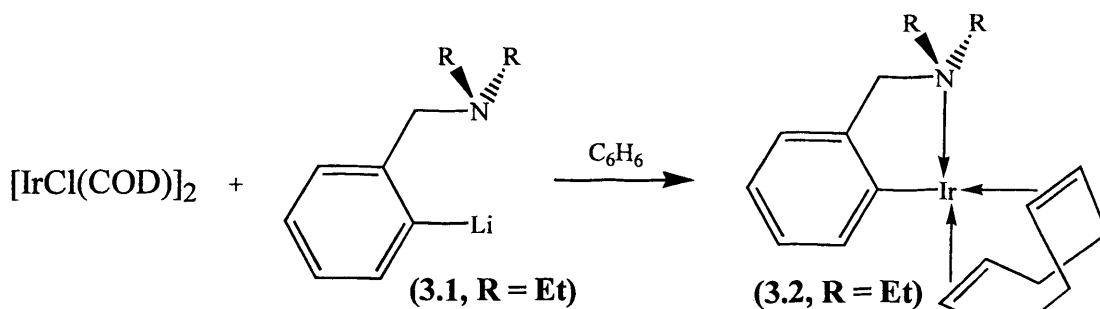
Attempts to Make C-Bonded Phenyl- Oxazolines

Chapter Three – Attempts to Make C-Bonded Phenyl-Oxazolines

There has been much interest recently in monoanionic aryl ligands with functionalised heteroatom containing substituents, particularly *C,N*- or *N,C,N*-donor ligands. This chapter will describe the attempts to make *C*-bonded complexes of chiral phenyloxazoline ligands. At the commencement of this work a few palladium orthometallated phenyloxazoline complexes were known,¹⁵⁰ though none with chiral oxazoline ligands, and arene half-sandwich complexes with cyclometallated phenyloxazoline ligands were unprecedented.

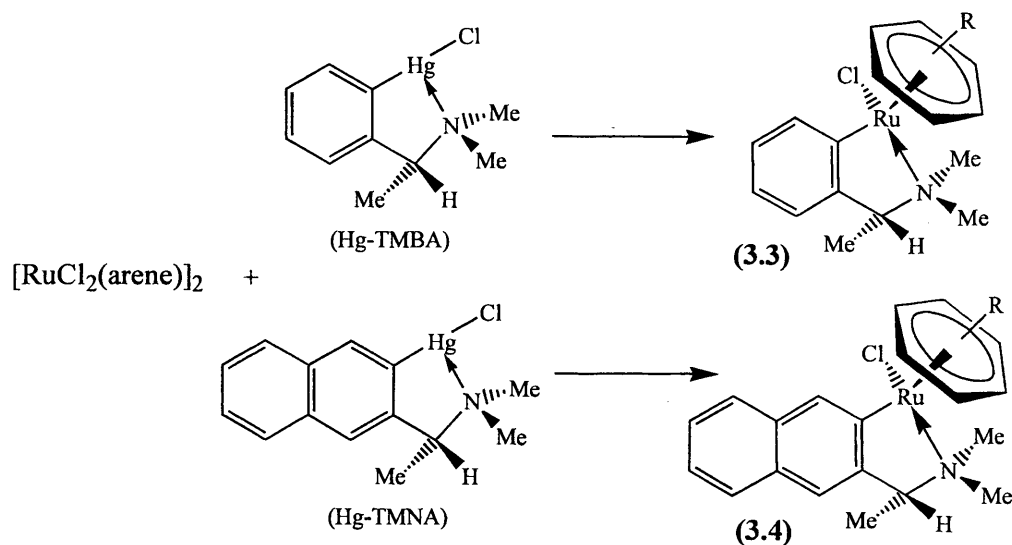
(3.1) – Introduction

Several methods have been reported for the synthesis of *ortho*-chelated functionalised σ -aryl complexes; notably transmetallation reactions, C-H activation and oxidative addition as described below. The group of Van Koten reported the formation of (3.2, R = Et) from the lithium reagent (3.1, R = Et) (Scheme 3.1).¹⁵¹



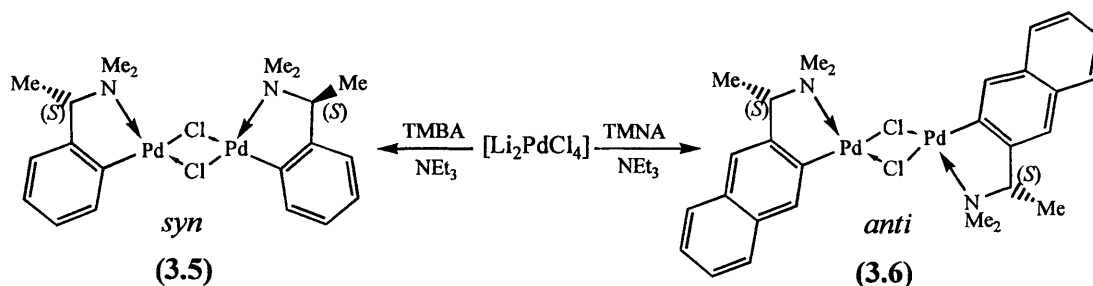
Scheme (3.1)

The methods for complexing structurally related arylamines, (*S*)-TMBA and (*S*)-TMNA (discussed in Section 1.4.3), are different for ruthenium and palladium metallacycles.^{86, 87, 152} Formation of monomeric ruthenacycles (3.3/3.4) required the use of the mercury complexes¹⁵³ and then transmetallation with the appropriate dimer $[\text{RuCl}_2(\text{arene})]_2$ (arene = C_6H_6 , $\text{C}_6\text{H}_5\text{CH}_3$, *p*-cy) in acetonitrile (Scheme 3.2).^{86, 87}



Scheme (3.2)

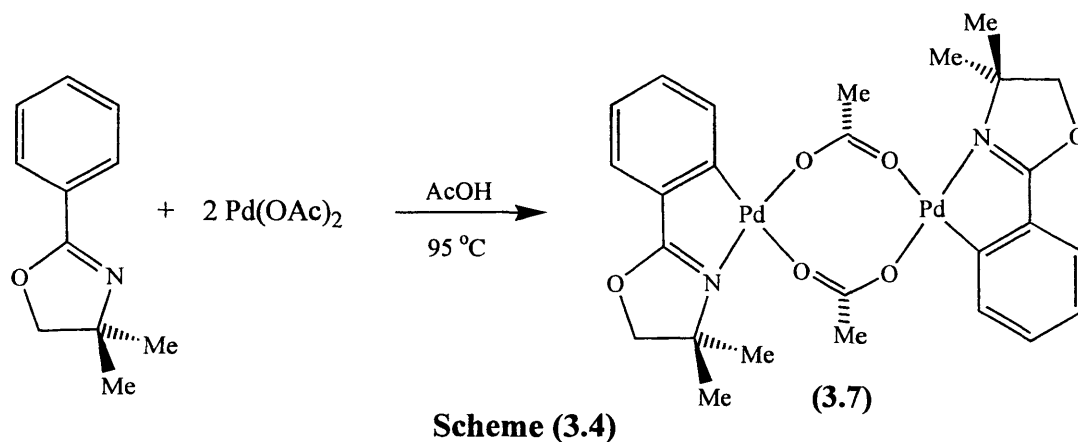
In contrast, palladium complexes (3.5) and (3.6) were formed directly by reacting TMBA and TMNA, respectively, with lithium tetrachloropalladate (Li_2PdCl_4) in the presence of NEt_3 (Scheme 3.3).¹⁵² These are examples of C-H bond activation, specifically cyclopalladation reactions which have been used to prepare a large number of C,N-bonded palladacycles. Extensive reviews on palladium-carbon cyclometallated complexes have been published,¹⁵⁴⁻¹⁵⁶ including recent detailed discussions of reaction mechanisms.^{156, 157} The TMBA complex (3.5) has *syn* geometry in the solid-state,¹⁵⁸ whereas the TMNA complex (3.6) adopted the *anti* arrangement,¹⁵² as shown by X-ray diffraction. Facile rearrangement of both complexes to an approximately 1:1 mixture of *syn* and *anti* isomers occurs in CDCl_3 , and is believed to proceed via a solvent-assisted associative process involving a pentacoordinated palladium transition state.¹⁵²



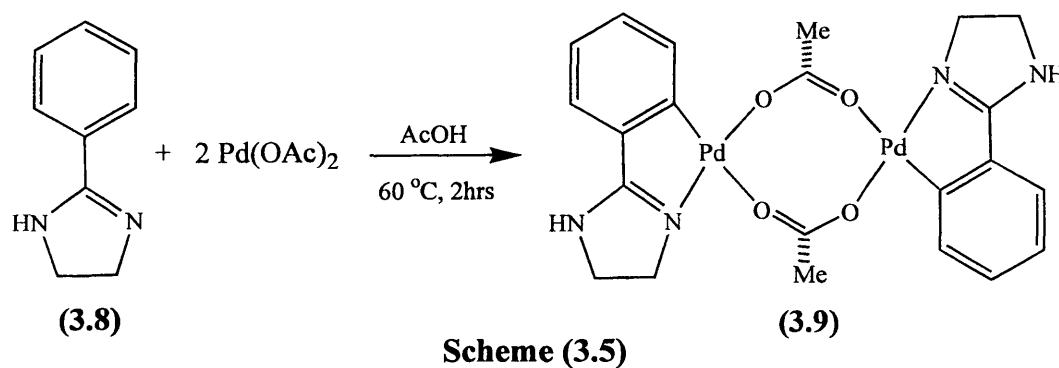
Scheme (3.3)

As indicated previously, some cyclometallated aryl oxazolines have been reported. Thus (3.7) was formed by reaction of $\text{C}_6\text{H}_5\text{-Me}_2\text{oxaz}$ with palladium acetate in glacial acetic acid (Scheme 3.4). The choice of solvent was critical since cyclopalladation was not observed in benzene, toluene or chloroform; in fact, heating to

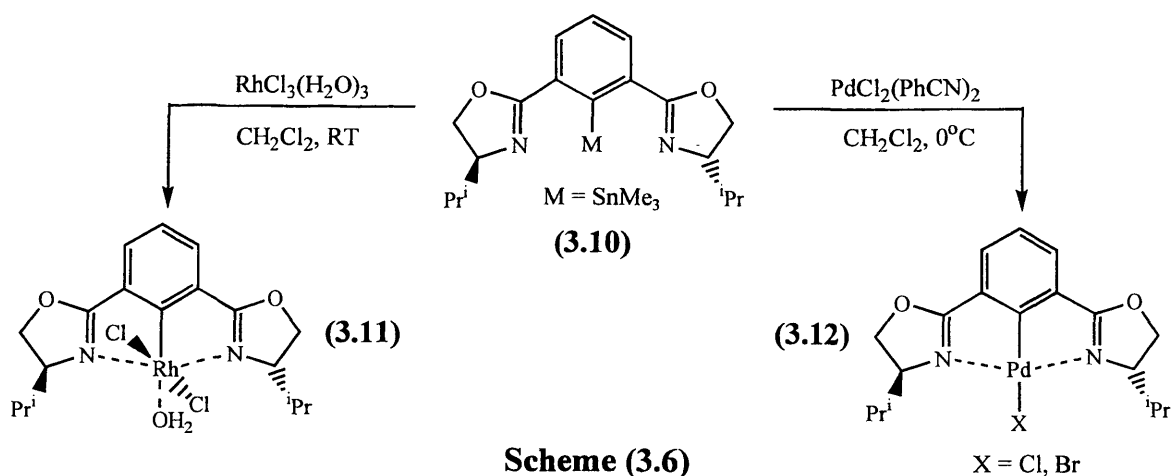
reflux in these solvents resulted in extensive decomposition only. The reaction was also sensitive to the palladium reagent; PdCl₂ reacted to give PdCl₂L₂ (L = *N*-coordinated). Characterisation of (3.7) by NMR and X-ray crystallography showed that only the *anti* stereoisomer was present in both solution and the solid-state.¹⁵⁰



The analogous achiral 2-phenylimidazoline ligand (3.8), also undergoes the cyclometallation reaction to form the acetate bridged palladium dimer (3.9) (Scheme 3.5).¹⁵⁹ Characterisation of (3.9) by NMR and X-ray crystallography showed that only the *anti* stereoisomer was present in both solution and the solid-state, as found for (3.7).¹⁵⁹

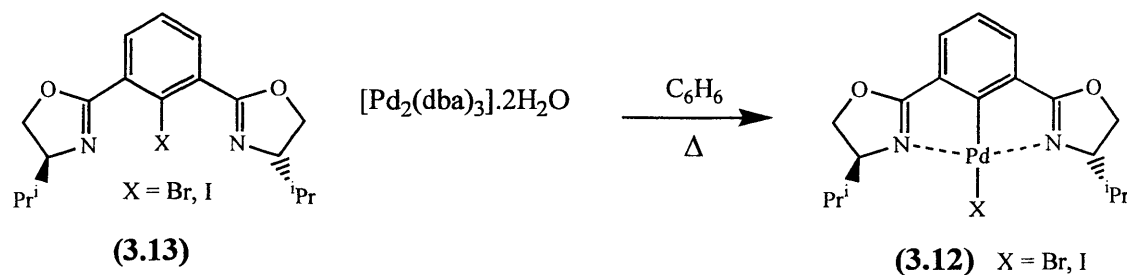


During the course of this work, tin reagents have also been used to synthesise rhodium and palladium complexes of anionic (*N,C,N*) bis(oxazoline)benzene (Scheme 3.6).¹⁶⁰ Reaction of the tin compound (3.10, M = SnMe₃) with RhCl₃(H₂O)₃ gave (3.11) in moderate yield (45%), whilst reaction with PdCl₂(PhCN)₂ gave (3.12, X = Cl) in 96% yield.¹⁶⁰ Formation of (3.12, X = Br) from the reaction of (3.10, M = Li) with PdBr₂(1,5-COD) was not as efficient (35% yield).¹⁶¹



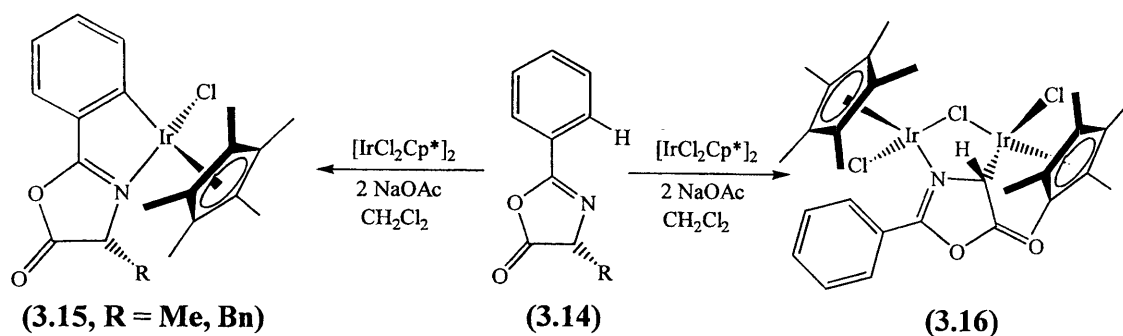
Scheme (3.6)

Alternatively, palladium complexes of anionic (*N,C,N*) bis(oxazoline)benzene can be conveniently formed via oxidative addition reactions (**Scheme 3.7**).¹⁶² Denmark *et al.* prepared complexes (3.12, X = Br, I) in 74 – 87% yield by heating (3.13, X = Br, I) with [Pd₂(dba)₃].2H₂O in benzene.



Scheme (3.7)

As regards half-sandwich species, no cyclometallated phenyl oxazolines were known prior to our work. However a half-sandwich complex of a phenyl oxazolone, which is similar to an oxazoline with the CH₂ of the heterocycle replaced by C=O, has been reported. Thus, reaction of enantiomerically pure phenyloxazolones (3.14, R = Me, Bn) with [IrCl₂Cp*]₂ in the presence of sodium acetate, formed mixtures of diastereomeric half-sandwich complexes (3.15, R = Me 5:1, Bn 20:1) (**Scheme 3.8**).¹⁶³ An unexpected complex was obtained with prochiral ligand (3.14, R = H); C-H bond activation on the oxazolone ring, instead of at the *o*-phenyl hydrogen, resulted in a chloride bridged diiridium complex.¹⁶³



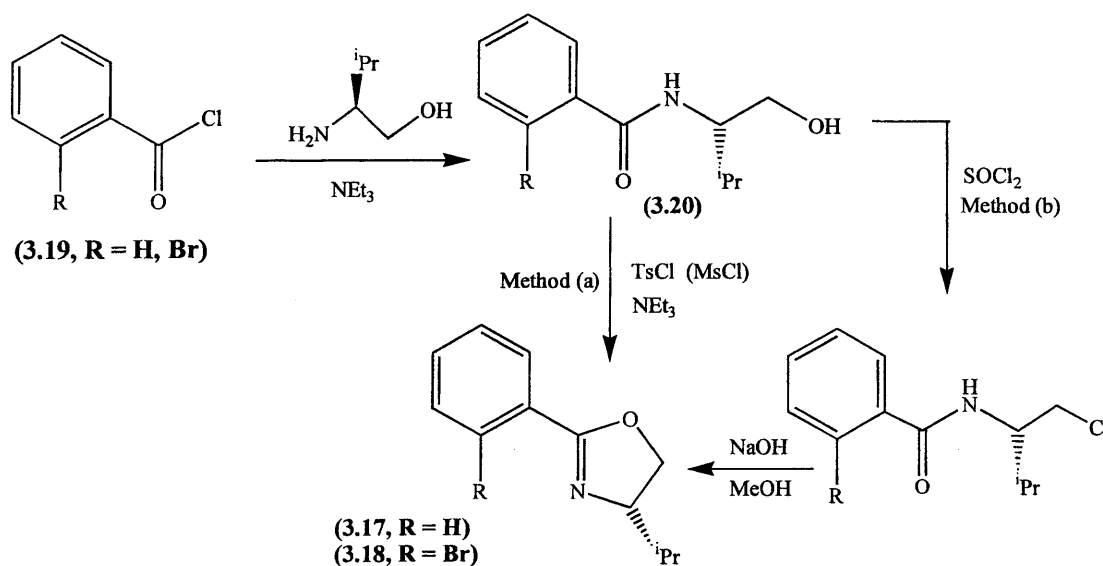
Scheme (3.8)

The remainder of this chapter will focus on complexation of the enantiopure C_6H_5 -ⁱProxaz ligand to form palladium complexes and the first phenyloxazoline half-sandwich complex.

(3.2) – Results and Discussion

(3.2.1) – Attempted Syntheses of Cyclometallated Phenyloxazoline Half-Sandwich Complexes

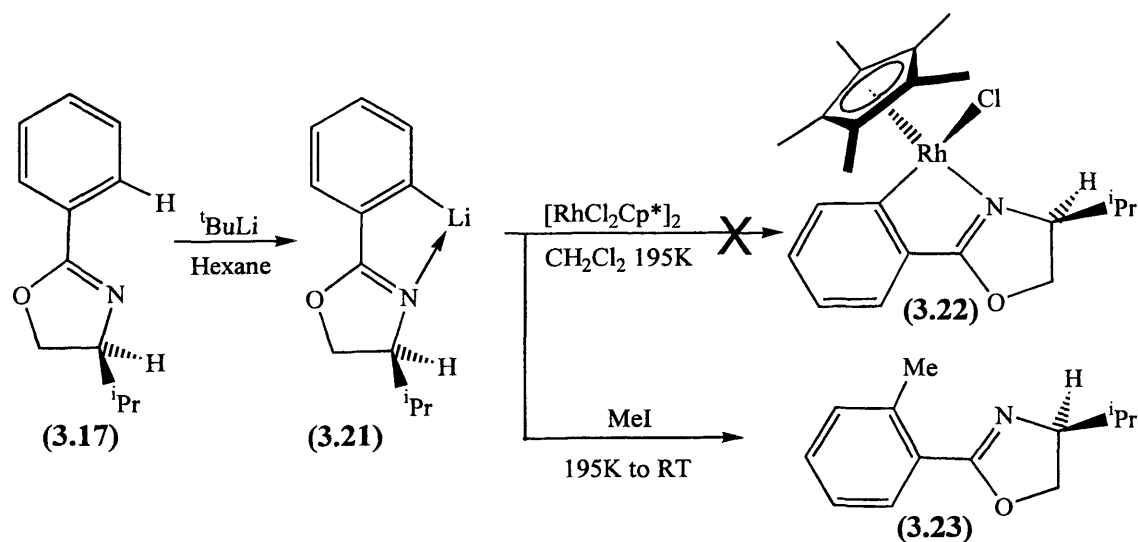
The phenyloxazoline ligands, C_6H_5 -ⁱProxaz (3.17) and *o*- BrC_6H_4 -ⁱProxaz (3.18), were inexpensively and conveniently synthesised by reaction of (L)-valinol with either benzoyl chloride or 2-bromobenzoyl chloride, respectively (Scheme 3.9), by the method of Denmark *et al.*¹¹³ Initially, the acyl chlorides (3.19, R = H, Br) were reacted with (L)-valinol to give stable hydroxy-amide species (3.20, R = H, Br). The terminal OH group was converted into a leaving group (Cl or, better, OTs or OMs), to allow base-induced cyclisation to occur, resulting in the desired oxazoline (3.17) or (3.18).



Scheme (3.9)

Ligands and complexes described in this chapter were characterised by a combination of mass spectrometry; microanalysis; ^1H NMR; ^1H - ^1H COSY and ^{13}C DEPT-135 NMR spectroscopy (Tables 3A/B; see Experimental), and where possible X-ray crystallography.

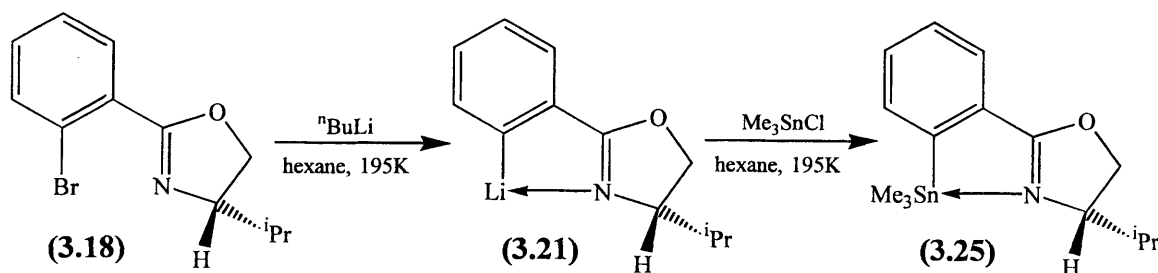
The first attempts to form cyclometallated complexes were via the lithium reagent (3.21) which was formed by treatment of (3.17) with $^t\text{BuLi}$ in hexane.¹⁵¹ A dichloromethane solution of $[\text{RhCl}_2\text{Cp}^*]_2$ was treated with (3.21) at 195K in an attempt to form $[\text{RhCl}(\text{C}_6\text{H}_4\text{-}^i\text{Proxaz})\text{Cp}^*]$ (3.22) (Scheme 3.10). The intense red reaction mixture was filtered through celite, to remove any LiCl by-product, and evaporated to give a brick-red solid. The ^1H NMR spectrum of the product contained signals consistent with unreacted ligand and dimer. The deprotonation step was checked by repeating the lithiation followed by addition of MeI; the ^1H NMR spectrum showed a mixture of starting material and methylated ligand (3.23) (*ca.* 30:70). Hence, failure of the reaction of (3.21) with $[\text{RhCl}_2\text{Cp}^*]_2$ was not due to failure of the lithiation step. The methodology (shown in Scheme 3.10) was also tested for the synthesis of the ruthenium analogue $[\text{RuCl}(\text{C}_6\text{H}_4\text{-}^i\text{Proxaz})(\text{mes})]$ (3.24); however, the reaction failed to give the desired ruthenacycle, instead unreacted dimer $[\text{RuCl}_2(\text{mes})]_2$ and ligand (3.17) were recovered.



Scheme (3.10)

The next approach was to convert the lithium complex (3.21) to the corresponding trimethylstannyl reagent (3.25) and then react this with either $[\text{RhCl}_2\text{Cp}^*]_2$ or $[\text{RuCl}_2(\text{mes})]_2$. The previously unreported compound (3.25) was prepared in 99% yield by reaction of (3.18) with $^n\text{BuLi}$ (a higher yielding route to

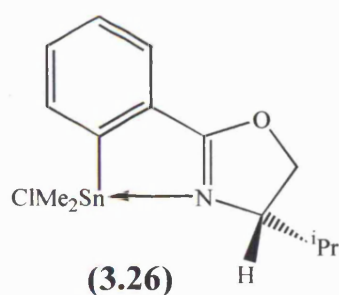
lithium reagent **3.21**) followed by addition of Me₃SnCl (**Scheme 3.11**). The air- and moisture-stable compound (**3.25**) was purified by column chromatography yielding a white crystalline solid.



The ¹H NMR spectrum of (**3.25**) is similar to that of (**3.18**); however, tin satellites (^{117,119}Sn-¹H) are observed for the signals at δ 7.67 (Ar-6-*H*) and there is a 9H singlet at δ 0.27 (SnMe₃) also with tin satellites. The electrospray (recorded in MeOH/water) and FAB mass spectra of (**3.25**) (see **Table 3B**) contain a minor ion pattern (10%) centred at *m/z* 354 due to [M + H]⁺ and a major pattern (90%) at *m/z* 338 due to [M - Me]⁺, suggesting relatively easy loss of a methyl from tin. Crystallisation of (**3.25**) from CH₂Cl₂/pentane gave crystals suitable for X-ray diffraction, the structure is discussed later (**Figure 3.1** and **Table 3.1**)

The transmetalation reactions between (**3.25**) and either [RhCl₂Cp*]₂ or [RuCl₂(mes)]₂ were carried out over a range of different temperatures (20-65°C) and in a range of solvents (CH₂Cl₂, MeOH and MeCN). The ¹H NMR spectra of the reaction mixtures, recorded after filtration through celite to remove unreacted dimer, did not contain signals consistent with the expected complex, nor the expected by-product (SnMe₃Cl) but no unreacted (**3.25**) was observed. One product was common to all the reactions, the ¹H NMR spectrum of which contained two 3H singlets (with Sn satellites) at δ 0.80 and δ 0.78 (X-SnMeMe') with additional signals for a C₆H₄-ⁱProxaz moiety suggesting an *o*-Me₂XSn-C₆H₄-ⁱProxaz species. The reaction mixtures were chromatographed to yield, after recrystallisation, a pure tin-containing complex. The electrospray mass spectra of the isolated product (see **Table 3B**) contained a minor ion pattern (10%) at *m/z* 373 consistent with [*o*-Me₂ClSn-C₆H₄-ⁱProxaz + H]⁺ and a major pattern (100%) at *m/z* 338, consistent with loss of chlorine. The above data are consistent with transfer of methyl to ruthenium or rhodium, rather than transfer of C₆H₄-ⁱProxaz, with formation of *o*-Me₂ClSn-C₆H₄-ⁱProxaz (**3.26**) rather than Me₃SnCl. The

resultant methyl complexes $[MCl(Me)(ring)]$ ($M = Ru$, ring = mes; $M = Rh$, ring = Cp*) would be formally 16-electron and presumably unstable, in the case of ruthenium reactions free mesitylene is observed in the NMR spectrum. In order to confirm this hypothesis, the reaction with $[RuCl_2(mes)]_2$ was repeated with the addition of dppe in an attempt to trap out the unstable methylated ruthenium species by forming $[Ru(Me)(dppe)(mes)]^+$ (**3.27**). The 1H NMR spectrum from this reaction mixture showed signals for (**3.26**) and a 3H singlet at δ 1.01 (Ru–Me) possibly due to (**3.27**), though other signals were present and the mixture could not be separated.



Crystallisation of (**3.26**) from CH_2Cl_2 /pentane gave X-ray quality crystals and the structure confirms that a methyl of (**3.25**) has been substituted by chloride. The structures of (**3.25**) and (**3.26**) are shown in **Figures (3.1)** and **(3.2)**, respectively, with selected bond lengths and angles in **Table (3.1)**.

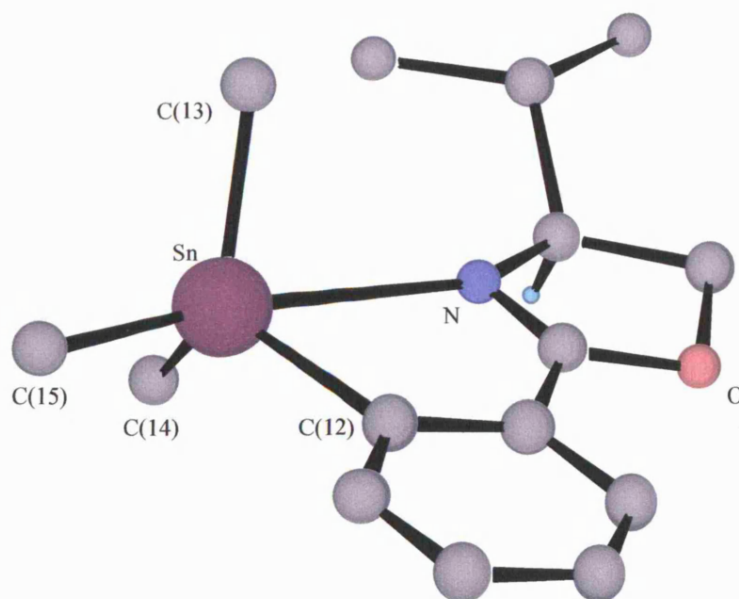


Figure (3.1): X-ray Structure of (3.25)

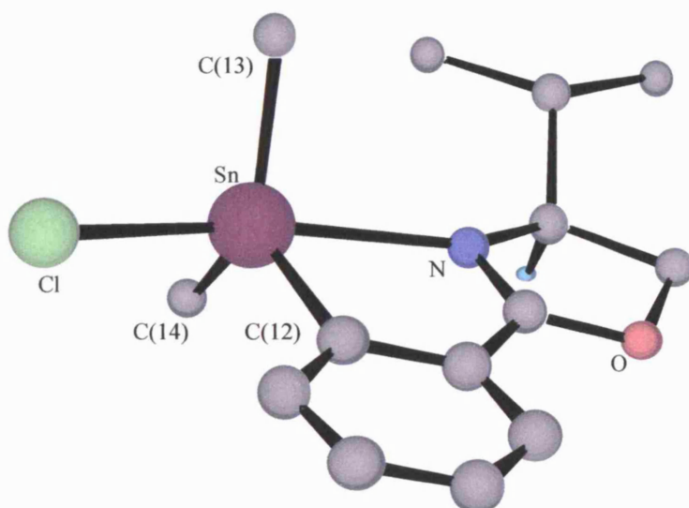


Figure (3.2): X-ray Structure of (3.26)

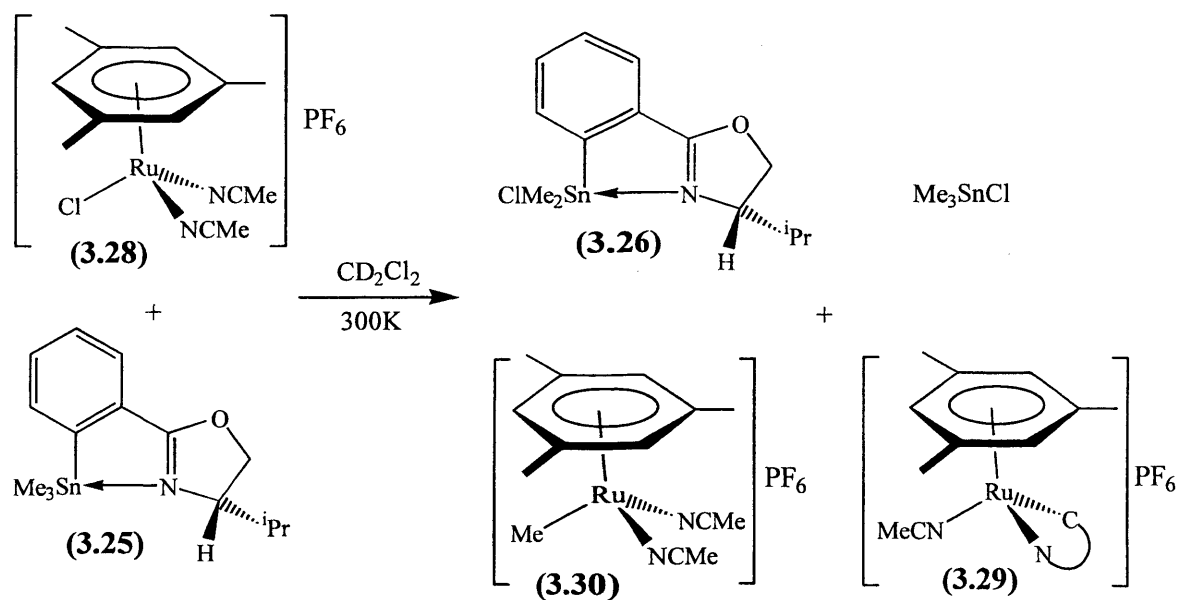
Table (3.1): Selected Bond Distances (Å) and Angles (°) of (3.25) and (3.26)

	(3.25)	(3.26)		(3.25)	(3.26)
Sn – C(12)	2.157 (9)	2.146 (5)	C(12)–Sn–C(13)	112.7 (4)	120.3 (3)
Sn – C(13)	2.133 (10)	2.126 (5)	C(12)–Sn–C(14)	115.9 (4)	116.3 (3)
Sn – C(14)	2.139 (9)	2.123 (5)	C(12)–Sn–C(15)	103.2 (4)	-
Sn – C(15)	2.161 (10)	-	C(12)–Sn–Cl(1)	-	94.67 (15)
Sn – Cl(1)	-	2.4957 (15)	C(12)–Sn–N(1)	68.74	75.78 (17)
Sn – N(1)	2.871 (5)	2.449 (4)			

The crystal structures show that in each case the tin has a distorted trigonal bipyramidal coordination geometry as a result of *C,N*-chelate bonding of the C_6H_4 -¹Proxaz ligand. In (3.26) the more electronegative nitrogen and chlorine atoms occupy the axial positions and the C_{phenyl} and methyl ligands are at the equatorial sites, as found for related complex *o*-{BrMe(Ph)Sn}- C_6H_4 -Me₂oxaz.¹⁶⁴ Whereas, in (3.25) the nitrogen and C(15) methyl group occupy the axial positions. In both complexes the nitrogen atom of the oxazoline preferentially coordinates to tin, although Sn–O coordination would result in a sterically less crowded molecule. The Sn–N(1) bond in (3.26) [2.449(4) Å] is shorter than in (3.25) [2.871(5) Å] probably due to the increased Lewis acidity of the tin centre due to the presence of the chlorine atom. The electron donating property of nitrogen increases the reactivity of the group *trans* to it; hence in (3.25) the Sn–C(15) bond should be weaker than Sn–C(13) and Sn–C(14), as found for

related tin compounds.^{165, 166} Hence transfer of methyl, instead of the aryl (C_6H_4 -ⁱProxaz), in the reactions of (3.25), might be due to this axial relationship between N and C(15).

In an attempt to prevent methyl transfer, the use of a more reactive ruthenium reagent was investigated. The labile salt $[RuCl(MeCN)_2(mes)]PF_6$ (3.28) has previously been shown to be a versatile synthetic intermediate in organoruthenium chemistry, as described in Section (1.4.2).⁵¹ The reaction of (3.25) and (3.28) in CD_2Cl_2 was monitored by 1H NMR spectroscopy. If the oxazoline fragment had been transferred, $SnMe_3Cl$ and $[Ru(MeCN)(C_6H_4$ -ⁱProxaz)(mes)] PF_6 (3.29) would be produced, compared to $[Ru(Me)(MeCN)_2(mes)]PF_6$ (3.30) and o - Me_2Cl Sn- C_6H_4 -ⁱProxaz (3.26) if methyl was transferred (Scheme 3.12).

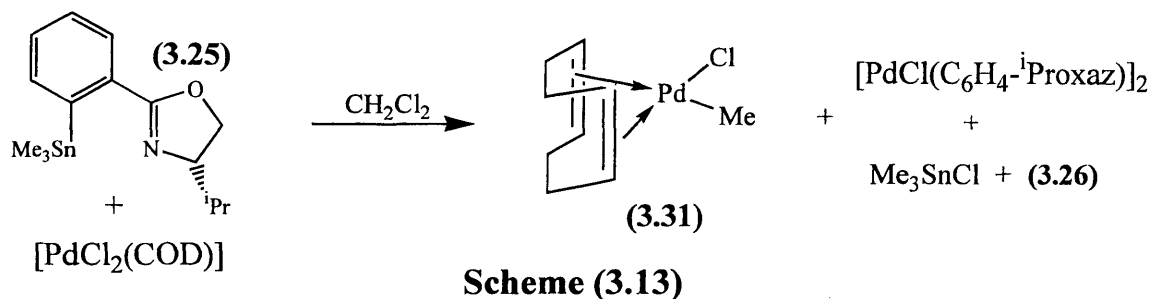


Scheme (3.12)

In the 1H NMR spectrum recorded after *ca.* 20 minutes had elapsed, two major species were observed. One of these corresponded to (3.26), indicating methyl had been transferred, the other major component contained a 3H(s) at δ 0.97 (Ru-*Me*), a 6H(s) at δ 2.43 (2 x *MeCN*) and mesitylene signals (δ 2.09 and 4.82) consistent with $[Ru(Me)(MeCN)_2(mes)]PF_6$ (3.30). Two minor species (~15 % total) were also present, a singlet at δ 0.70 (with tin satellites) is assigned to $SnMe_3Cl$ the other minor species showed signals for the moiety C_6H_4 -ⁱProxaz (and mesitylene at δ 2.09 and 4.82), possibly due to formation of (3.29) via transfer of C_6H_4 -ⁱProxaz. Electrospray mass spectrometry samples of the crude reaction mixture were made up in both MeOH and

MeCN. Irrespective of solvent the spectra each contained distinguishable ion patterns at m/z 408 (20%) $[\text{Ru}(\text{C}_6\text{H}_4\text{-}^i\text{Proxaz})(\text{mes})]^+$ and m/z 338 (50%) $[\text{o-Me}_2\text{Sn-C}_6\text{H}_4\text{-}^i\text{Proxaz}]^+$. Thus, corroborating the results of the NMR experiment that although transfer of methyl is favoured $\sim 85\%$, it is not specific, some transfer of $\text{C}_6\text{H}_4\text{-}^i\text{Proxaz}$ also occurs.

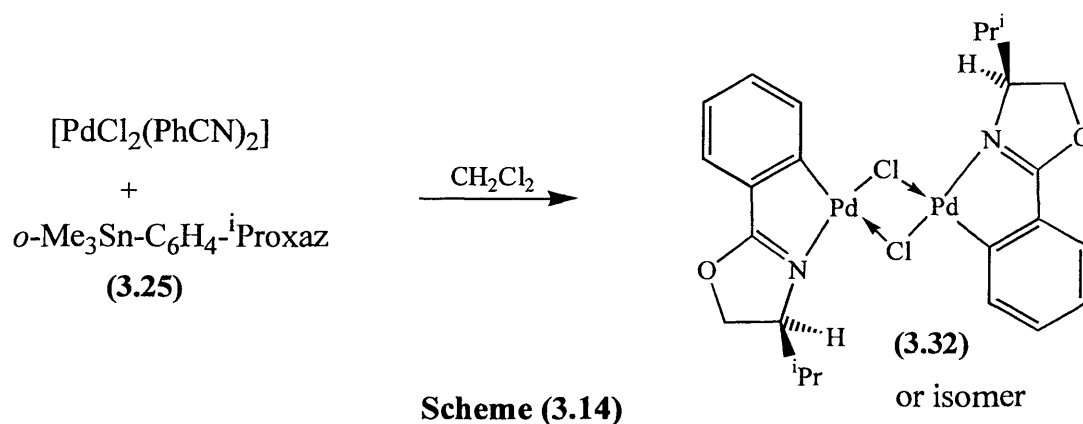
As mentioned previously, in the reaction with $[\text{PdCl}_2(\text{PhCN})_2]$, the tin reagent (**3.10**) transfers the functionalised phenyl rather than methyl.¹⁶⁰ However, with half-sandwich ruthenium and rhodium complexes the mono functionalised reagent (**3.25**) appears to transfer methyl in preference to $\text{C}_6\text{H}_4\text{-}^i\text{Proxaz}$. To test if this selectivity is due to the reagent or the metal we attempted reactions of (**3.25**) with various palladium complexes. Thus, $[\text{PdCl}_2(\text{COD})]$ and (**3.25**) were stirred overnight in CH_2Cl_2 (Scheme 3.13).



The ^1H NMR spectrum of the crude reaction mixture contained many signals including a singlet (δ 0.70) and two singlets (δ 0.80 and 0.78), both with tin satellites, assigned to SnMe_3Cl and $\text{o-Me}_2\text{ClSn-C}_6\text{H}_4\text{-}^i\text{Proxaz}$ (**3.26**), respectively. These products are consistent with transfer of $\text{C}_6\text{H}_4\text{-}^i\text{Proxaz}$ and methyl, respectively. Washing the reaction mixture with hexane and drying the resulting yellow solid under high vacuum removed both of the tin-containing by-products and free COD, leaving the signals for two remaining species in a ratio of 5:3, as determined by ^1H NMR spectroscopy. The minor species showed multiplets at δ 2.50, 2.60, 5.17 and 5.90 integrating to 12H and a 3H singlet at δ 1.20 consistent with $[\text{PdClMe}(\text{COD})]$ (**3.31**). The major product from the reaction only contains NMR signals derived from $\text{C}_6\text{H}_4\text{-}^i\text{Proxaz}$, *i.e.* no Pd-Me signal. Two aromatic proton signals integrating to 4H are observed and the resonances are shifted downfield compared to free $\text{C}_6\text{H}_5\text{-}^i\text{Proxaz}$ (**3.17**); consistent with a Pd coordinated $\text{C}_6\text{H}_4\text{-}^i\text{Proxaz}$ complex, presumably the chloride bridged dimer $[\text{PdCl}(\text{C}_6\text{H}_4\text{-}^i\text{Proxaz})]_2$ (confirmed by later experiments). This experiment indicates that the reaction

of **(3.25)** and $[\text{PdCl}_2(\text{COD})]$ is not selective, products from both C_6H_5 -ⁱProxaz and methyl transfer were formed.

The next palladium precursor to be tested was $[\text{PdCl}_2(\text{PhCN})_2]$, as used by Nishiyama *et al.* and chosen for the greater lability of the benzonitrile ligands compared to COD. It was predicted that unidentate PhCN would be displaced more readily by coordination of the oxazoline nitrogen, than would the chelating COD, thus, potentially promoting transfer of C_6H_4 -ⁱProxaz. Hence, $[\text{PdCl}_2(\text{PhCN})_2]$ and **(3.25)** were stirred overnight in CH_2Cl_2 in an attempt to form $[\text{PdCl}(\text{C}_6\text{H}_4$ -ⁱProxaz)]₂ **(3.32)** (Scheme 3.14).



The ¹H NMR spectrum (Table 3A) of the crude reaction mixture contained slightly broad signals, including a 12H multiplet assigned to CHMeMe' groups (δ 0.94) and two 4H multiplets (δ 7.09 and 7.41), identical to those of the major product from the reaction of $[\text{PdCl}_2(\text{COD})]$ and **(3.25)**. The FAB mass spectrum of the NMR sample contained three ion patterns at m/z 660 (40%) $[\text{M} + \text{H}]^+$, m/z 625 (100%) $[\text{M} + \text{H} - \text{Cl}]^+$ and m/z 294 (60%) $[\text{Pd}(\text{C}_6\text{H}_4$ -ⁱProxaz)]⁺, indicating the chloride dimer had been formed. Recording the electrospray mass spectrum in MeCN gave ion patterns m/z 376 $[\text{Pd}(\text{MeCN})_2(\text{C}_6\text{H}_4$ -ⁱProxaz)]⁺ and m/z 335 $[\text{Pd}(\text{MeCN})(\text{C}_6\text{H}_4$ -ⁱProxaz)]⁺, indicating that the dimer is easily cleaved by a coordinating solvent such as acetonitrile. The ¹H NMR spectrum recorded in CD_2Cl_2 at 253K contained sharp resonances at similar chemical shifts to those found at room temperature, indicating that only one isomer of **(3.32)** was present, as found for related complex $[\text{PdCl}(\text{C}_6\text{H}_4\text{-Me}_2\text{oxaz})]_2$.¹⁵⁰ The ¹³C DEPT 135 NMR spectrum showed (Table 3A, p 176) signals consistent with a single isomer and confirmed the presence of three quaternary carbons, δ 129.29 (Ar-C-C_{ox}), 144.41 (O=CN) and δ 173.56 (Ar-C-Pd), consistent with C_6H_4 -ⁱProxaz bound to palladium.

The two C₆H₄-ⁱProxaz ligands of **(3.32)** would be equivalent in both the *syn* and *anti* isomers therefore the exact structure of **(3.32)** could not be determined.

The differing selectivities for the two palladium reactions can be rationalised by the proposed mechanisms shown in **Figure (3.3)**. With [PdCl₂(COD)], dissociation/breaking of the COD chelate is disfavoured so direct Pd–C bond formation occurs. There is a preference for transfer of methyl as this is the weakest Sn–C bond (*trans* to N), thus forming *o*-Me₂ClSn–C₆H₄-ⁱProxaz (**(3.26)**) and [PdClMe(COD)] (**(3.31)**) as major products and some **(3.32)** and Me₃SnCl by transfer of Sn–C(Ph). In contrast, with [PdCl₂(PhCN)₂], one PhCN ligand can dissociate enabling coordination of oxazoline (**(3.25)**) to palladium, *i.e.* forming **(3.32a)**, followed by intramolecular transfer of Sn–C(Ph). Thus, generating Me₃SnCl by-product and [PdCl(PhCN)(C₆H₄-ⁱProxaz)] (**(3.32b)**), which forms the more stable chloro-bridged dimer [PdCl(C₆H₄-ⁱProxaz)]₂ (**(3.32)**). In this case, transfer of the Sn–C(Ph) rather than Sn–Me occurs exclusively, as is usually observed for Me₃SnPh,¹⁵⁴ since there is no longer any intramolecular coordination of nitrogen to tin in **(3.32a)**. Thus, the transmetalation reaction is sensitive to the palladium precursor used.

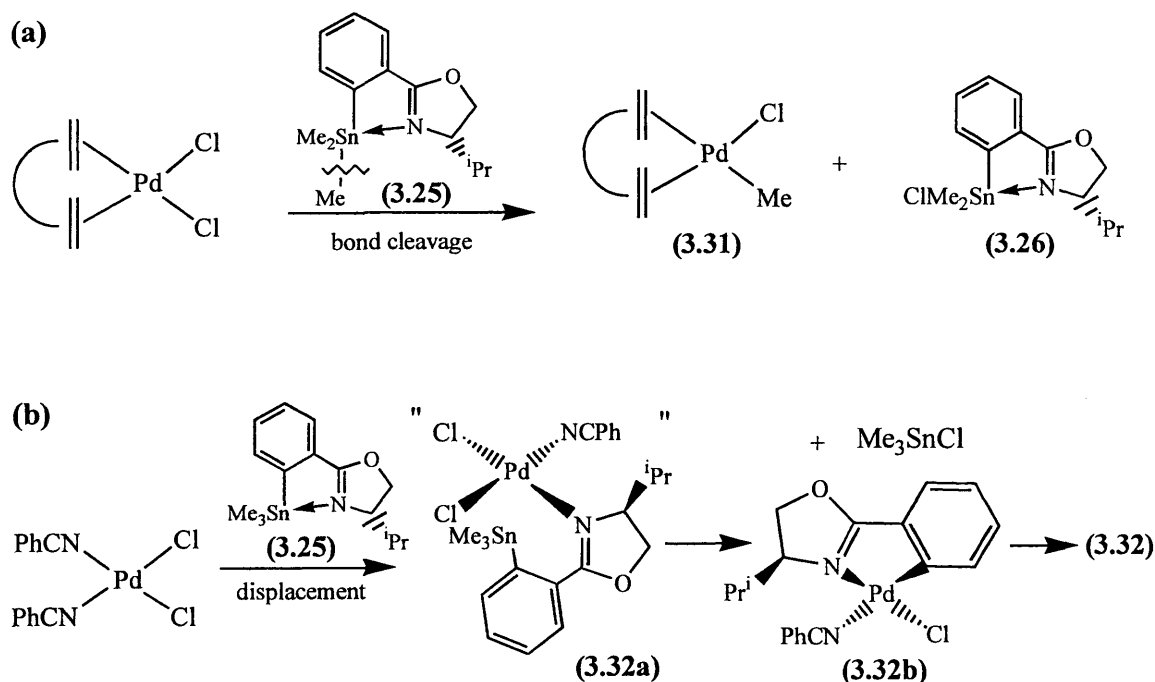
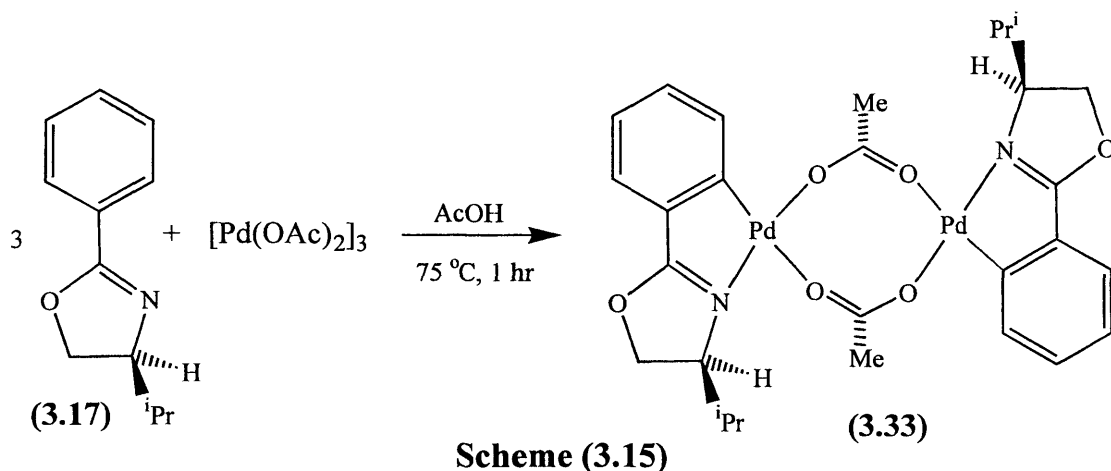


Figure (3.3)

As discussed in Section 3.1 the achiral orthometallated complex, [Pd(OAc)(C₆H₄-Me₂oxaz)] (**(3.7)**) has previously been formed by reaction of C₆H₅-

Me₂oxaz with [Pd(OAc)₂]₃, and the complex had been characterised by X-ray diffraction.¹⁵⁰ Using different reaction conditions (temperature and concentration) the synthesis of complex [Pd(OAc)(C₆H₄-ⁱProxaz)]₂ (**3.33**) was attempted by heating C₆H₅-ⁱProxaz (**3.17**) and [Pd(OAc)₂]₃ in acetic acid at 75°C (**Scheme 3.15**).



The ¹H NMR spectrum (**Table 3A**) of the crude reaction mixture contained signals for C₆H₄-ⁱProxaz and acetate in ratio 1:1, indicating the desired product (**3.33**) had been formed. The chemical shifts of the chelated ligands are to higher field than the uncomplexed phenyloxazoline (**3.17**). The observation of only one acetate signal (δ 2.12) in the ¹H NMR spectrum, indicates that in solution the complex must adopt the *anti* geometry making the two acetates equivalent; as observed for the related complex [Pd(OAc)(C₆H₄-Me₂oxaz)]₂.¹⁵⁰ The ¹³C DEPT 135 spectrum of (**3.33**) contained a single set of signals including four quaternary carbons, *i.e.* only one acetate group; again consistent with only the *anti* isomer. Careful recrystallisation from acetone/pentane gave crystals suitable for X-ray diffraction. The X-ray structure contained four independent molecules in the unit cell, none of which differed greatly. The structure of one of the molecules is shown in **Figure (3.4)**, with the ranges (for all four molecules) of selected bond distances and angles in **Table (3.2)**. The complex adopts the expected *anti* geometry, as observed in solution, with the acetate bridges enabling the molecule to fold into an “open book” arrangement. A similar geometry has been reported by Boubekeur¹⁵⁰ for [Pd(OAc)(C₆H₄-Me₂oxaz)]₂ and recently by Zhao for [Pd(OAc)(C₆H₄-ⁱBuoxaz)]₂.¹⁶⁷

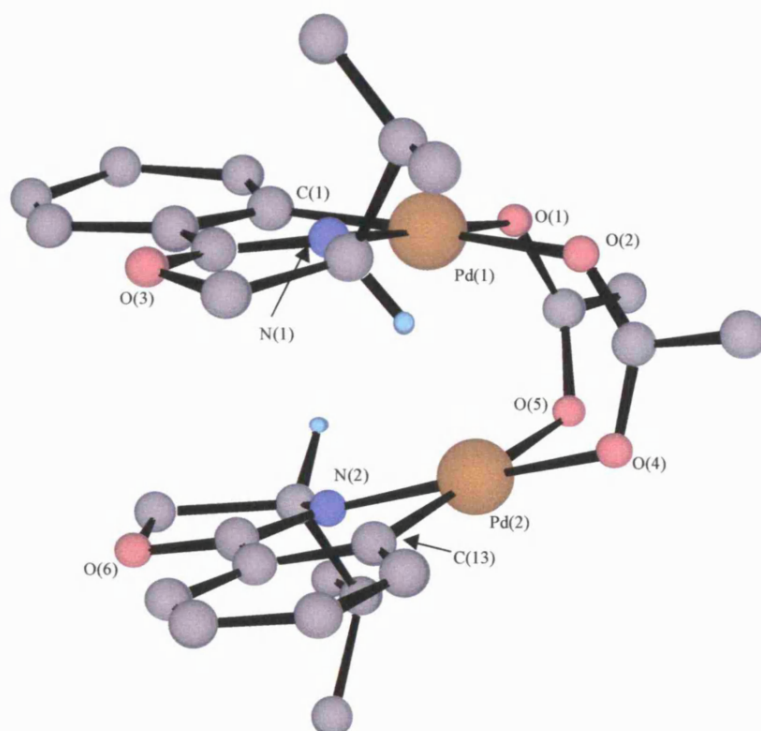


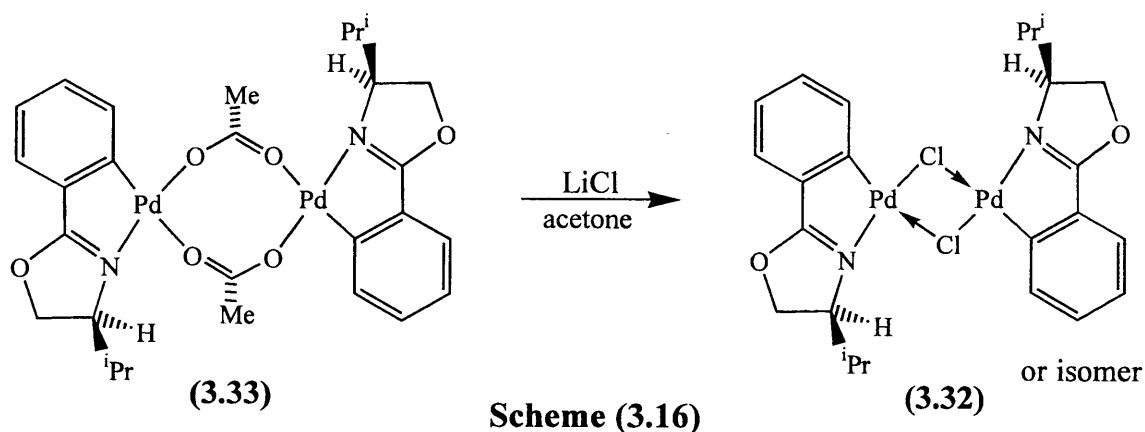
Figure (3.4): X-ray Structure of (3.33)

Table (3.2): Ranges of Selected Bond Distances (Å) and Angles (°) of (3.33)

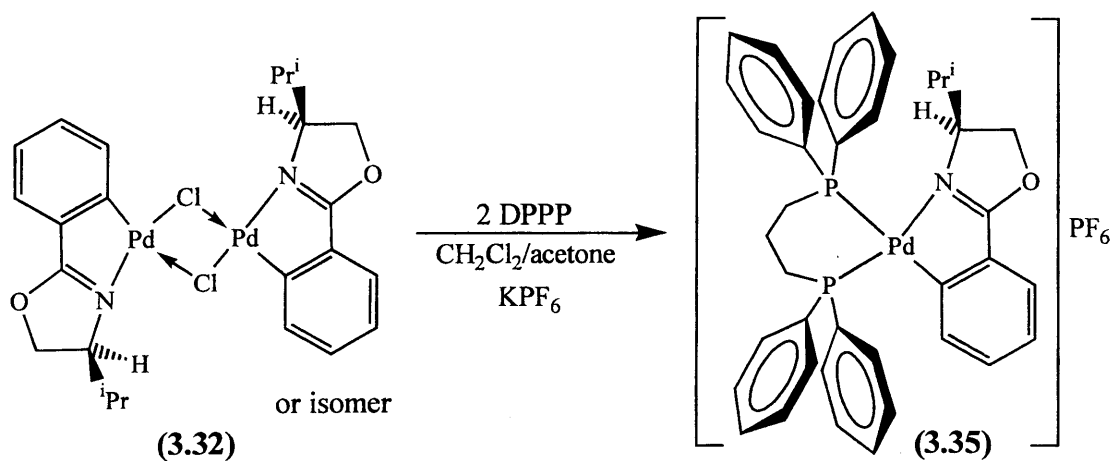
Pd(1)-O(1)	2.027(11) - 2.058(9)	Pd(2)-O(4)	2.022(13) - 2.059(14)
Pd(1)-O(2)	2.114(12) - 2.131(13)	Pd(2)-O(5)	2.109(12) - 2.146(12)
Pd(1)-N(1)	1.998(14) - 2.022(12)	Pd(2)-N(2)	1.993(13) - 2.022(12)
Pd(1)-C(1)	1.936(16) - 1.951(17)	Pd(2)-C(13)	1.941(14) - 1.954(16)
N(1)-Pd(1)-C(1)	90.3(7) - 81.7(8)	N(2)-Pd(2)-C(13)	81.1(9) - 83.0(14)
O(1)-Pd(1)-O(2)	88.7(5) - 92.1(6)	O(4)-Pd(2)-O(5)	88.7(7) - 91.7(5)

The coordination geometry around each palladium atom is approximately square-planar. The C–Pd distances [1.936(16) to 1.954(16) Å] are the same as those [1.967(4) Å] for the related complex [Pd(OAc)(C₆H₄-Me₂oxaz)]₂ (**3.7**).¹⁵⁰ The *trans* influence of a σ -bonded carbon is illustrated by the lengthening of the Pd–O bond *trans* to carbon [2.109(12) to 2.146(12) Å] relative to those *trans* to nitrogen atoms [2.022(13) to 2.059(14) Å].

The synthesis of the chloro-bridged complex [PdCl(C₆H₄-ⁱProxaz)]₂ (**3.32**), was accomplished by metathesis with lithium chloride in acetone in nearly quantitative yield (**Scheme 3.16**). The ¹H NMR and FAB mass spectra of the complex are identical to those obtained from the product of the transmetalation reaction between *o*-Me₃Sn-C₆H₄-ⁱProxaz (**3.25**) and [PdCl₂(PhCN)₂], see **Scheme (3.14)**.



The reactivity of the palladium dimers was assessed by reactions with PPh_3 , dppp and 4,4'- Me_2 -bipy. The synthesis of $[\text{Pd}(\text{C}_6\text{H}_4\text{-}^i\text{Proxaz})(\text{PPh}_3)_2]\text{PF}_6$ (**3.34**) was attempted by treating one equivalent of (**3.33**) with four equivalents of PPh_3 and three equivalents of KPF_6 in $\text{CH}_2\text{Cl}_2/\text{acetone}$ (1:1). After filtering through celite to remove excess KPF_6 and KCl by-product, the reaction mixture was analysed by mass spectrometry, ^1H and ^{31}P NMR spectroscopy. The ^{31}P (and ^1H) NMR spectra contained several signals indicating a mixture of species which have not been characterised, although free PPh_3 was identified in the ^{31}P spectrum. FAB and electrospray mass spectra contained an ion pattern at m/z 556 (100%) due to $[\text{Pd}(\text{C}_6\text{H}_4\text{-}^i\text{Proxaz})(\text{PPh}_3)]^+$, but signals consistent with the molecular ion were not present. These data indicate phosphine products have been formed but that the major product is certainly unstable to loss of PPh_3 . Therefore, the reaction was attempted using the chelating bisphosphine, dppp, with the aim of inhibiting dissociation of phosphine. One equivalent of (**3.32**) was stirred with two equivalents of dppp and KPF_6 in $\text{CH}_2\text{Cl}_2/\text{acetone}$ (1:1) to afford $[\text{Pd}(\text{C}_6\text{H}_4\text{-}^i\text{Proxaz})(\text{dppp})]\text{PF}_6$ (**3.35**) (Scheme 3.17).

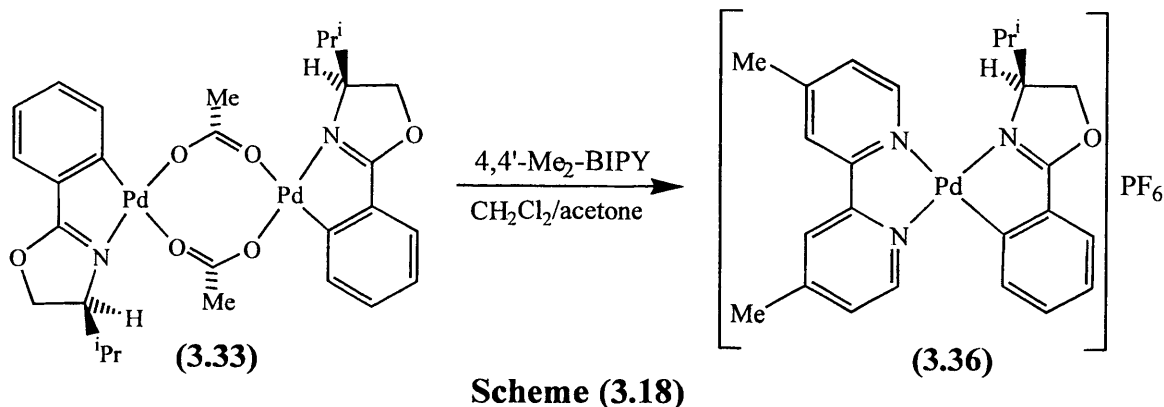


The electrospray mass spectrum shows the molecular ion at m/z 706 (100%) $[\text{Pd}(\text{C}_6\text{H}_4\text{-}^i\text{Proxaz})(\text{dppp})]^+$, indicating that $[\text{Pd}(\text{C}_6\text{H}_4\text{-}^i\text{Proxaz})(\text{dppp})]\text{PF}_6$ (**3.35**) had been synthesised. The ^1H NMR spectrum recorded in CD_2Cl_2 at 300K contained signals consistent with $\text{C}_6\text{H}_4\text{-}^i\text{Proxaz}$ and dppp , however many signals were broad suggesting the complex is fluxional. At 253K additional signals appeared; for example at δ 6.95, 6.78 and 6.69 (Ar-3,4,5-*H*) compared to δ 7.08, 7.01 and 6.85 at 300K. Variable temperature $^{31}\text{P}\{^1\text{H}\}$ NMR spectra were recorded on the sample. At 323K a slightly broad doublet (δ -2.55, $\{J = 57\text{Hz}\}$) and very broad signal (δ 26.1) were observed. Lowering the temperature through to 233K resolved the lowfield signal into a doublet (δ 26.3, $\{J = 56\text{Hz}\}$) and sharpened the highfield signal. These observations indicate the complex is fluxional and that the process(es) are “frozen-out” at low temperatures. The spectra are extremely complicated and there are several possibilities for the variable temperature observations including:

1. Dissociation of one end of the dppp chelate. There is supporting evidence for PPh_3 loss from (**3.34**), although a chelate is much more difficult to open and the phosphorus to phosphorus coupling is retained in the highfield signal.
2. Dissociation of the nitrogen of the oxazoline. It is not clear which phosphorus signal would be most affected by this process; a heteronuclear NOESY experiment may determine which phosphorus.
3. Restricted rotation of a phenyl(s) on dppp . It is likely that this would have greater effect on the phosphorus *cis* to nitrogen, since it is more sterically crowded than the other.

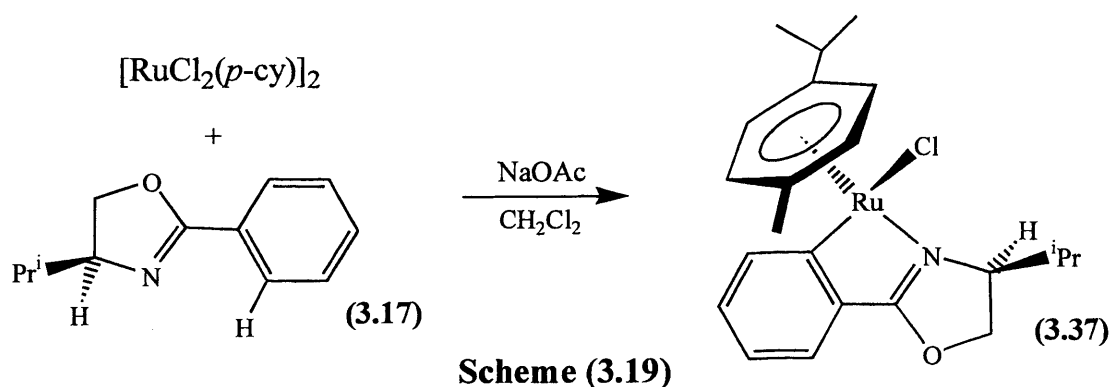
The fluxional behaviour of the dppp and PPh_3 complexes suggests that in the phosphine complexes there may be too much steric bulk near the ^iPr -substituent. In contrast, the use of a planar coordinating ligand, i.e. 4,4'- Me_2 -bipy, may reduce steric congestion since the bipy-6-*H* is in the palladium square plane, hence is not sterically interfering with the isopropyl.

Treating one equivalent of $[\text{Pd}(\text{OAc})(\text{C}_6\text{H}_4\text{-}^i\text{Proxaz})]_2$ (**3.33**) with two equivalents of 4,4'- Me_2 -bipy and KPF_6 in $\text{CH}_2\text{Cl}_2/\text{acetone}$ (1:1) gave $[(\text{C}_6\text{H}_4\text{-}^i\text{Proxaz})\text{Pd}(4,4'\text{-Me}_2\text{-bipy})]\text{PF}_6$ (**3.36**) in 72% yield (**Scheme 3.18**).



The ^1H NMR spectrum of **(3.36)** (Table 3A) contained well-resolved signals for complexed 4,4'-Me₂-bipy and C₆H₄-ⁱProxaz, shifted downfield by up to 0.3 and 1.20 ppm compared to free 4,4'-Me₂-bipy and **(3.33)**, respectively. The ^{13}C DEPT 135 NMR spectrum contained the expected signals for **(3.36)** and facilitated assignment of the oxazoline ring resonances. The ^1H NMR spectrum of the sample showed no sign of decomposition after two weeks at ambient temperature; in contrast [Pd(C₆H₄-Me₂oxaz)(py)₂] PF_6 , is unstable in solution decomposing to the dimer over a few weeks at 253K.¹⁵⁰ The use of the chelating 4,4'-Me₂-bipy ligand, would be expected to prevent dissociation. The electrospray mass spectrum contains the molecular ion m/z 478 [Pd(C₆H₄-ⁱProxaz)(4,4'-Me₂-bipy)]⁺, which is further evidence for formation of the complex.

The best method, in terms of convenience and yield, to form palladium C₆H₄-ⁱProxaz complexes proved to be C-H bond activation in acetic acid (Scheme 3.15). As mentioned previously, a similar approach had been used to synthesise half-sandwich iridium oxazolone complexes **(3.15)**, see Scheme (3.8),¹⁶³ and hence a C-H bond activation reaction was investigated as a route to the cyclometallated arene ruthenium C₆H₄-ⁱProxaz complexes. Thus, [RuCl₂(*p*-cy)]₂ was treated with two equivalents of C₆H₅-ⁱProxaz **(3.17)** and NaOAc in CH₂Cl₂ in an attempt to form [RuCl(C₆H₄-ⁱProxaz)(*p*-cy)] **(3.37)** (Scheme 3.19).



The reaction mixture was stirred overnight, filtered through celite to remove NaCl by-product and evaporated. The ^1H NMR spectrum of the yellow/brown oily residue contained a mixture of three species each containing *p*-cy and C_6H_4 - ^iPr oxaz ligands; for example, three doublets are observed at δ 7.96, 8.08 and 8.13 due to Ph-6-*H*. The oily residue was recrystallised from a concentrated CH_2Cl_2 /pentane solution to afford a crop of platelet crystals, which were then fully characterised. The ^1H NMR spectrum of the crystals (**Table 3A**) showed signals for C_6H_4 - ^iPr oxaz, at higher-field by up to 0.44 ppm compared to free ligand, whilst, the signals due to the NCH and the OCH_2 protons of the oxazoline ring were moved downfield upon coordination due to donation of electron density to the metal. Unusually, the CHMe_2 proton was deshielded compared to that of the free ligand by almost 0.7 ppm from δ 1.86 to δ 2.55; as observed previously for $[\text{RuCl}(^i\text{Pr-phenmox})(p\text{-cy})]$ (**2.13**, $\text{R} = ^i\text{Pr}$) (see Section 2.2) and this effect was attributed to the electronegativity of the Cl^- atom in close proximity to the proton. The *p*-cy exhibits two doublets at δ 0.90 and 1.04 (ArCHMe_2), as expected for a chiral complex. The FAB mass spectrum of (**3.37**) showed an ion (~60%) due to $[\text{M}]^+$ m/z 459, with a minor ion due to $[\text{M} - \text{HCl}]^+$ m/z 423. These data are consistent with formation of the desired half-sandwich C_6H_4 - ^iPr oxaz complex.

The crystals were found to be of X-ray diffraction quality; the X-ray structure is shown in **Figure (3.5)**, with selected bond distances and angles in **Table (3.3)**. The complex adopts the expected pseudo-octahedral structure, with the C_6H_4 - ^iPr oxaz ligand coordinated such that the isopropyl substituent adjacent to the imine nitrogen is pointing towards the chloride (isomer B), rather than the *p*-cy ring (isomer-A), thus minimising unfavourable steric interactions; as found in related pymox and phenmox complexes (Section 2.2).^{97, 100} The configuration at the ruthenium centre is (*S*), based on priority arene > Cl > N_{ox} > C_{ph} ; the configuration at the chiral carbon is also (*S*), as (*S*)-valinol was used in the synthesis.^{104, 134}

Table (3.3): Selected Bond Distances (Å) and Angles (°) of (3.37)

Ru – N(1)	2.081 (10)	N(1) – C(7)	1.294 (14)
Ru – C(1)	2.038 (9)	C(7) – C(2)	1.459 (15)
Ru – Cl(1)	2.419 (2)	C(2) – C(1)	1.437 (13)
N(1) – Ru - C(1)	77.2 (4)	C(1) – C(6)	1.415 (15)

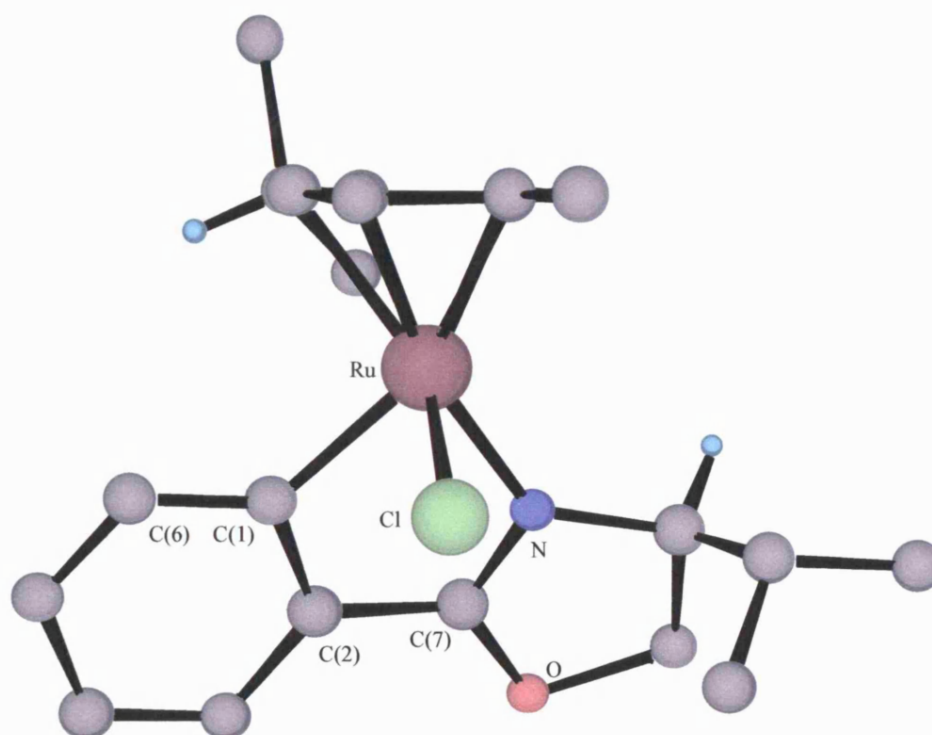


Figure (3.5) : X-ray Structure of (3.37)

The Ru-C(1) bond length [2.038(9) Å] in **(3.37)** is similar to that [2.064(3) Å] in the related five-membered chelate complex [RuCl(TMBA)(*p-cy*)] (**3.3**, *arene* = *p-cy*).⁸⁶ In addition, the Ru-N(oxazoline) bond length in **(3.37)** [2.081(10) Å] is similar to those [2.103(5) to 2.118(4) Å] observed in related pymox complexes [RuCl(R-pymox)(mes)]SbF₆ (**1.41**)¹⁰⁰ (both ligand types form five-membered chelates) and that [2.075(10) Å] in [RuCl(ⁱPr-phenmox)(mes)] (**2.12**, *R* = ⁱPr) (containing another anionic ligand). As expected, the chelate bond angle [77.2(4)°] for **(3.37)** is statistically similar to that in [RuCl(ⁱPr-pymox)(mes)]SbF₆ (**2.26**) [76.4(2)°] (replacing phenyl with pyridine) and **(3.3**, *arene* = *p-cy*) [77.8(1)°] (*i.e.* replacing imine with amine).

To determine whether the solid-state structure of **(3.37)** is retained in solution, the ¹H-¹H NOESY NMR spectrum of the crystals was recorded (at 400 MHz). Based on the crystal structure, the most informative nOes would be between the NCH proton (δ 4.19) and some of the *p-cy* signals; if the other diastereomer were present, one might expect to see nOes between the *p-cy* and either of the oxazoline ⁱPr methyls (δ 0.98 and 1.07). The NOESY spectrum contains nOe cross peaks from δ 4.19 (NCH) to δ 4.98 and δ 5.55 (*p-cy-H* signals) consistent with the crystal structure (isomer-B) and the absence of those expected for isomer-A; hence, the solid-state structure is retained in solution.

The C₆H₄-ⁱPr-oxaz complex (**3.37**) was isolated as a single diastereomer, which did not epimerise to a mixture after a week in CDCl₃, indicating the thermodynamic diastereoselectivity may be very high. The related ⁱPr-phenmox/pymox complexes (discussed in section 2.2), also give single isomers whereas, the diastereoselectivity of TMBA complex (**3.3**, arene = *p*-cy) is lower (discussed in section 1.4.3), presumably because in the minor diastereomer of (**3.3**, arene = *p*-cy) there is less steric congestion between the arene and ligand substituent compared to that in the oxazoline-containing complexes.

To summarise our attempts to make C-bonded phenyl-oxazolines, there are two main conclusions:

1. *Ortho* C-H bond activation was found to be the preferred method of palladium complex formation, though transmetallation using a tin reagent was successful with PdCl₂(PhCN)₂.
2. Novel arene ruthenium phenyloxazoline complexes can be isolated as single diastereomers in high yield via C-H bond activation. The favoured isomer possesses isomer B structure, where the ligand substituent is oriented towards the chloride ligand.

(3.3) - Experimental

All reagents were used as received and solvents were purified as described in Chapter Two. The spectroscopic techniques/instruments used were as described in Chapter Two. $[\text{PdCl}_2(\text{PhCN})_2]$ and $[\text{PdCl}_2(\text{COD})]$ were prepared by literature methods.¹⁶⁸

Preparation of chiral ligands

Preparation of Phenyloxazoline ligands

The ligands C_6H_5 -ⁱProxaz (**3.17**) and *o*-BrC₆H₄-ⁱProxaz (**3.18**) were synthesised by literature methods, or modifications thereof.¹¹³

Attempted synthesis of $[\text{RhCl}(\text{C}_6\text{H}_4$ -ⁱProxaz)(Cp)] (**3.22**)*

To a dry degassed solution of C_6H_5 -ⁱProxaz (**3.17**) (65 mg, 0.34 mmol) in hexane (3 ml) at 195K was slowly added ^tBuLi (1.7M in hexane, 0.201 ml, 0.34 mmol), the solution turned pale purple in colour. After stirring for four hours a red solution of $[\text{RhCl}_2(\text{Cp}^*)]_2$ (63 mg, 0.34 mmol) in dry CH₂Cl₂ (1 ml) was added by syringe, a colour change was not observed at 195K, so the reaction mixture was allowed to slowly warm to room temperature over two hours, this was accompanied by a slight lightening of the solution. Evaporation gave a red oily residue, which was shown by ¹H NMR and mass spectrometry to be unreacted dimer and ligand (**3.17**). Deprotonation of (**3.17**) was investigated by repeating the procedure, but with the addition of MeI (0.65 ml, 3.4 mmol) instead of $[\text{RhCl}_2(\text{Cp}^*)]_2$, to make *o*-MeC₆H₄-ⁱProxaz (**3.23**). The ¹H NMR and mass spectrum of the evaporated reaction mixture indicated that (**3.23**) had been formed.

*Preparation of *o*-Me₃Sn-C₆H₄-ⁱProxaz (**3.25**)*

To a dry degassed colourless solution of *o*-Br-C₆H₄-ⁱProxaz (**3.18**) (371 mg, 1.38 mmol) in hexane (5 ml) at 195K was added ⁿBuLi (1.6M in hexane, 0.865 ml, 1.38 mmol), the solution immediately turned red/orange. After stirring for two hours a dry hexane (1 ml) solution of Me₃SnCl (276 mg, 1.38 mmol) was added, a colour change was not observed at 195K, so the reaction mixture was allowed to slowly warm to room

temperature over two hours, giving a colour change to violet, finally giving a pale yellow solution at room temperature. A white precipitate (presumed to be LiCl by-product) was separated from the solution by cannular filtration. Evaporation of the solvent gave a pale yellow residue which was purified by chromatography on silica, with CH₂Cl₂ as eluent. Evaporation of the fore-run gave an oil, which was recrystallised from CH₂Cl₂/ether to give **(3.25)** as a white crystalline solid (497 mg, 99%). ¹H NMR data is given in **Table (3A)** and microanalysis and mass spectrometry results in **Table (3B)**.

Attempted syntheses of [MCl(C₆H₄-ⁱProxaz)(ring)] (M = Rh, ring = Cp*, **3.22**; M = Ru, ring = mes, **3.24**)

A representative example, for **(3.24)**, is given below:

To a solution of *o*-Me₃Sn-C₆H₄-ⁱProxaz (**3.25**) (150 mg, 0.426 mmol) in CH₂Cl₂ (5 ml) was added [RuCl₂(mes)]₂ (125 mg, 0.213 mmol) and the resulting suspension stirred overnight, giving a brown/red precipitate (unreacted dimer) and indigo solution. The mixture was filtered through celite and evaporated to give an indigo/black residue which was chromatographed (using silica gel and 90:10 CHCl₃/MeOH as eluent) and recrystallised from CH₂Cl₂/ether to give **(3.26)** as fine grey/indigo crystals (125 mg, 75%). The ¹H NMR data is in **Table (3A)**, and mass spectrometry data and elemental analysis in **Table (3B)**.

Attempted preparation of [Ru(MeCN)(C₆H₄-ⁱProxaz)(mes)]PF₆ (**3.27**)

A Young's tap NMR tube was charged with [RuCl(MeCN)₂(mes)]PF₆ (**3.28**) (23 mg, 0.05 mmol) and *o*-Me₃Sn-C₆H₄-ⁱProxaz (**3.25**) (17 mg, 0.05 mmol), degassed and CD₂Cl₂ (0.5 ml) added resulting in a purple solution. The reaction was monitored by ¹H NMR spectroscopy. The spectra showed the presence of **(3.26)** (**Table 3A**) and signals at δ 0.97 (s, 3H, Ru-Me), 2.09 (s, 9H, C₆H₃Me₃), 2.43 (s, 6H, 2*MeCN-Ru) and 4.82 (s, 3H, C₆H₃Me₃) consistent with [Ru(Me)(MeCN)₂(mes)]PF₆ (**3.30**). In addition, two minor species were observed (~15% of total) with signals including 2.09 (s, 9H, C₆H₃Me₃), 4.82 (s, 3H, C₆H₃Me₃) possibly due to [Ru(MeCN)(C₆H₄-ⁱProxaz)(mes)]PF₆ (**3.27**) and a signal at δ 0.70 (s, 9H, {J = (^{117,119}Sn-¹H) 72 Hz}, SnMe₃Cl). Mass spectrometry (Es): m/z 408 (20%) [Ru(C₆H₄-ⁱProxaz)(mes)]⁺ and m/z 338 (50%) [*o*-Me₂Sn-C₆H₄-ⁱProxaz]⁺.

Attempted preparation of [PdCl(C₆H₄-ⁱProxaz)]₂ (3.32)

A degassed solution of [PdCl₂(COD)] (41 mg, 0.142 mmol) and *o*-Me₃Sn-C₆H₄-ⁱProxaz (**3.25**) (50 mg, 0.142 mmol) in CH₂Cl₂ (3 ml) was stirred overnight at room temperature. The resultant pale green solution was evaporated to give a solid residue. The ¹H NMR spectrum showed signals for a mixture of species, including (**3.26**) and SnMe₃Cl. The bulk sample was washed with hexane (4 x 20 ml) and the resultant yellow powder dried *in vacuo*. The ¹H NMR spectrum of this solid showed signals for a major species (63%) (**3.32**) (see **Table 3A**) and a minor species (37%) at δ 1.20 (s, 3H, Pd-Me), 2.50 (m, 4H, COD-CH₂), 2.60 (m, 4H, COD-CH₂), 5.17 (m, 2H, COD-CH), 5.90 (m, 2H, COD-CH) consistent with literature values for [PdCl(Me)(COD)].¹⁶⁹

Preparation of [PdCl(C₆H₄-ⁱProxaz)]₂ (3.32) from [PdCl₂(PhCN)₂]

A degassed solution of [PdCl₂(PhCN)₂] (84 mg, 0.22 mmol) and *o*-Me₃Sn-C₆H₄-ⁱProxaz (**3.25**) (76 mg, 0.22 mmol) in CH₂Cl₂ (5 ml) was stirred at room temperature for one hour. The resultant pale yellow solution was evaporated and the solid residue washed with hexane prior to recrystallisation from CH₂Cl₂/ether to give (**3.32**) as a yellow powder (60 mg, 83%). ¹H NMR data is given in **Table (3A)** and microanalysis and mass spectrometry results in **Table (3B)**.

Preparation of [Pd(OAc)(C₆H₄-ⁱProxaz)]₂ (3.33)

A degassed solution of [Pd(OAc)₂]₃ (190 mg, 0.28 mmol), C₆H₅-ⁱProxaz (**3.17**) (160 mg, 0.85 mmol) and glacial acetic acid (8 ml) was stirred for one hour at 75°C. The resultant orange/yellow solution was evaporated and the solid recrystallised by slow diffusion from acetone/pentane to afford (**3.33**) as orange/brown needle shaped crystals (288 mg, 96%). ¹H NMR data is given in **Table (3A)** and microanalysis and mass spectrometry results in **Table (3B)**.

Preparation of [PdCl(C₆H₄-ⁱProxaz)]₂ (3.32) from [Pd(OAc)(C₆H₄-ⁱProxaz)]₂ (3.33)

To a degassed solution of (**3.33**) (67 mg, 0.095 mmol) in acetone (4 ml) was added LiCl (8.5 mg, 0.20 mmol) and the resulting suspension stirred for three hours. A yellow coloured solution was obtained, which was then evaporated and the crude residue was re-dissolved in CH₂Cl₂. Filtration through celite (to remove excess LiCl and LiOAc), gave a yellow solution, which was evaporated to afford the crude product.

Recrystallisation from CH₂Cl₂/ether gave **(3.32)** (59 mg, 94%) as a brown powder. ¹H NMR data is given in **Table (3A)** and microanalysis and mass spectrometry results in **Table (3B)**.

Reactions of [Pd(OAc)(C₆H₄-ⁱProxaz)]₂ (**3.33**)

General Method: To a yellow solution of [Pd(OAc)(C₆H₄-ⁱProxaz)]₂ (**3.33**) (1.0 equivalents) and Ligand L (2n equivalents) in 1:1 CH₂Cl₂/acetone (8 ml) was added KPF₆ (3.0 equivalents). The mixture was stirred at room temperature for four hours. The solvent was evaporated and the residue re-dissolved in CH₂Cl₂ and filtered through celite. The resulting yellow/brown solution was evaporated to afford the crude product. The products were analysed by ¹H and ³¹P{¹H} NMR spectroscopy, where applicable, and by mass spectrometry.

Attempted Preparation of [Pd(C₆H₄-ⁱProxaz)(PPh₃)₂]/PF₆ (**3.34**)

Following the general method, using [Pd(OAc)(C₆H₄-ⁱProxaz)]₂ (**3.33**) (100 mg, 0.152 mmol), and PPh₃ (159 mg, 0.61 mmol) and KPF₆ (84 mg, 0.454 mmol). FAB-MS: m/z 556 (100%) [Pd(C₆H₄-ⁱProxaz)(PPh₃)]⁺. The ³¹P (and ¹H) NMR spectra contained several signals indicating a mixture of species which have not been characterised, although free PPh₃ was identified in the ³¹P spectrum.

Preparation of [Pd(C₆H₄-ⁱProxaz)(dppp)]PF₆ (**3.35**)

Following the general method, using [Pd(OAc)(C₆H₄-ⁱProxaz)]₂ (**3.33**) (100 mg, 0.152 mmol), dppp (125 mg, 0.304 mmol) and KPF₆ (84 mg, 0.454 mmol) gave **(3.35)** as a white powder (231 mg, 89%). ¹H NMR data is given in **Table (3A)** and microanalysis and mass spectrometry results in **Table (3B)**.

Preparation of [Pd(C₆H₄-ⁱProxaz)(4,4'-Me₂-bipy)]PF₆ (**3.36**)

Following the general method, using [Pd(OAc)(C₆H₄-ⁱProxaz)]₂ (**3.33**) (113 mg, 0.160 mmol), 4,4'-Me₂-bipy (59 mg, 0.32 mmol) and KPF₆ (59 mg, 0.32 mmol) gave **(3.36)** as a yellow/brown powder (143 mg, 72 %). ¹H NMR data is given in **Table (3A)** and microanalysis and mass spectrometry results in **Table (3B)**.

*Preparation of [RuCl(C₆H₄⁻ⁱProxaz)(*p*-cy)] (3.37)*

A colourless solution of C₆H₅⁻ⁱProxaz (**3.17**) (124 mg, 0.655 mmol) and NaOAc (54 mg, 0.655 mmol) in CH₂Cl₂ (2 ml) was added to [RuCl₂(*p*-cy)]₂ (200 mg, 0.327 mmol) and the resulting red solution was stirred overnight at room temperature. The reaction mixture was filtered through celite (to remove NaCl and any decomposition) and evaporation of the solvent afforded a brown/yellow oily residue. Recrystallisation (slow diffusion) from CH₂Cl₂/pentane resulted in dark yellow/brown crystals of (**3.37**) (284 mg, 95%). ¹H NMR data is given in **Table (3A)** and microanalysis and mass spectrometry results in **Table (3B)**

Table (3A): NMR spectroscopic data (300 MHz) for complexes (3.25 – 3.33) in CDCl₃ (δ / ppm)

Compound (Code)	NMR Data
<i>o</i> -Me ₃ Sn-C ₆ H ₄ - ¹ Proxaz (3.25)	¹ H NMR: δ 0.27 (s, 9H, { ² J = (^{119,121} Sn- ¹ H) 54 Hz}, SnMe ₃), 0.93 (d, 3H, {J = 7.5 Hz}, MeCHMe'), 1.07 (d, 3H, {J = 8 Hz}, MeCHMe'), 1.90 (m, 1H, MeMe'CH), 4.07 (m, 2H, OCH + NCH), 4.46 (t, 1H, {J = 8 Hz}, OCH), 7.38 (m, 1H, Ar-4-H), 7.44 (m, 1H, Ar-5-H), 7.67 (d, 1H, { ³ J = (^{119,121} Sn- ¹ H) 48, 46 Hz; 8.5 Hz}, Ar-6-H), 7.93 (d, 1H, {J = 8 Hz}, Ar-3-H).
<i>o</i> -Me ₂ ClSn-C ₆ H ₄ - ¹ Proxaz (3.26)	¹ H NMR: δ 0.78 (s, 3H, { ² J = (^{117,119} Sn- ¹ H) 73, 75 Hz}, MeSnMe'), δ 0.80 (s, 3H, { ² J = (^{117,119} Sn- ¹ H) 73, 75 Hz}, MeSnMe'), 0.90 (d, 3H, {J = 7 Hz}, MeCHMe'), 1.04 (d, 3H, {J = 7 Hz}, MeCHMe'), 2.02 (m, 1H, MeMe'CH), 4.13 (m, 1H, NCH), 4.45 (t, 1H, {J = 10 Hz}, OCH), 4.68 (t, 1H, {J = 10.5 Hz}, OCH), 7.49 (t, 1H, {J = 7.5 Hz}, Ar-4-H), 7.68 (t, 1H, {J = 7.5 Hz}, Ar-5-H), 7.82 (d, 1H, {J = 8 Hz}, Ar-3-H), 8.38 (d, 1H, { ³ J = (^{117,119} Sn- ¹ H) 65, 63 Hz; J = 8.5 Hz}, Ar-6-H).
[PdCl(C ₆ H ₄ - ¹ Proxaz)] ₂ (3.32)	¹ H NMR: δ 0.94 (m, 12H, 2*CHMeMe' + 2*CHMeMe'), 2.55 (m, 2H, 2*MeCHMe'), 4.20 (br. s, 2H, 2*NCH), 4.57 (br. d, 4H, 2*OCH ₂), 7.09 (m, 6H, Ar-H), 7.41 (m, 2H, Ar-H). ¹³ C NMR: δ 13.36 (MeCHMe'), 17.85 (MeCHMe'), 28.33 (MeCHMe'), 65.97 (NCH), 69.22 (OCH ₂), 123.51 (C ₆ H ₄), 125.06 (C ₆ H ₄), 129.29 (C ₆ H ₄), 130.14 (C ₆ H ₄), 131.85 (C ₆ H ₄), 144.41 (O=CN), 173.56 (PhC-Pd).
[Pd(OAc)(C ₆ H ₄ - ¹ Proxaz)] ₂ (3.33)	¹ H NMR: δ 0.77 (d, 6H, {J = 3.5 Hz}, 2*MeCHMe'), 0.79 (d, 6H, {J = 2.6 Hz}, 2*MeCHMe'), 2.03 (m, 2H, 2*MeCHMe'), 2.12 (s, 6H, 2*OC(O)CH ₃), 3.06 (ddd, 2H, {J = 9, 5.5, 4 Hz}, 2*NCH), 3.37 (t, 2H, {J = 9 Hz}, 2*OCH ^{up}), 4.07 (dd, 2H, {J = 9, 5.5 Hz}, 2*OCH ^{down}), 7.04 (m, 4H, 2*Ph-2H), 7.11 (m, 2H, 2*Ph-1H), 7.18 (m, 2H, 2*Ph-1H).

Table (3A) continued: NMR spectroscopic data for complexes (3.33 – 3.35) in CDCl₃ (δ / ppm)

Compound (Code)	NMR Data
[Pd(OAc)(C ₆ H ₄ - ¹ Proxaz)] ₂ (3.33) (300 MHz)	¹³ C: δ 15.67 (<i>MeCHMe'</i>), 18.93 (<i>MeCHMe'</i>), 24.53 (<i>MeCHMe'</i>), 30.01 (CH ₃ COO), 66.65 (NCH), 71.09 (OCH ₂), 124.01 (C ₆ H ₄), 125.71 (C ₆ H ₄), 130.51 (C ₆ H ₄), 131.42 (C ₆ H ₄), 131.58 (C ₆ H ₄), 148.10 (OC=N), 173.68 (PhC-Pd), 181.35 (CH ₃ COO).
[Pd(C ₆ H ₄ - ¹ Proxaz)(dppp)]PF ₆ (3.35) (d ₆ -acetone, 400 MHz, 300K)	¹ H NMR: δ 0.34 (br. s, 3H, <i>MeCHMe'</i>), 0.78 (d, 3H, {J = 7.5 Hz}, <i>MeCHMe'</i>), 2.15 (m, 1H, <i>MeCHMe'</i>), 2.71 (m, 8H, 6H-dppp + <i>OCH</i>), 4.33 (t, 1H, {J = 10.5 Hz}, <i>OCH'</i>), 4.53 (m, 1H, NCH), 6.85 (br. s, 1H, <i>Ar-H</i>), 7.01 (br. s, 1H, <i>Ar-H</i>), 7.08 (br. s, 1H, <i>Ar-H</i>), 7.50 – 8.12 (m, 21H, 20H-dppp + <i>Ar-H</i>).
[Pd(C ₆ H ₄ - ¹ Proxaz)(dppp)]PF ₆ (3.35) (d ₆ -acetone, 400 MHz, 233K)	¹ H NMR: 0.22 (d, 3H, {J = 7.5 Hz}, <i>MeCHMe'</i>), 0.67 (d, 3H, {J = 7.5 Hz}, <i>MeCHMe'</i>), 2.25 (m, 1H, <i>MeCHMe'</i>), 2.54 (m, 2H, CH ₂ -dppp), 2.78 (m, 2H, CH ₂ -dppp), 2.291 (m, 1H, <i>OCH</i>), 2.95 (m, 2H, CH ₂ -dppp), 4.38 (t, 1H, {J = 10.5 Hz}, <i>OCH'</i>), 4.60 (m, 1H, NCH), 6.69 (m, 1H, <i>Ar-H</i>), 6.78 (m, 1H, <i>Ar-H</i>), 6.95 (m, 2H, <i>Ph-H</i>), 7.40 – 7.91 (m, 18H, dppp- <i>Ph-H</i> + 2* <i>Ar-H</i>), 8.30 (m, 2H, dppp- <i>Ph-H</i>). ³¹ P { ¹ H} NMR: δ 26.3 (d, {J = 56 Hz}, dppp- <i>P</i>), -4.2 (d, {J = 57 Hz}, dppp- <i>P</i>).
[Pd(C ₆ H ₄ - ¹ Proxaz)(dppp)]PF ₆ (3.35) (d ₆ -acetone, 400 MHz, 323K)	³¹ P { ¹ H} NMR: δ 26.1 (br. s, dppp- <i>P</i>), -2.7 (d, {J = 56.5 Hz}, dppp- <i>P</i>).

Table (3A) continued: NMR spectroscopic data for complexes in CDCl₃ (δ / ppm)

Compound (Code)	NMR Data
<p>[Pd(C₆H₄-¹Proxaz)(4,4'-Me₂-bipy)]PF₆ (3.36) (CD₂Cl₂, 300 MHz)</p>	<p>¹H NMR: δ 0.81 (d, 3H, {J = 6.5 Hz}, MeCHMe'), 0.92 (d, 3H, {J = 7 Hz}, MeCHMe'), 1.95 (m, 1H, MeCHMe'), 2.49 (s, 3H, 4-Me-bipy), 2.52 (s, 3H, 4'-Me-bipy), 4.37 (m, 1H, NCH), 4.51 (t, 1H, {J = 9 Hz}, OCH^{up}), 4.63 (dd, 1H, {J = 9, 4 Hz}, OCH^{down}), 7.16 (m, 4H, C₆H₄-Ph), 7.42 (d, 1H, {J = 6 Hz}, bipy-5-H), 7.46 (d, 1H, {J = 5.5 Hz}, bipy-5'-H), 7.88 (s, 1H, bipy-3'-H), 7.91 (s, 1H, bipy-3-H), 8.28 (d, 1H, {J = 5.5 Hz}, bipy-6'-H), 8.68 (d, 1H, {J = 6 Hz}, bipy-6-H).</p> <p>¹³C: δ 14.90 (MeCHMe'), 18.69 (MeCHMe'), 22.04 (4-Me-bipy), 22.11 (4'-Me-bipy), 31.30 (MeCHMe'), 66.32 (NCH), 70.99 (OCH₂), 124.73 (Ar-C-H), 125.42 (Ar-C-H), 126.34 (Ar-C-H), 127.62 (Ar-C-H), 128.70 (Ar-C-H), 128.97 (Ar-C-H), 132.38 (4°), 132.90 (Ar-C-H), 133.24 (Ar-C-H), 150.15 (Ar-C-H), 152.05 (4°), 152.42 (Ar-C-H), 154.21 (4°), 154.28 (4°), 154.92 (4°), 157.92 (PhC-Pd), 177.17 (4°).</p> <p>³¹P{¹H} NMR: δ -144.17 (septet, PF₆⁻).</p>
<p>[RuCl(C₆H₄-¹Proxaz)(p-cy)] (3.37) (250 MHz)</p>	<p>¹H NMR: δ 0.90 (d, 3H, {J = 7 Hz}, ArCHMeMe'), 0.98 (d, 3H, {J = 6.5 Hz}, CHMeMe'), 1.04 (d, 3H, {J = 3.5 Hz}, ArCHMeMe'), 1.07 (d, 3H, {J = 4 Hz}, CHMeMe'), 2.09 (s, 3H, Ar-Me), 2.47 (m, 1H, ArCHMeMe'), 2.55 (m, 1H, CHMeMe'), 4.19 (ddd, 1H, {J = 9, 7, 3 Hz}, NCH), 4.59 (m, 2H, OCH + OCH'), 4.82 (dd, 1H, {J = 6, 1 Hz}, p-cy-H), 4.98 (dd, 1H, {J = 6, 0.5 Hz}, p-cy-H), 5.55 (d, 2H, {J = 6 Hz}, p-cy-H), 6.97 (dt, 1H, {J = 7.5, 1.5 Hz}, Ph-4-H), 7.21 (dt, 1H, {J = 7.5, 1 Hz}, Ph-5-H), 7.32 (dd, 1H, {J = 7.5, 1.5 Hz}, Ph-3-H), 8.08 (d, 1H, {J = 7.5 Hz}, Ph-6-H).</p>

Table (3B): Analysis data for compounds (3.25 – 3.37)

Compound (Code)	Elemental Analysis			Mass	Spectrometry
	Found (calculated)			Molecular ion	Other ions
	C %	H %	N %	M ⁺ (m/z)	(m/z)
<i>o</i> -Me ₃ Sn-C ₆ H ₄ - ¹ Proxaz (3.25)	50.01 (49.90)	6.81 (6.70)	3.88 (3.88)	354	[M – MeH] ⁺ = 338
<i>o</i> -Me ₂ ClSn-C ₆ H ₄ - ¹ Proxaz (3.26)	44.69 (44.61)	5.32 (5.48)	3.32 (3.71)	373	[M – Cl] ⁺ = 338
[PdCl(C ₆ H ₄ - ¹ Proxaz)] ₂ (3.32)	-	-	-	660	[M – Cl] ⁺ = 625
[Pd(OAc)(C ₆ H ₄ - ¹ Proxaz)] ₂ (3.33)	47.15 (47.54)	4.62 (4.84)	3.43 (3.96)	-	[M – OAc] ⁺ = 649
[Pd(C ₆ H ₄ - ¹ Proxaz)(PPh ₃) ₂][PF ₆] (3.34)	-	-	-	-	[M – PPh ₃] ⁺ = 557
[Pd(C ₆ H ₄ - ¹ Proxaz)(dppp)][PF ₆] (3.35)	52.59 (54.97)	4.63 (4.73)	1.26 (1.64)	706	-
[Pd(C ₆ H ₄ - ¹ Proxaz)(4,4'-Me ₂ -bipy)][PF ₆] (3.36)	45.68 (46.21)	3.95 (4.20)	6.51 (6.74)	478	-
[RuCl(C ₆ H ₄ - ¹ Proxaz)(p-cy)] (3.37)	57.00 (57.57)	6.12 (6.15)	3.02 (3.05)	459	[M – HCl] ⁺ = 423

Chapter Four:

Chiral Half-Sandwich Complexes as Asymmetric Catalysts

Chapter Four – Chiral Half-Sandwich Complexes as Asymmetric Catalysts

(4.1) – Introduction

The active component of many pharmaceuticals, pesticides and biochemicals are chiral. It is often the case that when drugs interact with enzymes/cell receptors only one enantiomer will have the desired effect; this can be rationalised since nature has evolved using amino acids with only *L*-configuration and sugars with only *D*-configuration about their chiral centre(s). The other enantiomer may be inactive or even have a deleterious affect, as in the well-documented case of Thalidomide (the *R*-isomer helps prevent morning sickness and the *S*-isomer is a teratogen). In conjunction with reduced side-effects and increased activity of a single enantiomer drug, legislation passed in 1992 by the US Food and Drugs Administration (FDA) and the European Committee for Proprietary Medicinal Products requires that for drugs that are to be sold as a racemate, each enantiomer must be fully characterised. These factors have resulted in single-isomer drugs being the most commercially viable alternative.

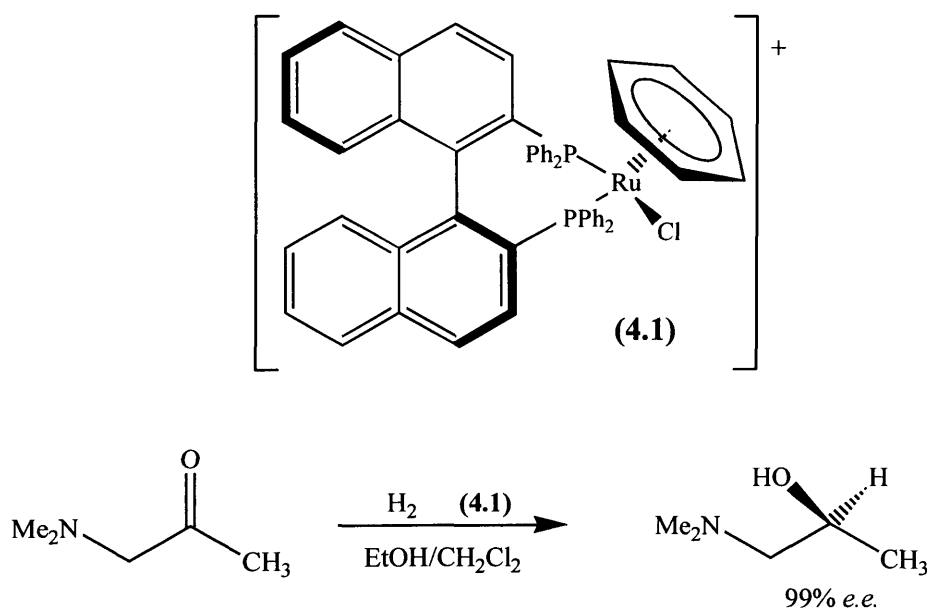
In nature, enzymes are the catalysts used to carry out highly efficient and stereoselective transformations on a wide range of organic substrates. However, enzymes have some drawbacks for industrial use, they are difficult to extract and purify and in the majority of cases are rather reagent specific. These obstacles have lead to research into alternative methods for obtaining enantiopure compounds.

There are three main routes to obtaining single-enantiomers, these are:

1. **Stoichiometric synthesis** – the desired configuration of starting material is used and maintained throughout the synthesis this involves no amplification of chirality and so is usually expensive.
2. **Resolution** – the chemical or physical separation of enantiomers. This method has a maximum possible yield of 50% (the desired enantiomer), requiring disposal of the unwanted enantiomer if it is not recycled.
3. **Asymmetric catalysis** – is often the most efficient method since one molecule of chiral catalyst can produce thousands of enantiopure product molecules by introducing asymmetry directly into achiral starting reagents, eradicating the need for resolution methods. These inherent advantages have brought asymmetric

catalysis to the forefront of modern industrial chemistry and, in some cases, the stereoselectivity and efficiency is now approaching that of enzymes.

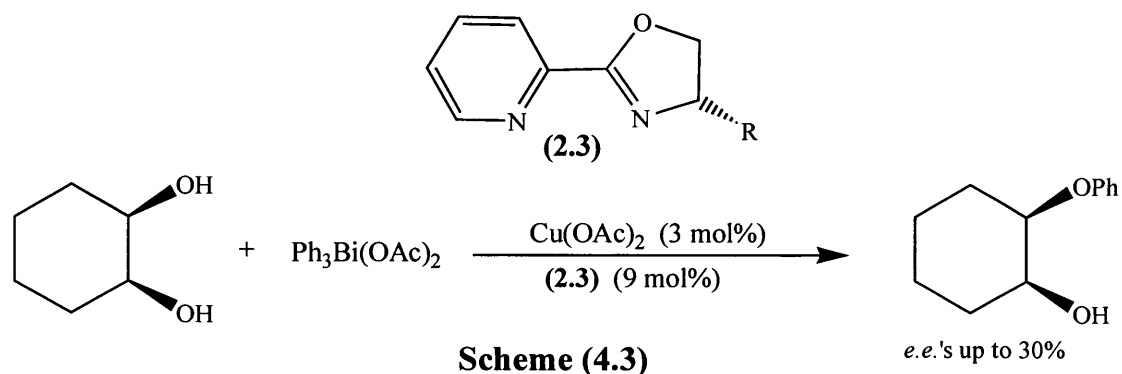
The most successful early asymmetric catalysts were Rh(I) complexes with chiral diphosphines, which catalyse the asymmetric reduction of various functionalised alkenes.¹⁷⁰ More recently, ruthenium complexes *e.g.* [RuCl(BINAP)(C₆H₆)]BF₄ (**4.1**), have been used for the asymmetric hydrogenation reaction of substituted alkenes and ketones (**Scheme 4.1**).⁶⁵ The reactions are carried out under mild conditions (30 – 40°C) with excellent yields ≥99% and *e.e.* >99% being achieved. It should be noted that during these catalyses the arene ring dissociates from the complex such that the catalytically active species no longer has a half-sandwich structure.⁶⁵



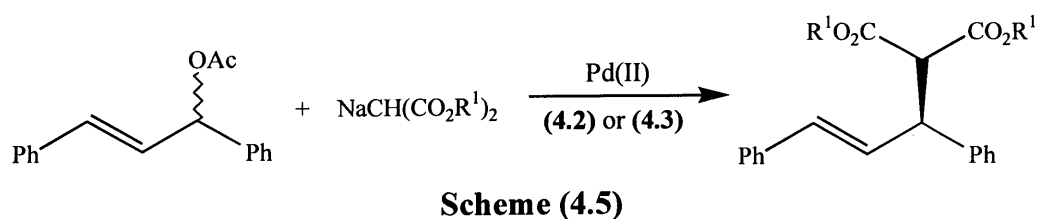
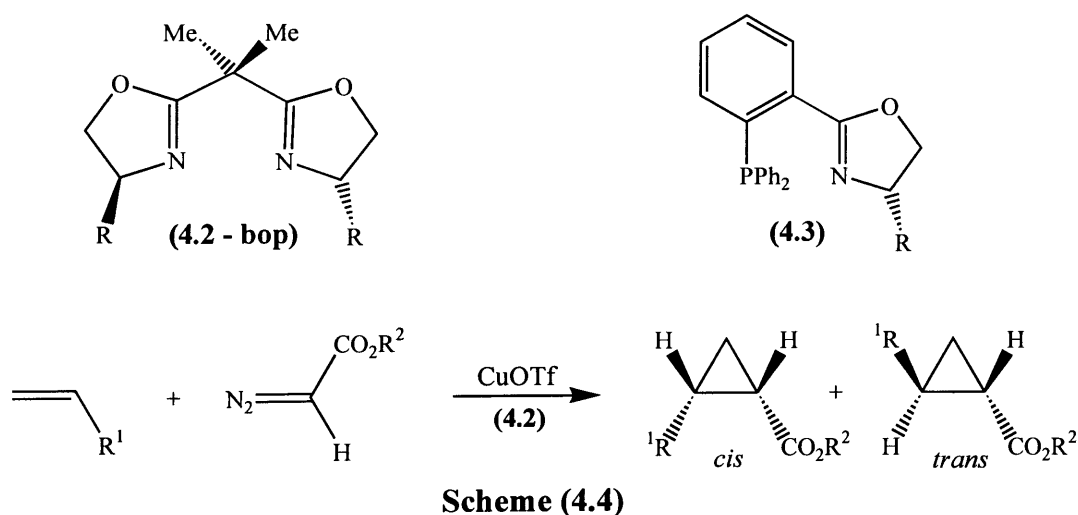
Scheme (4.1)

Whilst chiral phosphines have proved excellent ligands for catalytic reductions, their susceptibility towards oxidation and reaction with species such as diazo-compounds makes them unsuitable in catalytic cyclopropanation or epoxidation. These reactions often require less electron-rich catalysts, which contain 'hard'-donor ligands such as N or O. Recently there has been much interest in the use of chiral *N*-donor ligands in asymmetric catalysis, especially in oxidations, aziridinations, cyclopropanations, allylic substitutions, ketone reductions, nucleophilic additions and Lewis-acid catalysed cycloadditions and the area has been well reviewed.^{3, 105, 171}

Chiral oxazolines have been used in stoichiometric synthesis for many decades, but it is only since the late 1980's that their potential as ligands in asymmetric catalysis was recognised. The first example of using chiral oxazoline-containing ligands in asymmetric catalysis was the mono-phenylation of *meso*-diols with $\text{Ph}_3\text{Bi}(\text{OAc})_2$, by Brunner *et al.* in 1986 (Scheme 4.3), *e.e.*'s of up to 30% being obtained.¹⁷²

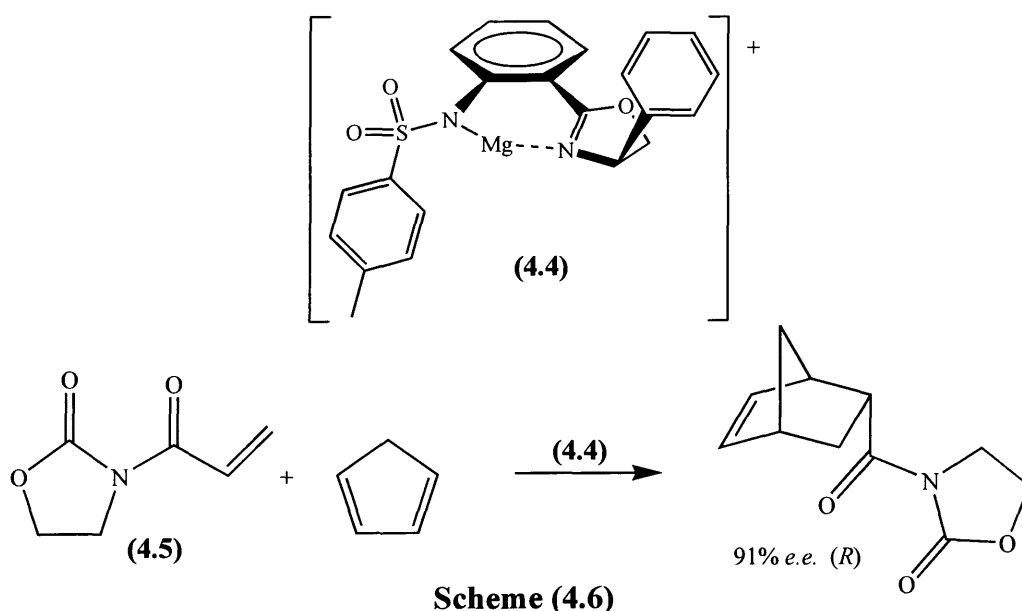


The logical progression from Brunner's results was to introduce C_2 -symmetry into ligand design. Many research groups have independently investigated the application of catalysts derived from C_2 -symmetric bis(oxazoline) ligands with various metal salts.¹⁷³⁻¹⁷⁹ As a result of which, Cu/bis-oxazolanyl propane (bop – 4.2) complexes have emerged as excellent enantioselective catalysts for the cyclopropanation of olefins with diazoacetates (*e.e.*'s up to 99%) (Scheme 4.4),¹⁷⁵ amongst other reactions.



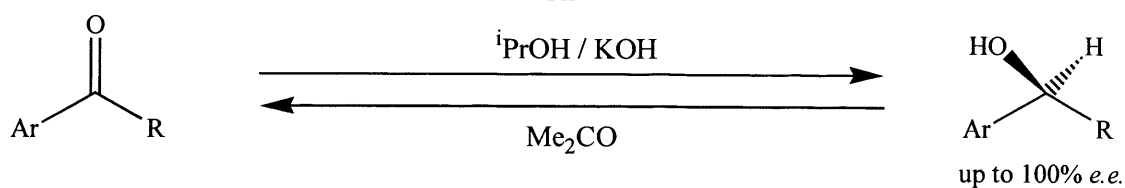
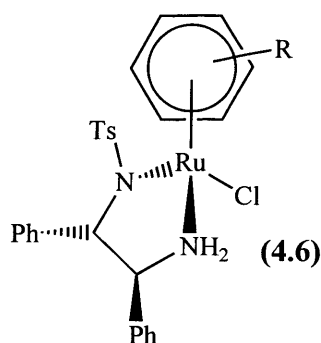
Pfaltz *et al.* have shown that Pd(II) complexes of oxazoline ligands can be used as allylic alkylation catalysts (**Scheme 4.5**).¹⁸⁰ Using (**4.2**, **R** = **Bn**), attack of a nucleophile (*e.g.* malonate) is preferentially directed by steric interactions to one end of the allyl, with *e.e.*'s of up to 88% being obtained. Replacing (**4.2**) with a diphenylphosphino-oxazoline (**4.3**), gives an improved catalyst, in which regioselectivity is controlled by electronic effects; one end of the intermediate allyl species being *trans* to phosphorus the other *trans* to nitrogen. Fast rates and excellent enantioselectivity (*e.e.*'s up to 99%) are achieved, demonstrating that C₂-symmetry is not essential for obtaining high selectivity with oxazoline ligands.¹⁸¹

A recent publication by Fujisawa *et al.* demonstrates that unsymmetrical oxazoline ligands are also capable of inducing high levels of enantiocontrol in the Diels-Alder reaction.¹⁴¹ The magnesium cation (**4.4**), was found to be an asymmetric catalyst for the Diels-Alder reaction of bidentate oxazolidinone dienophiles (**4.5**) with cyclopentadiene (**Scheme 4.6**); *e.e.*'s of up to 91% were obtained.



Chiral diamines have also attracted study, in particular half-sandwich complexes [RuCl(*p*-TsDPEN)(arene)] (**4.6**) were shown by Noyori to be excellent catalyst precursors for asymmetric transfer hydrogenation of ketones. As mentioned in Section 2.1, the catalysts promote the reaction of an unsymmetrical ketone (or imine) with a hydrogen source, such as 2-propanol, to give secondary alcohols (or amines) with very high enantioselectivity (*e.e.*'s up to 100% being obtained) (**Scheme 4.7**).⁸⁰ Noyori's catalysts can also exploit the reversibility of the transfer hydrogenation reaction to

convert a secondary alcohol to a ketone, thus providing a means of kinetic resolution of racemic alcohols.⁸¹



Carbon-carbon bond forming reactions are particularly important in organic synthesis, for example the Diels-Alder¹⁸², hetero Diels-Alder¹⁸³ and Mukaiyama aldol reactions,¹⁸⁴ which have all been well reviewed.¹⁸⁵⁻¹⁸⁷ These reactions are usually catalysed by traditional Lewis acids *e.g.* B(III), Al(III) or Ti(IV); and the topic has been well reviewed.^{105, 185, 188-190}

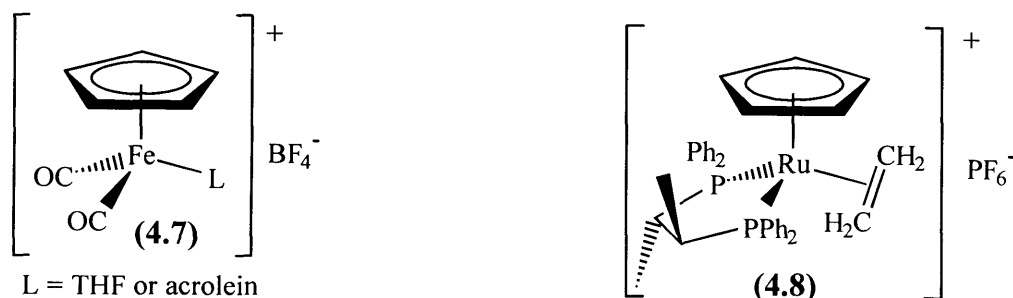
Asymmetric variants of these Lewis acid catalysts are often formed from halide, alkyl or alkoxy complexes of B(III), Al(III) or Ti(IV) (strong Lewis-acids) with chiral chelating ligands, such as, binaphthol; there are several extensive reviews of such chiral Lewis-acid catalysts.^{188, 189} These complexes, whilst being excellent stereo- and enantioselective catalysts for many Lewis-acid catalysed reactions, were often found to promote undesired polymerisation, or even decomposition, of more sensitive substrates. Further disadvantages of these catalysts are: they are highly oxophilic, so both the reactants and the products of catalysis bind very strongly to the Lewis-acid and hence, the reaction is often product inhibited hence has slow turnover. In addition, the catalysts are often very water sensitive and as a result, the Lewis-acids are often employed at very high loadings (up to 20%); although the metals are fairly inexpensive, the chiral auxiliary must be reclaimed after catalysis is complete as the complex ligands necessary to obtain high enantioselectivity are often difficult and expensive to synthesise. Many chiral Lewis acid catalysts, are formed *in situ* and have not been fully characterised, so understanding the molecular basis for enantioselectivity is often complicated (*e.g.*

Cu(II) / bop catalysed reactions discussed earlier). To aid such understanding, the use of a well-defined, structurally stable metal complex would be desirable. As a result of these disadvantages, the use of an appropriate transition metal catalyst might be preferable. An ideal transition metal Lewis acid should:

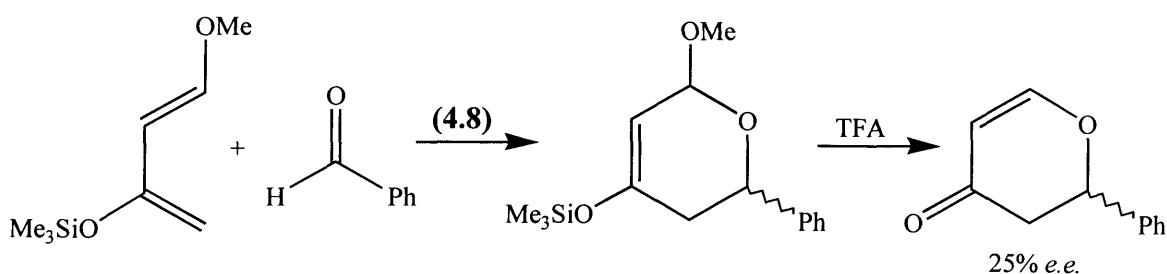
1. accelerate the reaction so that there is no competing thermal reaction (> 100 fold acceleration), but should not be so Lewis acidic that reactants are decomposed or polymerised. The complex should, therefore, have at least one overall positive charge, and/or electron withdrawing or π -acidic ligands.
2. have a stable, well-defined geometry with only one catalytically active species in solution.
3. not be air and/or oxygen sensitive and should not be dramatically affected by trace amounts of water (from solvent).
4. form a σ -bond to the oxygen of the carbonyl group in the substrate, in preference to with alkenes, as this would inhibit catalysis. The coordination of the carbonyls should be rapid and reversible, to allow fast catalytic turnover.

Noyori's catalysts illustrate that chiral half-sandwich complexes and nitrogen-donor ligands can produce highly asymmetric catalytic systems and, as outlined in this section, oxazoline ligands have been used with great effect in asymmetric catalysis. On this basis, the incorporation of oxazoline or related hard donor ligands in ruthenium or rhodium half-sandwich complexes offers great potential, particularly for reactions in which only one coordination site is required by the substrate.

The remainder of this section will focus on the development of Lewis acidic half-sandwich catalysts. Examples of some of the early catalysts for the Diels-Alder reaction, extensively investigated by Hersh *et al.*, were $[\text{Fe}(\text{CO})_2\text{LCp}]^+$ (**4.7**, L = THF or acrolein).¹⁹¹ These complexes catalysed the reactions of acrylic dienophiles with simple dienes, with higher *exo/endo* selectivities than the thermal reactions. However, the possibility that adventitious impurities or small amounts of decomposition products were responsible for some, or even most, of the catalysis was difficult to exclude.¹⁹¹ It was found that addition of small amounts of a hindered (*i.e.* non-coordinating) base, such as 2,6-di-*tert*-butyl pyridine, significantly lowered the yield of adduct in many cases. The species scavenged by the hindered base was difficult to identify; the most plausible candidates were thought to be H^+ or BF_3 (derived from the BF_4^- counter-ion).



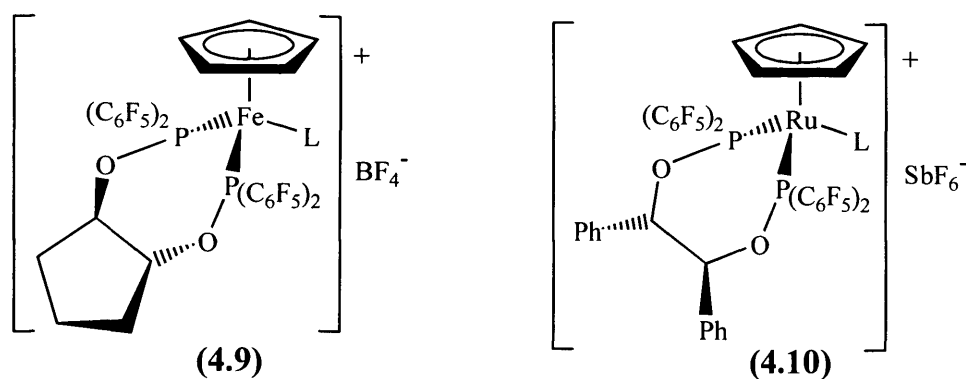
The first chiral half-sandwich complex to be used as an asymmetric Lewis-acid catalyst, developed by Faller *et al.*, was $[\text{Ru}(\text{C}_2\text{H}_4)(\{S,S\}\text{-CHIRAPHOS})\text{Cp}]\text{PF}_6$ (**4.8**).¹⁹² This mildly Lewis-acidic complex catalysed the hetero Diels-Alder reaction between benzaldehyde and Danishefsky's diene (**Scheme 4.8**), with moderate enantioselectivity (25% *e.e.*).



Scheme (4.8)

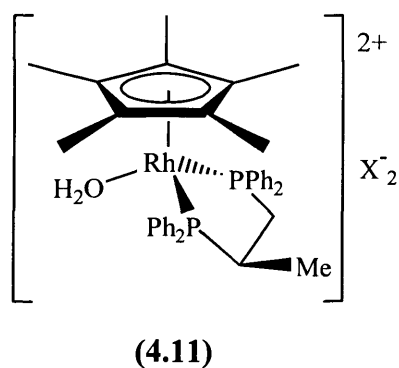
Complex (**4.8**), however, is not Lewis-acidic enough to catalyse the classical Diels-Alder reaction. This latter reaction is also disfavoured due to preferential binding of the Lewis-acid to the alkene over the carbonyl. Despite this, coordination of benzaldehyde in the hetero Diels-Alder reaction presumably occurs via an η^1 -interaction (*i.e.* σ -binding). In “arene-Ru” and “Cp*Rh” complexes, σ -aldehyde coordination has been established in some cases (see Section 4.2.1).^{72, 193}

High enantioselectivity for the Diels-Alder reaction catalysed by chiral half-sandwich complexes, $[\text{Fe}(\text{L})\{(\text{C}_6\text{F}_5)_2\text{POC}_5\text{H}_8\text{OP}(\text{C}_6\text{F}_5)_2\}\text{Cp}]\text{BF}_4$ (**4.9**, L = dienophile, MeCN), was first reported by Kundig *et al.* in 1994.¹⁹⁴ The electron poor chiral bis-phosphinite ligand is electronically similar to CO (due to the electron-withdrawing C_6F_5 substituents) and the complexes are thus chiral analogues of complexes (**4.7**). Very high enantioselectivity was obtained for the Diels-Alder reaction of acrylic dienophiles with simple dienes; for example, 99% *e.e.* was obtained for the major *endo* reaction product of bromoacrolein and cyclohexadiene. The use of complexes (**4.9**), however, is limited by their low thermal stability, they decompose above 253K.



During the course of our work, the thermally stable ruthenium analogues $[\text{Ru}(\text{L})\{(\text{C}_6\text{F}_5)_2\text{POCH}(\text{Ph})\}_2\text{Cp}]\text{SbF}_6$ (**4.10**, $\text{L} = \text{dienophile, acetone}$), were reported by Kundig *et al.*¹⁹³ These complexes catalysed the Diels-Alder reaction between methacrolein and cyclopentadiene at 253K with high enantioselectivity (up to 92% *e.e.*), and have also provided valuable structural information about catalyst-substrate interactions (see Section 4.2.1).

The first enantioselective half-sandwich rhodium catalysts for the Diels-Alder reaction were reported in 1996, by Carmona *et al.* The dicationic complexes $[\text{Rh}(\text{H}_2\text{O})(\text{R-Prophos})\text{Cp}^*]\text{X}_2$ (**4.11**, $\text{X} = \text{BF}_4, \text{SbF}_6$), gave *e.e.*'s of up to 71% for the reaction between methacrolein and cyclopentadiene.¹⁹⁵ The rate and enantioselectivity of catalysis were found to be greater when SbF_6^- was used as the anion instead of BF_4^- , this was ascribed to a different degree of association of the anions with the metal cation, as found for copper¹⁹⁶ and ruthenium¹⁹³ catalysts.



Previous work in our group has shown that dicationic complexes $[\text{Ru}(\text{OH}_2)(\text{R-pymox})(\text{arene})](\text{SbF}_6)_2$ (**4.12**) will catalyse the Diels-Alder reaction between methacrolein and cyclopentadiene with high enantioselectivity (*e.e.*'s of up to 83% being obtained).¹⁰⁰ We have also shown that Cp^* -rhodium complexes with various oxazoline ligands will catalyse the same Diels-Alder reaction and that the

enantioselectivity is dependent on the specific ligand used,⁹⁸ thus evaluating related ligand systems could lead to highly selective catalysts. Furthermore, the rate of dissociation/exchange of the ligand at the sixth coordination site is dependent on the ligand, being slower in pymox-containing dicationic complexes compared to monocationic phenmox-containing complexes, as discussed in Chapter Two. Therefore, it might be expected that by using monocationic complexes (formed from anionic bidentate ligands), the rate of substrate/product exchange will be faster and so the catalyst may be more active. Alternatively, the reduced Lewis-acidity of monocationic complexes may reduce the activation of the dienophile and hence reduce catalysis.

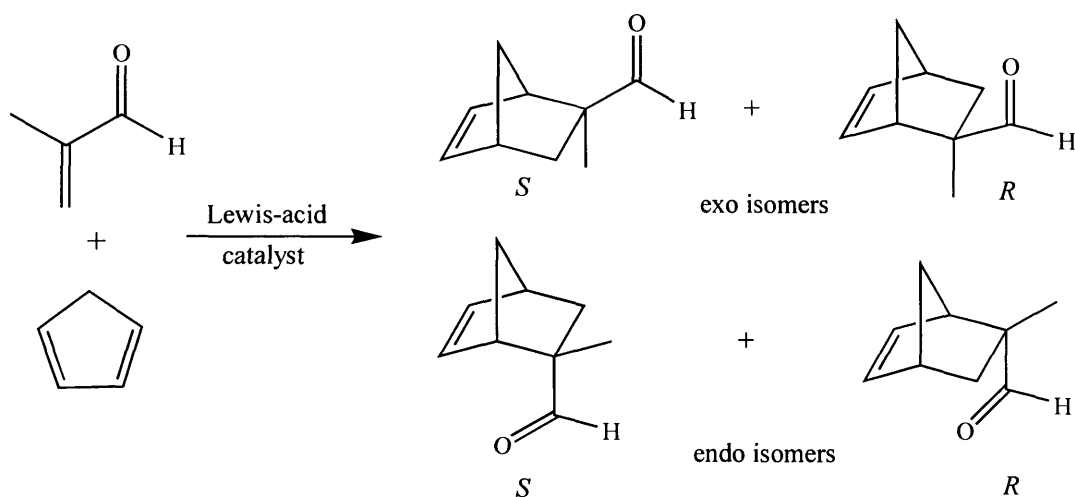
These hypotheses have been investigated by testing various complexes $[\text{MCl}(\text{L})(\text{ring})]^{n+}$ ($n = 0$, L = anionic chelate and $n = 1$, L = neutral chelate) as Lewis-acid catalyst precursors as described below.

(4.2) – Results and Discussion

As mentioned in section 2.2, in order to use the half-sandwich complexes $[\text{MCl}(\text{L})(\text{ring})]^{n+}$ ($n = 0, 1$) as catalysts the chloride ligand needs to be abstracted, which is done using AgSbF_6 . The resulting cationic species $[\text{M}(\text{solvent})(\text{L})(\text{ring})]^{(n+1)+}$ can be isolated and purified or can be used *in situ* after filtering through celite to remove AgCl by-product, similar catalytic results being observed in either case. The results with phenmox-containing (*i.e.* N,O^- -donor) catalysts (**2.12** - **2.15**) will be discussed first (**Tables 4.1 – 4.6**) followed by those containing N,N -donors (**Tables 4.7 – 4.9**). The Diels-Alder reaction of methacrolein and cyclopentadiene (**Scheme 4.9**) was chosen as a model catalytic reaction. The ratio of *exo:endo* products from the thermal reaction is ~80:20, but with a Lewis acid catalyst, the ratio can be >95:5.¹⁹⁷ This reaction can often be catalysed by mild Lewis acids and standard methods exist to determine the *exo:endo* ratio and enantioselectivity.¹⁹⁸ In addition, the reaction has been catalysed by most of the known transition metal catalysts, so comparison of the relative reactivities and selectivities can be made.

The solvent used in all of the catalytic reactions described below was dichloromethane, which is polar enough to dissolve the catalysts (particularly in the presence of dienophile), but does not coordinate to the metal centre. Previous work in our group, has shown that with the complex $[\text{Ru}(\text{OH}_2)(^i\text{Pr-pymox})(\text{mes})](\text{SbF}_6)_2$ (**2.29**), the use of acetone instead of dichloromethane slows the rate of catalysis but does not

effect selectivity; whilst, the use of either THF or nitromethane as solvent gave none of the desired product, suggesting they coordinated to the ruthenium centre.¹⁰⁰



Scheme (4.9)

In the general procedure, one equivalent of dienophile and two equivalents of diene were reacted, with 1 – 5 mol % catalyst in CH_2Cl_2 in the presence of hindered base 2,6-di-*tert*-butylpyridine (equimolar with catalyst) used to scavenge protons, which may also catalyse the Diels-Alder reaction.¹⁹¹

Using (*S*)-configured ligands, the major product was identified as *exo* (1*R*,2*S*,4*R*)-2-methylbicyclo[2.2.1]hept-5-ene-2-carbaldehyde, by comparison of the sign of the optical rotation $[\alpha_D]$, and the GC behaviour of the acetal formed from (2*R*,4*R*)-pentanediol with literature values.¹⁹⁸ Enantiomeric excess refers to the major *exo* product unless stated otherwise. All yields quoted are isolated yields and so are not necessarily indicative of activity.

(4.2.1) – Phenmox Catalysts

In an initial screening, a series of complexes $[\text{M}(\text{OH}_2)(\text{R-phenmox})(\text{ring})]\text{SbF}_6$ ($\text{M} = \text{Ru}$, ring = mes; $\text{M} = \text{Rh}$, ring = Cp^* ; $\text{R} = \text{}^i\text{Pr}$ or Ph) were tested as catalysts for the Diels-Alder reaction shown in **Scheme (4.9)**, with 2 mol % catalyst loading at 0°C (all other conditions as described above) (**Table 4.1**).

Table (4.1): Comparison of ruthenium and rhodium catalysts [M(Cl)(R-phenmox)(ring)] (2.12 and 2.15)^a for the reaction of methacrolein and CpH

Entry	Metal	R-group	Diastereomer Ratio (B:A) ^b	Yield (%)	Time / h	Isomer Ratio (<i>exo:endo</i>)	<i>E.e.</i> (%)
1	Ru	¹ Pr	100:0	93	24	95:5	40
2	Rh	¹ Pr	100:0	46	72	94:6	8
3	Ru	Ph	24:76	91	65	93:7	13
4	Rh	Ph	76:24	36	72	91:9	3

a These were performed on isolated samples of the water cation.

b Diastereomer ratios refer to chlorides.

The two ruthenium catalysed reactions were performed in an NMR tube in CD₂Cl₂ (spectra were obtained at 2-4 hour intervals for first 12 hours, then every subsequent 5-10 hours). The ¹Pr-phenmox catalyst (entry 1) is faster (> 75% yield after 10 hours) and more selective (40% *e.e.*) than the Ph-phenmox catalyst (entry 3) (~ 75% yield in 35 hours with 13% *e.e.*). For both catalysts, the *exo:endo* ratios were considerably higher than the thermal ratio (~80:20). The main conclusions that can be drawn from **Table (4.1)** is that ruthenium complexes (entries 1 and 3) are more active and enantioselective for this reaction than their rhodium analogues (entries 2 and 4) and moderate enantioselectivity can be obtained with the non-optimised Ru/¹Pr-phenmox catalyst. The rhodium catalysed reactions (entries 2 and 4) had not gone to completion after 72 hours, presumably due to reduced Lewis-acidity. In these cases, the low enantioselectivity may be due to intrinsic low selectivity and/or that the thermal adduct has contributed to the Diels-Alder reaction product, as a consequence of low activity. Hence, the use of the rhodium phenmox complexes was not investigated further.

The ruthenium phenmox catalysts have been studied in more detail, varying catalyst loading, reaction temperature, R-substituent and arene-ligand. Firstly, the effects of loading and temperature were studied using [Ru(OH₂)(¹Pr-phenmox)(mes)]SbF₆ as catalyst (**Table 4.2**).

Table (4.2): Effect of temperature and catalyst loading on reaction of methacrolein and CpH using [Ru(OH₂)(ⁱPr-phenmox)(mes)][SbF₆] (2.17, R = ⁱPr) as catalyst^a

Entry	Catalyst (mol %)	T/ °C	t/h	Yield (%)	Isomer Ratio (<i>exo:endo</i>)	<i>E.e.</i> (%)
1	1	0	24	>95	95:5	40
2	2	0	24	93	95:5	40
3	5	0	23	94	94:6	41
4	2	RT	15	>95	94:6	37
5	2	-20	72	77	95:5	44

a These were performed on isolated samples of the water cation.

At room temperature the reactions reached completion in under 15 hours, as monitored by ¹H NMR spectroscopy. At 0°C the rate did not alter significantly when using 1, 2 or 5 mol % of catalyst. High *exo:endo* selectivity (~95:5) and modest enantioselectivity (40% *e.e.*) were obtained, even with 1 mol % catalyst (entry 1). Increasing the catalyst ratio (entries 2 and 3), had little effect on the *exo:endo* or enantioselectivity, but lowering the reaction temperature from room temperature to 0 and -20°C led to improvements in the enantioselectivity (entries 4, 2 and 5), an *e.e.* of 44% being obtained at -20°C, with 2 mol % catalyst.

Table (4.3): Effect of varying the R-substituent on the reaction of methacrolein and CpH using [Ru(OH₂)(R-phenmox)(mes)][SbF₆] (2.17) as catalyst^a

Entry	R-group	Diastereomer Ratio (B:A) ^b	Yield (%)	Isomer Ratio (<i>exo:endo</i>)	<i>E.e.</i> (%) (abs. config.)
1	^t Bu	100:0	92	97:3	38 (<i>S</i>)
2	ⁱ Pr	100:0	93	95:5	40 (<i>S</i>)
3	Bn	78:22	89	92:8	6 (<i>S</i>)
4	Ph	24:76	91	93:7	13 (<i>S</i>)

a All reactions carried out at 0°C, for 72 hours with 2 mol % catalyst formed *in situ*.

b Diastereomer ratios refer to chlorides.

The effect of varying the R-substituent was investigated using [Ru(OH₂)(R-phenmox)(mes)]SbF₆ as catalyst (Table 4.3). The enantioselectivity was found to increase with increasing steric bulk of the R-group up to a point. However, R = ⁱPr and

^tBu (entry 1 to 2) give rather similar *e.e.*'s, 40% and 38% respectively. Also, oxazoline substituents containing aryl groups (*i.e.* R = Bn, Ph) gave rather low *e.e.*'s with, surprisingly, the slightly smaller R = Ph (entry 4) giving higher *exo:endo* ratio and higher enantioselectivity than R = Bn (entry 3).

The poor enantioselection achieved with (**2.12**, R = Bn, Ph) (entry 3 and 4) is consistent with low diastereoselectivity in the complexes (see Section 2.2); hence there may be two competing catalysts (shown in **Figure 4.1**). The isomer-B structure is likely to impose some face shielding of the coordinated methacrolein by the R-group, therefore some enantioselection is expected. Whereas in the isomer-A structure, the oxazoline substituent is on the opposite side to the coordinated methacrolein and hence would not be expected to influence the enantioselectivity significantly, *i.e.* isomer-A is expected to give a racemic product. A combination of these two diastereomers catalysing the reaction would be expected to give reduced enantiomeric excess.

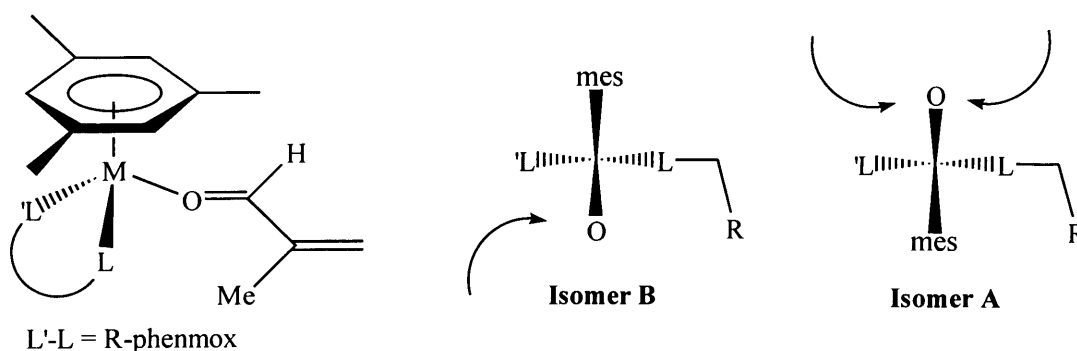


Figure (4.1): Model for proposed enantioselection

In conclusion, changing the R-group of the phenmox ligand, has a significant effect on the enantioselectivity of the reaction between methacrolein and cyclopentadiene. In contrast, lowering the reaction temperature and the catalyst loading has a much smaller effect.

The nature of the arene ligand in the precatalysts [RuCl(R-phenmox)(arene)] (**2.12 – 2.14**) was also investigated (**Table 4.4**).

Table (4.4): Effect of changing the η^6 -arene on the reaction of methacrolein and CpH using [RuCl(ⁱPr-phenmox)(arene)] (2.12 –2.14) as precatalysts^a

Entry	Catalyst	R-group	Arene	Diastereomer Ratio (B:A) ^b	Yield (%)	Exo:endo	E.e. (%)
1	2.14	ⁱ Pr	C ₆ H ₆	89:11	67	95:5	48
2	2.13	ⁱ Pr	<i>p</i> -cy	89:11	80	95:5	47
3	2.12	ⁱ Pr	mes	100:0	93	95:5	40
4	2.13	^t Bu	<i>p</i> -cy	100:0	73	93:7	37
5	2.12	^t Bu	mes	100:0	92	97:3	38

a All reactions at 0°C for 72 hours, with 2 mol % catalyst formed *in situ*.

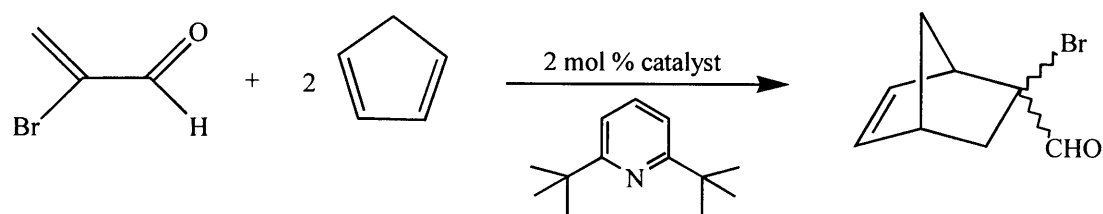
b Diastereomer ratios refer to chlorides.

Using the ⁱPr-phenmox complexes (entries 1 - 3) the mesitylene-containing catalyst (entry 3), was found to be inferior in terms of enantioselectivity (40 % *e.e.*) to the C₆H₆ or *p*-cy catalysts (entries 1 and 2 ~ 48 % *e.e.*). Using ^tBu-phenmox complexes, *p*-cy and mesitylene-containing catalysts (entries 4 and 5) give essentially the same enantioselectivity though the mesitylene complex gives a somewhat higher *exo:endo* ratio. A sterically more bulky arene might be expected to restrict rotation of coordinated methacrolein (see later) and hence provide higher enantioselectivity. However, using the related [RuCl(ⁱPr-pymox)(arene)][SbF₆] (arene = C₆H₆, *p*-cy, mes, C₆Me₆)¹⁰⁰ as catalyst precursors for this reaction, our group has shown that the highest selectivity was found with the mesitylene-containing complex rather than the more bulky hexamethylbenzene complex. Noyori found that in asymmetric transfer hydrogenation reactions of ketones catalysed by [RuCl(*p*-TsDPEN)(arene)], the maximum enantioselectivity was observed when the arene is mesitylene.⁸⁰ These results suggest that when increasing the steric bulk of the arene and the R-substituent in arene-ruthenium half-sandwich complexes, there is a point where the sterics of the arene/R-substituent combination become too large for optimum enantioselectivity of a catalysed reaction. In the case of [RuCl(R-phenmox)(arene)] (entries 1 - 3) optimum enantioselectivity clearly occurs with a less bulky arene than mesitylene. Using [RuCl(^tBu-phenmox)(arene)] (entry 4 and 5) the enantioselectivity with *p*-cy and mesitylene are less than with ⁱPr-phenmox suggesting that optimum enantioselectivity would occur with less bulky arenes than have been tested.

As mentioned in the introduction, the rate of water exchange is much faster in phenmox (*N,O*) complexes $[\text{Ru}(\text{OH}_2)(\text{R-phenmox})(\text{arene})][\text{SbF}_6]$ than in the related pymox (*N,N*) complexes $[\text{Ru}(\text{OH}_2)(\text{R-pymox})(\text{arene})][\text{SbF}_6]_2$. However, using the pymox-containing catalysts for the Diels-Alder reaction of methacrolein and cyclopentadiene, the rates and enantioselectivities are considerably higher than those with phenmox complexes.¹⁰⁰ Under standard conditions (2 mol % catalyst and 0°C) the best arene-ruthenium pymox results (83% *e.e.*, 94% yield in 5 hours) and Cp*-rhodium pymox results (68% *e.e.*, 81% yield in 3 days), were significantly better than the phenmox catalysts $[\text{MCl}(\text{R-phenmox})(\text{ring})]$. It would appear that the increased Lewis acidity of the dicationic complexes formed with neutral pymox ligands outweighs the increased rate of ligand exchange with anionic phenmox ligands. Thus, substrate coordination or product loss are unlikely to be the rate determining steps in the catalytic cycle. The smaller chelate ring size for pymox (5-membered) compared to phenmox (6-membered) may contribute to the increased enantioselectivity with the pymox catalysts.

Previously our group has shown that using pymox catalysts $[\text{Ru}(\text{OH}_2)(^i\text{Pr-pymox})(\text{mes})][\text{SbF}_6]_2$ changing the dienophile has a marked effect on the *exo:endo* ratio and enantioselection. Thus, using acrolein (α -substituent = H) instead of methacrolein (α -substituent = Me), led to a considerable reduction in selectivity; the *exo:endo* ratios were all 1:2, with the highest *e.e.* obtained (for the major *endo* product) being 46%. Whilst bromoacrolein (α -substituent = Br) gave very poor yields; only a 20% yield of product was obtained after 90 minutes at 0°C with an *exo:endo* ratio of 80:20, indicative of thermal reaction.¹⁰⁰ Since bromoacrolein is a more activated dienophile and phenmox catalysts may have a larger active site, phenmox complexes were tested as catalysts for the reaction of bromoacrolein with cyclopentadiene. This reaction is known to proceed with high enantioselectivity, with a number of chiral catalysts.^{100, 194, 199} Bromoacrolein is a very reactive dienophile, the uncatalysed reaction with cyclopentadiene proceeding rapidly at room temperature (> 90% yield after 2 hours in CD_2Cl_2 solution, with an *exo:endo* ratio of 78:22), so to minimise competing thermal reaction, fairly reactive Lewis acid catalysts are required. Furthermore, to obtain the optimum selectivity low temperatures are usually employed in the catalysed reactions.

The reaction was carried out as before with bromoacrolein in place of methacrolein (**Scheme 4.13**). The effect of varying the R-substituents and temperature are shown in **Table (4.5)**.



Scheme (4.13)

Table (4.5):^a Effect of varying R-substituent and temperature for the reaction of bromoacrolein and CpH using [Ru(OH₂)(R-phenmox)(mes)]SbF₆ (2.17) as catalyst

Entry	R-group	Diastereomer Ratio (B:A) ^b	T/°C	Yield (%) ^c	Isomer Ratio (<i>exo:endo</i>)	<i>E.e.</i> (%)
1	^t Bu	100:0	0	80	93:7	41
2	ⁱ Pr	100:0	0	92	95:5	44
3	Bn	78:22	0	82	92:8	15
4	Ph	24:76	0	59	88:12	12
5	^t Bu	100:0	-20	80	98:2	48
6	ⁱ Pr	100:0	-20	93	97:3	49
7	Bn	78:22	-20	86	94:6	18
8	Ph	24:76	-20	92	95:5	23

a Reactions at 0°C for 2 hrs or at -20°C for 24 hrs, with 2 mol % catalyst formed *in situ*.

b Diastereomer ratios refer to chlorides.

c Isolated yields are quoted and so are not necessarily indicative of activity.

Comparing entries (1 - 4) the enantioselectivity and *exo:endo* ratio change with size of R-group as found for methacrolein, with a marked difference between R = ⁱPr or ^tBu (entry 1 and 2) and R = Ph or Bn (entry 3 and 4). The much reduced enantioselectivity with Ph and Bn may be an indication that two diastereomeric catalysts are present as found for the chloride precursors, however a single diastereomer was observed for [Ru(OH₂)(Ph-phenmox)(mes)]SbF₆ (2.17, R = Ph), but water exchange was rapid indicating the spectrum may have been time-averaged. The reduced enantioselectivity may also result from reduced face protection of the coordinated dienophile by the less sterically bulky R-groups. In addition, at 0°C the maximum enantioselectivity is with R = ⁱPr (entry 2), rather than with R = ^tBu (entry 1); as found with methacrolein and cyclopentadiene. This is further evidence that the pairing of two bulky groups

(mesitylene and ^tBu) may result in a too sterically congested active site, thus reducing the enantioselectivity. As expected, selectivity is greater at lower temperature (compare entries 5 - 8 with 1 - 4, respectively) as found with methacrolein and cyclopentadiene.

The effect of varying the arene ligand in the precatalysts [RuCl(R-phenmox)(arene)] (2.12 – 2.14) on the reaction of bromoacrolein and cyclopentadiene is shown in Table (4.6).

Table (4.6): Effect of variation in η^6 -arene for the reaction of bromoacrolein and CpH using [Ru(OH₂)(R-phenmox)(arene)]SbF₆] (2.17) as catalysts^a

Entry	Catalyst	R-group	Arene	Diastereomer Ratio (B:A) ^b	T (°C)	Yield (%) ^c	Exo:endo	E.e. (%)
1	2.12	ⁱ Pr	Mes	100:0	0	92	95:5	44
2	2.13	ⁱ Pr	<i>p</i> -cy	89:11	0	>95	95:5	53
3	2.14	ⁱ Pr	C ₆ H ₆	89:11	0	>95	92:8	44
4	2.12	^t Bu	Mes	100:0	0	80	93:7	41
5	2.13	^t Bu	<i>p</i> -cy	100:0	0	>95	97:3	51
6	2.12	ⁱ Pr	Mes	100:0	-20	93	97:3	49
7	2.13	ⁱ Pr	<i>p</i> -cy	89:11	-20	76	96:4	57
8	2.12	^t Bu	Mes	100:0	-20	80	98:2	48
9	2.13	^t Bu	<i>p</i> -cy	100:0	-20	>95	98:2	58

a Reactions at 0°C for 2 hrs or at -20°C for 1 day, with 2 mol % catalyst formed *in situ*.

b Diastereomer ratios refer to chlorides.

c Isolated yields are quoted and so are not necessarily indicative of activity.

The size of the arene was found to have a significant effect on the selectivity of the Diels-Alder reaction (entries 1 - 3). Thus, using [RuCl(ⁱPr-phenmox)(arene)] as catalyst, as the size of the arene increased from C₆H₆ to *p*-cy the enantioselectivity increased significantly (44% to 53% *e.e.* entry 1 and 2, respectively), however with the more bulky mesitylene-containing catalyst the *e.e.* decreased to 44% (entry 3). Similar trends were observed with R = ^tBu (entries 4 and 5) and at different temperatures (entries 6 & 7 and, 8 & 9). These results suggest that for the reaction of bromoacrolein and cyclopentadiene using a sterically bulky R-substituent (R = ⁱPr, ^tBu), the enantioselectivity reaches an optimum with *p*-cy as arene, whereas with methacrolein and cyclopentadiene, C₆H₆ and *p*-cy were equally enantioselective using ⁱPr-phenmox.

Clearly with the more activated dienophile bromoacrolein, the reduced Lewis acidity of the phenmox catalysts is not an important factor. The reduced reactivity with the pymox catalysts is then either due to too great steric hindrance of the bromoacrolein or possibly by competing side reaction, as suggested for (4.10) (Section 4.1).¹⁹³

In order to try to understand the observed selectivities and rates for these Diels-Alder reactions, it is helpful to consider the likely reaction mechanism (Scheme 4.14). In the reaction of methacrolein and cyclopentadiene catalysed by (2.12 – 2.15) and (2.29) containing (*S_C*)-configured oxazoline ligands, the absolute configuration of the major *exo* product is 1*R*, 2*S*, 4*R*.¹⁰⁰ To account for this selectivity a model of the transition state was proposed with the isopropyl shielding the *Si* face of the coordinated methacrolein leading to attack of the cyclopentadiene at the *Re* face (Figure 4.2).

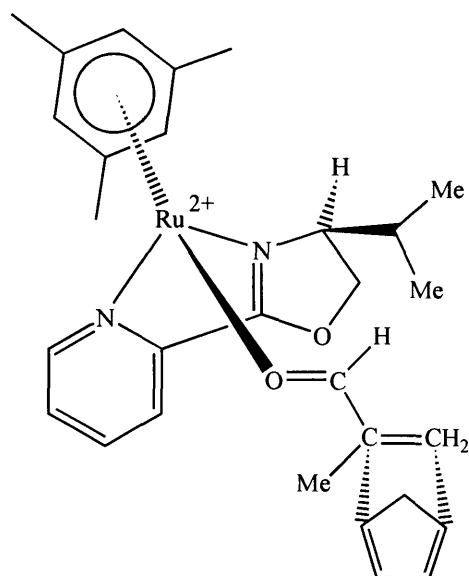
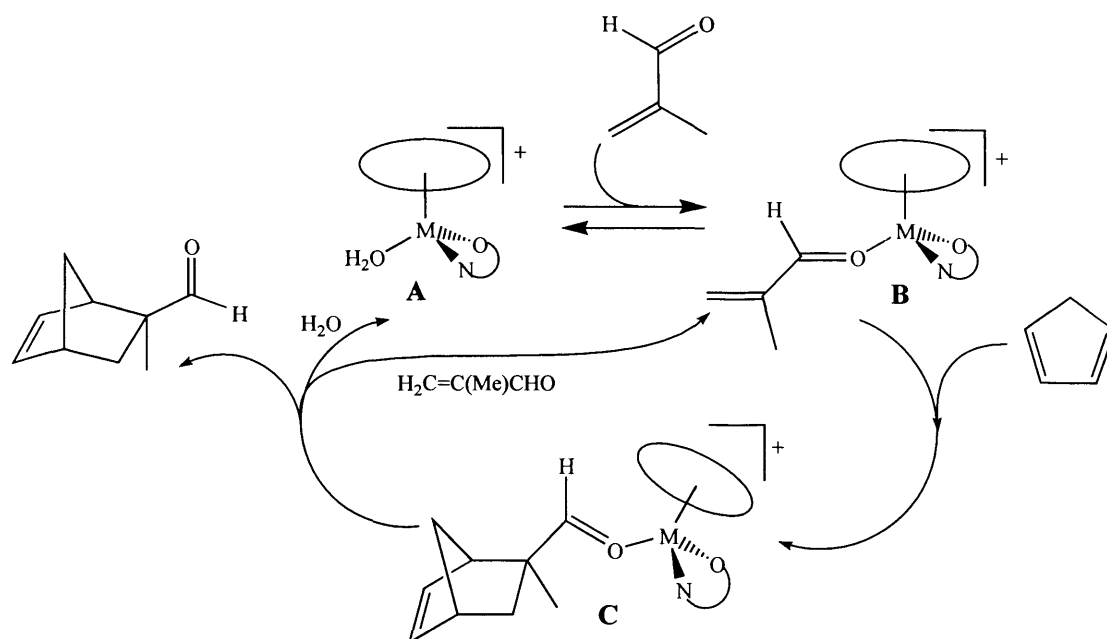


Figure (4.2): Model of catalytic transition state

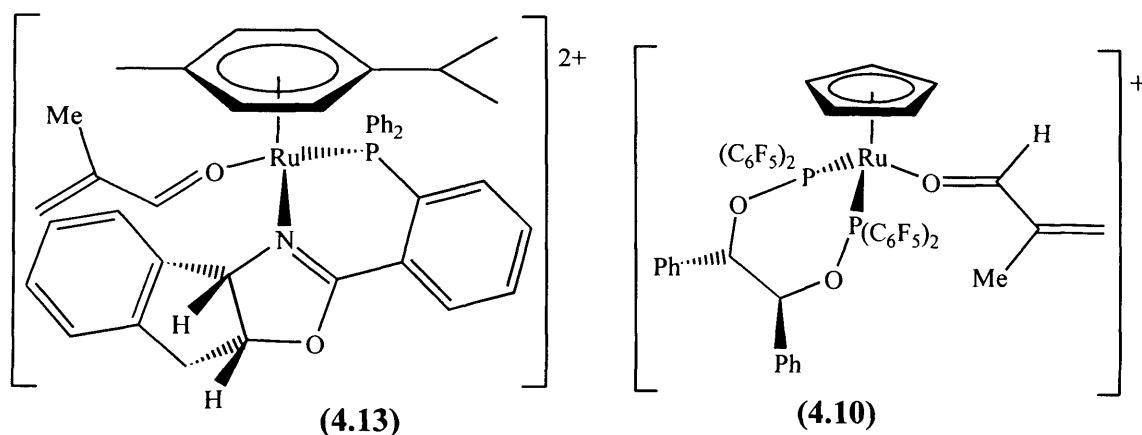
Addition of excess methacrolein to aqua species **A** (Scheme 4.14) favours formation of methacrolein-coordinated species **B** (which may exist as two diastereomers), which reacts with cyclopentadiene to form adduct-coordinated species **C**. Dissociation of the Diels-Alder product and coordination of another methacrolein molecule, or water, completes the cycle. It is possible there is a different equilibrium mixture (**A** \leftrightarrow **B**) of coordinated water and methacrolein for each catalyst and between different experiments due to varying amounts of water present, which may account for some variation in catalytic activity. In the proposed reaction mechanism (Scheme 4.14), **B** to **C** corresponds to the transition state (Figure 4.2) therefore it would be advantageous to observe and study dienophile-coordinated complex **B**.



Scheme (4.14)

We have established (Section 2.2) that exchange between free and coordinated water in $[\text{Ru}(\text{OH}_2)(^i\text{Pr-phenmox})(\text{mes})]\text{SbF}_6$ (**2.17**) is fast on the NMR timescale at room temperature. Therefore, studying the methacrolein-coordinated complex is also likely to be difficult due to rapid exchange of coordinated methacrolein and water. However, rate of aqua exchange is slower for $[\text{Ru}(\text{OH}_2)(^i\text{Pr-pymox})(\text{mes})](\text{SbF}_6)_2$ (**2.29**), such that signals for both free and coordinated water were observed with ^1H NMR spectroscopy.¹⁰⁰ Hence, studying the coordination of methacrolein in the “[$\text{Ru}(^i\text{Pr-pymox})(\text{mes})$]²⁺” system is more likely to provide detailed information in support of the reaction mechanism (**Scheme 4.14**).

In Lewis acid-catalysed Diels-Alder reactions, it is assumed that activation occurs by η^1 -coordination of the carbonyl group to the metal centre, though there is little direct evidence for this mechanism. During the course of this work, Carmona *et al.* have reported an X-ray structure of a Lewis acid-dienophile adduct, (**4.13**).⁷² Complex (**4.13**) was formed as a 9:1 mixture of diastereomers, the major one being shown below. The methacrolein coordinates in the expected η^1 -fashion, adopting an *S-trans* configuration (such that the carbonyl and C=C are parallel), with the methyl group oriented most towards the arene. This complex and the precursor aqua-complex were both found to be active catalysts for the reaction of methacrolein and cyclopentadiene, with moderate enantioselectivity being observed (*e.e.* up to 48%).



As mentioned in Section 4.1, in 1999 Kundig *et al.* reported the formation of a related methacrolein-coordinated complex, **(4.10)**.¹⁹³ The ^1H - ^1H NOESY NMR spectrum at 253K, indicated an *S-trans* geometry with the aldehyde proton pointing towards the cyclopentadienyl ring (the opposite rotamer to that found in **4.13**). The preferred structure of **(4.10)** in solution, coincides with that found in the X-ray structure; hydrogen bond interactions ($\text{H}\cdots\text{F}$) between the SbF_6^- anion with the cyclopentadienyl ring and aldehyde hydrogen, fix the methacrolein moiety in the chiral pocket and impede rotation about the Ru–O bond. This control of the geometry is believed to be responsible for the high enantioselectivity observed, up to 92% *e.e.* at 253K for the reaction of methacrolein and cyclopentadiene.¹⁹³

Coordination of methacrolein has been studied by treatment of $[\text{RuCl}(\text{}^i\text{Pr-pymox})(\text{mes})]\text{SbF}_6$ (**2.26**) with AgSbF_6 and methacrolein in CD_2Cl_2 , in the presence of activated molecular sieves to remove water. The ^1H NMR spectrum showed signals due to the methacrolein complex $[\text{Ru}\{\text{OHC}(\text{Me})=\text{CH}_2\}(\text{}^i\text{Pr-pymox})(\text{mes})][\text{SbF}_6]_2$ (**4.14**), a small amount of the aqua complex (**2.29**) as well as signals due to methacrolein and a small amount of water. The coordinated aldehyde proton signal is observed at δ 9.10, a shift of 0.44 ppm upfield on coordination. This is much larger than the 0.02 ppm shift reported for aldehyde coordination to an arene ruthenium bisphosphine monoxide complex.⁶⁸ Assuming the methacrolein lies in the plane roughly perpendicular to the pymox ligand four distinct orientations are possible (**Figure 4.3**). The aldehyde can coordinate through the lone pair *syn* to the aldehyde proton (I and II) or the lone pair (III and IV), *anti*. In each case there are two rotamers corresponding to rotation about the Ru–O bond. The orientation of the methacrolein was probed using a phase-sensitive NOESY experiment; the observed cross peaks are shown in **Figure (4.3)** (structure I).

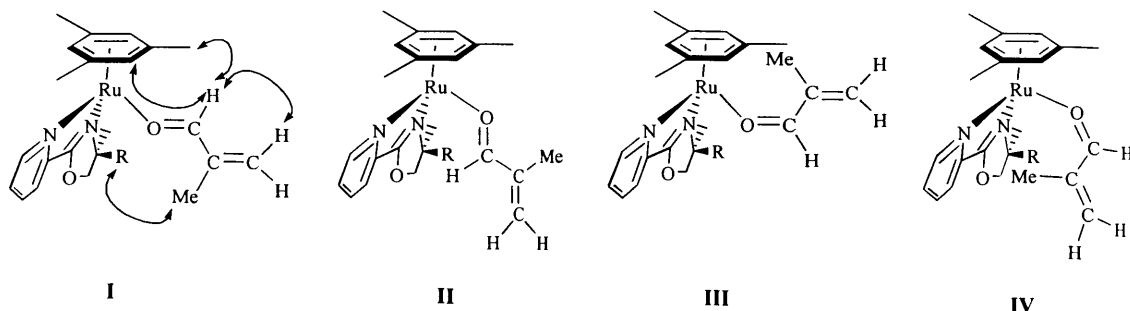


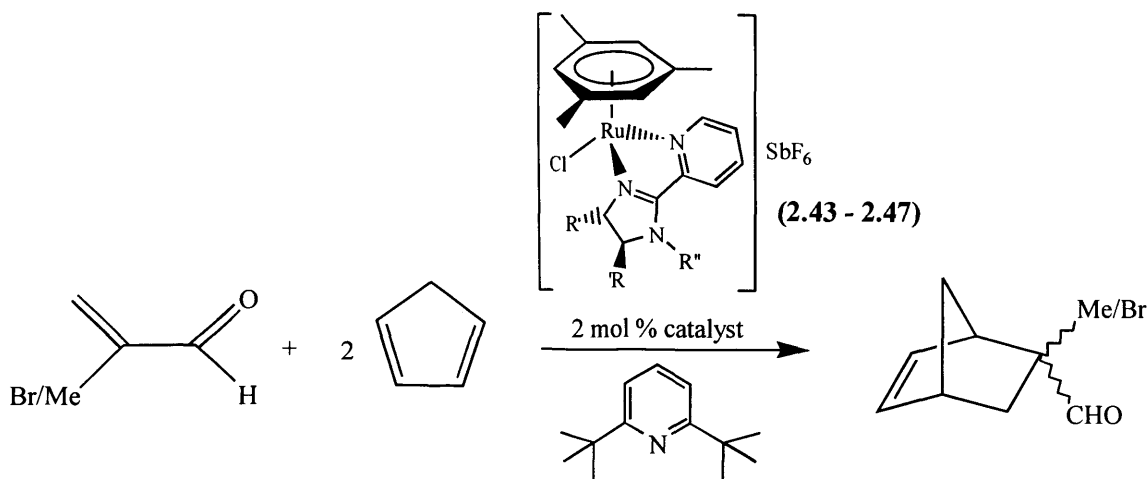
Figure (4.3): Possible geometries for $[\text{Ru}\{\text{OCHC}(\text{Me})=\text{CH}_2\}(\text{}^i\text{Pr-pymox})(\text{mes})]^{2+}$

Within the coordinated methacrolein cross peaks were observed between the aldehyde $\text{O}=\text{CH}$ proton (δ 9.10) and one hydrogen of the CH_2 (δ 6.59), consistent with an *S-trans* arrangement. Cross peaks were also observed between the $\text{O}=\text{CH}$ (δ 9.10) and the protons on the mesitylene ring (δ 5.65 $\text{C}_6\text{H}_3\text{Me}_3$ and δ 2.30 $\text{C}_6\text{H}_3\text{Me}_3$) and between the methyl of the methacrolein and one of the methyls of the isopropyl. Notably there are no cross peaks between the methyl of the methacrolein and any of the mesitylene signals. Of the four possible orientations I to IV these observations are only consistent with orientation I. This is similar to the orientation found in solution and in the solid state by Kundig *et al.*¹⁹³ in ruthenium complex (4.10), whereas an orientation similar to II was observed in the solid state by Carmona *et al.*⁷² in rhodium complex (4.13). In addition to the nOe cross peaks, chemical exchange cross peaks were observed between free and coordinated methacrolein so this exchange is occurring within the timescale of the NOESY experiment; thus, binding of the carbonyl group is not too strong, as required for catalyst turnover.

Having established that the faster rate of aqua exchange for phenmox complexes does not give higher catalyst turnover (at least for methacrolein with cyclopentadiene) we decided to evaluate complexes of the other neutral *N-N*-donor ligands, described in Chapter Two, *i.e.* imidazolines and Schiff-bases.

(4.2.2) – *N,N*-Donor Catalysts

The imidazoline-containing complexes $[\text{RuCl}(\text{R},\text{R}'\text{-pymimR}'')(\text{mes})]\text{SbF}_6$ (**2.43** – **2.47**) were tested as precatalysts for the Diels-Alder reaction of methacrolein or bromoacrolein with cyclopentadiene shown in **Scheme (4.15)**, using the same conditions as before (**Table 4.7**).



Scheme (4.15)

Table (4.7): Diels-Alder reactions of CpH using $[\text{Ru}(\text{OH}_2)(\text{R},\text{R}'\text{-pymimR}'')(\text{mes})](\text{SbF}_6)_2$ (**2.43** – **2.47**) as catalysts.^a

Entry	R,R',R''	Diastereomer Ratio (B:A)	Dienophile	Yield (%)	Exo:endo	E.e. (%)
1	Ph, Ph, H	53:47	Methacrolein	90	94:6	45
2	Ph, Ph, H ^b	53:47	Methacrolein	93	94:6	43
3	Ph, Ph, Me	47:53	Methacrolein	62	90:10	15
4	Ph, Ph, H	53:47	Bromoacrolein	66	84:16	17
5	Ph, Ph, Me	47:53	Bromoacrolein	68	91:9	26
6	ⁱ Pr, H, Ph	100:0	Methacrolein	>95	93:7	26
7	ⁱ Pr, H, ⁿ Bu	100:0	Methacrolein	87	95:5	58
8	Bn, H, ^t Bu	100:0	Methacrolein	48	93:7	19
9	ⁱ Pr, H, Ph	100:0	Bromoacrolein	45	83:17	10
10	ⁱ Pr, H, ⁿ Bu	100:0	Bromoacrolein	92	93:7	50
11	Bn, H, ^t Bu	100:0	Bromoacrolein	50	90:10	3

^a Reactions at 0°C for 72 hours, with 2 mol % catalyst formed *in situ*.

^b Without hindered base.

There are two main catalyst systems shown in **Table (4.7)**, ligands containing two chiral centres (entries 1 - 5) or ligands containing one chiral centre (entries 6 - 11). In general, both catalyst types give promising selectivity with methacrolein as dienophile (entries 1 – 3 and 6 - 8), however with bromoacrolein the selectivity and activity of the catalysts are more variable (entries 4 – 5 and 9 - 11). For the methacrolein/CpH reaction, with Ph₂-pymimH as ligand, the resulting catalyst gave higher selectivity (94:6 and 45% *e.e.*) than with Ph₂-pymimMe (90:10 and 15% *e.e.*) as ligand (entries 1 and 3). Surprisingly, with the same two catalysts the observed selectivity is reversed for the bromoacrolein/CpH reaction (entries 6 and 7); 84:16 *exo:endo* selectivity and 17% *e.e.* was obtained with Ph₂-pymimH, whereas 91:9 and 26% *e.e.* was achieved with Ph₂-pymimMe as ligand. The low *exo:endo* selectivity (84:16) with Ph₂-pymimH (entry 4) is similar to that of the thermal reaction (~80:20), indicating that the catalyst formed from **(2.43)** may not be the active species. Comparing Entries 1 and 2 confirms that the presence/absence of hindered base does not greatly effect the catalyst performance, *i.e.* not much, if any, of a deprotonated species was generated under the reaction conditions. The moderate *e.e.*'s obtained with **(2.43)**, indicate that low equilibrium diastereoselectivity (53:47) in the chloride precursor complexes may not be significant; the ratio of the aqua diastereomers (100:0) may be a better guide to the catalyst's selectivity. Comparing these catalysts to the analogous Ph-pymox catalyst (*exo:endo* ratio of 94:6 and 58% *e.e.* for methacrolein, but inactive for bromoacrolein)¹⁰⁰ shows that the increased electron donor properties of imidazolines leads to a decrease in Lewis acidity and a reduction in selectivity for the methacrolein/CpH reaction, but an increase in activity and selectivity for the bromoacrolein/CpH reaction.

The effect of differing electronic properties of the R'' group is most clearly demonstrated by comparing R'' = Ph (entries 6 and 9) and R'' = ⁿBu (entries 7 and 10) for the R = ⁱPr catalysts. With the ⁿBu group the catalyst gives good enantioselection (58 and 50% *e.e.*) and *exo:endo* selectivity (95:5 and 93:7) with methacrolein or bromoacrolein as dienophile. In comparison, the selectivities are dramatically reduced, (26 and 10% *e.e.*) and (93:7 and 83:17 *exo:endo*), for the comparable reactions with R'' = Ph, suggesting an element of electronic control is possible, by selecting an electron donating (ⁿBu) or withdrawing (Ph) R'' group. It should be noted that the *exo:endo* ratio 83:17 (entry 9) is similar to that of the thermal reaction, indicating complex **(2.45)** (containing ⁱPr-pymimPh) is a poor catalyst for the reaction of bromoacrolein and CpH.

Substituting R = ⁱPr with Bn, lowers the enantioselectivity of both reactions from 58 to 19% *e.e.* for methacrolein/CpH (entries 8 and 9) and from 50 to 3% *e.e.* (entries 10 and 11) for bromoacrolein/CpH. Reduced selectivity with Bn rather than ⁱPr is consistent with the results from pymox¹⁰⁰ and phenmox-containing catalysts Section 4.1. The fact that the *exo:endo* selectivities observed with Bn-pymimⁱBu as ligand are reasonable, suggests that this ruthenium complex is the active catalyst, but that it is not very enantioselective.

The complexes of neutral imidazolines (**2.43 – 2.47**) (five-membered chelate) are more selective catalysts than those with anionic phenmox (**2.12 – 2.14**) (six-membered chelate) for the reactions of methacrolein or bromoacrolein with cyclopentadiene. Furthermore, the imidazoline complexes are less active and selective than the analogous pymox complexes⁹⁷ for the methacrolein/CpH reaction, but they are more active for the bromoacrolein/CpH reaction; consistent with reduced Lewis acidity of imidazolines.

The Schiff-base ketimine-containing complexes [RuCl(N-N')(mes)]SbF₆ (**2.49 – 2.53**) were tested as catalysts for the Diels-Alder reaction of methacrolein or bromoacrolein with cyclopentadiene, as described previously (**Table 4.8**).

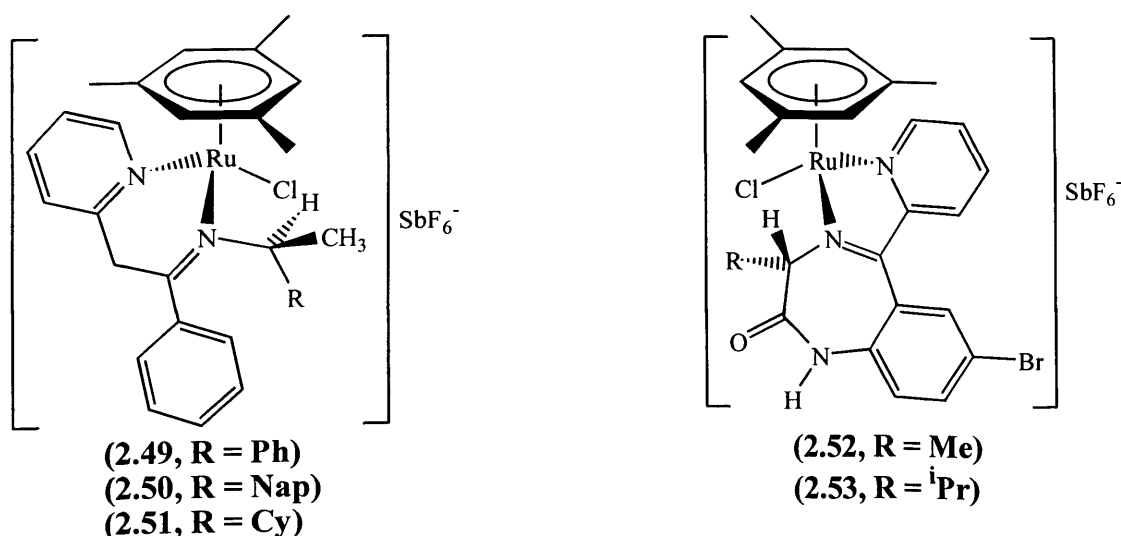


Table (4.8): Diels-Alder reactions of CpH using [Ru(OH₂)(N-N')(mes)](SbF₆)₂ (2.49 – 2.53) as catalysts^a

Entry	Code	Diastereomer Ratio (II:I), R =	Dienophile	Yield (%) ^b	<i>exo:endo</i>	<i>E.e.</i> (%) (abs. config.)
1	2.49	8:92 Ph	Methacrolein	87	92:8	8 (<i>R</i>)
2	2.50	34:66 Nap	Methacrolein	55	90:10	9 (<i>R</i>)
3	2.51	65:35 Cy	Methacrolein	68	97:3	41 (<i>S</i>)
4	2.49	8:92 Ph	Bromoacrolein	70	83:17	2 (<i>R</i>)
5	2.50	34:66 Nap	Bromoacrolein	>95	83:17	2 (<i>R</i>)
6	2.51	65:35 Cy	Bromoacrolein	>95	94:6	47 (<i>S</i>)
7	2.52	71:29 ^c Me	Methacrolein	30	90:10	8 (<i>S</i>)
8	2.53	92:8 ¹ Pr	Methacrolein	78	93:7	32 (<i>S</i>)
9	2.52	71:29 ^c Me	Bromoacrolein	92	88:18	0 (<i>S</i>)
10	2.53	92:8 ¹ Pr	Bromoacrolein	81	85:15	0 (<i>S</i>)

a Reactions at 0°C for 72 hours, with 2 mol % catalyst prepared *in situ*.

b Isolated yields are quoted and so are not necessarily indicative of activity.

c Three isomers: two conformers of diastereomer II.

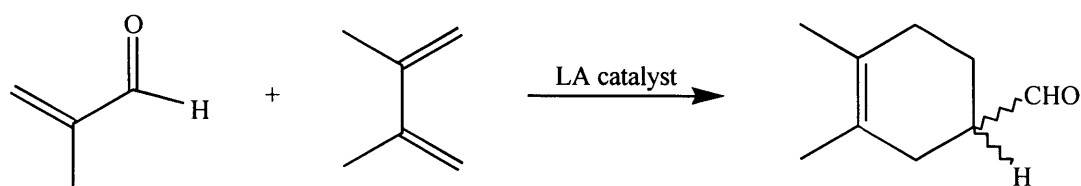
With ketimine complexes (2.49 – 2.51), there appears to be a correlation between diastereomer ratio and enantioselectivity for the reactions of methacrolein or bromoacrolein with cyclopentadiene (entries 1 – 3 and 4 – 6, respectively). The highest *exo:endo* selectivity and enantioselectivity are obtained when the diastereomer ratio favours isomer-II structure; *i.e.* with (2.51, R = Cy) (entries 3 and 6). Furthermore, greater selectivity also correlates with increasing size of the R-substituent, Cy > Nap > Ph. The poor selectivity with R = Ph (and hence Nap), may be related to the structure. The crystal structure and nOe experiments on (2.49, R = Ph) indicate that the C–H bond of the N–CH(Me)Ph fragment is oriented towards the chloride; *i.e.*, if this orientation were retained by the “active” catalyst, poor enantioselectivity would be expected. It should be noted that complexes (2.49, R = Ph and 2.50, R = Nap) having electron withdrawing R-substituents do not catalyse the reaction of bromoacrolein and CpH; the isolated products have an isomer ratio of 83:17 and 2% *e.e.* (entries 4 and 5), which are indicative of a thermal reaction. An important correlation is between catalyst structure (either similar to isomer-II or -I, see Section 2.2.3) and the absolute configuration of the Diels-Alder adducts formed. With (2.51, R = Cy) diastereomer ratio 65:35, the (2*S*)-

configured adduct is favoured (as found for related pymox¹⁰⁰ and phenmox catalysts see Section 4.2.1), whereas with (**2.49**, **R = Ph**) 8:92 and (**2.50**, **R = Nap**) 34:66 (both complexes favouring isomer-I type structure), the (2*R*)-configured adduct is preferred (compare entries 1 – 3 and 4 -6). This observation is consistent with the proposed transition state discussed in Section 4.2.1. Even with a sterically bulky Cy-substituent, the ketimine complex (**2.51**) is less enantioselective (41% *e.e.* compared to 75% *e.e.*) than the analogous ⁱPr-pymox complex (**2.26**). The lower selectivity with (**2.51**) might be attributed to free rotation about the N—CH(Me)Cy bond, hence the face-shielding in the transition state may be provided by Me rather than Cy. Note, the size of the chelate ring may also have an effect on the enantioselectivity of the reaction.

Using the ketimine complexes (**2.52** - **2.53**), as catalysts for the reaction of methacrolein and CpH the enantioselectivity and *exo:endo* selectivity improved from 8% and 90:10 with R = Me (entry 7) to 32% and 93:7 with R = ⁱPr (entry 8). This is consistent with the higher diastereoselectivity (92:8) of (**2.53**) compared to 71:29 for (**2.52**). In addition, (**2.52**) is formed as three isomers (see Section 2.2.3) (hence, three potentially active catalysts), which might also contribute to the lower enantioselectivity. Complexes (**2.52** and **2.53**) are inactive for the reaction of bromoacrolein and cyclopentadiene as found with related ketimines (**2.49/2.50**, **R = Ph/Nap**) and pymox complexes (**4.12**).¹⁰⁰

The complexes of neutral ketimines (**2.49** – **2.53**) were found to be the least selective catalysts for the reactions of methacrolein or bromoacrolein with cyclopentadiene. Furthermore, only complex (**2.51**, **R = Cy**) catalysed the reaction of bromoacrolein/CpH; consistent with reduced Lewis acidity due to an electron donating R-substituent.

The Diels-Alder reaction with other dienes, instead of dienophiles, was tested using those complexes which gave the best catalytic results for the reaction of methacrolein with cyclopentadiene. Complexes [Ru(OH₂)(N-N')(mes)](SbF₆)₂ (N-N' = ⁱPr-pymox, ⁱPr-pymimPh, ⁱPr-pymimⁿBu, Ph₂-pymimH, Ph₂-pymimMe, Cy-ketimine) were also tested as catalysts for the Diels-Alder reaction of methacrolein with 2,3-dimethylbutadiene (DMBD) (**Scheme 4.16**), with all reactions being carried out at room temperature with 2 mol % catalyst for 12 hours (**Table 4.9**).



Scheme (4.16)

Table (4.9): Diels-Alder reaction of DMBD and CpH using $[\text{Ru}(\text{OH}_2)(\text{Ligand})(\text{mes})](\text{SbF}_6)_2$ as catalysts.^a

Entry	Code	Ligand	Diastereomer Ratio (B:A) ^b	Yield (%) ^c	<i>E.e.</i> (%)
1	2.26	ⁱ Pr-pymox	100:0	89	69
2	2.45	ⁱ Pr-pymimPh	100:0	>95	62
3	2.46	ⁱ Pr-pymim ⁿ Bu	100:0	90	58
4	2.43	Ph ₂ -pymimH	53:47	40	26
5	2.44	Ph ₂ -pymimMe	47:53	43	23
6	2.51	Cy-ketimine	35:65	26	6

a All reactions at RT for 12 hours using 2 mol% catalyst prepared *in situ*.

b Diastereomer ratios refer to chlorides.

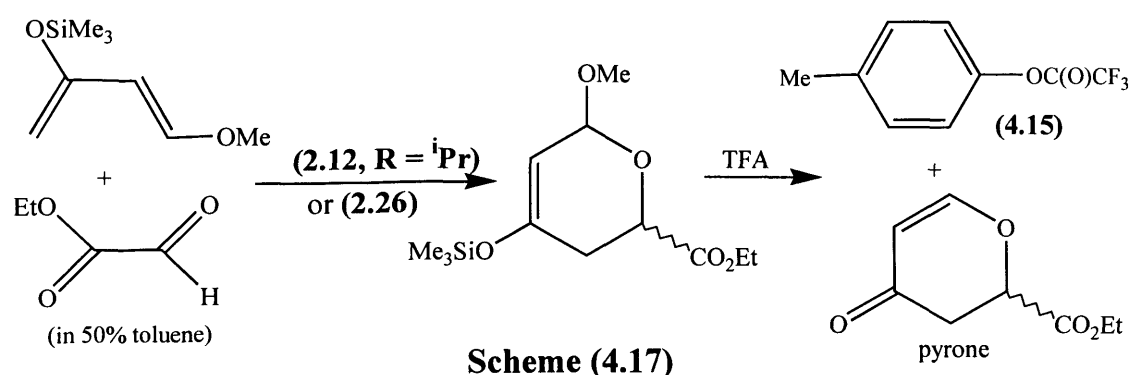
c Isolated yields are quoted and so are not necessarily indicative of activity.

The reaction was initially monitored by NMR (NMR tube reaction in CD_2Cl_2) using (2.29) as catalyst, the reaction took 5 hours to go to completion. Consequently, the remaining reactions were run for 12 hours to ensure that reactions with less active catalysts will have gone to completion. With ⁱPr-substituted ligands (entries 1 - 3), the product was obtained in high enantioselectivity (58 – 69% *e.e.*). Interestingly, the nature of the N-R'' substituent on the imidazolines (Ph or ⁿBu) does not greatly affect either the activity (both ~90% yield after 12 hours) or the enantioselectivity (62% *e.e.* versus 58% *e.e.*, respectively) in this reaction. This is in contrast to larger differences observed for the reaction of cyclopentadiene with methacrolein or bromoacrolein (see Table 4.7). The two imidazoline catalysts with R = Ph substituents (entries 4 and 5) are less active (both ~40% yield after 12 hours) and enantioselective (~25% *e.e.*) compared to R = ⁱPr (entries 2 and 3 ~90% yield, ~60% *e.e.*). The reduced enantioselectivity with R = Ph compared to R = ⁱPr is similar to that observed with the analogous R-phenmox (Table 4.5) and R-pymox¹⁰⁰ complexes. The Schiff-base Cy-ketimine complex (2.51) was found to be a poor catalyst (26% yield and 6% *e.e.*) for this reaction.

From the results obtained so far, $[\text{RuCl}(\text{}^i\text{Pr-pymox})(\text{mes})](\text{SbF}_6)$ (**2.26**) is best for methacrolein, whilst $[\text{RuCl}(\text{}^i\text{Pr-phenmox})(\text{mes})]$ (**2.12**, $\text{R} = \text{}^i\text{Pr}$) seems to give similar results with methacrolein and bromoacrolein and so, is more versatile. Therefore both precatalysts were chosen to test a range of other Lewis-acid catalysed reactions; ${}^i\text{Pr}$ substituents were chosen since they generally give good enantioselectivity and are much less expensive than the corresponding ${}^t\text{Bu}$ complexes. As mentioned previously, main group Lewis acid complexes have been used as catalysts for hetero Diels-Alder¹⁸³, inverse electron-demand hetero Diels-Alder²⁰⁰ and Mukaiyama aldol¹⁸⁴ reactions. The complexes containing N,N - or N,O -donor ligands, discussed in this report, were evaluated as asymmetric catalysts for these reactions.

(4.2.3) – Additional Reactions

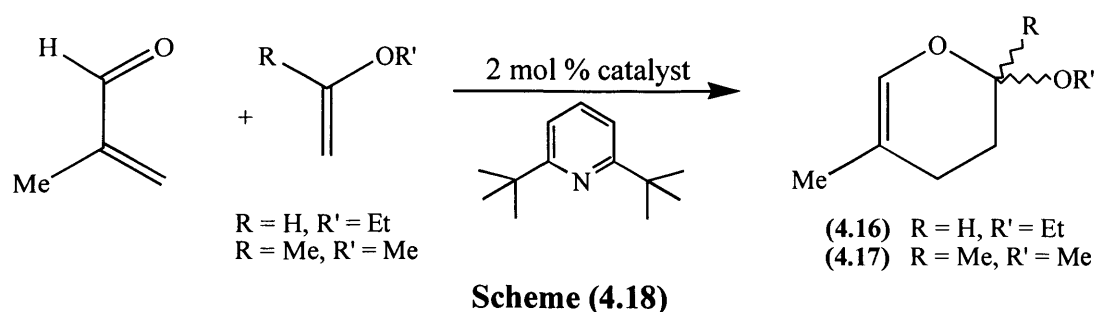
Previously in our group, complex (**2.26**) was shown not to catalyse the hetero Diels-Alder reaction between benzaldehyde and Danishefsky's diene (see **Scheme 4.8**); only unreacted or hydrolysed substrates were recovered, thus it was postulated that a more reactive aldehyde than PhCHO might be needed.¹⁰⁰ Therefore, the use of ethylglyoxylate might facilitate the transformation. Hence, the diene was added under N_2 , to a solution of ethylglyoxylate (50% solution in toluene), hindered base and aqua cation in CH_2Cl_2 , the mixture stirred for 2 days, before addition of a catalytic quantity of trifluoroacetic acid (TFA), to hydrolyse the silyl intermediate species to the desired pyrone see **Scheme (4.17)**; the procedure of Jacobsen *et al.*²⁰¹ was followed.



Both complexes tested were found to catalyse the hetero Diels-Alder reaction; in each case, the ${}^1\text{H}$ NMR of the reaction products showed two sets of signals in 13:7 ratio and no signals consistent with unreacted ethylglyoxylate. The major species was identified as the desired pyrone product, signals for the minor compound were consistent with (**4.15**) presumably a product from a side-reaction between toluene and

TFA. Column chromatography failed to separate the mixture of the pyrone product and by-product (60% yield of pyrone). As a result, the enantioselectivity of the pyrone has not been measured, although the reaction does warrant further investigation.

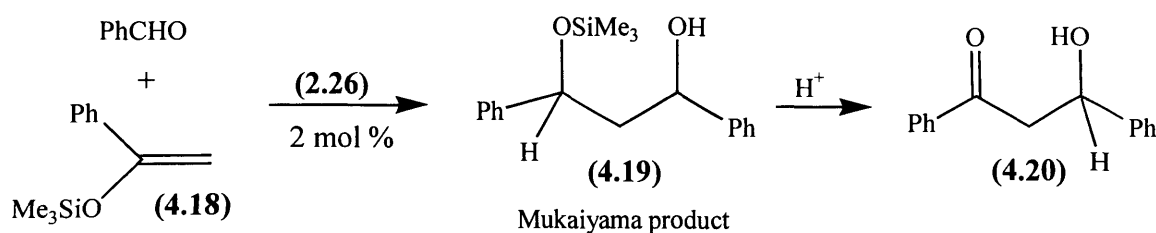
In the inverse electron-demand hetero Diels-Alder (ied-HDA) reaction of methacrolein with either ethyl vinyl ether (EVE) or 2-methoxy propene (MPP), the methacrolein acts as “diene”, with the latter reagents acting as “dienophile” (**Scheme 4.18**). The reactions were carried out using one equivalent of methacrolein, two equivalents of “dienophile” and 2 mol % of catalyst prepared *in situ* from either (**2.12**, $R = \textit{iPr}$) or (**2.26**) and hindered base (2 mol %) in CH_2Cl_2 for 48 hours at room temperature.



The reaction of methacrolein and EVE was attempted first, of the two catalysts, phenmox-containing (**2.12**, $R = \textit{iPr}$) was very slow, after 2 days only 5% conversion had been achieved. In contrast, 89% yield of adduct was obtained after 2 days using pymox catalyst (**2.26**); the remaining reactions, therefore, were only tested with catalyst (**2.26**). The adduct was identified as (**4.16**), by ^1H and 2D-COSY NMR spectroscopy and had an optical rotation of $([\alpha_D]^{25} = -24.6)$. This suggests that some asymmetric induction had occurred, but no literature value could be found for comparison, as the reaction has only been studied with achiral Lewis-acid catalysts.²⁰² Addition of one molar equivalent of a chiral lanthanide shift reagent (0.1M $\text{Eu}(\text{hfbc})_3$ in CDCl_3) to an NMR sample of the adduct, split the singlet at δ 6.06 into two singlets. Integration gave an enantiomeric excess of 18% *e.e.* for the reaction. The low enantioselectivity achieved with EVE, might be due to partial racemisation during work-up via deprotonation at the chiral carbon of the adduct. To avoid this possibility MPP was used instead of EVE. For this reaction, a 76% yield of (**4.17**) was obtained after 48 hours. The optical rotation of the product was $([\alpha_D]^{25} = -29.2)$, suggesting that the reaction had been performed with a degree of asymmetric induction (unfortunately literature values for comparison of

specific rotation were not found and addition of various chiral shift reagents only resulted in broadening of the NMR signals).

Another Lewis-acid reaction that has attracted a lot of interest is the Mukaiyama aldol reaction¹⁸⁴ of benzaldehyde with 1-phenyl-1-trimethylsilyloxy-ethylene (**4.18**) (**Scheme 4.20**). Bosnich *et al.* has shown that the complex $[\text{Ru}(\text{OH}_2)(\text{NO})(\text{salen})]\text{SbF}_6$ is a very efficient catalyst for this reaction, a 90% yield of Mukaiyama product (**4.19**) being observed after only 6 minutes (however the catalyst was prone to decomposition due to reduction by the silyl enol ethers used).²⁰³



Scheme (4.20)

It seemed reasonable, therefore, that similar activity, in addition to potential enantioselectivity, might be obtained with **(2.26)** as catalyst. The Mukaiyama reaction was performed by treating a CD_2Cl_2 solution of **(2.26)** (2 mol%) with AgSbF_6 in the presence of one equivalent of benzaldehyde and molecular sieves, this solution was filtered onto one equivalent of silyl-reagent **(4.18)**, hindered base (2 mol %) and molecular sieves in an NMR tube and the reaction monitored by ^1H NMR spectroscopy. The reaction had gone to completion after 12 hours, giving 75% yield of **(4.19)**. The product was treated with acid to hydrolyse the silylenol ether, forming hydroxyketone **(4.20)**. The products were found to be optically inactive ($[\alpha_D = 0]$) both before and after acid treatment. In an attempt to determine the catalytically active species, the reaction was repeated in the following ways: (i) without molecular sieves, (ii) without hindered base, (iii) without precatalyst **(2.26)**, and finally (iv) with substrates only. Conditions (i) and (ii) gave racemic product in good yield (70 – 80%) after 12 hours; however in contrast, conditions (iii) and (iv) did not yield any Mukaiyama product **(4.19)**. These exploratory reactions appeared to indicate that complex **(2.26)** was essential for catalysis to proceed, therefore studying the coordination of benzaldehyde might explain the absence of enantioselectivity from the reaction. Thus, $[\text{Ru}(\text{PhCHO})(^i\text{Pr-pymox})(\text{mes})](\text{SbF}_6)_2$ (**4.21**) was formed by reaction of $[\text{RuCl}(^i\text{Pr-pymox})(\text{mes})]\text{SbF}_6$ (**2.26**) with AgSbF_6 and one equivalent of benzaldehyde in the presence of molecular

sieves in CD_2Cl_2 . After filtration to remove AgCl the ^1H NMR spectrum showed signals due to complex (4.21), a small amount of the aqua complex (2.29) and free benzaldehyde. The coordinated aldehyde proton signal is observed at δ 9.40, a shift of 0.52 ppm upfield on coordination, similar to that observed upon methacrolein coordination in complex (4.14), 0.44 ppm. As described for complex (4.14), there are four distinct orientations of the benzaldehyde, the two most likely structures are shown in Figure (4.4). The orientation of the benzaldehyde was probed using a phase-sensitive NOESY experiment; the observed cross peaks are shown in Figure (4.4) (structure I). NOe cross peaks were observed between the coordinated aldehyde proton and the methyl and arene protons on the mesitylene ring, and also between an isopropyl Me signal and aldehyde phenyl. Notably there are no cross peaks between the phenyl and any of the mesitylene signals. Of the two orientations shown in Figure (4.4), these observations are only consistent with orientation I. As mentioned previously, a similar orientation was found in solution for complex (4.14). In addition, chemical exchange cross peaks were observed between free and coordinated benzaldehyde so this exchange is occurring within the timescale of the NOESY experiment. The orientation of benzaldehyde in (4.21) (structure I), suggests that some enantioselectivity should be expected if (4.21) was the sole catalytically active species.

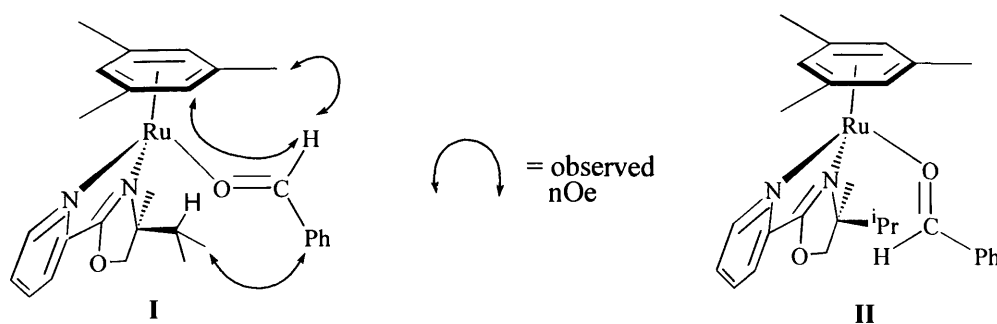


Figure (4.4): Proposed geometries for $[\text{Ru}(\text{PhCHO})(\text{iPr-pymox})(\text{mes})]^{2+}$

Given the investigative experiments discussed above, there are three possible explanations for the formation of a racemic product:

1. A small amount (such that it was not observed by NMR) of an extremely active species with structure II orientation is also catalysing the reaction. This catalyst would be expected to form the opposite enantiomer product (to structure I). However, the enantiomer from the minor catalyst isomer must be formed in an identical yield to that obtained from the major catalyst isomer (4.21) (structure I), in order for a racemate to be formed; this is extremely unlikely.

2. Ionisation of $[\text{Ru}(\text{H}_2\text{O})(^i\text{Pr-pymox})(\text{mes})](\text{SbF}_6)_2$ (**2.29**) could produce “free H^+ ions”, which would hydrolyse the silylenol ether to give Me_3Si^+ (an achiral Mukaiyama aldol catalyst).²⁰⁴ However, Me_3Si^+ is an extremely active catalyst (forms 95% yield after 10 minutes)²⁰⁵; clearly the observed rate of reaction (75% yield after 12 hours) suggests that not even a small amount of Me_3Si^+ is likely to have been the active catalyst.
3. Ag^+ is a proven achiral catalyst for these reactions.¹⁹¹ If a small quantity of Ag^+ was soluble in dichloromethane (therefore not removed by filtration), this would be consistent with zero product in the absence of $[\text{RuCl}(^i\text{Pr-pymox})(\text{mes})]\text{SbF}_6$ (**2.26**) (*i.e.* no AgSbF_6 had been used) and, the product formed in the presence of “[$\text{Ru}(^i\text{Pr-pymox})(\text{mes})$]²⁺”, being a racemate.

The most likely explanation is 3. (Ag^+ catalysing the reaction), since this is the only hypothesis which has not been ruled out.

To summarise the results with phenmox-containing $[\text{MCl}(\text{R-phenmox})(\text{ring})]$ (**2.12 – 2.15**) and pymox-containing $[\text{RuCl}(^i\text{Pr-pymox})(\text{mes})][\text{SbF}_6]$ (**2.26**) catalysts described above, there are 4 main conclusions:

1. Ruthenium phenmox catalysts are significantly better than rhodium phenmox
2. Alkyl R-substituents give greater selectivity than those containing an aryl group
3. Oxazoline ligands generally give good chiral induction.
4. Catalyst activity doesn't correlate well with rate of aqua exchange; phenmox catalysts are worse than pymox catalysts for the reaction of methacrolein with cyclopentadiene, but are better for bromoacrolein with cyclopentadiene. Increased activity/selectivity of the catalyst correlates better to increased Lewis acidity.

The general conclusion regarding the use of the half-sandwich complexes as asymmetric Lewis acid catalysts is that the rate of aqua exchange doesn't correlate well with the rate of catalysis. The rate of the reaction may be due to differences in Lewis acidity. Further work would be to investigate other Lewis acid catalysed reactions using the *N,N*-donor catalysts discussed above.

(4.3) – Experimental

Diels-Alder reagents were dried and distilled from the following reagents:

1. Methacrolein from CaH_2
2. 2,3-Dimethyl-1,3-butadiene from 4Å Molecular Sieves
3. Benzaldehyde from 4Å Molecular Sieves

Bromoacrolein was prepared by the literature method²⁰⁶ and cyclopentadiene was freshly cracked prior to use. All other reagents were used as received and other solvents were purified as described in Chapter Two.

Diels-Alder Reactions

NMR tube experiments (under N_2): Dienophile[‡] (*ca.* 0.25 mmol) was added to a yellow/orange coloured degassed CD_2Cl_2 (0.5 ml) solution of catalyst (2.5, 5 or 12.5 μmol) in a Young's tap NMR tube. To the solution was added 2,6-di-*tert*-butylpyridine (1 equivalent/mol of catalyst) and diene[†] (0.5 mmol). The ^1H NMR spectrum was recorded immediately and then repeated after suitable time intervals.

Schlenk reactions (under N_2): Dienophile[‡] (1 mmol) and 2,6-di-*tert*-butylpyridine (1 equivalent/mol of catalyst) were added to a solution of catalyst (0.01, 0.02 or 0.05 mmol) in CH_2Cl_2 (2 ml). The yellow/orange solution was cooled to the appropriate temperature before addition of diene[†] (2 mmol). At the end of the reactions, the mixture was passed through a silica plug (to remove catalyst), the solvent was removed and the product was obtained as a colourless oil. The *exo:endo* ratio (where appropriate) was determined by NMR spectroscopy. The catalysts could also be prepared *in situ*, from the corresponding chloride complex and one equivalent of AgSbF_6 in CH_2Cl_2 , filtration through celite to remove AgCl and then addition of the reagents as described above.

[‡]Dienophile = Methacrolein or bromoacrolein

[†]Diene = Cyclopentadiene or 2,3-Dimethyl-1,3-butadiene

The enantiomeric excesses were determined by several routes:

1. The *e.e.*'s of adduct from methacrolein with cyclopentadiene was determined by GC after conversion to the acetal with (2*R*,4*R*)-pentanediol, according to the method of Evans *et al.*¹⁹⁶

2. The *e.e.*'s of adducts from methacrolein with 2,3-Dimethyl-1,3-butadiene were determined by GC after conversion to the acetal with (2*R*,4*R*)-pentanediol and by ¹H NMR {by integration of the singlets due to RCH(OR')₂}.
3. The *e.e.*'s of adducts from bromoacrolein with cyclopentadiene were determined by ¹H NMR {by integration of the singlets due to RCH(OR')₂}, after conversion to the acetal with (2*R*,4*R*)-pentanediol (a reaction time of 4 days was required to synthesise the acetal).

Hetero Diels-Alder reaction

To a degassed solution of catalyst (11 μmol), 2,6-di-*tert*-butylpyridine (2.6 μl, 11 μmol) and ethylglyoxylate (50% solution in toluene) (50 μl, 0.22 mmol) in CH₂Cl₂ (2 ml) was added 1-methoxy-3-trimethylsilyloxy-1,3-butadiene (50 μl, 0.23 mmol) via syringe. The resulting solution was stirred for 2 days at room temperature under N₂, before addition of a drop of trifluoroacetic acid, giving a brown-coloured solution. The mixture was evaporated and a crude ¹H NMR spectrum obtained.

Inverse-electron demand hetero Diels-Alder reaction

To a degassed solution of catalyst (0.02 μmol) and 2,6-di-*tert*-butylpyridine (1 equivalent/mol of catalyst) in CH₂Cl₂ (2 ml), was added methacrolein (1 mmol) and dienophile[‡] (2 mmol) by syringe. The solution was stirred at room temperature for 2 days, then filtered through a plug of silica, to remove the catalyst. The resulting colourless solution was evaporated and dried *in vacuo* to afford a colourless oil.

[‡]Dienophile = ethyl vinyl ether: product (127 mg, 89% yield) identified as 2-ethoxy-5-methyl-3,4-dihydro-2H-pyran (**4.16**), by comparison of the ¹H NMR spectrum with that for similar known compounds and by 2D-COSY NMR. The optical rotation was measured at $[\alpha_D]^{25} = -24.6$. The enantiomeric excess, 18% *e.e.*, was determined by ¹H NMR after addition of one molar equivalent of a chiral lanthanide shift reagent (0.1M Eu(hfbc)₃ in CDCl₃).

[‡]Dienophile = 2-methoxy propene: product (108 mg, 76% yield) identified as 2-methoxy-2,5-methyl-3,4-dihydro-2H-pyran (**4.17**), by comparison of the ¹H NMR spectrum with that for similar known compounds. The optical rotation was measured at $[\alpha_D]^{25} = -29.2$. Addition of various CLSR only resulted in broadening the NMR signals; enantiomer separation was not achieved.

Mukaiyama aldol reaction (under N₂)

To a CD₂Cl₂ solution of **(2.26)** (9 mg, 10 μmol) and PhCHO (53 μl, 0.50 mmol) was added AgSbF₆ (4 mg, 11 μmol) and 4Å molecular sieves, this solution was stirred for 30 minutes (in darkness) prior to being filtered using a canula (to remove AgCl) into a Young's tap NMR tube containing 1-phenyl-1-(trimethylsilyloxy)ethylene (102.5 μl, 0.50 mmol), 2,6-di-*tert*-butylpyridine (2.4 μl, 10.5 μmol) and a molecular sieve. The ¹H NMR spectrum was recorded immediately and then repeated after suitable time intervals. At the end of the reaction (12 hours), the mixture was passed through a silica plug (to remove catalyst and molecular sieve), the solvent was removed and the product obtained as a colourless oil (113 mg, 75% yield). Addition of a 1:1 solution of 2M HCl/THF (4 ml) removed the silylenol ether group, yielding hydroxyketone product as an off-white oil, after silica gel chromatography (with EtOAc/hexane 3:17 as eluent). The optical rotation was measured at $[\alpha_D]^{25} = 0$.

General Preparation of Substrate Coordinated Complexes (4.14, 4.21)

To a CD₂Cl₂ (1 ml) solution of **(2.26)** (15 mg, 22 μmol) and substrate (26.5 μmol) was added AgSbF₆ (10 mg, 29 μmol) and 4Å molecular sieves. The resulting suspension was stirred for 30 minutes (in darkness) prior to being filtered by using a canula (to remove AgCl and molecular sieves) into a Young's tap NMR tube.

In situ preparation of [Ru(methacrolein)(ⁱPr-pymox)(mes)](SbF₆)₂ (4.14)

Following the general synthesis, with methacrolein (2.2 μl, 26.5 μmol) as substrate. ¹H NMR (CD₂Cl₂, 400 MHz, 300K): δ 0.70 (d, 3H, {J = 6.5 Hz}, CHMeMe'), 1.15 (d, 3H, {J = 6.5 Hz}, CHMeMe'), 1.74 (s, 3H, CHOC{=CH₂}Me), 2.30 (s, 9H, C₆H₃Me₃), 2.30 (m, 1H, CHMeMe'), 4.89 (m, 1H, OCH), 5.12 (m, 1H, OCH'), 5.38 (m, 1H, NCH), 5.65 (s, 3H, C₆H₃Me₃), 6.59 (d, 1H, {J = 0.5 Hz}, CHOC{=CH^{up}H}Me), 6.70 (d, 1H, {J = 0.5 Hz}, CHOC{=CH^{down}}Me), 8.00 (m, 1H, Py-5-*H*), 8.10 (td, 1H, {J = 5.5, 1.5 Hz}, Py-3-*H*), 8.29 (m, 1H, Py-4-*H*), 9.10 (s, 1H, CHOC{=CH₂}Me), 9.62 (d, 1H, {J = 5 Hz}, Py-6-*H*).

In situ preparation of [Ru(benzaldehyde)(ⁱPr-pymox)(mes)](SbF₆)₂ (4.21)

Following the general synthesis, with benzaldehyde (2.7 μl, 26.5 μmol) as substrate. ¹H NMR (CD₂Cl₂, 400 MHz, 300K): δ 0.60 (d, 3H, {J = 6.5 Hz}, CHMeMe'),

1.07 (d, 3H, {J = 6.5 Hz}, CHMeMe'), 2.21 (s, 9H, C₆H₃Me₃), 2.37 (m, 1H, CHMeMe'), 4.78 (m, 1H, OCH), 5.06 (m, 1H, OCH'), 5.06 (m, 1H, NCH), 5.60 (s, 3H, C₆H₃Me₃), 7.48 (m, 2H, PhCHO), 7.57 (m, 1H, PhCHO), 7.79 (m, 2H, PhCHO), 7.88 (d, 1H, {J = 5 Hz}, Py-3-H), 8.03 (m, 1H, Py-4-H), 8.18 (m, 1H, Py-5-H), 9.40 (s, 1H, PhCHO), 9.63 (d, 1H, {J = 5.5 Hz}, Py-6-H).

Appendix

APPENDIX

Figure (5.1): Graph to calculate Rate Constants for Epimerisation of [RuCl(ⁱPr-pymox)(mes)]SbF₆ (2.26) at 313 K (40°C).

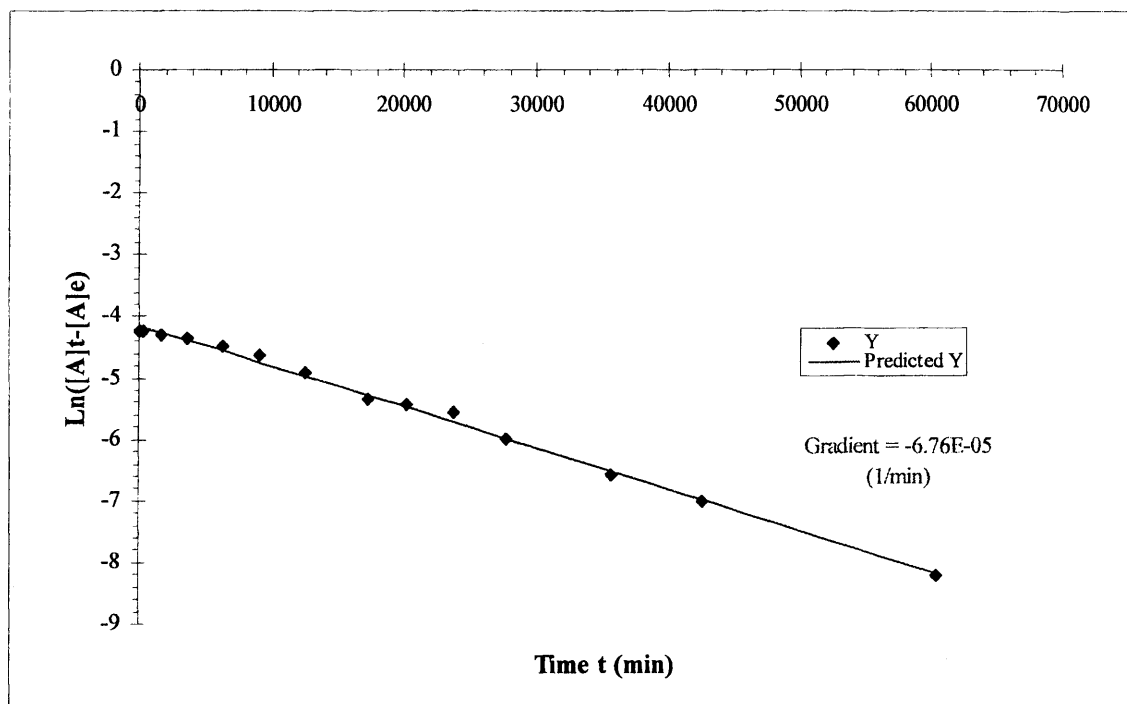


Figure (5.2): Graph to calculate Rate Constants for Epimerisation of [RuBr(ⁱPr-pymox)(mes)]SbF₆ (2.27) at 313 K (40°C)

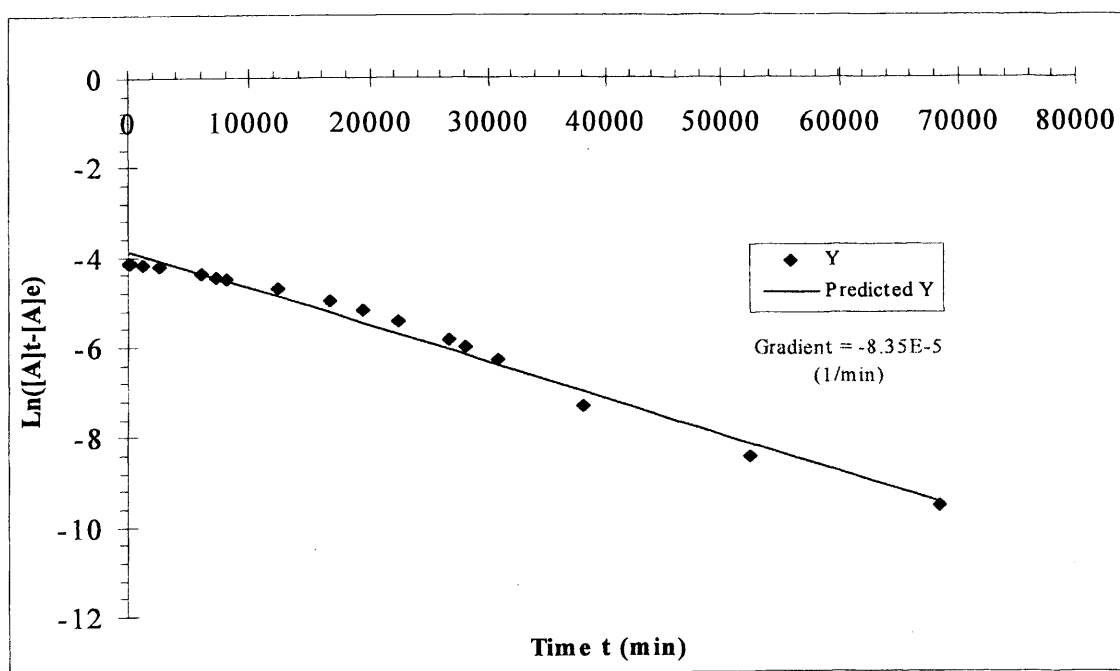


Figure (5.3): Graph to calculate Rate Constants for Epimerisation of [RuBr(ⁱPr-pymox)(mes)]SbF₆ (2.27) at 327 K (54°C)

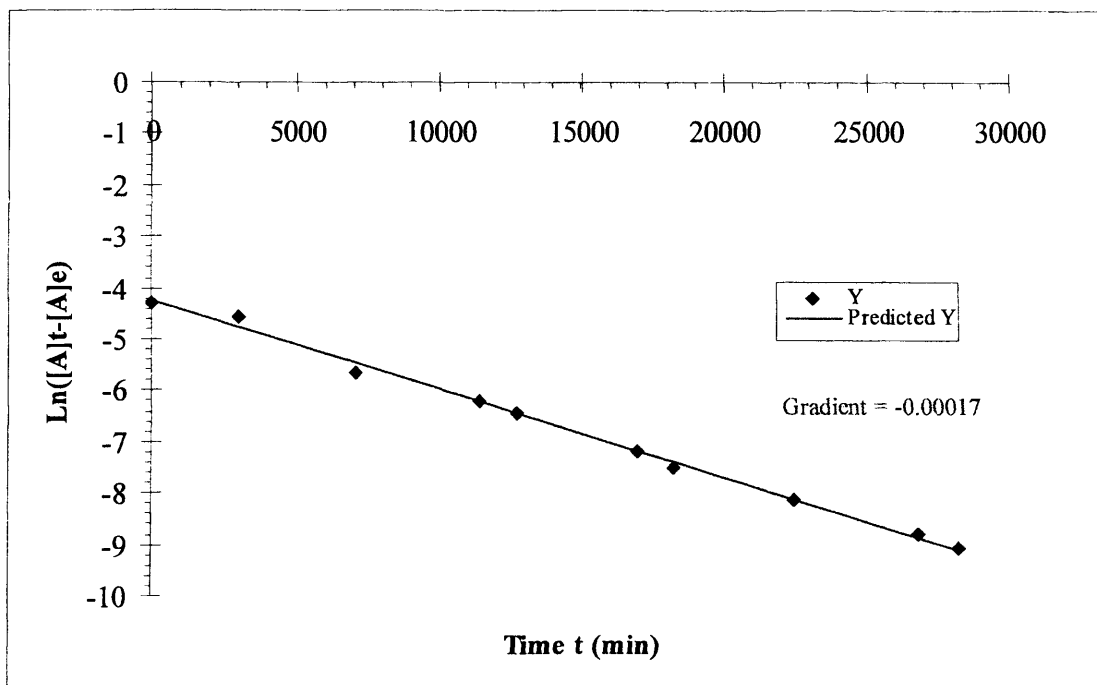


Figure (5.4): Graph to calculate Rate Constants for Epimerisation of [RuBr(ⁱPr-pymox)(mes)]SbF₆ (2.27) at 333 K (60°C)

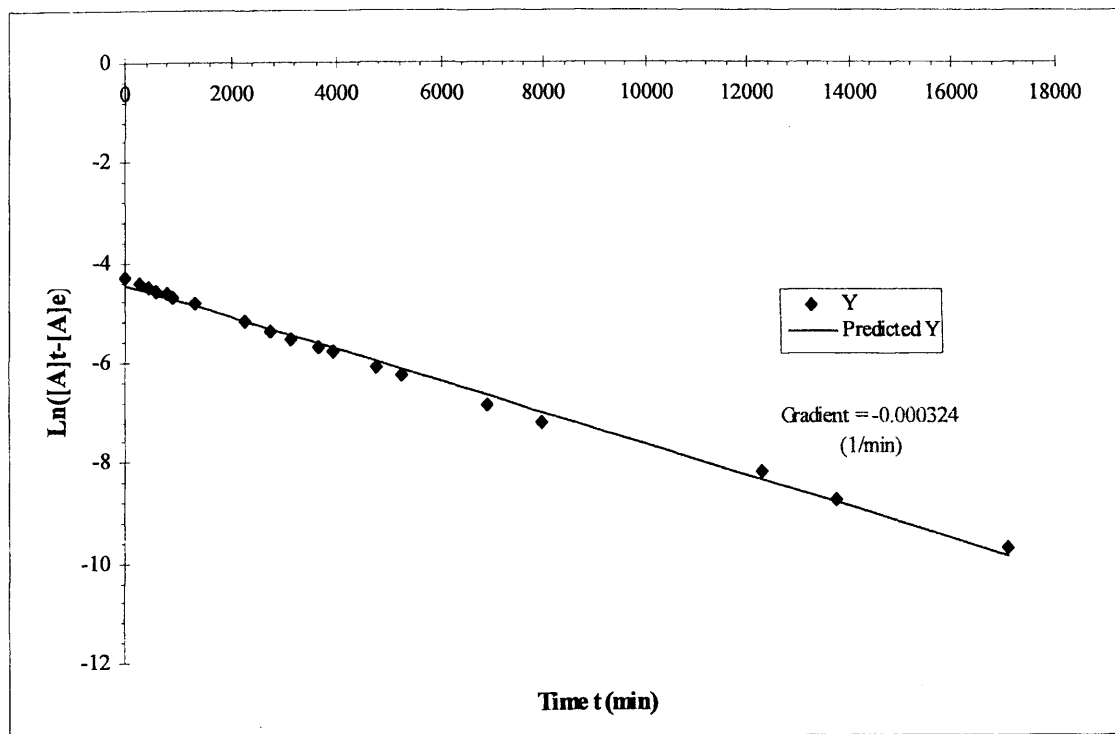


Figure (5.5): Graph to calculate Rate Constants for Epimerisation of [RuI(ⁱPr-pymox)(mes)]SbF₆ (2.27) at 313 K (40°C)

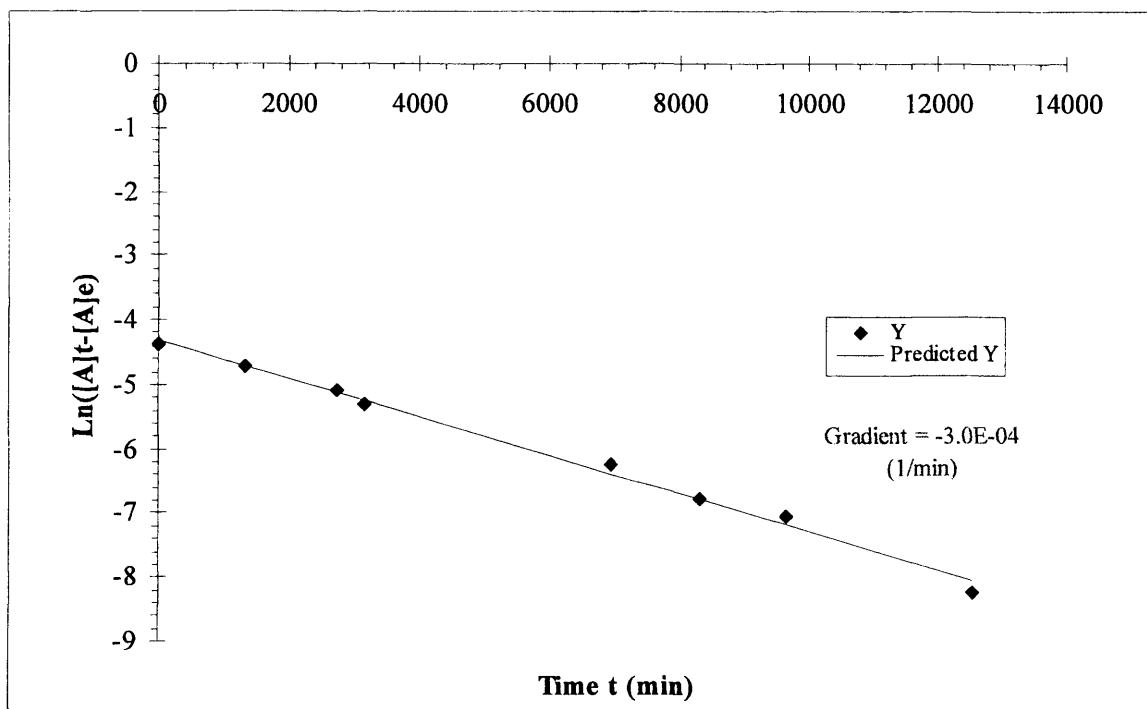


Figure (5.6): Graph to calculate Rate constants for Epimerisation of [RuCl(Ph₂-pymimH)(mes)]SbF₆ (2.43) at 317 K (44°C).

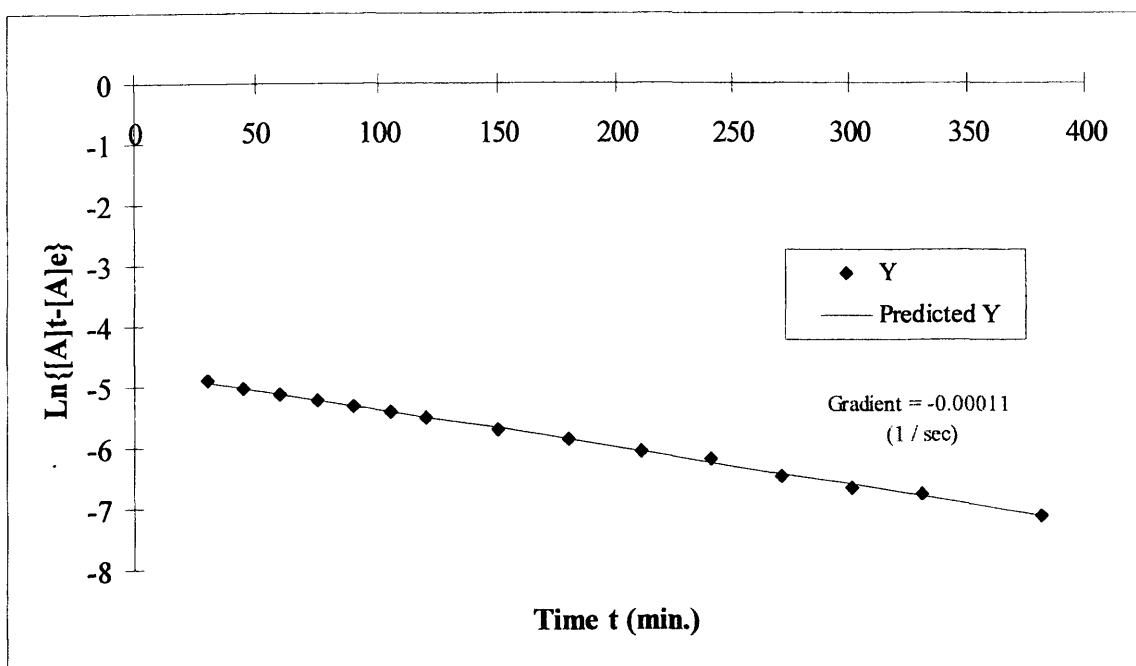


Figure (5.7): Graph to calculate Rate Constants for Epimerisation of $[\text{RuCl}(\text{Ph}_2\text{-pymimH})(\text{mes})]\text{SbF}_6$ (2.43) at 320 K (47°C).

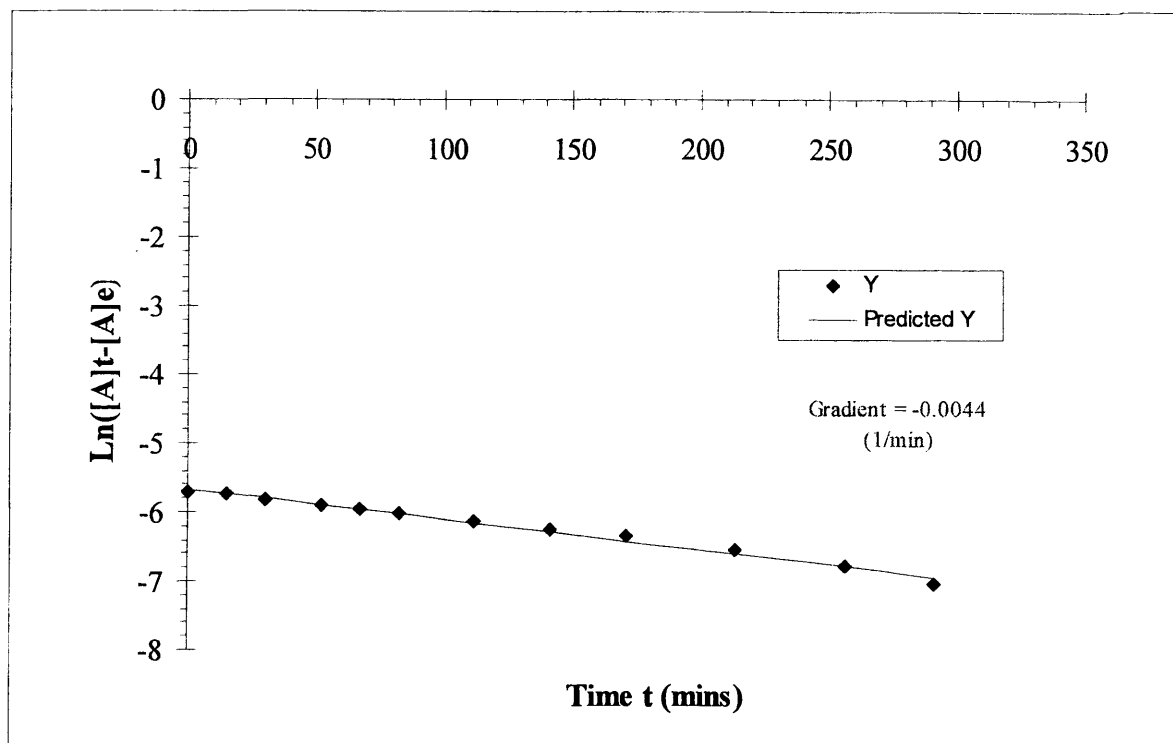


Figure (5.8): Graph to calculate Rate Constants for Epimerisation of $[\text{RuCl}(\text{Ph}_2\text{-pymimH})(\text{mes})]\text{SbF}_6$ (2.43) at 323 K (50°C).

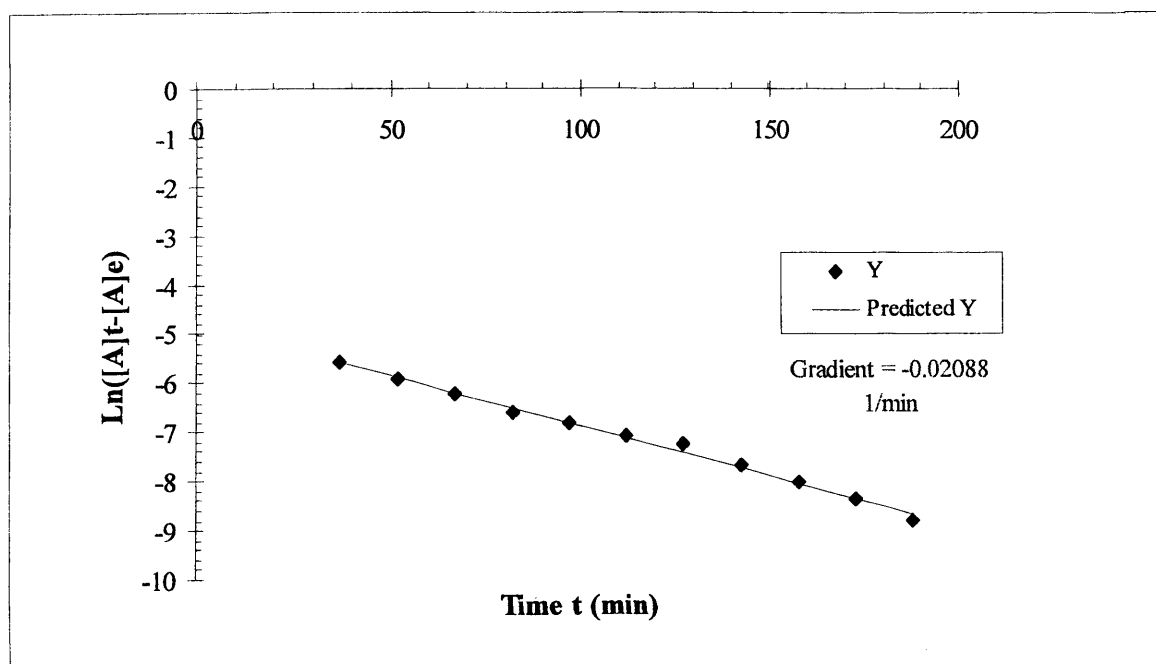


Figure (5.9): Graph to calculate Rate Constants for Epimerisation of [RuCl(Ph₂-pymimMe)(mes)]SbF₆ (2.44) at 323 K (50°C)

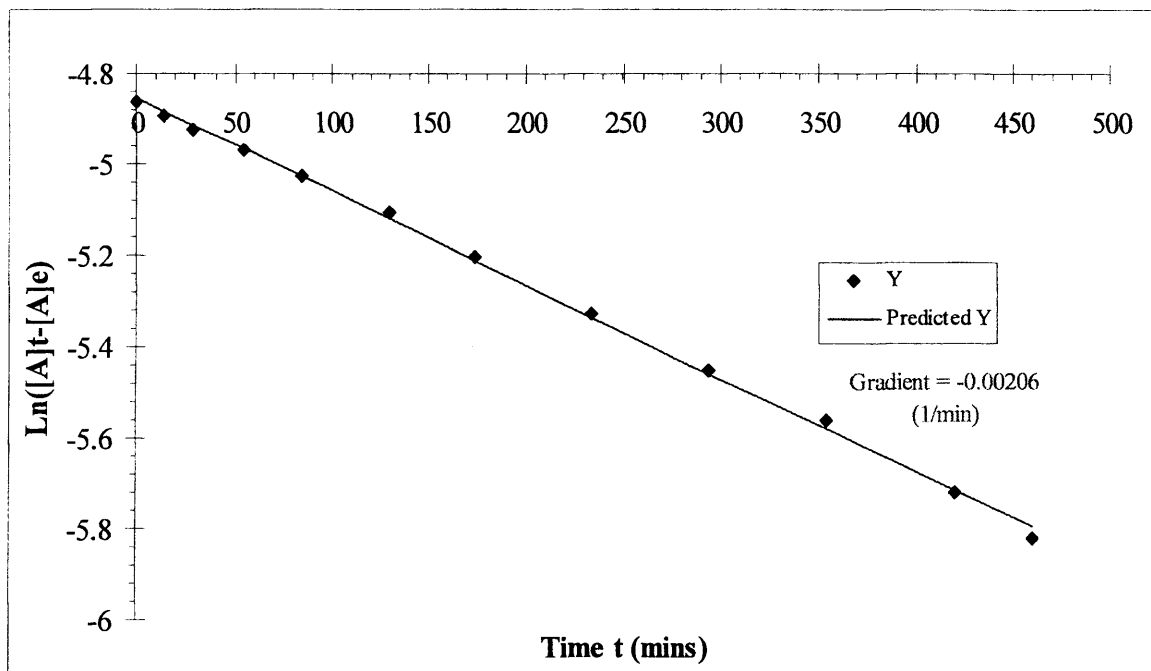
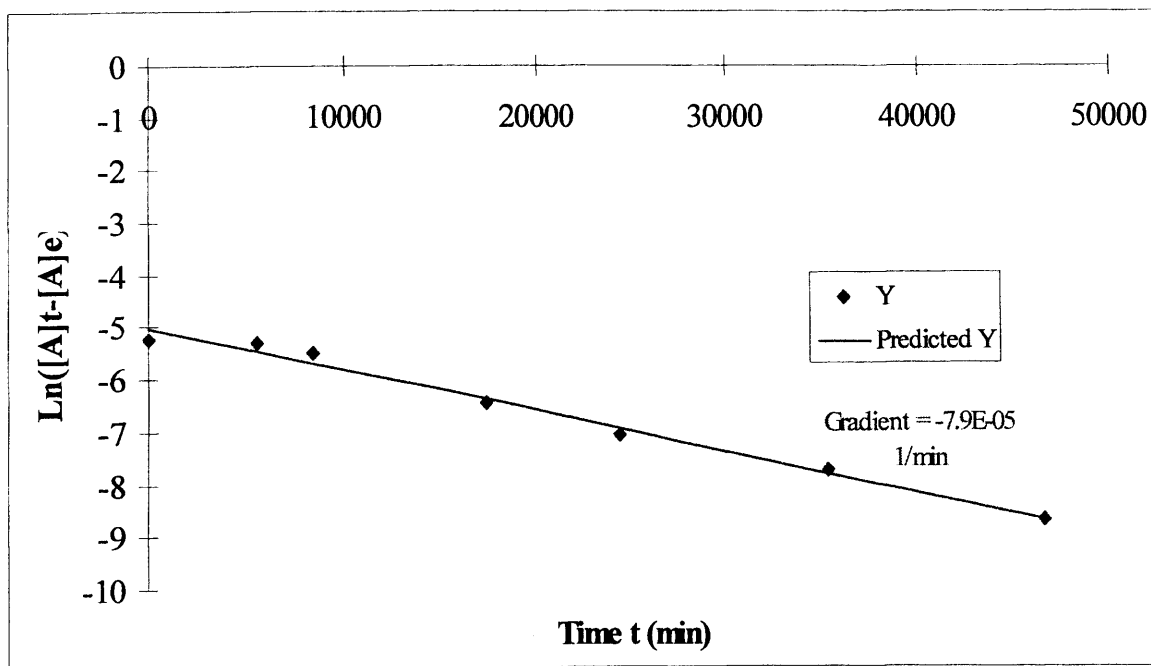


Figure (5.10): Graph to calculate Rate Constants of Epimerisation for [RuCl(Ph-pymox)(mes)]SbF₆ (1.42, R = Ph) at 313 K (40°C)



**Figure (5.11): Eyring Plot for $[\text{RuBr}(\text{}^i\text{Pr-pymox})(\text{mes})]\text{SbF}_6$ (2.27)
between 313 K and 333 K.**

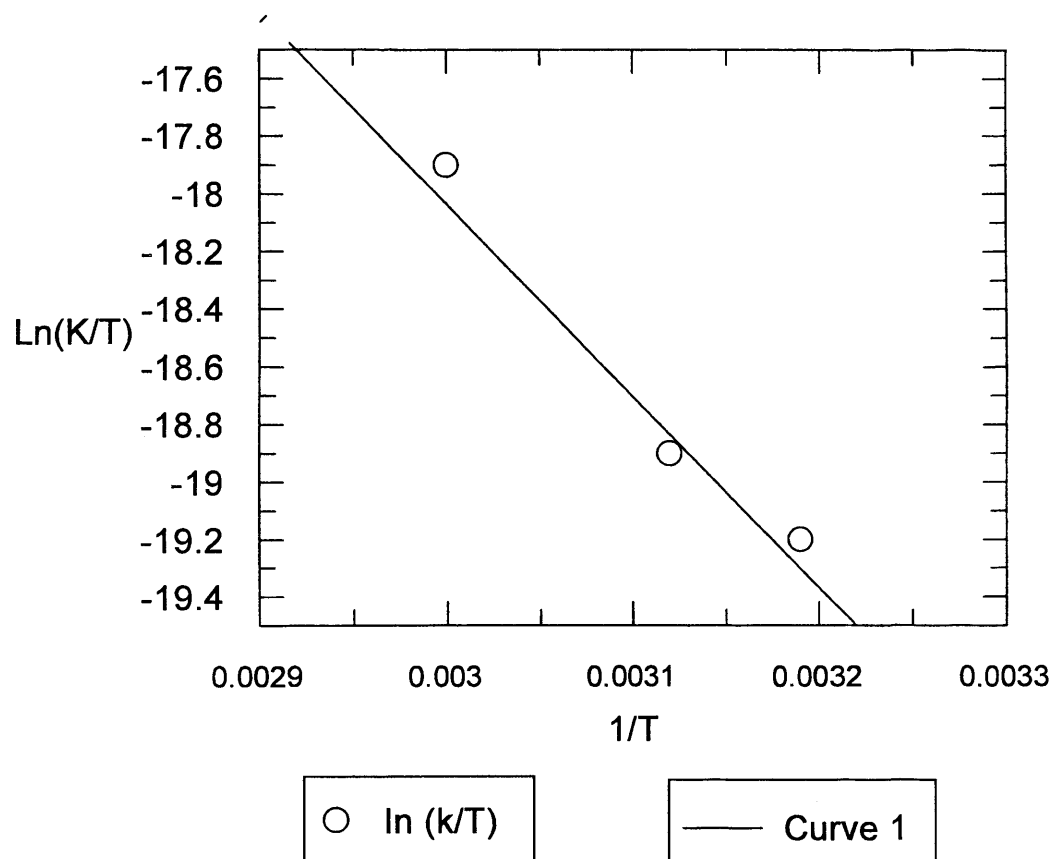


Table (5.1): Crystal data and structure refinement for (2.11)

Empirical formula	C21 H27 Cl N O2 Rh	
Formula weight	463.80	
Temperature	190 (2) K	
Wavelength	0.71073 Å	
Crystal system	Monoclinic	
Space group	P2(1) / c	
Unit cell dimensions	a = 10.238(2) Å	$\alpha = 90^\circ$.
	b = 13.548(3) Å	$\beta = 91.1(2)^\circ$.
	c = 14.959(3) Å	$\gamma = 90^\circ$.
Volume	2074.5(7) Å ³	
Z	4	
Density (calculated)	1.485 Mg/m ³	
Absorption coefficient	0.966 mm ⁻¹	
F(000)	952	
Crystal size	0.33 x 0.16 x 0.15 mm ³	
Theta range for data collection	2.72 to 25.00°.	
Index ranges	-1 ≤ h ≤ 12, -1 ≤ k ≤ 16, -17 ≤ l ≤ 17	
Reflections collected	4360	
Independent reflections	3631 [R(int) = 0.0246]	
Completeness to theta = 27.02°	1.039	
Absorption correction	Psi Scan:Xemp,Shelxtlpc	
Max. and min. transmission	0.778 and 0.691	
Refinement method	Full-matrix least-squares on F ²	
Data / restraints / parameters	3631 / 0 / 235	
Goodness-of-fit on F ²	1.039	
Final R indices [I > 2sigma(I)]	R1 = 0.0426, wR2 = 0.0994	
R indices (all data)	R1 = 0.0562, wR2 = 0.1082	
Largest diff. peak and hole	0.863 and -0.837 e.Å ⁻³	

Table (5.2): Crystal data and structure refinement for (2.15, R = ¹Pr)

Empirical formula	C22 H29 Cl N O2 Rh	
Formula weight	477.82	
Temperature	190(2) K	
Wavelength	0.71073 Å	
Crystal system	Orthorhombic	
Space group	P2(1)2(1)2(1)	
Unit cell dimensions	a = 7.978(1) Å	$\alpha = 90^\circ$.
	b = 10.496(1) Å	$\beta = 90^\circ$.
	c = 25.860(3) Å	$\gamma = 90^\circ$.
Volume	2165.5(5) Å ³	
Z	4	
Density (calculated)	1.466 Mg/m ³	
Absorption coefficient	0.928 mm ⁻¹	
F(000)	984	
Crystal size	0.48 x 0.27 x 0.18 mm ³	
Theta range for data collection	2.67 to 27.00°.	
Index ranges	-1 ≤ h ≤ 6, -1 ≤ k ≤ 13, -1 ≤ l ≤ 33	
Reflections collected	2667	
Independent reflections	2489 [R(int) = 0.0395]	
Absorption correction	Psi-scan	
Max. and min. transmission	0.810 and 0.569	
Refinement method	Full-matrix least-squares on F ²	
Data / restraints / parameters	2489 / 0 / 244	
Goodness-of-fit on F ²	1.070	
Final R indices [I > 2sigma(I)]	R1 = 0.0303, wR2 = 0.0711	
R indices (all data)	R1 = 0.0376, wR2 = 0.0781	
Absolute structure parameter	-0.08(6)	
Largest diff. peak and hole	0.462 and -0.466 e.Å ⁻³	

Table (5.3): Crystal data and structure refinement for (2.12, R = 'Pr)

Empirical formula	C ₂₁ H ₂₆ Cl N O ₂ Ru	
Formula weight	460.95	
Temperature	190(2) K	
Wavelength	0.71073 Å	
Crystal system	Tetragonal	
Space group	P4(1)2(1)2	
Unit cell dimensions	a = 12.259(2) Å	α = 90°.
	b = 12.284(5) Å	β = 90°.
	c = 27.260(13) Å	γ = 90°.
Volume	4105.2(25) Å ³	
Z	8	
Density (calculated)	1.492 Mg/m ³	
Absorption coefficient	0.908 mm ⁻¹	
F(000)	1888	
Crystal size	0.11 x 0.42 x 0.55 mm ³	
Theta range for data collection	2.78 to 25.97°.	
Index ranges	0 ≤ h ≤ 15, -1 ≤ k ≤ 15, -1 ≤ l ≤ 33	
Reflections collected	4694	
Independent reflections	3846 [R(int) = 0.0415]	
Absorption correction	None	
Refinement method	Full-matrix least-squares on F ²	
Data / restraints / parameters	3845 / 0 / 235	
Goodness-of-fit on F ²	1.112	
Final R indices [I > 2σ(I)]	R1 = 0.0681, wR2 = 0.1475	
R indices (all data)	R1 = 0.1054, wR2 = 0.1815	
Absolute structure parameter	-0.11(13)	
Largest diff. peak and hole	1.082 and -1.514 e.Å ⁻³	

Table (5.4): Crystal data and structure refinement for (2.12, R = Ph)

Empirical formula	C ₂₅ H ₂₆ Cl ₃ N O ₂ Ru (with CH ₂ Cl ₂)	
Formula weight	579.89	
Temperature	190(2) K	
Wavelength	0.71073 Å	
Crystal system	Monoclinic	
Space group	P2~1~	
Unit cell dimensions	a = 7.737(1) Å	α = 90°.
	b = 16.171(1) Å	β =
	93.38(1)°.	
	c = 9.984(1) Å	γ = 90°.
Volume	1247.0(2) Å ³	
Z	2	
Density (calculated)	1.544 Mg/m ³	
Absorption coefficient	0.972 mm ⁻¹	
F(000)	588	
Crystal size	0.64 x 0.46 x 0.33 mm ³	
Theta range for data collection	2.04 to 27.00°.	
Index ranges	-1 ≤ h ≤ 9, -20 ≤ k ≤ 1, -12 ≤ l ≤ 12	
Reflections collected	3353	
Independent reflections	3008 [R(int) = 0.0185]	
Absorption correction	Psi scan (XEMP; SHELXTL/PC)	
Max. and min. transmission	0.694 and 0.517	
Refinement method	Full-matrix least-squares on F ²	
Data / restraints / parameters	3008 / 1 / 270	
Goodness-of-fit on F ²	1.062	
Final R indices [I > 2σ(I)]	R1 = 0.1096, wR2 = 0.3056	
R indices (all data)	R1 = 0.1104, wR2 = 0.3065	
Absolute structure parameter	0.05(17)	
Largest diff. peak and hole	6.255 and -1.915 e.Å ⁻³	

Table (5.5): Crystal data and structure refinement for (2.13, R = 'Bu)

Empirical formula	C23 H30 Cl N O2 Ru	
Formula weight	489.00	
Temperature	190(2) K	
Wavelength	0.71073 Å	
Crystal system	Ortorhombic	
Space group	P2(1)2(1)2(1)	
Unit cell dimensions	a = 6.666(1) Å	$\alpha = 90^\circ$.
	b = 17.697(5) Å	$\beta = 90^\circ$.
	c = 18.595(8) Å	$\gamma = 90^\circ$.
Volume	2193.6(12) Å ³	
Z	4	
Density (calculated)	1.481 Mg/m ³	
Absorption coefficient	0.854 mm ⁻¹	
F(000)	1008	
Crystal size	0.76 x 0.20 x 0.12 mm ³	
Theta range for data collection	2.19 to 26.97°.	
Index ranges	-8 ≤ h ≤ 0, -22 ≤ k ≤ 1, -23 ≤ l ≤ 1	
Reflections collected	3049	
Independent reflections	2982 [R(int) = 0.0376]	
Absorption correction	Psi-scan (XEMP; SHELXTL/PC ver5.0)	
Max. and min. transmission	0.734 and 0.547	
Refinement method	Full-matrix least-squares on F ²	
Data / restraints / parameters	2982 / 0 / 253	
Goodness-of-fit on F ²	1.049	
Final R indices [I > 2σ(I)]	R1 = 0.0383, wR2 = 0.0916	
R indices (all data)	R1 = 0.0443, wR2 = 0.0962	
Absolute structure parameter	-0.05(5)	
Largest diff. peak and hole	0.980 and -1.126 e.Å ⁻³	

Table (5.6): Crystal data and structure refinement for (2.16)

Empirical formula	C22 H29 Cl2 F6 N O3 Rh Sb	
Formula weight	765.02	
Temperature	190(2) K	
Wavelength	0.71073 Å	
Crystal system	Triclinic	
Space group	P-1	
Unit cell dimensions	a = 9.403(2) Å	$\alpha = 79.92(2)^\circ$.
	b = 11.130(3) Å	$\beta = 77.22(2)^\circ$.
	c = 14.418(3) Å	$\gamma = 87.33(3)^\circ$.
Volume	1448.8(6) Å ³	
Z	2	
Density (calculated)	1.754 Mg/m ³	
Absorption coefficient	1.748 mm ⁻¹	
F(000)	752	
Crystal size	0.32 x 0.26 x 0.18 mm ³	
Theta range for data collection	2.22 to 27.00°.	
Index ranges	0 ≤ h ≤ 11, -13 ≤ k ≤ 13, -17 ≤ l ≤ 18	
Reflections collected	6425	
Independent reflections	6077 [R(int) = 0.0190]	
Absorption correction	None	
Max. and min. transmission	0.732 and 0.525	
Refinement method	Full-matrix least-squares on F ²	
Data / restraints / parameters	6077 / 6 / 361	
Goodness-of-fit on F ²	1.076	
Final R indices [I > 2σ(I)]	R1 = 0.0476, wR2 = 0.1306	
R indices (all data)	R1 = 0.0558, wR2 = 0.1390	
Largest diff. peak and hole	1.884 and -0.819 e.Å ⁻³	

Table (5.7): Crystal data and structure refinement for (2.20, L^m = 4-Me-py)

Empirical formula	C27 H33 F6 N2 O2 RuSb	
Formula weight	754.37	
Temperature	190(2) K	
Wavelength	0.71073 Å	
Crystal system	Orthorhombic	
Space group	P2(1)2(1)2(1)	
Unit cell dimensions	a = 10.561(3) Å	α = 90°.
	b = 16.194(5) Å	β = 90°.
	c = 16.851(5) Å	γ = 90°.
Volume	2881.9(12) Å ³	
Z	4	
Density (calculated)	1.739 Mg/m ³	
Absorption coefficient	1.527 mm ⁻¹	
F(000)	1496	
Crystal size	0.62 x 0.09 x 0.08 mm ³	
Theta range for data collection	2.52 to 25.99°.	
Index ranges	0 ≤ h ≤ 13, -19 ≤ k ≤ 1, -1 ≤ l ≤ 20	
Reflections collected	3376	
Independent reflections	3302 [R(int) = 0.0273]	
Absorption correction	Psi-scan (XEMP; SHELXTL/PC ver5.0)	
Max. and min. transmission	0.877 and 0.678	
Refinement method	Full-matrix least-squares on F ²	
Data / restraints / parameters	3302 / 0 / 352	
Goodness-of-fit on F ²	1.004	
Final R indices [I > 2σ(I)]	R1 = 0.0567, wR2 = 0.1252	
R indices (all data)	R1 = 0.0879, wR2 = 0.1433	
Absolute structure parameter	-0.04(7)	
Largest diff. peak and hole	1.243 and -0.751 e.Å ⁻³	

Table (5.8): Crystal data and structure refinement for (2.27 A)

Empirical formula	C20 H26 Br F6 N2 O Ru Sb	
Formula weight	727.16	
Temperature	200(2) K	
Wavelength	0.71073 Å	
Crystal system	Orthorhombic	
Space group	P2(1)2(1)2(1)	
Unit cell dimensions	a = 7.7030(7) Å	α = 90°.
	b = 12.0995(17) Å	β = 90°.
	c = 27.223(2) Å	γ = 90°.
Volume	2537.2(5) Å ³	
Z	4	
Density (calculated)	1.904 Mg/m ³	
Absorption coefficient	3.293 mm ⁻¹	
F(000)	1408	
Crystal size	0.72 x 0.34 x 0.29 mm ³	
Theta range for data collection	1.84 to 25.99°.	
Index ranges	0 ≤ h ≤ 9, -1 ≤ k ≤ 14, -33 ≤ l ≤ 1	
Reflections collected	3234	
Independent reflections	3152 [R(int) = 0.0238]	
Completeness to theta = 25.99°	99.2 %	
Absorption correction	Psi scan	
Max. and min. transmission	0.49 and 0.41	
Refinement method	Full-matrix least-squares on F ²	
Data / restraints / parameters	3152 / 0 / 290	
Goodness-of-fit on F ²	1.058	
Final R indices [I > 2σ(I)]	R1 = 0.0579, wR2 = 0.1566	
R indices (all data)	R1 = 0.0871, wR2 = 0.1804	
Absolute structure parameter	-0.06(4)	
Extinction coefficient	0.0020(4)	
Largest diff. peak and hole	1.344 and -0.900 e.Å ⁻³	

Table (5.9): Crystal data and structure refinement for (2.27 B)

Empirical formula	C20 H26 Br F6 N2 O Ru Sb	
Formula weight	727.16	
Temperature	190(2) K	
Wavelength	0.71073 Å	
Crystal system	Orthorhombic	
Space group	P2(1)2(1)2(1)	
Unit cell dimensions	a = 8.5892(9) Å	$\alpha = 90^\circ$.
	b = 9.5732(14) Å	$\beta = 90^\circ$.
	c = 29.369(3) Å	$\gamma = 90^\circ$.
Volume	2414.9(5) Å ³	
Z	4	
Density (calculated)	2.000 Mg/m ³	
Absorption coefficient	3.460 mm ⁻¹	
F(000)	1408	
Crystal size	0.44 x 0.36 x 0.24 mm ³	
Theta range for data collection	2.24 to 27.00°.	
Index ranges	-10 ≤ h ≤ 1, -1 ≤ k ≤ 12, -1 ≤ l ≤ 37	
Reflections collected	3782	
Independent reflections	3570 [R(int) = 0.0429]	
Absorption correction	Analytical SHELXTL/PC	
Max. and min. transmission	0.411 and 0.273	
Refinement method	Full-matrix least-squares on F ²	
Data / restraints / parameters	3569 / 0 / 289	
Goodness-of-fit on F ²	1.090	
Final R indices [I > 2σ(I)]	R1 = 0.0534, wR2 = 0.1326	
R indices (all data)	R1 = 0.0587, wR2 = 0.1364	
Absolute structure parameter	0.00(3)	
Largest diff. peak and hole	1.134 and -2.099 e.Å ⁻³	

Table (5.10): Crystal data and structure refinement for (2.43)

Empirical formula	C29 H29 Cl F6 N3 Ru Sb	
Formula weight	791.82	
Temperature	200(2) K	
Wavelength	0.71073 Å	
Crystal system	Orthorhombic	
Space group	P2(1)2(1)2(1)	
Unit cell dimensions	a = 8.159(3) Å	$\alpha = 90^\circ$.
	b = 17.370(5) Å	$\beta = 90^\circ$.
	c = 21.182(7) Å	$\gamma = 90^\circ$.
Volume	3002.0(17) Å ³	
Z	4	
Density (calculated)	1.752 Mg/m ³	
Absorption coefficient	1.553 mm ⁻¹	
F(000)	1560	
Crystal size	0.44 x 0.26 x 0.20 mm ³	
Theta range for data collection	1.92 to 26.99°.	
Index ranges	-10 ≤ h ≤ 0, -22 ≤ k ≤ 1, -27 ≤ l ≤ 1	
Reflections collected	4137	
Independent reflections	4051 [R(int) = 0.0192]	
Completeness to theta = 26.99°	99.6 %	
Absorption correction	Psi scan (XEMP; SHELXL-97)	
Max. and min. transmission	0.58 and 0.47	
Refinement method	Full-matrix least-squares on F ²	
Data / restraints / parameters	4051 / 0 / 370	
Goodness-of-fit on F ²	1.088	
Final R indices [I > 2σ(I)]	R1 = 0.0471, wR2 = 0.0931	
R indices (all data)	R1 = 0.0742, wR2 = 0.1064	
Absolute structure parameter	-0.07(5)	
Largest diff. peak and hole	1.047 and -0.816 e.Å ⁻³	

Table (5.11): Crystal data and structure refinement for (2.44)

Empirical formula	C30 H31 Cl F6 N3 Ru Sb	
Formula weight	805.85	
Temperature	195 K	
Wavelength	0.71073 Å	
Crystal system	Orthorhombic	
Space group	P2(1)2(1)2(1)	
Unit cell dimensions	a = 8.566(3) Å	$\alpha = 90^\circ$.
	b = 17.569(8) Å	$\beta = 90^\circ$.
	c = 20.345(5) Å	$\gamma = 90^\circ$.
Volume	3062(2) Å ³	
Z	4	
Density (calculated)	1.748 Mg/m ³	
Absorption coefficient	1.525 mm ⁻¹	
F(000)	1592	
Crystal size	0.54 x 0.50 x 0.15 mm ³	
Theta range for data collection	2.00 to 27.02°	
Index ranges	0 ≤ h ≤ 10, -22 ≤ k ≤ 1, -25 ≤ l ≤ 1	
Reflections collected	4130	
Independent reflections	4049 [R(int) = 0.0361]	
Completeness to theta = 27.02°	99.1 %	
Absorption correction	Psi Scan:Xemp,Shelxtpc	
Max. and min. transmission	0.432 and 0.324	
Refinement method	Full-matrix least-squares on F ²	
Data / restraints / parameters	4049 / 0 / 379	
Goodness-of-fit on F ²	1.038	
Final R indices [I > 2sigma(I)]	R1 = 0.0461, wR2 = 0.1050	
R indices (all data)	R1 = 0.0615, wR2 = 0.1130	
Absolute structure parameter	-0.03(4)	
Largest diff. peak and hole	1.596 and -0.844 e.Å ⁻³	

Table (5.12): Crystal data and structure refinement for (2.46)

Empirical formula	C24 H35 Cl F6 N3 Ru Sb	
Formula weight	737.82	
Temperature	200(2) K	
Wavelength	0.71073 Å	
Crystal system	Orthorhombic	
Space group	P2(1)2(1)2(1)	
Unit cell dimensions	a = 9.0831(10) Å	$\alpha = 90^\circ$.
	b = 15.031(4) Å	$\beta = 90^\circ$.
	c = 20.902(3) Å	$\gamma = 90^\circ$.
Volume	2853.8(8) Å ³	
Z	4	
Density (calculated)	1.717 Mg/m ³	
Absorption coefficient	1.626 mm ⁻¹	
F(000)	1464	
Crystal size	0.51 x 0.42 x 0.37 mm ³	
Theta range for data collection	1.95 to 48.03°	
Index ranges	-19 ≤ h ≤ 1, -21 ≤ k ≤ 0, -29 ≤ l ≤ 11	
Reflections collected	5453	
Independent reflections	5249 [R(int) = 0.0185]	
Completeness to theta = 48.03°	31.3 %	
Absorption correction	Psi scan (XEMP; SHELXTL/PC)	
Refinement method	Full-matrix least-squares on F ²	
Data / restraints / parameters	5249 / 0 / 361	
Goodness-of-fit on F ²	1.033	
Final R indices [I > 2sigma(I)]	R1 = 0.0421, wR2 = 0.0847	
R indices (all data)	R1 = 0.0652, wR2 = 0.0943	
Absolute structure parameter	-0.07(4)	
Largest diff. peak and hole	1.051 and -0.960 e.Å ⁻³	

Table (5.13): Crystal data and structure refinement for (2.47)

Empirical formula	C ₂₈ H ₃₅ Cl F ₆ N ₃ Ru Sb	
Formula weight	785.86	
Temperature	200(2) K	
Wavelength	0.71073 Å	
Crystal system	Orthorhombic	
Space group	P2(1)2(1)2(1)	
Unit cell dimensions	a = 8.0067(13) Å	α = 90°.
	b = 17.323(2) Å	β = 90°.
	c = 22.141(3) Å	γ = 90°.
Volume	3071.0(7) Å ³	
Z	4	
Density (calculated)	1.700 Mg/m ³	
Absorption coefficient	1.517 mm ⁻¹	
F(000)	1560	
Crystal size	0.74 x 0.30 x 0.17 mm ³	
Theta range for data collection	2.18 to 27.00°.	
Index ranges	0 ≤ h ≤ 9, -1 ≤ k ≤ 22, -1 ≤ l ≤ 28	
Reflections collected	3920	
Independent reflections	3854 [R(int) = 0.0485]	
Absorption correction	Psi scan (XEMP; SHELXTL/PC ver5.0)	
Max. and min. transmission	0.652 and 0.569	
Refinement method	Full-matrix least-squares on F ²	
Data / restraints / parameters	3854 / 0 / 362	
Goodness-of-fit on F ²	1.008	
Final R indices [I > 2σ(I)]	R1 = 0.0542, wR2 = 0.1340	
R indices (all data)	R1 = 0.0724, wR2 = 0.1621	
Absolute structure parameter	-0.01(7)	
Extinction coefficient	0.0015(3)	
Largest diff. peak and hole	1.051 and -1.616 e.Å ⁻³	

Table (5.14): Crystal data and structure refinement for (2.49)

Empirical formula	C ₃₀ H ₃₂ Cl F ₆ N ₂ Ru Sb	
Formula weight	792.85	
Temperature	190 (2) K	
Wavelength	0.71073 Å	
Crystal system	Monoclinic	
Space group	P2(1)	
Unit cell dimensions	a = 8.141(2) Å	α = 90°.
	b = 10.849(2) Å	β = 94.18(2)°.
	c = 17.313(2) Å	γ = 90°.
Volume	1525.2(5) Å ³	
Z	2	
Density (calculated)	1.726 Mg/m ³	
Absorption coefficient	1.528 mm ⁻¹	
F(000)	784	
Crystal size	0.80 x 0.76 x 0.60 mm ³	
Theta range for data collection	2.22 to 31.01°.	
Index ranges	0 ≤ h ≤ 11, -10 ≤ k ≤ 15, -25 ≤ l ≤ 25	
Reflections collected	7104	
Independent reflections	6662 [R(int) = 0.0227]	
Absorption correction	Psi Scan:Xemp,Shelxtlpc	
Max. and min. transmission	0.271 and 0.230	
Refinement method	Full-matrix least-squares on F ²	
Data / restraints / parameters	6662 / 1 / 407	
Goodness-of-fit on F ²	1.065	
Final R indices [I > 2σ(I)]	R1 = 0.0321, wR2 = 0.0840	
R indices (all data)	R1 = 0.0338, wR2 = 0.0856	
Absolute structure parameter	0.15(2)	
Largest diff. peak and hole	0.520 and -1.141 e.Å ⁻³	

Table (5.15): Crystal data and structure refinement for (3.25)

Empirical formula	C15 H23 N O Sn	
Formula weight	352.03	
Temperature	190(2) K	
Wavelength	0.71073 Å	
Crystal system	Orthorhombic	
Space group	P2(1)2(1)2(1)	
Unit cell dimensions	a = 7.7059(17) Å	$\alpha = 90^\circ$.
	b = 11.2951(18) Å	$\beta = 90^\circ$.
	c = 18.111(6) Å	$\gamma = 90^\circ$.
Volume	1576.4(7) Å ³	
Z	4	
Density (calculated)	1.483 Mg/m ³	
Absorption coefficient	1.611 mm ⁻¹	
F(000)	712	
Crystal size	0.44 x 0.42 x 0.23 mm ³	
Theta range for data collection	2.12 to 26.01°	
Index ranges	-9<=h<=1, -1<=k<=13, -22<=l<=1	
Reflections collected	2399	
Independent reflections	2223 [R(int) = 0.0418]	
Completeness to theta = 26.01°	99.8 %	
Absorption correction	Psi-scan	
Max. and min. transmission	0.218 and 0.163	
Refinement method	Full-matrix least-squares on F ²	
Data / restraints / parameters	2223 / 0 / 166	
Goodness-of-fit on F ²	1.038	
Final R indices [I>2sigma(I)]	R1 = 0.0536, wR2 = 0.1304	
R indices (all data)	R1 = 0.0642, wR2 = 0.1382	
Absolute structure parameter	-0.01(8)	
Largest diff. peak and hole	1.413 and -1.775 e.Å ⁻³	

Table (5.16): Crystal data and structure refinement for (3.26)

Empirical formula	C14 H20 Cl N O Sn	
Formula weight	372.45	
Temperature	200(2) K	
Wavelength	0.71073 Å	
Crystal system	Orthorhombic	
Space group	P2(1)2(1)2(1)	
Unit cell dimensions	a = 7.570(2) Å	$\alpha = 90^\circ$.
	b = 13.984(5) Å	$\beta = 90^\circ$.
	c = 14.563(6) Å	$\gamma = 90^\circ$.
Volume	1541.6(9) Å ³	
Z	4	
Density (calculated)	1.605 Mg/m ³	
Absorption coefficient	1.820 mm ⁻¹	
F(000)	744	
Crystal size	0.58 x 0.27 x 0.18 mm ³	
Theta range for data collection	2.02 to 27.01°	
Index ranges	-1<=h<=9, -17<=k<=14, -15<=l<=18	
Reflections collected	5721	
Independent reflections	2797 [R(int) = 0.0635]	
Completeness to theta = 27.01°	100.0 %	
Absorption correction	Psi-scan	
Max. and min. transmission	0.771 and 0.465	
Refinement method	Full-matrix least-squares on F ²	
Data / restraints / parameters	2797 / 0 / 163	
Goodness-of-fit on F ²	1.031	
Final R indices [I>2sigma(I)]	R1 = 0.0357, wR2 = 0.0804	
R indices (all data)	R1 = 0.0433, wR2 = 0.0848	
Absolute structure parameter	0.01(6)	
Largest diff. peak and hole	0.539 and -0.673 e.Å ⁻³	

Table (5.17): Crystal data and structure refinement for (3.33)

Empirical formula	C ₂₈ H ₃₄ N ₂ O ₆ Pd ₂	
Formula weight	707.37	
Temperature	200(2) K	
Wavelength	0.71073 Å	
Crystal system	Triclinic	
Space group	P1	
Unit cell dimensions	a = 9.6973(15) Å	α = 83.799(13)°
	b = 15.045(3) Å	β = 83.044(13)°
	c = 21.616(3) Å	γ = 73.291(13)°
Volume	2989.4(8) Å ³	
Z	4	
Density (calculated)	1.572 Mg/m ³	
Absorption coefficient	1.244 mm ⁻¹	
F(000)	1424	
Crystal size	0.62 x 0.27 x 0.23 mm ³	
Theta range for data collection	1.90 to 25.00°	
Index ranges	-11 ≤ h ≤ 0, -17 ≤ k ≤ 17, -25 ≤ l ≤ 25	
Reflections collected	11177	
Independent reflections	11177 [R(int) = 0.0000]	
Completeness to theta = 25.00°	99.7 %	
Absorption correction	Psi-scan	
Max. and min. transmission	0.77 and 0.67	
Refinement method	Full-matrix least-squares on F ²	
Data / restraints / parameters	11177 / 3 / 1369	
Goodness-of-fit on F ²	1.035	
Final R indices [I > 2σ(I)]	R1 = 0.0683, wR2 = 0.1684	
R indices (all data)	R1 = 0.0861, wR2 = 0.1831	
Absolute structure parameter	0.04(5)	
Largest diff. peak and hole	1.702 and -2.035 e.Å ⁻³	

Table (5.18): Crystal data and structure refinement for (3.37)

Empirical formula	C ₂₂ H ₂₈ Cl N O Ru	
Formula weight	458.97	
Temperature	200(2) K	
Wavelength	0.71073 Å	
Crystal system	Monoclinic	
Space group	P2(1)	
Unit cell dimensions	a = 12.343(2) Å	α = 90°
	b = 16.081(4) Å	β = 94.46(2)°
	c = 21.341(5) Å	γ = 90°
Volume	4223.2(17) Å ³	
Z	8	
Density (calculated)	1.444 Mg/m ³	
Absorption coefficient	0.879 mm ⁻¹	
F(000)	1888	
Crystal size	0.60 x 0.55 x 0.33 mm ³	
Theta range for data collection	1.85 to 26.00°	
Index ranges	-15 ≤ h ≤ 0, -1 ≤ k ≤ 19, -26 ≤ l ≤ 26	
Reflections collected	9242	
Independent reflections	8851 [R(int) = 0.1106]	
Completeness to theta = 26.00°	96.4 %	
Absorption correction	Analytical	
Max. and min. transmission	0.723 and 0.573	
Refinement method	Full-matrix least-squares on F ²	
Data / restraints / parameters	8851 / 1 / 941	
Goodness-of-fit on F ²	1.033	
Final R indices [I > 2σ(I)]	R1 = 0.0618, wR2 = 0.1546	
R indices (all data)	R1 = 0.0765, wR2 = 0.1671	
Absolute structure parameter	-0.01(5)	
Largest diff. peak and hole	1.170 and -2.441 e.Å ⁻³	

Bibliography

BIBLIOGRAPHY

- 1 B. Cornils, in 'Applied Homogeneous Catalysis with Organometallic Compounds', ed. B. Cornils and W. A. Hermann, Cambridge, 1996.
- 2 K. H. Dotz and J. Pfeiffer, in 'Transition Metals for Organic Synthesis', ed. M. Beller and C. Bolm, 1998.
- 3 B. Bosnich, *Encyclopedia of Inorganic chemistry*, 219.
- 4 G. Natta, R. Ercoli, and F. Calderazzo, *Chimica Industria*, 1958, **40**, 287.
- 5 M. F. Bailey and L. F. Dahl, *J. Am. Chem. Soc.*, 1965, 1298.
- 6 L. S. Hegedus, 'Transition Metals in the Synthesis of Complex Organic Molecules', University Science Books, 1999.
- 7 M. Uemura, R. Miyake, K. Nakayama, M. Shiro, and Y. Hayashi, *J. Org. Chem.*, 1993, **58**, 1238.
- 8 G. Winkaus and H. Singer, *J. Organomet. Chem.*, 1967, **7**, 487.
- 9 A. Davison, J. A. McCleverty, and G. Wilkinson, *J. Chem. Soc., Chem. Commun.*, 1963, 1133.
- 10 E. O. Fischer and K. Bitler, *Z. Naturforsch.*, 1961, **16**, 225.
- 11 M. I. Bruce, M. Z. Iqbal, and F. G. A. Stone, *J. Chem. Soc., Dalton Trans.*, 1971, **127**, C55.
- 12 H. Brunner, *Angew. Chem., Int. Ed. Engl.*, 1969, **81**, 395.
- 13 J. I. Seeman and S. G. Davies, *J. Am. Chem. Soc.*, 1985, **107**, 6522.
- 14 G. J. Baird, J. A. Bandy, S. G. Davies, and K. Prout, *J. Chem. Soc., Chem. Commun.*, 1983, 1202.
- 15 S. G. Davies, *Pure Appl. Chem.*, 1988, **60**, 13.
- 16 Y. Kondo, J. R. Green, and J. Ho, *J. Org. Chem.*, 1993, **58**, 6182.
- 17 P. M. Treichel and D. A. Komar, *Inorg. Chim. Acta*, 1980, **42**, 277.
- 18 C. Bolm and K. Muniz, *Chem. Soc. Rev.*, 1999, **28**, 51.
- 19 S. G. Davies, *Chem. and Ind.*, 1986, 506.
- 20 M. Uemura, T. Minami, and Y. Hayashi, *J. Am. Chem. Soc.*, 1987, **109**, 5277.
- 21 P. Pertici, F. Borgherini, G. Uitulli, P. Salvadori, C. Rosini, C. Moise, and J. Besancon, *Inorg. Chim. Acta*, 1998, **268**, 323.
- 22 H. Brunner and J. Doppelberger, *Chem. Ber.*, 1978, **111**, 673.
- 23 H. Brunner, *Angew. Chem., Int. Ed. Engl.*, 1999, **38**, 1194.
- 24 H. Asano, K. Katayama, and H. Kurosawa, *Inorg. Chem.*, 1996, **35**, 5760.

- 25 G. Consiglio and F. Morandini, *Chem. Rev.*, 1987, **87**, 761.
- 26 J. D. Korp and I. Bernal, *Inorg. Chem.*, 1981, **20**, 4065.
- 27 H. Brunner and R. G. Gastinger, *J. Organomet. Chem.*, 1978, **145**, 365.
- 28 T.-S. Peng, A. M. Arif, and J. A. Gladysz, *J. Chem. Soc., Dalton Trans.*, 1995, 1857.
- 29 J. H. Merrifield, C. E. Strouse, and J. A. Gladysz, *Organomet.*, 1982, **1**, 1204.
- 30 J. H. Merrifield, M. Fernandez, W. E. Buhro, and J. A. Gladysz, *Inorg. Chem.*, 1984, **23**, 4022.
- 31 J. Fernandez and J. A. Gladysz, *Inorg. Chem.*, 1986, **25**, 2672.
- 32 T. R. Ward, O. Schafer, C. Daul, and P. Hofmann, *Organomet.*, 1997, **16**, 3207.
- 33 M. A. Dewey, Y. Zhou, Y. Liu, and J. A. Gladysz, *Organomet.*, 1993, **12**, 3924.
- 34 G. Capper, L. C. Carter, D. L. Davies, J. Fawcett, and D. R. Russell, *J. Chem. Soc., Dalton Trans.*, 1996, 1399.
- 35 G. Consiglio, F. Morandini, and F. Bangerter, *Inorg. Chem.*, 1982, **21**, 455.
- 36 G. Consiglio, F. Morandini, G. Ciani, and A. Sironi, *Angew. Chem., Int. Ed. Engl.*, 1983, **95**, 322.
- 37 F. Morandini, G. Consiglio, and V. Lucchini, *Organomet.*, 1985, **4**, 1202.
- 38 F. Morandini, G. Consiglio, B. Straub, G. Ciani, and A. Sironi, *J. Chem. Soc., Dalton Trans.*, 1983, 2293.
- 39 M. A. Bennett, T. Huang, T. W. Matheson, and A. K. Smith, *Inorg. Synth.*, 1982, **21**, 75.
- 40 C. White, A. Yates, and P. M. Maitlis, *Inorg. Synth.*, 1992, **29**, 228.
- 41 M. R. Churchill and S. A. Julis, *Inorg. Chem.*, 1977, **16**, 1488.
- 42 J. W. Hull, Jr. and W. L. Gladfelter, *Organomet.*, 1984, **3**, 605.
- 43 M. A. Bennett, M. I. Bruce, and T. W. Matheson, in 'Comprehensive Organometallic Chemistry 2'; ed. G. Wilkinson, F. G. A. Stone, and E. W. Abel, Oxford, 1982.
- 44 J. W. Kang, K. Moseley, and P. M. Maitlis, *J. Am. Chem. Soc.*, 1969, **91**, 5970.
- 45 W. Rigby, H. Lee, P. M. Bailey, and J. A. McCleverty, *J. Chem. Soc., Dalton Trans.*, 1979, 387.
- 46 P. R. Sharp, in 'Comprehensive Organometallic Chemistry 2'; ed. G. Wilkinson, F. G. A. Stone, and E. W. Abel, Oxford, 1995.
- 47 M. A. Bennett, in 'Comprehensive Organometallic Chemistry 2'; ed. G. Wilkinson, F. G. A. Stone, and E. W. Abel, Oxford, 1995.

- 48 P. M. Maitlis, *Acc. Chem. Res.*, 1978, **11**, 301.
- 49 R. P. Hughes, in 'Comprehensive Organometallic Chemistry'; ed. G. Wilkinson, F. G. A. Stone, and E. W. Abel, Oxford, 1982.
- 50 M. A. Bennett, T. W. Matheson, G. B. Robertson, W. L. Steffen, and T. W. Turney, *J. Chem. Soc., Chem. Commun.*, 1979, 32.
- 51 F. B. McCormick, D. D. Cox, and W. B. Gleason, *Organomet.*, 1993, **12**, 610.
- 52 L. Carter, D. L. Davies, J. Fawcett, and D. R. Russell, *Polyhedron*, 1993, **12**, 1599.
- 53 R. Lang, K. Polborn, T. Severin, and K. Severin, *Inorg. Chim. Acta*, 1999, **294**, 62.
- 54 M. A. Bennett, T.-N. Huang, and T. W. Turney, *J. Chem. Soc., Chem. Commun.*, 1978, 582.
- 55 H. LeBozec, D. Touchard, and P. H. Dixneuf, *Adv. Organomet. Chem.*, 1989, **29**, 163.
- 56 D. Carmona, C. Vega, F. J. Lahoz, R. Atencio, L. A. Oro, P. M. Lamata, F. Viguri, and E. San Jose, *Organomet.*, 2000, **19**, 2273.
- 57 G. Consiglio, F. Morandini, G. Ciani, and A. Sironi, *Organomet.*, 1986, **5**, 1976.
- 58 M. A. Bennett and A. K. Smith, *J. Chem. Soc., Dalton Trans.*, 1974, 233.
- 59 H. Werner, H. Kletzin, A. Hohn, W. Paul, W. Knaup, M. L. Ziegler, and Serhadli, *J. Organomet. Chem.*, 1986, **306**, 227.
- 60 H. Werner and H. Kletzin, *J. Organomet. Chem.*, 1982, **228**, 289.
- 61 M. Otto, J. Parr, and A. M. Z. Slawin, *Organomet.*, 1998, **17**, 4527.
- 62 D. Carmona, F. J. Lahoz, L. A. Oro, M. P. Lamata, F. Viguri, and E. San Jose, *Organomet.*, 1996, **15**, 2961.
- 63 L. Dadci, H. Elias, U. Frey, A. Hornig, U. Koelle, A. E. Merbach, H. Paulus, and J. S. Schneider, *Inorg. Chem.*, 1995, **34**, 306.
- 64 A. Cusanelli, L. Nicula-Dadci, U. Frey, and A. E. Merbach, *Inorg. Chem.*, 1997, **36**, 2211.
- 65 K. Mashima, K. Kusano, T. Ohta, R. Noyori, and H. J. Takaya, *J. Chem. Soc., Chem. Commun.*, 1989, 1208.
- 66 A. Bader and E. Lindner, *Coord. Chem. Rev.*, 1991, **108**, 27.
- 67 V. V. Grushin, *J. Am. Chem. Soc.*, 1999, **121**, 5831.
- 68 J. Faller and J. Parr, *Organomet.*, 2000, **19**, 1829.

- 69 J. Faller, B. P. Patel, M. A. Albrizzio, and M. Curtis, *Organomet.*, 1999, **18**, 3096.
- 70 D. D. Sternbach, D. M. Rossana, and K. D. Onan, *Tetrahedron Lett.*, 1985, **26**, 591.
- 71 E. L. Eliel, S. H. Wilen, and L. N. Mander, 'Stereochemistry of Organic Compounds', Wiley-Interscience, 1994.
- 72 D. Carmona, C. Cativiela, S. Elipe, F. J. Lahoz, M. P. Lamata, M. P. Lopez-Ram de Viu, L. A. Oro, C. Vega, and F. Viguri, *Chem. Commun.*, 1997, 2351.
- 73 D. F. Dersnah and M. C. Baird, *J. Organomet. Chem.*, 1977, **127**, C55.
- 74 G. Capper, 'PhD Thesis', University of Leicester, 1995.
- 75 D. L. Davies, J. Fawcett, R. Krafczyk, and D. R. Russell, *J. Organomet. Chem.*, 1997, **545-546**, 581.
- 76 R. Kramer, K. Polborn, H. Wanjek, I. Zahn, and W. Beck, *Chem. Ber.*, 1990, **123**, 767.
- 77 W. S. Sheldrick and S. Heeb, *J. Organomet. Chem.*, 1989, **377**, 357.
- 78 L. C. Carter, 'PhD Thesis', University of Leicester, 1994.
- 79 L. C. Carter, D. L. Davies, K. T. Duffy, J. Fawcett, and D. R. Russell, *Acta Crystallogr., Sect. C*, 1994, **50**, 1559.
- 80 R. Noyori and S. Hashiguchi, *Acc. Chem. Res.*, 1997, **30**, 97.
- 81 K.-J. Haack, S. Hashiguchi, A. Fujii, T. Ikariya, and R. Noyori, *Angew. Chem., Int. Ed. Engl.*, 1997, **36**, 285.
- 82 D. B. Grotjahn, C. Joubran, and J. L. Hubbard, *Organomet.*, 1996, **15**, 1230.
- 83 D. Carmona, A. Medoza, F. J. Lahoz, L. A. Oro, M. P. Lamata, and E. San Jose, *J. Organomet. Chem.*, 1990, **396**, C17.
- 84 D. Carmona, F. J. Lahoz, R. Atencio, L. A. Oro, M. P. Lamata, F. Viguri, E. San Jose, C. Vega, J. Reyes, F. Joo, and A. Katho, *Chem. Eur. J.*, 1999, **5**, 1544.
- 85 S. Attar, V. J. Catalano, and J. H. Nelson, *Organomet.*, 1996, **15**, 2932.
- 86 S. Attar, J. H. Nelson, J. Fischer, A. Decian, J. P. Sutter, and M. Pfeffer, *Organomet.*, 1995, **14**, 4559.
- 87 N. Gul and J. H. Nelson, *Organomet.*, 1999, **18**, 709.
- 88 H. D. Hansen, K. Maitra, and J. H. Nelson, *Inorg. Chem.*, 1999, **38**, 2150.
- 89 S. Fernandez, M. Pfeffer, V. Ritleng, and C. Sirlin, *Organomet.*, 1999, **18**, 2390.
- 90 H. Brunner and T. Zwack, *Organomet.*, 2000, **19**, 2423.

- 91 H. Brunner, R. Oeschey, and B. Nuber, *J. Chem. Soc., Dalton Trans.*, 1996, 1499.
- 92 H. Brunner, R. Oeschey, and B. Nuber, *Inorg. Chem.*, 1995, **34**, 3349.
- 93 S. K. Mandal and A. R. Chakravarty, *J. Chem. Soc., Dalton Trans.*, 1992, 1627.
- 94 S. K. Mandal and A. R. Chakravarty, *Inorg. Chem.*, 1993, **32**, 3851.
- 95 M. L. Loza, J. Parr, and A. M. Z. Slawin, *Polyhedron*, 1997, **16**, 2321.
- 96 H. Brunner, R. Oeschey, and B. Nuber, *Organomet.*, 1996, **15**, 3616.
- 97 D. L. Davies, J. Fawcett, S. A. Garratt, and D. R. Russell, *Chem. Commun.*, 1997, 1351.
- 98 A. J. Davenport, D. L. Davies, J. Fawcett, S. A. Garratt, L. Lad, and D. R. Russell, *Chem. Commun.*, 1997, 2347.
- 99 D. L. Davies and S. A. Garratt, 'Unpublished results'.
- 100 S. A. Garratt, 'PhD Thesis', University of Leicester, Leicester, 1998.
- 101 W. S. Sheldrick and S. Heeb, *Inorg. Chim. Acta*, 1990, **168**, 93.
- 102 H. Brunner, R. Oeschey, and B. Nuber, *J. Organomet. Chem.*, 1996, **518**, 47.
- 103 H. Brunner, B. Nuber, and M. Prommesberger, *Tetrahedron-Asymmetry*, 1998, **9**, 3223.
- 104 K. Stanley and M. C. Baird, *J. Am. Chem. Soc.*, 1975, **97**, 6598.
- 105 A. K. Ghosh, P. Mathivanan, and J. Cappiello, *Tetrahedron-Asymmetry*, 1998, **9**, 1.
- 106 H. Nishiyama, M. Kondo, T. Nakamura, and K. Itoh, *Organomet.*, 1991, **10**, 500.
- 107 A. Pfaltz, *Acc. Chem. Res.*, 1993, **26**, 339.
- 108 G. Helmchen, A. Krotz, K.-T. Ganz, and D. Hansen, *Synlett*, 1991, 257.
- 109 F. G. Schaefer and G. A. Peters, *J. Org. Chem.*, 1961, **26**, 412.
- 110 J. Hall, J. Lehn, A. DeCian, and J. Fischer, *Helv. Chim. Acta*, 1991, **74**, 1.
- 111 C. Bolm, K. Weickharott, M. Zender, and T. Ranff, *Chem. Ber.*, 1991, **124**, 1173.
- 112 M. Peer, J. C. D. Jong, M. Kiefer, T. Langer, H. Rieck, H. P. Sennhenn, J. Sprinz, H. Steinhagen, B. Wiese, and G. Helmchen, *Tetrahedron*, 1996, **52**, 7547.
- 113 S. E. Denmark, N. Nakajima, O. J.-C. Nicaise, A.-M. Faucher, and J. P. Edwards, *J. Org. Chem.*, 1995, **60**, 4884.
- 114 H. Brunner and U. Obermann, *Chem. Ber.*, 1989, **122**, 499.

- 115 A. J. Davenport, D. L. Davies, J. Fawcett, S. A. Garratt, and D. R. Russell, *Chem. Commun.*, 1999, 2331.
- 116 C. Bolm, K. Weickharott, M. Zender, and D. Glasmacher, *Helv. Chim. Acta*, 1991, **74**, 717.
- 117 C. Bolm, G. Schlingloff, and K. Weickhardt, *Angew. Chem., Int. Ed. Engl.*, 1994, **33**, 1848.
- 118 H. Bieraugel, R. Plemp, H. C. Hiemstra, and U. K. Pandit, *Tetrahedron*, 1983, **39**, 3971.
- 119 Y. Ito, Y. Inubushi, M. Z. S. Tomita, and T. Saegusa, *J. Am. Chem. Soc.*, 1973, 4447.
- 120 B. Cetinkaya, B. Alici, I. Ozdemir, C. Bruneau, and P. Dixneuf, *J. Organomet. Chem.*, 1999, **575**, 187.
- 121 B. Cetinkaya, E. Cetinkaya, P. B. Hitchcock, M. F. Lappert, and I. Ozdemir, *J. Chem. Soc., Dalton Trans.*, 1997, 1359.
- 122 C. Dauwe and J. Buddrus, *Synthesis*, 1995, 171.
- 123 T. Morimoto, K. Tachibana, and K. Achiwa, *Synlett*, 1997, 783.
- 124 H. Schiff, *Anal. Chem.*, 1864, **131**, 118.
- 125 J. Costamagna, J. Vargas, R. Latorre, A. Alvarado, and G. Mena, *Coord. Chem. Rev.*, 1992, **119**, 67.
- 126 J. Parr, A. T. Ross, A. M. Z. Slawin, D. F. Evans, and D. A. Jakubovic, *J. Chem. Soc., Dalton Trans.*, 1996, 2927.
- 127 M. Calligaris and L. Randaccio, in 'Comprehensive Coordination Chemistry'; ed. G. Wilkinson, R. D. Gillard, and J. A. McClerverty, Oxford, 1987.
- 128 K. Reedijk, in 'Comprehensive Coordination Chemistry'; ed. G. Wilkinson, R. D. Gillard, and J. A. McClerverty, Oxford, 1987.
- 129 R. Uhrhammer, D. G. Black, T. G. Gardner, J. D. Olsen, and R. F. Jordan, *J. Am. Chem. Soc.*, 1993, **115**, 8493.
- 130 E. B. Tjaden, D. G. Swenson, R. F. Jordan, and J. L. Peterson, *Organomet.*, 1995, **14**, 371.
- 131 V. Sunjic, D. Sepac, B. Kojic-Prodic, R. Kiralj, K. Mlinaric-Majerski, and V. Vinkovic, *Tetrahedron-Asymmetry*, 1993, **4**, 575.
- 132 Z. Majer, M. Hollosi, S. I. Kirin, and V. Sunjic, *Chirality*, 1996, **8**, 244.
- 133 V. Vinkovic, Z. Raza, and V. Sunjic, *Spectroscopy Letters*, 1994, **2**, 269.
- 134 T. E. Sloan, *Top. Stereochem.*, 1981, **12**, 1.

- 135 P. S. Pregosin and R. W. Kunz, 'NMR 16 Basic Principles and Progress', ed. P. Diehl, E. Fluck, and R. Kosfield, Springer-Verlag, 1989.
- 136 A. J. Davenport, D. L. Davies, J. Fawcett, S. A. Garratt, and D. R. Russell, *J. Chem. Soc., Dalton Trans.*, 2000, 4432.
- 137 H. Brunner, *Adv. Organomet. Chem.*, 1980, **18**, 151.
- 138 R. J. Leatherbarrow, in 'Graft', 1989-1995.
- 139 P. I. Dalko and Y. Langlois, *Chem. Commun.*, 1998, 331.
- 140 P. I. Dalko and Y. Langlois, *J. Org. Chem.*, 1998, **63**, 8107.
- 141 T. Ichiyangi, M. Shimizu, and T. Fujisawa, *J. Org. Chem.*, 1997, **62**, 7937.
- 142 O. Keller, W. E. Keller, G. Look, and G. Wersin, *Organic Syntheses*, **63**, 160.
- 143 T. Miyazawa, T. Otamatsu, Y. Fukui, T. Yamada, and S. Kuwata, *J. Chem. Soc., Chem. Commun.*, 1988, 419.
- 144 M. Cernerud, H. Adolfsson, and C. Moberg, *Tetrahedron-Asymmetry*, 1997, **8**, 2655.
- 145 H. M. I. Osborn, A. A. Cantrill, J. B. Sweeney, and W. Howson, *Tetrahedron Lett.*, 1994, **35**, 3159.
- 146 D. Carmona, C. Vega, F. J. Lahoz, S. Elipe, L. A. Oro, P. M. Lamata, F. Viguri, R. Garcia-Correas, C. Cativiela, and M. P. Lopez-Ram deViu, *Organomet.*, 1999, **18**, 3364.
- 147 N. L. Allinger and D. Y. Chung, *J. Am. Chem. Soc.*, 1976, **98**, 6798.
- 148 M. J. McKennon, A. I. Meyers, K. Drauz, and M. Scharm, *J. Org. Chem.*, 1993, **58**, 3568.
- 149 J. H. Espenson, 'Chemical Kinetics and Reaction Mechanisms', ed. McGraw-Hill, 1995.
- 150 B. Boubekur, *J. Organomet. Chem.*, 1990, **389**, 259.
- 151 I. C. M. Ewhman-Ooyevaar, I. F. Luitwieler, K. Vatter, D. M. Grove, W. J. J. Smeets, E. Horn, A. L. Spek, and G. van Koten, *Inorg. Chim. Acta*, 1996, **252**, 55.
- 152 N. Gul and J. H. Nelson, *Organomet.*, 2000, **19**, 91.
- 153 S. Attar, J. H. Nelson, and J. Fischer, *Organomet.*, 1995, **14**, 4776.
- 154 P. K. Byers, A. J. Canty, and R. T. Honeyman, *Adv. Organomet. Chem.*, 1992, **34**, 1.
- 155 G. R. Newkome, W. E. Puckett, V. K. Gupta, and G. E. Kiefer, *Chem. Rev.*, 1986, **86**, 451.

- 156 A. D. Ryabov, *Chem. Rev.*, 1990, **90**, 403.
- 157 P. L. Alsters, P. F. Engel, M. P. Hogerheide, M. Copinj, A. L. Spek, and G. van Koten, *Organomet.*, 1993, **389**, 1831.
- 158 D. C. R. Hockless, P. A. Gugger, and S. B. Wibl, 'Unpublished Results'.
- 159 C. Navarro-Ranninger, F. Zamora, I. Lopez-Solera, A. Monge, and J. R. Masaguer, *J. Organomet. Chem.*, 1996, **506**, 149.
- 160 Y. Motoyama, N. Makihara, Y. Mikami, K. Aoki, and H. Nishiyama, *Bull. Chem. Soc. Jpn.*, 1997, 951.
- 161 M. A. Stark, G. Jones, and C. J. Richards, *Organomet.*, 2000, **19**, 1282.
- 162 S. E. Denmark, R. A. Stavenger, A.-M. Faucher, and J. P. Edwards, *J. Org. Chem.*, 1997, **62**, 3375.
- 163 W. Bauer, M. Prem, K. Polborn, K. Sunkel, W. Steglich, and W. Beck, *Eur. J. Inorg. Chem.*, 1998, 485.
- 164 J. T. B. H. Jastrzebski, E. Wehman, J. Boersma, and G. van Koten, *J. Organomet. Chem.*, 1991, **409**, 157.
- 165 E. Vedejs, A. R. Haight, and W. O. Moss, *J. Am. Chem. Soc.*, 1992, **114**, 6556.
- 166 J. W. Suggs and K. S. Lee, *J. Organomet. Chem.*, 1986, **299**, 297.
- 167 G. Zhao, O. G. Wang, and T. C. Mak, *J. Chem. Soc., Dalton Trans.*, 1998, 1241.
- 168 J. Chatt, L. M. Vallarino, and L. M. Venanzi, *J. Chem. Soc.*, 1957, 3413.
- 169 R. Uson, J. Fornies, R. Navarro, M. P. Garcia, and B. Bergarache, *Inorg. Chim. Acta*, 1977, **25**, 269.
- 170 R. Noyori and H. Takaya, *Acc. Chem. Res.*, 1990, **23**, 345.
- 171 A. Togni and L. M. Venanzi, *Angew. Chem., Int. Ed. Engl.*, 1994, **33**, 497.
- 172 H. Brunner, U. Obermann, and P. Wimmer, *J. Organomet. Chem.*, 1986, **316**, C1.
- 173 R. E. Lowenthal, A. Abiko, and S. Masamune, *Tetrahedron Lett.*, 1990, **31**, 6005.
- 174 D. Muller, G. Umbricht, B. Weber, and A. Pfaltz, *Helv. Chim. Acta*, 1991, **74**, 232.
- 175 D. A. Evans, K. A. Woerpel, M. M. Hinman, and M. M. Faul, *J. Am. Chem. Soc.*, 1991, **113**, 726.
- 176 D. A. Evans, K. A. Woerpel, and M. J. Scott, *Angew. Chem., Int. Ed. Engl.*, 1992, **31**, 430.

- 177 H. Nishiyama, Y. Itoh, Y. Sugawara, H. Matsumoto, K. Aoki, and K. Itoh, *Bull. Chem. Soc. Jpn.*, 1995, **68**, 1247.
- 178 T. G. Gant, M. L. Noe, and E. J. Corey, *Tetrahedron Lett.*, 1995, **52**, 8745.
- 179 R. Tokunoh, H. Tomiyama, M. Sodeoka, and M. Shibasaki, *Tetrahedron Lett.*, 1996, **37**, 2449.
- 180 P. von Matt, G. C. Lloyd-Jones, A. B. E. Minidis, A. Pfaltz, L. Macko, M. Neuberger, M. Zehnder, H. Reugger, and P. S. Pregosin, *Helv. Chim. Acta*, 1995, **78**, 265.
- 181 A. Pfaltz, *Acta Chem. Scand.*, 1996, **50**, 189.
- 182 J. Sauer and R. Sustmann, *Angew. Chem., Int. Ed. Engl.*, 1980, **19**, 779.
- 183 H. Waldmann, *Synthesis*, 1994, 535.
- 184 T. Mukaiyama, K. Narasaka, and K. Bunno, *Chem. Lett.*, 1973, 1011.
- 185 T. Naota, H. Takaya, and S.-I. Murahashi, *Chem. Rev.*, 1998, **98**, 2599.
- 186 A. C. Regan, *Chem. Soc.-Perkin Trans.*, 1998, **1**, 1151.
- 187 K. A. Jorgensen, M. Johansen, H. Audrain, and J. Thorhauge, *Acc. Chem. Res.*, 1999, **32**, 605.
- 188 H. B. Kagan and O. Riant, *Chem. Rev.*, 1992, **92**, 1007.
- 189 K. Narasaka, *Synthesis*, 1991, 1.
- 190 J. A. Gladysz and B. J. Boone, *Angew. Chem., Int. Ed. Engl.*, 1997, **36**, 550.
- 191 P. V. Bonnesen, C. L. Puckett, R. V. Honeychuck, and W. H. Hersh, *J. Am. Chem. Soc.*, 1989, **111**, 6070.
- 192 J. W. Faller and C. J. Smart, *Tetrahedron Lett.*, 1989, **30**, 1189.
- 193 E. P. Kundig, C. M. Saudan, and G. Bernardinelli, *Angew. Chem., Int. Ed. Engl.*, 1999, **38**, 1220.
- 194 E. P. Kundig, B. Bourdin, and G. Bernardinelli, *Angew. Chem., Int. Ed. Engl.*, 1994, **33**, 1856.
- 195 D. Carmona, C. Cativiela, R. Garcia-Correas, F. J. Lahoz, M. P. Lamata, J. A. Lopez, M. P. Lopez-Ram de Viu, L. A. Oro, E. San Jose, and F. Viguri, *Chem. Commun.*, 1996, 1247.
- 196 D. A. Evans, J. A. Murry, P. v. Matt, R. D. Norcross, and S. J. Miller, *Angew. Chem., Int. Ed. Engl.*, 1995, **34**, 798.
- 197 D. Kaufmann and R. Boese, *Angew. Chem., Int. Ed. Engl.*, 1990, **29**, 545.
- 198 D. A. Evans, J. A. Murry, and M. C. Kozlowski, *J. Am. Chem. Soc.*, 1996, **118**, 5814.

- 199 K. Ishihara, Q. Gao, and H. Yamamoto, *J. Org. Chem.*, 1993, **58**, 6917.
- 200 L. F. Tietze, C. Schneider, and A. Grote, *Chem. Eur. J.*, 1996, **2**, 139.
- 201 S. E. Schaus, J. Branalt, and E. N. Jacobsen, *J. Org. Chem.*, 1998, **63**, 403.
- 202 S. Danishefsky and M. Bednarski, *Tetrahedron Lett.*, 1984, **25**, 721.
- 203 T. K. Hollis, W. Odenkirk, N. P. Robinson, J. Whelan, and B. Bosnich, *Tetrahedron*, 1993, **49**, 5415.
- 204 W. W. Ellis and B. Bosnich, *Chem. Commun.*, 1998, 193.
- 205 T. K. Hollis and B. Bosnich, *J. Am. Chem. Soc.*, 1995, **117**, 4570.
- 206 R. H. Baker, S. W. Tinsley, D. Butler, and B. Riegel, *J. Am. Chem. Soc.*, 1950, **72**, 393.